The dynamics and control of bubbling fluidised beds[†]

Chin Nam Lim

February 2004

[†] A thesis submitted to the University of Bristol in accordance with the requirements for the degree of Doctor of Philosophy in the Faculty of Engineering, Department of Mechanical Engineering.

ABSTRACT

The objective of the dissertation is to improve the understanding of the complicated dynamics of the bubbling process in a fluidised bed. This will enable the implementation of effective control to achieve a desirable fluidisation quality. Techniques in the field of dynamics and automatic control were employed to study the bed. A planar fluidised bed was used to enable bubbling to be directly observable and measurable using real-time image analysis instrumentation. The bubble void fraction, BVF, in the bed was measured, which is the proportion of the bed occupied by the voids associated with bubbles.

A simulated bubbling bed devised based on the Clift & Grace (1970, 1971a, 1971b) bubble interaction model was validated experimentally using frequency domain analysis techniques. This led to the dynamical modelling of the fluidised bed by capturing the important features that governs the overall dynamics of the bed. The fluidised bed can be thought to be a temporary store of gas and the model related the introduction of a packet of gas and its nucleation as a bubble, to the changes in the bed BVF. The model works for cases of single bubbles and freely bubbling beds, showing that activities such as bubble interaction and coalescence cause non-linearity within the bed. The criteria for good fluidisation quality were defined and were related closely to bubble population and spatial distribution in the bed. The major causes affecting it were identified as bubble interaction and the influence of geometry allowing techniques to improve the quality of the process to be proposed.

A closed-loop system permitted thorough system identification of the bubbling fluidisation process, enabling the process dynamics to be extracted for controller design purposes. Fixed gain (Proportional + Integral + Derivative) and adaptive (Minimal Control Synthesis) controller schemes were implemented to control the process producing good experimental results.

To

My family

Acknowledgements

Dr. Andrew Harrison, my primary supervisor, presented me with the wonderful opportunity to continue my studies at Bristol. I have been grateful for his advice and counsel, as well as his flexibility as I manoeuvred many challenges. His brilliant ideas and insights have been a kernel that led to great discoveries in this research. Dr. Mark Gilbertson has made his warm and intelligent presence felt in personal ways over the years, contributed directly with enthusiasm and provided support and sage advice through his expertise in the field of fluidisation. His role as my second supervisor has never been better played and has been a crucial supportive element in the advisor-advisee structure. Their support has played a vital and pivotal role in making the attainment of this dissertation possible. I am deeply indebted to them. It has been a great honour having worked under them. Thank you Andrew and Mark...

The band of technicians has set a high standard of technical competence, providing a context to motivate this work, and have been personal friends. Dedicated appreciation is extended to Clive Rendall, Michael Darby and John Byles for having provided assistance with equipment, insights, machining help, moral support and friendship. Departmental staff including the secretaries has been fabulous, complimenting the support mechanism of the department. Where would the rest of us be without them sorting out the paper work?

Wallace Wong, BoonPing Koh, Leo Ngan, YewJun Chai and BengSin Lee have been valued compatriots and virtual labmates. We undertaken similar journeys side by side and often offered support and helping hand to each other so that none of us will fall behind. The sense of their warm and communal presence has been inspirational, morale lifting and will be deeply missed. David Drury, Arkadijus Nikonovas and Anthony Croxford are fellow researchers I have worked with, amongst others, who have all bolstered a stimulating and supportive environment to work in.

Manor Hall warden Dr. Martin Crossley-Evans, I must say, has been a major part of my community life in Bristol. My great thanks to him for his patience and support as I juggle between my research and being a hall of residence tutor. It has been a pleasure to have

served alongside him. The pastoral care and support from the hall and staff have become a family away from home.

Finally, my wonderful family has supported me throughout the duration of this work, and tolerated my absence. The sweetest reward for completing this dissertation will be the ability to spend more time with them. My parents deserve much credit for this achievement. They fed my curiosity from an early age, and gave me countless opportunities to grow. Their continuous love, encouragement and backing fuelled my drive and gave me the momentous push towards achieving something I never thought at one time, possible.

Author's Declaration

Unless otherwise acknowledged, the content of this thesis is the original and sole work of the author. No portion of the work in this thesis has been submitted by the author in support of an application for any other degree or qualification, at this or any other university or institute of learning. The views expressed in this thesis are those of the author, and not necessarily those of the University of Bristol.

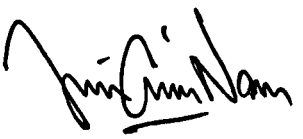

Chin Nam Lim

Copyright

Contents

CHAPTER 2

IMAGE ANALYSIS SYSTEM INSTRUMENTATION

CHAPTER 3

ASSESSMENT OF BED FLUIDISATION QUALITY

CHAPTER 4

RESOLVING BUBBLING PROCESS DYNAMICS WITH FREQUENCY DOMAIN TECHNIQUES

CHAPTER 5

THE SIMULATED BUBBLING FLUIDISED BED

List of Figures

List of Tables

Nomenclature

BNC	Bayonet Neil-Concelman / British Naval Connector	2.2
CPU	Central Processing Unit	2.2
DSP	Digital Signal Processor	2.2
D/A	Digital/Analogue (converter card)	2.2
DAC	Digital Analogue Converter	2.2
DLL	Dynamic Link Library	2.2
ISA	Industrial Standard Architecture (hardware bus interface)	2.2
SDK	Software Development Kit	2.2
ROI	Region Of Interest	2.2
NTSC	National Television System Committee (video format)	2.2
PC	Personal Computer	2.2
PAL	Phase Alternate Line (video format)	2.2
PCI	Peripheral Component Interconnect (hardware bus interface)	2.2
SIMD	Single Instruction Multiple Data	2.2
BVF	Bubble Void Fraction	2.3
LFG	Low Frequency Gain	4.2
PSD	Power Spectra Density	4.2
dB	Decibels	4.2
PDE	Partial Differential Equation	4.2
DC	Direct Current (very low/ null frequency signal)	4.3
ZOH	Zero Order Hold	7.3
PID	Proportional + Integral + Derivative (controller)	8.3
MRAC	Model Reference Adaptive Control	8.4
MSC	Minimal Control Synthesis	8.4
MSCIA	Minimal Control Synthesis + Integral Action	8.4
IPBM	Inverted Pyramid Bi-Modal (bubble introduction mode)	8.5
NBM	Normal-Bi-Modal (bubble introduction mode)	8.5

U_{mf}	superficial velocity at minimum point of fluidisation	1.3
U_{mb}	superficial gas flow at onset of bubbling fluidisation	1.3
ρ_p	particle density	1.3
d_p	particle diameter	1.3
$d_{b,e}$	equivalent bubble diameter, used for two-dimensional bed	3.2

$v_{b,L,av}$	average local bubble rise velocity (Werther & Molerus, 1976)	3.3
P	time period of measurement (Werther & Molerus, 1976)	3.3
$f_{b,L,av}$	average local bubble frequency over time period, P (Werther & Molerus, 1976)	3.3
$\delta_{b,L,av}$	average local bubble pulses (positive signal duration in sensor reading) over P (Werther & Molerus, 1976)	3.3.
$Q_{b,L}$	local bubble gas flow	3.3
ω	frequency in rad/s	4.2
r_i	magnitude of roots of a transfer function of order n (i = 1,2,..n)	4.2
θ_i	phase of roots of a transfer function of order n (i = 1,2,..n)	4.2
m	Mass	4.2
c	damping coefficient	4.2
k_s	spring constant	4.2
F	excitation force	4.2
x	horizontal displacement of a dynamical system	4.2
ω_n	undamped natural/characteristic frequency	4.2
λ	low frequency gain (LFG) denoted in transfer functions	4.2
ζ	damping ratio	4.2
g	gravitation acceleration	5.3
K_b	general coefficient relating bubble rise velocity to characteristic diameter	5.3
d_b	bubble characteristic diameter (general)	5.3
$d_{b,ev}$	diameter of sphere having the same volume as the spherical cap bubble	5.3
A_b	bubble projected area on a two-dimensional bed Pyle & Harrison, 1967	5.3
d_{bm}	diameter of modelled bubble	5.3
r_{bn}	radius of curvature at the nose of the bubble, (Davies & Taylor, 1950)	5.3
r_{bc}	bubble cloud radius	5.3
r_{bv}	bubble void radius	5.3
v_b	mean bubble rise velocity	5.3
$v_{b\infty}$	rise velocity of isolated bubble	5.3
v_{mf}	interstitial gas velocity for incipient fluidisation	5.3
α_b	$v_{b\infty} / v_{mf}$	5.3
S	r_{bc} / r_{bv}	5.3
d_{bi}	initial diameter of bubble at the distributor	5.3
h_b	bubble height in bed above distributor	5.3
t_c	bubble coalescence process duration	5.3
R_l	cloud radius of leading bubble in Farrokhalaee, 1979	5.3

R_2	cloud radius of trailing bubble in Farrokhalaee, 1979	5.3
x_b	horizontal bubble co-ordinate position	5.3
y_b	vertical bubble co-ordinate position	5.3
x_L	horizontal position of the leading bubble	5.3
y_L	vertical position of the leading bubble	5.3
x_T	horizontal position of the trailing bubble	5.3
y_T	vertical position of the trailing bubble	5.3
v_i	vertical velocity component of the i^{th} bubble	5.3
u_i	horizontal velocity component of the i^{th} bubble	5.3
r_{bm}	radius of modelled bubble	5.3
D	distance between the leading and trailing bubbles in Clift & Grace model	5.3
x_D	horizontal distance between the leading and trailing bubbles in Clift & Grace model	5.3
y_D	vertical distance between the leading and trailing bubbles in Clift & Grace model	5.3
$d_{bi,max}$	bubble maximum initial diameter	5.4
$d_{bi,min}$	bubble minimum initial diameter	5.4
f_{BVF}	Bubble Void Fraction factor for ratio of void to bubble area	5.4
A_{gb}	area (volume per unit thickness) of gas introduced as bubbles per unit time	6.4
A_p	amplitude of impulse signal mm/s	7.2
u_H	Zero Order Hold output	7.3
u^*	Zero Order Hold input	7.3
$K_{b,ZOH}$	constant of proportionality in BVF measurement relating to bubble size	7.3
K_{ZOH}	t/Δ	7.3
Δ	discrete time, sampling interval	7.3
T	bubble residence time in the bed	7.3
c_1	coefficient of bubble expansion (step) in (7.13)	7.5
c_2	coefficient of bubble expansion (ramp) in (7.13)	7.5
c_3	coefficient of bubble expansion (parabolic) in (7.13)	7.5
t	Time	7.5
d_{b1}	diameter of bubble 1	7.6
d_{b2}	diameter of bubble 2	7.6
$d_{b1,2}$	diameter of bubble product of coalescence of b_1 and b_2	7.6
$W_{b,i}$	weighting function of bubble i affecting (7.13) (i = 1,2,..n)	7.6
G_{b1}	theoretical model transfer function of bubble 1	7.6
G_{b2}	theoretical model transfer function of bubble 2	7.6
H_{bed}	gassed bed height	7.7

b_i	an arbitrary bubble (i = 1,2,..n)	7.7
$b_{1,2}$	bubble product of coalescence of b_1 and b_2	7.7
$h_{1,2}$	coalescence height between bubble b_1 and b_2	7.7
α_{tf}	transfer function zero (numerator root)	8.2
z	system zero roots in the s-transform transfer function equation	8.3
p	system pole roots in the s-transform transfer function equation	8.3
t_s	settling time of a dynamical system	8.3
k_p	PID controller proportional gain	8.3
T_i	PID controller integral gain	8.3
T_d	PID controller derivative gain	8.3
α	MCS weighting parameter	8.4
β	MCS weighting parameter	8.4
k_r	MCS forward/reference gain	8.4
K_r	MCS reference gain matrix	8.4
K	MCS gain matrix	8.4
k_1	MCS feedback position gain	8.4
k_2	MCS feedback velocity gain	8.4
k_i	MCSIA integral gain	8.4
b_L	leading bubble	8.5
b_T	trailing bubble	8.5
$b_{i,aj}$	arbitrary adjacent bubble	8.5

Chapter 1

Introduction

1.1 Introduction to fluidisation

Fluidisation is a process technology that typically combines the interaction effects of solid with gas or liquid to harness the unique characteristics of this mixture in many multi-phase contacting processes mainly in the chemical industry. Fluidisation manifests itself when a vessel filled with a bed of particles is supplied with gas from the bottom opposing the influence of gravity at a sufficient rate, causing the particles within to be agitated, mobilised and brought to suspension as the gas travels up the bed and leaves at the top. With insufficient flow, the fluid merely percolates through the spacing left by adjoining particles. Subsequent increases in flow bring the bed to a point of incipient fluidisation where sufficient aeration gives the bulk of particles fluid-like characteristics (i.e. when drag = weight).

When its buoyant weight is fully supported by drag, the bed of particles is said to be fluidised taking on behaviour equivalent to that of a fluid, e.g. zero-angle of repose and the floatation of light, as well as submergence of heavy objects. The behaviour of the agitated particles provides good mixing and contact between the gas and particles, with a pressure loss per unit area equivalent to the weight of the bed. The description of a typical fluidised bed and the fluidisation of particles are illustrated in *Figure 1.1.1*.

When gas is supplied in excess, causing the bed to expand to accommodate the increase, gas voids form in the emulsion phase, disturbing the homogeneity of the bed. Gas-fluidised beds typically operate in a regime in which the rising bubbles are dispersed within the emulsion phase of fluidised particles. The rising voids are referred to as bubbles if their size is significantly less than that of the cross section of the bed itself and as slugs

otherwise. The former process is termed bubbling or aggregative fluidisation and the latter, slugging fluidisation.

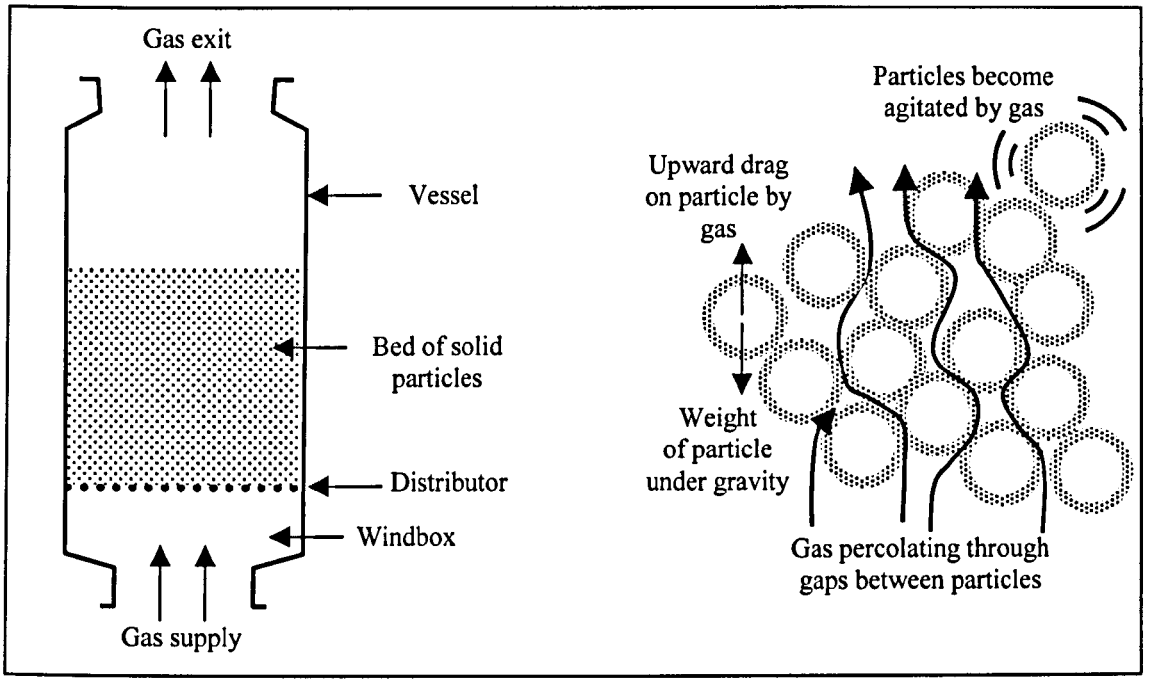

Figure 1.1.1: A typical arrangement of a fluidised bed and the phenomenon of a fluidisation process.

Fluidisation enables an easier and more efficient handling of solid materials through contact with a gas or liquid. This process has remarkable and intriguing characteristics and as a result, has generated a significant degree of engineering interest. Thus, engineering in the field of fluidisation is concerned with efforts to understand and exploit these features.

1.2 Practical uses of fluidisation technology

For the past two decades, the chemical-process industries have seen much development in expanding the application of numerous types of solid-handling techniques, ranging from moving-bed, mass-lift, suspension coolant, boiling bed and many others (Zabrodsky, 1966). All these have branched out from the commercialisation of the fluidised solid process used in the petroleum industry during the 1940s. However, references on the knowledge of the fluidisation technique have stretched as far back as 1878. The fluidisation process became a major industrial component, and was initiated by the pioneering work of the Standard Oil Development Company, the M. W. Kellogg Company

and the Standard Oil of Indiana in efforts to devise a better more efficient catalytic-cracking process than the previous fixed-bed method (Zenz & Othmer, 1960).

From a commercial and industrial point of view, it is clear that fluidisation is blessed with a number of advantages, principally with respect to temperature control, heat and mass transfer, continuity of operation and catalytic reactions. Good temperature control and the ability to reach isothermal conditions create an ideal environment to nurture efficient reactions. With good mixing and contact as the primary characteristics of fluidised particles, excellent mass and heat transfer capability inherent in this system is obvious. The turbulence within the bed is known to be able to disperse localised hot or cold regions throughout the bed resulting in an exceptionally good temperature uniformity and distribution. The high capacity of transfer surfaces available at any time allows high rates of heat transfer while the relatively high heat capacity of the bed compared to the fluidising gas ensures a stable bed temperature during operation, steadily absorbing surges of heat changes while incurring small temperature fluctuations.

The ability to handle solids as a mobile bulk allows fluidisation to be used in many continuous processes and is advantageous when particles are to be transported, circulated and rapidly mixed with minimum effort. The above-mentioned features enable the application of fluidisation in catalytic-reaction processes where maintenance of uniform (time and spatial) catalyst activity, continuous addition and removal of materials and a continuous operation with automatic control are required. Conveyance of solid material via pneumatic conveyers is evidence of fluidisation technology in such practice, transporting, for example, feed-corn into a silo for storage.

Processes like gas-gas, solid-solid and gas-solid mixing and reaction have been enhanced in production and quality when revolutionised to using fluidisation techniques. Incineration, material treatment, waste management and drying processes have also seen fluidisation being applied into their components of production line.

1.3 The state of the bed, the bubbling regime and structure and behaviour of bubbles

1.3.1 State of fluidisation

The phenomenon of gas-solid fluidisation occurs in several definable stages. Initially, with a small supply of gas through a bed of particles, the gas filters through the void around the particles hence, a bed at this state is called a fixed bed. Further gas flow increase mobilises the particles causing the bed to expand and this persists until the point when the bed becomes incipiently fluidised, with the bed taking on liquid-like behaviour.

Introduction of gas in excess of the quiescent state promotes formation of bubbles within the particulate fluidised bed. As the gas flow is increased further, the bed experiences several stages of transition from a bubbling bed to slugging bed, then finally into the pneumatic transport regime. *Figure 1.3.1* illustrates these regimes of fluidisation in sequence of gas flow increase into the bed.

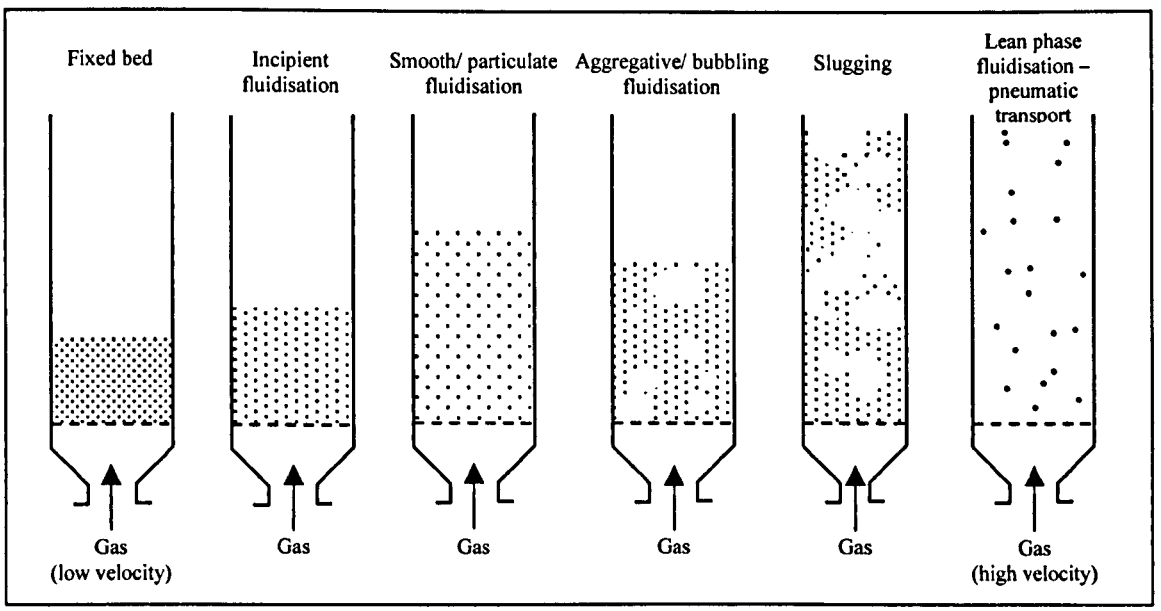

Figure 1.3.1: The regimes of fluidisation in sequence of gas flow increase into the bed. (Reproduced from Kunii & Levenspiel, 1969)

1.3.2 Fluidisation powder classification

The fluidisation of particles is also dependent on the properties of the particles to be fluidised, such as the particle size, density, shape and surface roughness. Geldart (1973) classified different particles into groups based on their size and density by the type of fluidisation characteristics, at ambient conditions, that are attributed to them. The classification is presented in the chart shown in *Figure 1.3.2*. Typically, group A powder beds with particles of size and density range of (~40 to 100 μm and < 1400 kg/m^3) expand considerably upon fluidisation above U_{mf} before bubbling commences at U_{mb} with additional supply of gas. Cutting the gas supply causes the bed to collapse slowly. Beds containing group B powders (approximately 40 μm to 500 μm, 1400 kg/m^3 to 4000 kg/m^3) begin to generate bubbles as soon as or slightly after achieving the state of minimum fluidisation ($U_{mf} \approx U_{mb}$) with negligible bed expansion. Bubbles form at the distributor and rise through the particulate phase coalescing and splitting before exiting at the top. Bubbles grow with height when rising in isolation.

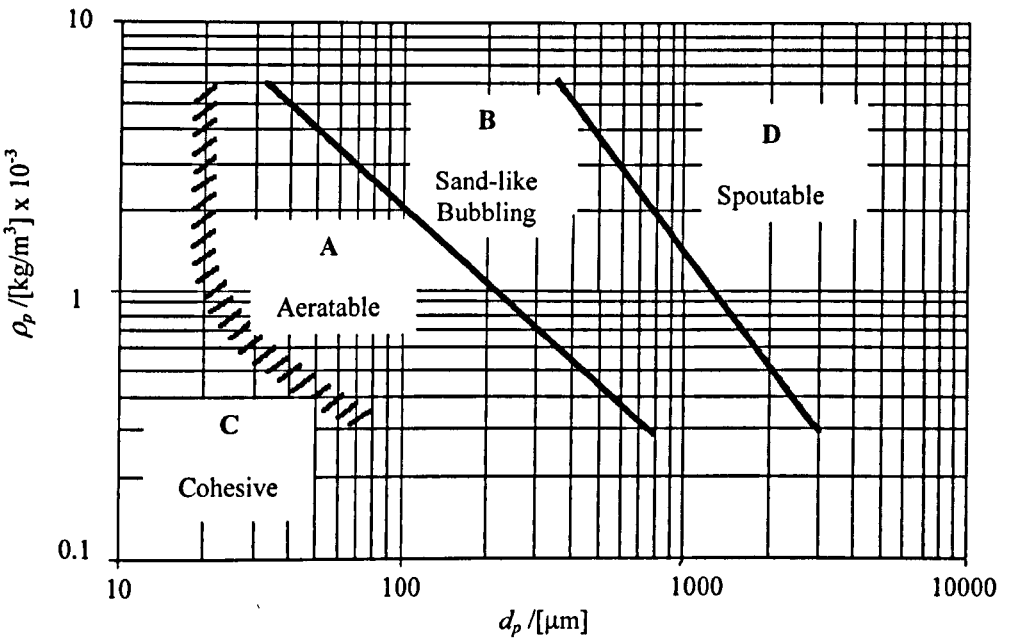

Figure 1.3.2: The Geldart's classification of powders according to their fluidisation properties. (Reproduced from Geldart, 1973).

Group C powders are fine and sticky, making the bed cohesive. Normal fluidisation of such powders will be extremely difficult. The bed expands due to the bulk of powders lifting up as a plug and will then tend to form channels through which the aeration gas

escapes rather than being dispersed and percolates through the interstices around the particles. This situation occurs because of the strong inter-particle forces and this usually arises from electrostatic charges or the presence of moisture and also due to sticky materials. Solid mixing and hence heat transfer is poorer compared to beds with group A or B powders. At the other extreme, beds with large and heavy particles cannot be properly fluidised either, as the fluidisation of the particles in these beds tends to be very turbulent and form spouts where the fluidising gas rushes through. These particles are categorised as group D powders in the Geldart's classification. The gas velocity in the dense phase can be high but the mixing of solids is poor.

1.3.3 Bubbles in fluidised bed

When operating in the bubbling regime, the existence of bubbles in fluidised systems has perhaps received the most attention and a tremendous amount of research effort has been put in to characterise and understand this phase. Bubbles in fluidised beds exist when gas is supplied in excess, such that packets of gas nucleate within the homogenous or emulsion phase. The existence of bubbles is important in some mixing processes because they drive mixing in the bed. Many (Davidson et al., 1977) workers have associated these bubbles closely with the gas bubbles in liquid. Yet, there are many dissimilarities in many aspects, particularly in their respective structure. A typical gas bubble in liquid consists of a packet of gas trapped within a spherical or spherical-cap like enclosure formed between the surface tension of the liquid and the equi-directional reaction of the gas pressure within the bubble.

On the other hand, a bubble in a gas-fluidised bed is somewhat different in that the observable void is merely an artefact of the existence of the bubble. The true bubble includes features not visible as a void. Shown in *Figure 1.3.3* is a diagram representing the structure of a bubble in gas-fluidised beds. A fluidised bed bubble comprises of several relatively concentric circumferential zones known as: the shell (Yates et al., 1994) where the voidage in the emulsion phase is increased by the bubble; the cloud, where parts of the bubble phase are hidden in the emulsion phase; and the void region, a particle-free region observable within the emulsion phase and it is easily recognisable and associated with the presence of the bubbling phase.

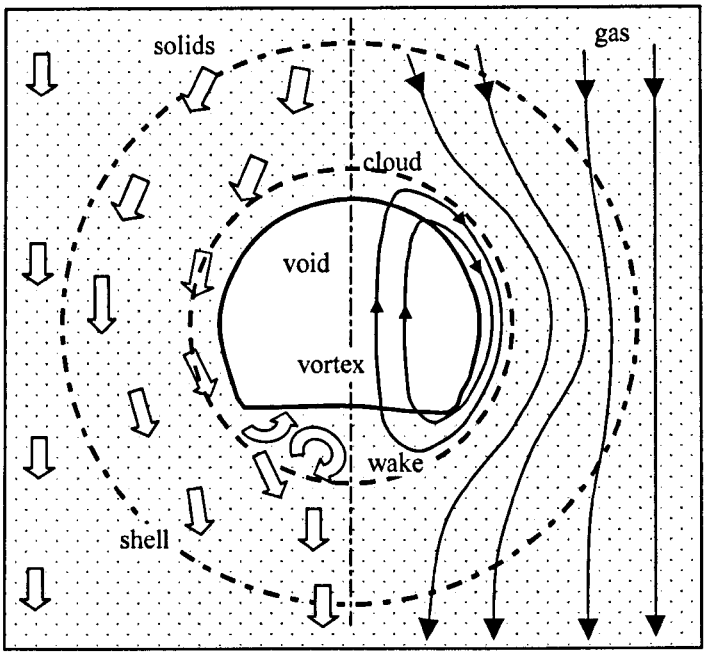

Figure 1.3.3: The structure of a fluidised bed bubble and the interaction of the gas and solids in the proximity of and within the bubble.

The cloud region is made out of a persistent vortex (observed as twin vortices in planar beds and a torus in three-dimensional beds) that is at the core of the existence of the bubble. Relative to the bubble's motion, the vortex maintains a continuous motion of gas through the bubble's vertical centreline and pushes upwards, holding the roof of the bubble where the mass of the gas circles around the sides, downwards and recirculates around to the centreline at the bottom. It is this perpetual vortex created at the distributor that generates a bubble and maintains its existence throughout the course of bubble rise, if the vortex is not disrupted.

Rowe *et al.* (1964) exhaustively investigated the cloud of a bubble, its formation, its shape and size as well as bubble splitting and coalescence. A better understanding of the cloud phenomenon could be the key to elucidating the complex relationship between bubble gas volume and the observable void shape and size. Other studies of bubble size and shape include Rowe (1976) who established a relationship to predict the bubble size in gas-fluidised beds indicating that the bubble volumetric average diameter is a function of the excess gas flow velocity and bed height. Horio & Nonaka (1987) derived a bubble diameter correlation to predict bubbling characteristics of fluidised beds of various powder categories. Lim & Agarwal (1990a, 1990b) used image analysis techniques to obtain the

pierced length and other statistical measures of bubble size and shape to obtain a theoretical prediction of bubble size measures using a geometrical probability approach.

Bubbles are often regarded as features where the gas within is not effectively fulfilling its primary purpose; that is to take part in reaction with the solid phase materials. The knowledge of the time scale these bubbles spend in the bed is crucial in assessing the requirement of an optimum bubble size, depending on the type of application of the process. Therefore, the rise rate of bubbles in fluidised beds has been extensively researched. As early as 1943, researchers such as Dumitrescu (1943) have been studying the rise of bubbles. The most significant contribution came from Davies & Taylor (1950). They mathematically described the relationship of bubble size to the rate of rise of gas bubbles in liquid such that

$$v_b = K_b\sqrt{gr_{bn}}$$

where v_b is the bubble rise velocity, r_{bn} is the radius of curvature at the nose of the bubble and K_b is a coefficient . Their semi-empirical formula was derived based on a gas bubble in an inviscid liquid of zero surface tension. Davidson et al. (1959) was later able to represent their results from experiments they conducted in fluidised beds with this relationship. Researchers such as Harrison & Leung (1961), Reuter (1963), Rowe & Partridge (1965) and Toei et al. (1965) have all studied the rise rate of bubbles in their various methods producing their individual interpretations of the quantitative empirical relationship between bubble size and velocity. Pyle & Harrison (1967) studied the rate of rise of bubble in planar beds with a photographic technique, allowing them to relate bubble velocity to the projected area of the bubble in the planar bed.

Davidson et al. (1959) developed a model of the bubble in fluidised systems. The model basically assumes the emulsion phase as a porous medium with constant voidage, such that the coupling of interaction between the solid and the gas is removed. The fluidising gas was assumed inviscid. The flow field around the modelled circles (or cylinders) is the flow pattern of the interaction between the objects through the surrounding medium. The model took into account both the movements of solid and gas and the pressure distribution about the rising bubbles. The fluidising gas was assumed to be incompressible and has negligible inertia such that the pressure was assumed to be uniform within the bubble and constant throughout any lateral plane remote from the bubble. Later, the model and theory were extended due to the follow-on efforts of other modellers such as Jackson (1963), Murray

(1965) and Collins (1965a, 1965b) by accounting for the actual shape of the bubbles rather than assuming a circular representation. The resulting models are, as a consequence, more cumbersome to use.

Stewart (1968) carried out detailed investigation into the models developed by these workers to compile a quantitative comparison between them and to attempt to provide an overall better understanding of the behaviour of bubbles in fluidised beds in terms of gas and particle movements. The measurement data obtained by Reuter (1963) on the pressure field around bubbles was compared with that predicted by the models established by these researchers. Stewart (1968) also derived a bubble model and found that no existing theoretical analysis fitted all the experimental facts exactly.

Generally, bubbles in fluidised beds become larger when they reach the top of the bed, due to the action of coalescence with other neighbouring bubbles during the course of their rise. However, Kunii et al. (1967) empirically investigated the behaviour of freely bubbling fluidised beds and found that bubbles grow as they rise in isolation. This is an important physical and dynamic feature in the bed with certain solid particle characteristics. The bubbling fluidisation of Geldart's group B powders is known to accommodate bubble expansion as the bubbles rise in isolation. There is no known explanation of the cause of growth of isolated rising bubbles and the actual mechanism causing this is badly understood. However, there were suggestions that hydrodynamic pressure changes and particle inertia could have contributed to this phenomenon. Also, Batchelor & Nitsche (1994) suggested that the growth of bubble with height could be caused by the time the vortex in the bubble takes to gradually empty the inside of the bubble. This gradually creates a void in the bubble that is seen to increase in size with height. Other researchers who also studied the growth of bubble size with height in the bed were Kobayashi et al. (1965) and Yasui and Johanson (1958).

The physical existence of individual bubbles within their surroundings and amongst their neighbouring bubbles results in complex bubble interactions with each other and the vessel, which determine the way bubbles travel up the bed. The local and global conditions in the bed dictate when the splitting of bubbles and coalescence of bubbles occur when interacting bubbles are in close enough proximity. These activities have been the

fundamental features that govern the overall behaviour of the process and it is crucial that they are properly studied and understood.

1.3.4 Behaviour of bubbles in fluidised beds

Clift & Grace (1972) and Clift *et al.* (1974) studied the stability of bubbles in fluidised beds by looking into the phenomenon of bubble splitting and its probable causes. They carried out a linearised stability analysis on the upper surface of a bubble in fluidised beds, and suggested that interstitial gas velocity has virtually no effect on the bubble roof stability, but instead that the effective kinematic viscosity of the dense phase plays the determining role. They were able to predict the initial growth rates of the dividing curtain of particles during bubble splitting and the sensitive wavelengths of disturbance that disrupt the stability of the solid-gas interface.

Clift and Grace have produced a series of papers studying the coalescence of bubbles. In their papers (Clift & Grace, 1970, 1971, 1972), Clift and Grace developed a bubble interaction model utilising potential flow theory to calculate the flow velocity of the flow field between neighbouring bubbles. The model predicts the sequence of bubble coalescence and was experimentally validated via comparison with measurements made from sequences of images of coalescing bubbles taken from a planar bed as well as by comparison with results obtained by other workers, e.g. Harrison & Leung (1962). The model, formulated for both the two- and three-dimensional beds, has already found its usage in many other researchers' work such as Korte et al. (2001) and Rafailidis & Clift (1991). Other research work on bubble coalescence and splitting include Rowe & Goldsmith (1975), Toei & Matsuno (1967), Shichi et al. (1968) and Grace & Venta (1973).

When bubbles interact, they translate laterally under the influence of the leading bubbles with the gross natural trend of migration concentrating the bubble population towards the centre region of the bed. This phenomenon changes the spatial distribution of bubbles progressively upwards from the distributor upon their introduction. The spatial distribution of bubbles has been the determining factor affecting the bubble population density and size distribution. The placement or distribution of successive bubbles within the vessel is constantly affected by how predecessor bubbles are placed.

Werther and Molerus (Werther & Molerus, 1973a, 1973b) spearheaded the investigation of bubble spatial distribution in three-dimensional vessels of different size aspect ratios. They found that bubble distribution takes on a profile that changes gradually with height from an annular profile of more intense bubble concentration near the walls to one that gradually tapers inwards towards the bed centre with bed height, ending with the merging of the annular rims into a single peaked profile of bubble concentration. However, they did not provide substantial reasoning on which the grounds of their findings were established. An equivalent investigation conducted on two-dimensional beds was carried out earlier by Grace & Harrison (1969) who found that due to coalescence, the distribution of bubbles was naturally non-uniform. They then suggested a simple coalescence model to describe the phenomenon of bubble spatial distribution transition with height.

As an alternative aspect of studying the profile of non-homogeneity in the bubbling bed, many researchers also looked into the solid concentration and bed voidage fraction distribution in the bed over various operating conditions. For example, Yates et al. (1993) and Lockett & Harrison (1967) studied the voidage distribution around bubbles and in fluidised beds while others looked at the phenomenon and characteristics of solid mixing. For example, Mostoufi & Chaouki (2001) used radioactive particle tracking technique to study the local mixing and diffusivity of solids over different fluidisation regimes.

The study of the cause and effect of bubble introduction profile is essentially related to fluidisation quality enhancement. Knowing and understanding how the introduction of bubbles at the distributor affects the instantaneous bubble distribution profile and consequently how that affects the subsequent profile as well as the bubbling properties enhances the ability to manipulate or control the process such that it complies with the required conditions that promote good quality of fluidisation.

1.4 Fluidisation quality

Fluidisation quality is a somewhat subjective term. Gibilaro (2001) laid out a series of criteria outlining the definition of fluidisation quality, which depending on the purpose or the operation, make up a definition that represents a good degree of fluidisation quality. For example, in a fluidised reactor the conversion process depends on the extent of the heat and mass transfer and therefore is strongly governed by the mixing within and between the phases made possible by the presence of bubbles in the bubbling mode. As a filtration bed on the other hand, the requirement is that the bed operates in a stable homogenous suspension where bubble formation is suppressed or kept to a minimum.

Harrison et al. (1961) pointed out that the quality of fluidisation is affected by several determining factors such as the solid and gas density ratio, solid particle size, operating pressure and temperature as well as the fluidising gas viscosity. Depending on these factors, the fluidised bed may observe a complete range of fluidisation regimes from smooth to bubbling. By controlling the choice of solid and fluidising medium characteristics, the fluidisation mode and hence the quality, depending on the type of operation, could also be controlled. However, often this is not possible when a certain selection of operating parameters have already been determined and quality of fluidisation only begins to vary during the process operation. Then, a dynamic means of control applies, e.g. via controlling the feed rate of solids or fluidising medium.

The appropriate ability to control the state of the bed becomes even more crucial when there are ever changing factors inherent within the bed, e.g. addition and removal of solids or agglomeration of particles. The generation of bubbles within a bed is typically perceived to be useful in inducing gross stirring and mixing, however, the gas associated with these bubbles does not serve its primary purpose of reacting with the solids. Therefore for convenience of study, a general definition of a good fluidisation quality is that the bed is in a state where there are large numbers of 'smallish' bubbles homogeneously distributed throughout the bed.

1.5 Measurement and analysis techniques

1.5.1 Measurement techniques

To understand a complicated system, it is good practice that the basic aspects of it be studied first to keep issues simple initially. Having fully grasped the fundamentals, the more complicated issues can be subsequently studied effectively. Currently, this is only possible with the use of a two-dimensional or planar bed. The planar bed was fabricated from two flat panels, usually transparent, placed a small distance apart so that the bed is essentially two-dimensional. Planar beds have provided great insight into the bubbling regime in the past (Rowe et al., 1964; Rowe, 1976; Lim et al., 1990a, 1990b, 1992, 1993).

In order to determine the state and condition of the fluidisation process, an appropriate measurement technique is required. Over the years, various techniques for measuring and characterising the state of the process have been developed, some of which have been successfully applied in industry as well as to research. An ideal technique would be non-intrusive, robust and effective, yet simple and cost-effective to implement.

The choice of measurement technique is based on the measurement requirement. Typically in a bubbling fluidised bed, the bubbling phase is the crucial element that requires measuring and characterising. The presence of bubbles and their behaviour and arrangement in the bed determines the degree of fluidisation quality in the bed at a given condition. Therefore indirectly, the quality of the bed can be inferred if the proper measurement of the condition of the bed based on the state of the bubbling phase can be made.

Previously, localised probes have been developed to detect and measure these bubbles. For example, Yasui & Johanson (1958) used optical sensors whereby a light source consisting of a 3.175mm-dia. tungsten filament lamp is coupled to a 2.38mm-o.d. metal tube. A prism was attached, which transmitted light from a lamp also attached, to a quartz tube. The apparatus was immersed into a fluidised bed column (~10 and 15 cm in diameter). When a bubble passed between the lamp and the prism, light was transmitted and converted into electrical energy, which was then processed and analysed.

A device by Whitehead & Young (1967) comprised of an array of probes which was also immersed into a three-dimensional bed (1.2 m^2) at varying depths to analyse bed behaviour and bubble properties. The device gave useful information on the formation and location of preferred bubble tracks within the bed. Okhi et al. (1976) devised a miniature optical fibre probe used to investigate bubble flow that had three fibres with one emitting strobe-like flashes with the other two picking it up and channelling it to a photo-multiplier. Other attempts are by means of electro-resistivity probe for fluidised bed with conductive particles (Park et al., 1969; Burgess & Calderbank, 1975).

Capacitance measurement techniques involve measuring the capacitance in a localised region of the bed (Morse & Ballou, 1951; Geldart & Kelsey 1972; Werther & Molerus 1973). The probes detected changes in capacitance in gas-fluidised beds due to changes in local solid concentrations during bubble formation. Werther & Molerus (1973) used the capacitance technique to measure the local void fraction around the bed to determine the spatial distribution of bubbles in the process of analysing their theory regarding the rise path of bubble in the bed from the distributor and the governing factors that determine these paths.

Many of these probes mentioned above were intrusive inserts installed protruding into the bed column. Their measuring tip was surrounded by the fluidised content of the bed such that these devices affected the nature of the process; their presence being the source of locally induced bubbling. Therefore, the data that these methods obtained were already altered by their presence. Rowe & Masson (1981) conducted extensive research into the effect of intrusive and invasive inserts of probes into the bed on the state of the bed, coming up with detailed conclusions indicating distortion of local measurements due to these devices. The physical presence of any probe locally modifies the flow field and hence tends to act as bubble nucleation site. Therefore, the obtained measurements will not be the true representation of the actual bed condition.

Pressure measurement is perhaps the most commonly used technique in the monitoring and sensing of conditions in fluidised systems due to its capability of measuring in opaque vessels. Pressure probes have been installed in many industrial fluidised systems in the past as well and present to measure the pressure fluctuation in the fluidised chamber caused by the perturbation of the pressure field caused by the activity of bubbles, from which the

state of the process could then be inferred. The measurement of pressure fluctuations has been used by many researchers in the study and characterisation of the fluidisation process. Reported literature includes Fan et al. (1981, 1983), Fan et al. (1990), Leckner et al. (2001). Bi et al. (1995) and Schaaf et al. (1998) who separately have used pressure measurements to look at the origin and phenomenon of pressure waves propagation in gas-fluidised beds to investigate the interaction between particles. Pressure measurements were also used to characterise the fluidisation regime such as in the work by Zijerveld et al. (1998) and Johnsson et al. (2000). Johnsson et al. (2002) on a separate piece of work also used pressure fluctuation data to study the interaction between the fluidised bed and the air-feed system.

1.5.2 Analysis techniques

Johnsson et al. (2002) applied several techniques when analysing the time series of pressure fluctuations, ranging from merely analysis done in the time domain, such as with statistical approach, to state-space analyses. In the frequency domain, they looked at the power spectra of the pressure fluctuations to determine its characteristics for different fluidisation regimes. The methods proved to be successful and to complement each other.

Frequency domain analysis techniques have been a very effective tool for studying the various aspects of the fluidisation process, ranging from detection of the various modes of fluidisation (Kage et al., 2000) to establishing scaling relationships for fluidised beds (Nicastro & Glicksman, 1984). Typically, frequency domain techniques were used to interpret the complicated measurement obtained from pressure fluctuations in the bed. Kage et al. (2000) have shown that through this technique, different dominating frequency contents could be identified characterising the regime at which the bed was operating.

Brue and Brown (Brue & Brown, 2001; Brown & Brue, 2001) also looked at the frequency domain of pressure measurements, to obtain an interpretation of the dynamics of the process using techniques common in the field of dynamics and automatic control. Their dynamical approach to analysis was unusual in that they assumed the bed could be treated as a dynamical system with an input parameter that is all the activities occurring within the bed, which include bubble formation, eruption and so on. This parameter was estimated to

have a frequency content equivalent to that of white noise of small amplitudes. The pressure fluctuation measurement (output) and the input parameter (a time series data) were then used to generate a transfer function describing the dynamics of the fluidisation condition from which the measurements were taken.

As pressure fluctuations are caused by various activities occurring within the bed, it is difficult to obtain a meaningful interpretation of how the measurements correspond to those which physically induced these measurements. It then becomes apparent that perhaps visual techniques are most suitable to study a complicated system such as this at the fundamental level. Through a transparent planar bed, the bubbling activity can be easily and readily observed, allowing studies of the bubbling phase to be carried out in its most direct and explicit form. This is a simple and fast technique, given the current technology of data processing and analysis, to effectively study the bubbling phase. It cannot be applied to opaque vessels, limiting its application to purely analytical purposes conducted on planar beds. Previously, photography was employed by researchers such as Pyle & Harrison (1967), Geldart (1970), Lim et al. (1990a, 1990b, 1992, 1993) and Mudde et al. (1994) to study the bubbling phase in planar beds.

Perhaps the most technologically advanced technique devised to characterise the fluidisation process is tomography. It is a completely non-intrusive method, capable of imaging in three-dimensions the voidage distributions within a fluidised bed at rates up to 100 Hz. Makkawi & Wright (2002a, 2002b) used electrical capacitance tomography (ECT) to study and verify the different classification of fluidisation regimes. ECT provided lateral cross-sectional view of the fluidisation column detailing information on the solid fraction content. This information allowed them to characterise the changes in solid fraction locally, and averaged over the bed to determine the regime in which the bed was operating. The solid fraction distribution profile then demonstrated the distribution of bubble development during bubbling from which the fluidisation quality in the bed could be inferred.

Many others have also developed techniques to study processes using tomography such as Dyakowski et al. (1997), Xu et al. (1997), Waterfall et al. (1997) and Halow & Nicoletti (1992). At present, the technique of tomography is becoming ever more affordable and readily available; perhaps it will become the next viable diagnostic and monitoring tool to

be widely used in industry in the near future. Tomography technique is currently applicable to only small sized (typically ~ 200 mm in diameter) non-metallic vessels and has yet to be developed so that it could process and analyse data in real-time. However, this is quickly improving.

For appropriate control of the bed to achieve the desired fluidisation quality requires that the instrumentation system provides measurements that characterise the state of the bed that are comprehensible and effective. This would only be possible if a good understanding of what is being measured could be established.

1.6 Control requirement and implementation

The control of the bubbling fluidisation process has become a crucial requirement when a good product and process operation are desired. Therefore, it is important to achieve a good degree of fluidisation quality and to continuously preserve this state in the bed. So far, the limited number of published sources is evidence that insufficient effort has been invested into developing credible tools and techniques for the control of the fluidisation process in various applications.

One prominent effort was by Schouten et al. (1998) who detailed the consequences of fluidisation quality alteration due to several factors ranging from changes in the fluidisation condition to variations in gas or solids feed. Preventive measures could be carried out to avoid problems such as defluidisation and agglomeration of solids if process condition changes could be detected early enough. They have developed a monitoring method using the short-term predictability of pressure signals from the process, which is claimed to be more successful in sensing changes in bed operation than the conventional average bed pressure drop measurement.

An example of a practical implementation of control over the fluidisation process was carried out by Chong et al. (Lee, Chong & Leung, 1986; Chong et al., 1987) who used pressure fluctuations in a tall three-dimensional bed to determine the bed condition. The variance of pressure fluctuations gave them a measure of excess gas build up at different heights within the tall bed, and was used to govern the removal of excess gas via installed

bleed valves at those heights. A conventional linear strategy was used to control the process. This technique was shown to suppress excessive bubbling that leads to slugging especially in tall beds hence maintaining a good fluidisation quality within.

Korte et al. (2001) also attempted to control the bed quality via the proper management of the spatial distribution of bubbles by deterring bubble coalescence in the bed. Carried out in the simulated environment, they analysed the prospect of doing so by controlling the sequence at which bubbles are introduced at the distributor and met some degree of success, however, this currently lacks experimental validation.

In the field of dynamics and automatic control, the definition of control takes on a different perspective. Generally, a system to be controlled is named the plant. The reference or demand, which is typically a value designating the state to which the plant should be controlled to approach and be maintained is given as the input. The output from the system is a measured parameter, characteristic of the state of the plant. In a closed-loop control implementation, the feedback of the output is compared with the demand so that appropriate control can be exerted to bring about the desired plant output. *Figure 1.6.1* shown below summarises the description of a closed-loop control implementation on a system.

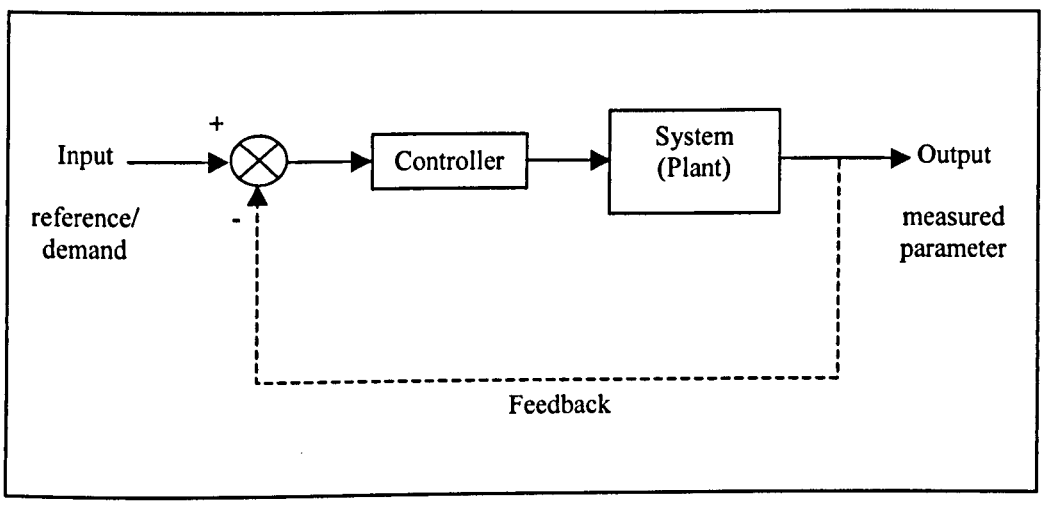

Figure 1.6.1: The block diagram of a typical treatment of a dynamical system in a closed-loop control implementation.

1.7 Research motivation and dissertation overview

Having reviewed the progress achieved in the technology of fluidisation and identified the issues that remain unexplored and the prospect of improvements that lies ahead, research objectives and motives were established constituting the content of this dissertation. The formation of gas voids or bubbles when gas is supplied in excess of that required for incipient fluidisation creates heterogeneity in the bed often associated with a discontinuity in the emulsion phase. The extent of study of the bubbling phenomenon is only exceeded by its complexity where throughout the years, it has been subject to much research effort, both experimental and theoretical, and remains an active topic of study.

It is of interest to further dwell into this area exploring only within the bubbling regime of Geldart's classification of group B powders with simplicity in the approach of study in mind. Group B powders are somewhat large in size that reach a bubbling state as soon as it becomes incipiently fluidised. The formation of bubbles upon achieving state of fluidisation immediately alters the dynamical behaviour of the bed from that of while it is just fluidised. From a dynamical point of view, the changes in the bed behaviour due to the formation of non-linear features and activities in the bed, governed by an input parameter, offers a great interest in study.

An understanding of the mechanism that governs the bubbling process in the bed would be beneficial to demonstrate that it is a process that gradually upsets homogeneity of smooth or particulate fluidisation, attributed to the effects of bubble interaction and coalescence, which are gas supply dependent. An instrumentation system is required and must be able to appropriately characterise these events, correlating the measurements to the physical state of the bed. *Chapter 2* describes the development of the imaging technique as the instrumentation method for characterising the bubbling phase. This chapter serves to demonstrate the complexity and difficulty in measuring processes such as fluidisation and to show how imaging techniques applied to a planar bed could help in the understanding of the process in its simplest and explicit form. The chapter includes the details of identifying measurable parameters that could appropriately and effectively characterise the bubbling process where direct observation of voids associated with presence of bubbles in the bed was made.

The control of the process with the purpose of achieving and preserving a good degree of fluidisation quality has been a real concern and is a necessity to ensure high process efficiency and product quality. On a fundamental level, the performance of the process should be studied and judged based on the assessment of the process quality not directly associated with the criterion common in any specific application in industry. What was studied was the fundamental physical behaviour of bubbling and the effects of the presence of the bubbles on the overall bed performance and looking to achieve a well-mixed homogeneous bubbling condition. The work in *Chapter 3* consolidates the spatial and time domain in which measurements could be conducted such that a more effective characterisation of the state of the bed can be achieved. The combination of spatial and temporal measurement provides a time varying two-dimensional resolution of activities occurring in the bed allowing the behaviour of bubbles to be carefully studied. Along with statistical measurements of the bubble population, the state of the bed can be directly related to the state of the fluidisation quality.

Several (e.g. Kage et al., 2000; Johansson et al., 2002) researchers have used analytical techniques carried out in the frequency domain in their work, bearing commendable results and implications to future efforts of process system characterisation and identification. *Chapter 4* explains the development of an effective technique to characterise the bubbling process, which analyses the frequency content of the measured parameter time series. Frequency domain analysis has been shown by many researchers to allow identification of the dynamical features of fluidised systems. The demonstration of the technique in interpreting data from the experimental bed is provided, accompanied by sets of rules and procedures to identify key features in the frequency content plots that correspond to the activities and events occurring in the bed. The relationship of the bubble spatial distribution in the bed to the overall bed dynamics was also made in this chapter using frequency domain techniques.

Again on a fundamental and analytical level, the experimental equipment and hence its data and results should be complimented by the development of a simulation, replicating its experimental counterpart, in efforts to further assist in comprehending the process. The simulation offers a domain in which ideas and theories could be worked on efficiently and effectively. In *Chapter 5*, a simulated bubbling fluidised bed was devised primarily to complement and support the study carried out on the experimental bed. The development

of the simulated bubbling bed is described, addressing several of the major features in the simulation in close detail with comparison made to related work by other researchers. The simulated bed is validated by comparison with the experimental version of the system.

Chapter 6 encompasses the efforts to conceptualise an idealised bed. The chapter also seeks to establish a set of criteria that defines a good degree of the fluidisation quality. The idealised bed was therefore conceived to represent an example bed, to which a normal operating bed should attempt to approach. An idealised bed sustains a condition that promotes good fluidisation quality, realistically achievable only when the normal bed is close to its quiescent state. Idealised conditions enabled the corresponding features in the bed to be studied leading to an improved understanding of the fundamental physical effect of bubbling activities on the overall behaviour of the bed.

In *Chapter 7*, the concept of idealised beds has led to the ability to derive a theoretical model of the bubbling process that assumes a bubbling bed is a temporary store of gas. The model was shown to appropriately describe the effect of presence of bubbles from the simple case of single bubbles progressing to the more complicated effect of having multiple bubbles in the bed.

In order to properly control a system, its behaviour has to be understood so that a suitable control method could be appropriately implemented, which is so far a challenge for such a process. The process of system identification, common in the field of automatic control, was extensively used to describe the behaviour of dynamic systems prior to designing suitable method to control them. To address this issue, system identification therefore became an essential tool in the dissertation to further study the dynamics of the bubbling process from which the transient response of the process to external changes can be fully understood.

Chapter 8 elaborates the definition and the purpose of system identification. The knowledge obtained from the study described particularly in *Chapters 2*, *3* and *6* is essential in the successful implementation of the system identification study on the fluidised system. Conventional control methods were shown to generally able to control the process properly although their performance is sensitive to changes in the bed dynamics. The capability of standard linear controllers indicated the advantages of

applying adaptive controller strategies to control systems such as this, which led to the usage of the Minimal Control Synthesis (MSC) adaptive scheme. A brief description of an alternative method of controlling the process by direct control of the bubble spatial distribution was also included with preliminary studies conducted in a simulated environment prospecting potential future research. This method of control has implications for further improvements of the process quality in the bed.

Chapter 9 summarises the findings realised throughout this research. Each research topic was given an overview complemented by summarising remarks. The dissertation then concludes with a list of future and potential challenges available in the research.

1.8 Dissertation contribution

The five most significant contributions of this dissertation are:

- An example showing how complicated system dynamics can be studied using simple approaches to identify key features that dominate the overall system behaviour.
- Development of a novel method to characterise the bubbling fluidisation process, via frequency domain analysis techniques.
- Construction of a theoretical model to describe the bubbling process based on dynamics techniques.
- Demonstration that bubble coalescence is the main driving factor causing the deterioration of good degree of fluidisation quality by upsetting the linear relationship between bubble size and their residency in the bed.
- Demonstration that a fluidised bed is non-linear but that it is possible to approximate it to a linear system, allowing implementation of linear control strategies to control the process.

Chapter 2

Image analysis system instrumentation

2.1 Introduction

In a fluidisation process, it is desirable for the components in the bed to be well mixed; this is promoted by the existence of bubbles. It is important to maintain uniformity of the bed properties and for the pressure drop throughout the bed to be stable for good fluidisation quality. Bubbles play a significant role in determining this quality, being the main mixing agent and for delivering uniform properties and good contacting in the bed. However, it is apparent that they also introduce heterogeneity to the process that reduces the efficiency of contact between solid and gas, and as they usually travel faster through the bed than the surrounding gas in the emulsion phase, the residence time associated with the gas in the bubbles is reduced (Kaart et al., 1999).

The characterisation and monitoring of the state of a bubbling bed and the determination of the fluidisation quality associated with the bubbles have been important subjects. The development of an instrumentation system that is able to properly measure and characterise the state of the bed and relate the measurements to the physical processes occurring in it is crucial if a good understanding of the dynamical behaviour of the fluidised system is to be had. This also leads to a proper definition of what is meant by a good quality of fluidisation so that the objective of controlling the bed could be established.

This chapter discusses the development of the instrumentation system to monitor the bubbling fluidisation process through the use of image analysis techniques. The chapter begins with a brief introduction to the experimental bed listing the challenges of effectively and consistently monitoring and characterising the behaviour of the process. This is followed by the description of the implementation of image analysis on digitally acquired

images of the two-dimensional bubbling bed, from which the proportion of the bed occupied by voids associated with bubbles termed the Bubble Void Fraction, BVF, was measured as the characterising parameter for the bed. The system set-up and development including details of software and hardware implementations and several important algorithms that were used are also presented.

Signal characterisation was carried out on the measured parameter by which salient features were identified, corresponding to respective dynamic features in the bubbling process. A brief assessment of the system performance, optimisation and limitations were conducted to benchmark the system before using it for further research application. The use of the image analysis system to measure the bed bubble spatial distribution and the standard deviation and switching frequency of local states in the bed was also demonstrated relating closely to the definition of fluidisation quality.

2.2 Development of the image analysis system

The objective of developing this system is not to present yet another means of characterising the fluidisation process when so many others are already available and their applications elaborately addressed by various workers (*Chapter 1*). It is a means developed to analyse and investigate the bubbling process at its most explicit and simple form. The presence of bubbles, which can be seen looking through the planar bed allows direct study of the behaviour of these bubbles and their influence on the overall condition of the bed. This allows the fundamental behaviour of such bubbles to be first understood before more complicated systems, e.g. three-dimensional beds, can be tackled.

To observe and ultimately to quantify the existence of bubbles within the planar bed, imaging techniques prove to be a viable means through which qualitative measurement can also be obtained. A computer is therefore used to carry out this qualitative analysis and also to serve as the automatic controller for the control of the bubbling process. The flow into the bed can be varied through the use of a valve to adjust the state of fluidisation in the bed.

Therefore a system was designed and the experimental arrangement of the fluidised system with the image analysis instrumentation system installed is represented in a diagram shown in *Figure 2.2.1*. The image acquisition device, a digital video camera, was placed at the front of the bed, allowing for adjustable lateral and vertical positions. Fluorescent light tubes were fitted at the back of the bed as backlighting to provide the wide-angle illumination needed for bubble voids detection.

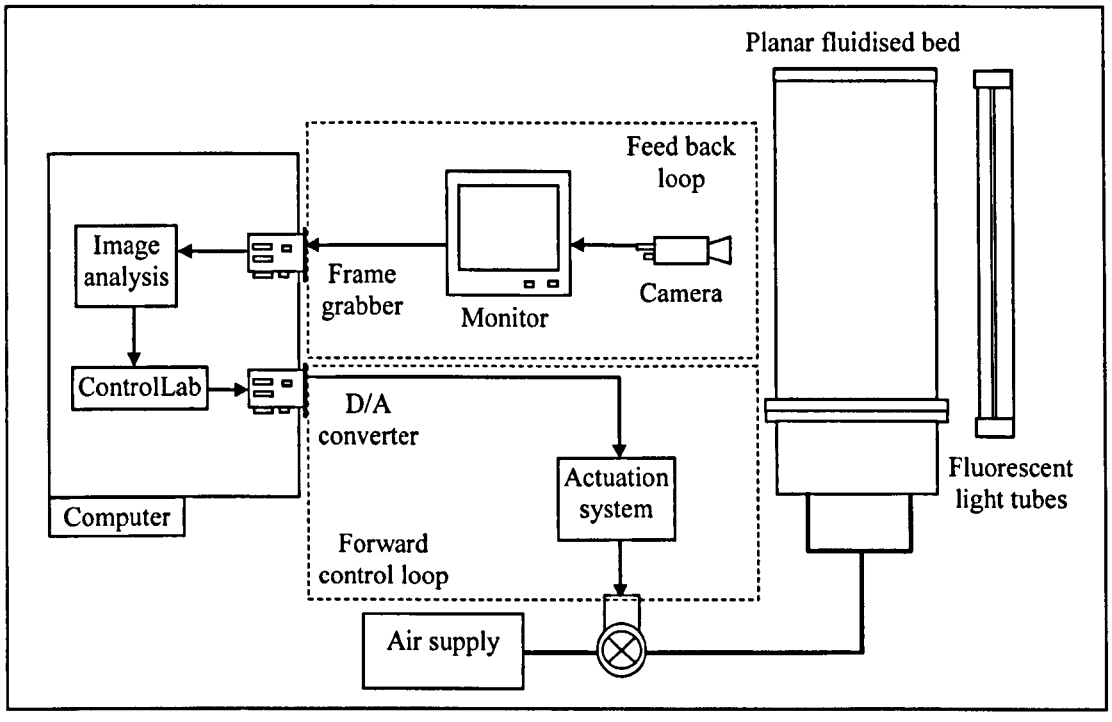

Figure 2.2.1: The arrangement of the experimental apparatus with the installation of image analysis system.

The digital video camera was connected to the frame grabber card via a monitor. The frame grabber fed the acquired image data from the camera into the CPU memory of a computer for further processing and analysis. A dedicated software module was written for image acquisition, processing and analysis from which the relevant measured parameters could be obtained. This was an open-loop operation with the cycle ending at the image analysis module. An actuation signal from the CPU could be sent via the D/A converter card to the servomotor that governs the amount of flow into the bed plenum by adjustments made to the pin-needle valve.

Bubbles in the bed can be detected because they create transparent areas on the flat cross-sectional plane of the two-dimensional bed, through which the illumination from the back

of the bed can shine pass and reach the camera. The amount of light shining through is dependent on the size of the bubble and bed thickness. The following sub-sections are dedicated to describing each element of the entire system in more detail.

2.2.1 Fluidised bed

The two-dimensional fluidised bed was constructed from Perspex (acrylic) with dimensions: 500 mm width, 1000 mm height and 13 mm depth, which allows bubbles to form and rise without immediately slugging. The sufficient height also enabled the complete development of bubble migration towards the bed centre (detailed in *Chapter 3*). A porous plate was used as the distributor. Geldart group B particles, ballotini glass beads (bulk density 1500 kg/m^3, particle density, $\rho_p \approx 3750$ kg/m^3, diameter 106 μm to 212 μm, and approximately 80% spherical) were used in all experiments. The distributor gave consistent uniform flow with formation of small bubbles well distributed symmetrically across it. No channelling of flow was observed during any bubbling conditions and the windbox pressure was stable and remained constant throughout the cross-section. *Figure 2.2.2(a)* shows a photograph of the experimental rig where the planar fluidised bed could be seen bubbling in the dark surrounding provided by a blackout tent where the illumination at the back of the bed shines through the bubble voids. In *Figure 2.2.2(b)* is a photograph of the bubbling planar fluidised bed.

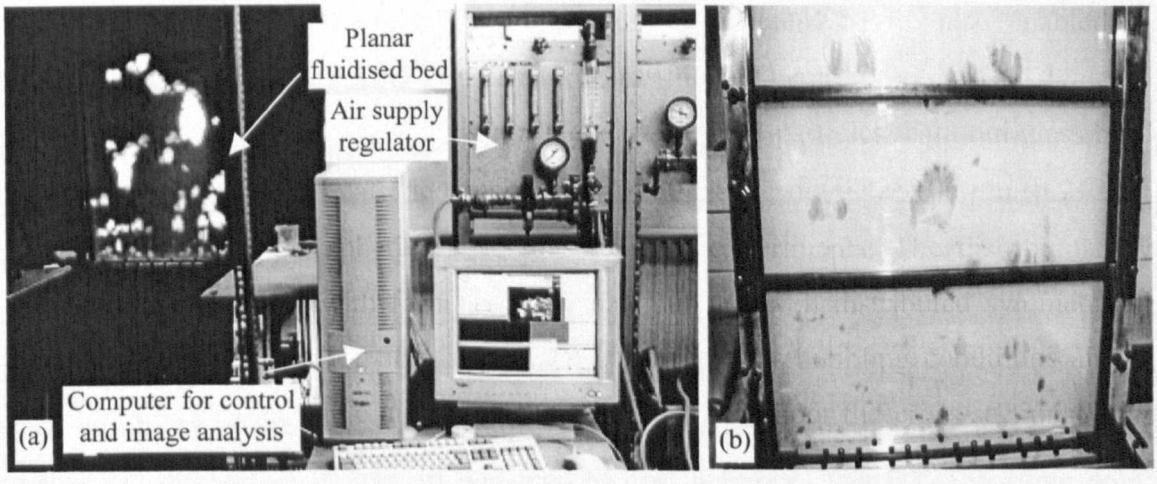

Figure 2.2.2: (a) A photo of the experimental rig where the planar fluidised bed can be seen bubbling in the dark surrounding with illumination shining from the back through the bubble voids, and (b) A photo of the fluidised bed up close while freely bubbling.

Measures were implemented by means of equipment earthing to minimise the effect of electrostatic charge generated between the Perspex panels and the particles. The counter-measure was sufficiently effective where the bed demonstrated non-cohesive particle fluidisation and the particles next to the walls of the bed were mobile and there was no obvious retardation to motion caused by electrostatic effect. The ungassed bed height was approximately 690mm, although, a variation of that height will also be used in some studies. The bed was fluidised by air at ambient temperature and pressure and was uniformly illuminated from the back. A nozzle was placed at the centre of the bed to introduce single bubbles into the system when required. The nozzle end was mounted flush to the porous plate distributor. A solenoid valve was placed before the single bubble nozzle to control the gas volume and flow rate. The solenoid was controlled by a control-box for both its close and open duration.

2.2.2 Digital video camera and video format

A commercially available digital video camera, the Panasonic NV-DX100B, was used. It captured and streamed frames video images at 25 frames per second in Phase Alternate Line (PAL, 50 Hz interlaced) format. Online streamings of video data were channelled directly to the frame grabber via a monitor using S-video and a BNC (Bayonet Neil-Concelman, or sometimes, British Naval Connector) ports.

2.2.3 Frame grabber and Digital Analogue Converter card

The frame grabber card used was the Data Translation Inc. DT3155 model. It is a high accuracy analogue monochrome frame grabber suitable for high-speed, low-noise imaging that could be used with standard PAL cameras. The DT3155 operated and interfaced with the computer via the Peripheral Component Interconnect (PCI) bus, transferring images continuously in real-time to system memory for further manipulation. Employing the high-speed capability of the PCI bus, the DT3155 could be programmed to transfer unlimited number of consecutive frames, in real-time to host memory. The DT3155 came with a versatile generalised Software Development Kit (SDK) containing a complete library of hardware-independent function calls that enabled the user to control the card via user-customised programme coded in virtually any coding languages. During an operation, the

SDK functions call on the specific low level commands that control the card in carrying out required tasks.

DT3155 frame grabber acquired frames of images at 1/30s (60 Hz interlaced) for NTSC format and at 1/25s (50 Hz interlaced) for PAL format. The corresponding maximum resolutions were 640x860 pixels and 768x576 pixels respectively with an aspect ratio of 1:1. The images were digitised to 8 bit, 256 grey levels monochrome quality. Pixel jitter had been minimised to approximately ± 3.5 ns typical and ± 5.0 ns maximum. Due to the acquisition formats (PAL, NTSC etc), the acquisition modes were interlaced.

The Digital Analogue Converter (DAC) card used was the Amplicon PC 30AT, 16-bit card. It operates on the Industry Standard Architecture (ISA) bus interface with the computer. The card has proven to be a robust and reliable hardware for what was required from previous applications operated using a currently available non-commercial written hardware controller software and driver, detailed further in *Section 2.2.4*.

2.2.4 Interfacing and instrumentation software

This section describes the software package used in the image analysis instrumentation of the bubbling process. The development of the software package provides a means of carrying out tasks specifically required in the research as well as acting as an interface for the user to instruct the computer to communicate with and operate the various hardware in service.

Throughout the research, instrumentation and control software were frequently used in many of the experimental work. The software, ControlLab, is an object-orientated software developed proprietarily within the Control Research Group in the University of Bristol Mechanical Engineering Department, which has been continually developed. The software was initiated by the programme Win Ctrl (Dye & Stoten, 1994) and developed by G.S. Beard (Beard, 1998). The software is implemented using a Pentium-based computer and was programmed using Delphi software development coding, incorporating various commercially available Software Development Kits (SDKs), designed to regulate the operation of the hardware ControlLab was instructed to work with.

ControlLab was constructed based on the concept of modular architecture. It consists of a main console, which is the front end of the software that interacts with the user and links all the modules of functions connected to it. Various modules performing specific functions could be linked to the main console when needed. In this way, unneeded modules could be removed and new modules with additional functions could continuously be developed without the main console as well as other modules undergoing any modifications. This allowed the software to operate and to be used efficiently, offering versatility on usage over various types of applications.

The image analysis instrumentation system was hence built around the functionality characteristic of ControlLab. With all the required functions programmed into a module, ControlLab could link to the instrumentation system when required. Additional features could be added to the existing module or a separate version of the instrumentation system could be developed without affecting compatibility with ControlLab.

ControlLab loads up with the main console as an executable file ('.exe' in Microsoft jargon) accompanied by the module library listing the available modules. Typically, a scope module, data logger module and a digital analogue converter (DAC) controller module are used in an application. For the application in this research, the image analysis module along with several other modules were used as shown in the diagram presented in *Figure 2.2.3*. All of the modules were linked directly to the main console enabling them to communicate efficiently during an operation.

Each of the modules is coded as Dynamic-Link-Libraries, DLLs (*.dll) that could be called upon or requested when the main programme of ControlLab requires so. A DLL is a piece of software that implements a set of routines collectively known as the interface of the DLL. These routines are called upon by other programmes at execution time. Implementation of programmes using DLL helps reduce the size of the calling main programme, as they are not statically linked to it. Besides that, the DLL codes could be reused and makes the structure of programmes simpler.

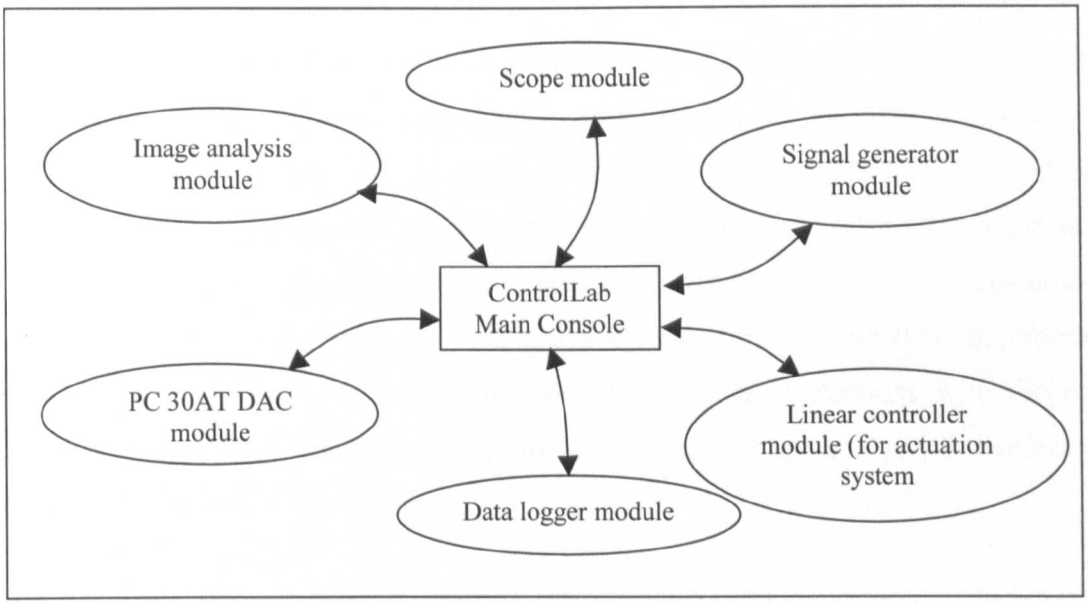

Figure 2.2.3: The modules that are dynamically linked to ControlLab when used for the image analysis instrumentation system.

A path linker window could be loaded up by ControlLab to administrate the connection of signal traffics between the modules to form a working system. The path linker window contains the forms of respective modules, each consisting of the input and output signals available from the module. Using the 'drag-drop' technique, a connection is formed between the input and the output of two modules, linking them together. *Figure 2.2.4* shows a snapshot of the path linker with the module connections for the system arrangement used in the research.

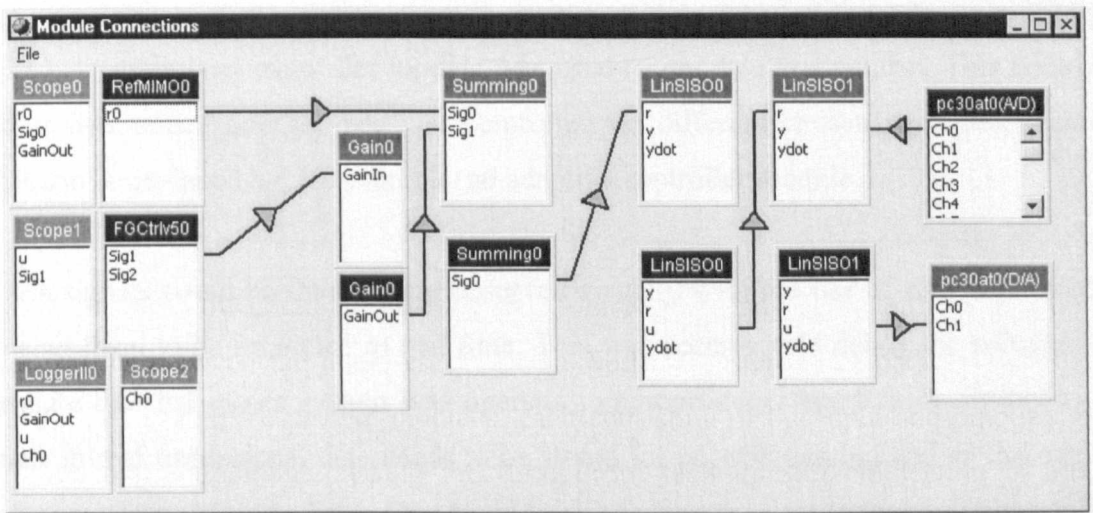

Figure 2.2.4: A snapshot of the path linker window use to administrate the connection of the modules to form a working system of the image analysis system.

The frame grabber used in the system was operated using the SDK supplied by the manufacturer (Data Translation Inc.). The supplied DLL files that communicate with the frame grabber with low-level instructions were written in C language. Additional programme interfacing files were needed to translate instruction from C to Delphi DLL and back during the execution of commands. Although this nature of programme structure adds to the overhead of the software, tests were carried out to validate that this does not increase the execution time of any instruction by significant proportion. Incorporating basic input-output commands as well as other operational instructions with the image processing and analysis functions, the frame grabber and image analysis instrumentation module was successfully implemented.

Figure 2.2.5 shows a snapshot of the image analysis module in operation with other modules, demonstrating how a general ControlLab operation platform looks. Referring back to *Figure 2.2.3*, the ControlLab main console linked the frame grabber, PC 30AT DAC controller, data logger, scopes, linear control suites and signal generator modules together via the path linker management window. The frame grabber module was responsible for managing the frame grabber card as well as all the image processing and analysis tasks. The signal generator produced the demand (reference) signal required to regulate the flow into the gas through which the PC 30AT module's administration of the DAC card would send the signal to the servomotor connected to the valve. The performance of the valve was controlled by the linear control module via a Proportional + Derivative Feedback method. In a closed-loop arrangement, such as that shown in *Figure 2.2.5*, which allowed the whole system to engage on the control of the state of bubbling in the bed, an additional controller module was used to regulate this control. This controller module determined how the bed was controlled via different chosen strategies, meaning that it can be replaced by, for example, an adaptive controller module.

All the signals could be tracked and observed visually with the use of the scope module allowing them to be inspected in real time. This was necessary to debug the software and to ensure that the whole system was operating appropriately. Apart from displaying the signals in real time, signal data needs to be stored for post-processing and so that records of an experiment could be kept. This could be done using the data logger module available in the ControlLab platform. The flow chart in *Figure 2.2.6* summarises the sequences of the tasks involved in the image analysis system.

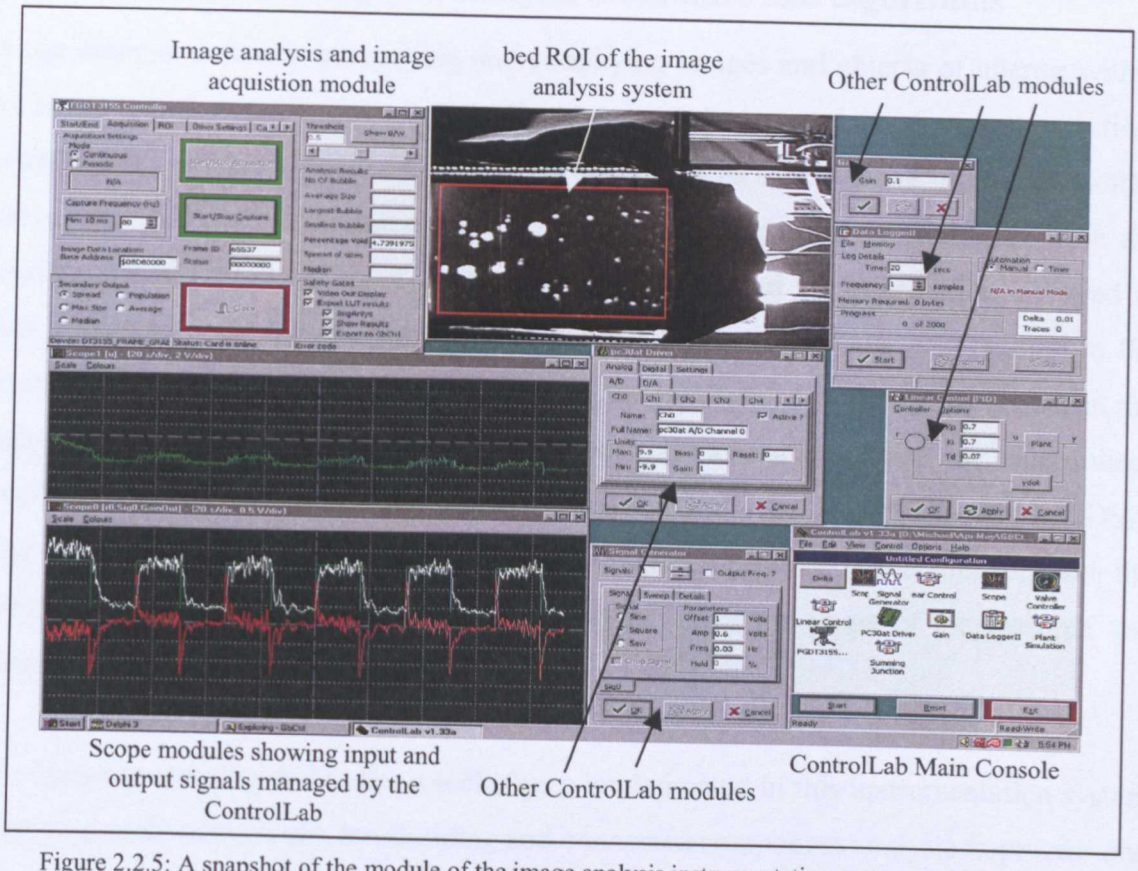

Figure 2.2.5: A snapshot of the module of the image analysis instrumentation system operating in the ControlLab platform.

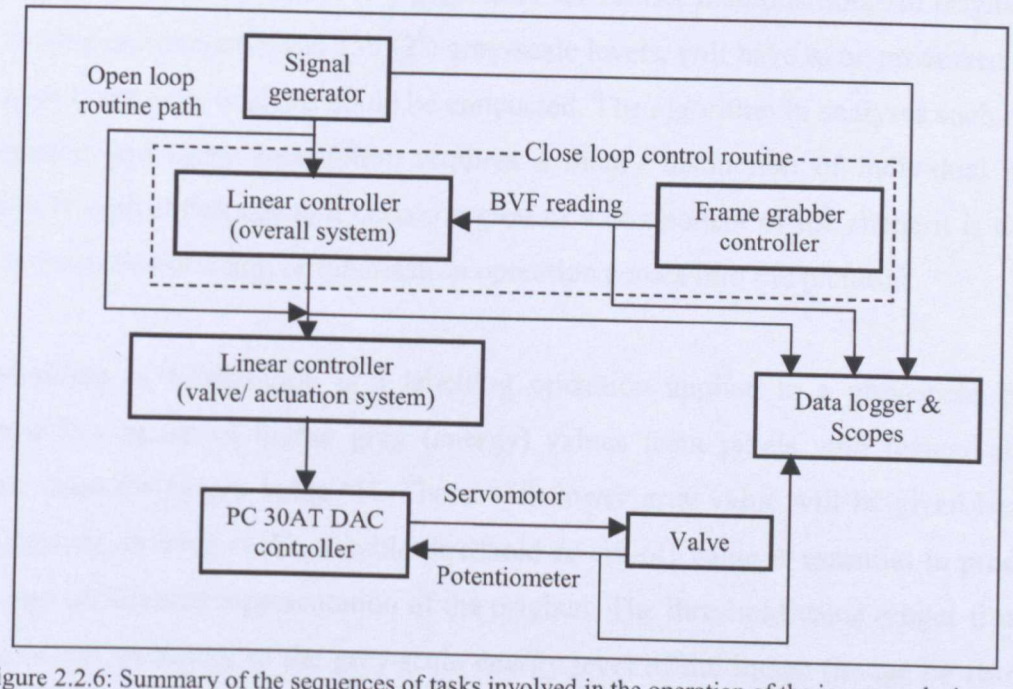

Figure 2.2.6: Summary of the sequences of tasks involved in the operation of the image analysis system.

2.2.5 Image processing and analysis mechanics and algorithms

Image analysis concerns quantifying and classifying images and objects of interest within an image under interrogation. Principally, image analysis consists of image capturing, segmentation, object detection, measurements and analysis in respective order and is often carried out iteratively after some form of image processing operations. Images from the source, once digitised are not susceptible to degradation and the information is stored in both spatial (pixels) and energy (grey levels) forms. Image analysis was applied to the acquired images of the bubbling bed to interrogate the changes of certain parameter in the images with time, correlating it to the corresponding behaviour of the bed that caused these changes. Ideally for high-speed analysis, dedicated digital signal processing (DSP) hardware would be programmed to execute the required analysis procedures and free the computer to perform other tasks. However, this is out of the scope of the research and hence not undertaken in the course of the work.

The image processing and analysis techniques implemented in this instrumentation system used grey-scale conversion, thresholding and connected component analysis to process and analyse the images. Grey-scale conversion involved converting certain number of precision level of energy information to another. Often in image analysis, images need to be in a 1-bit (binary black, '1' or white, '0') grey-scale for further manipulation. An original image say, in 8-bit monochrome has 256 (2^8) grey-scale levels, will have to be processed into a 1-bit image before any analysis could be conducted. The algorithm in analyses such as region segregation and shape recognition requires a binary distinction of individual pixels to identify if a pixel belongs to a certain region or a component of the shape it is detecting. This is when thresholding or binarisation operation comes into the picture.

Thresholding or binarisation is a labelling operation applied to a grey-scale image. It distinguishes pixels of higher grey (energy) values from pixels with lower values and assigns them the binary value '1'. Those with lower grey value will be given binary '0'. The decision on what is the suitable threshold or cut-off value is essential in producing a good and undistorted representation of the original. The threshold value ranges from 0 to 1 acting as the multiplier to the grey-scale energy level of the image (image bit resolution), the product of which will be compared with the pixels in the image to determine their binarised value ('0' or '1'). *Figure 2.2.7* shows the product of binarisation of the original

acquired image with different threshold values. The best conversion was obtained with a threshold value of 0.5 (thresholding at 50% of the grey-scale 256 levels). However, in some cases adjustment to the chosen threshold value had to be made depending on the illumination level. The criterion for the choice of threshold was based on obtaining the best distinction of true bubble voids from the emulsion phase, particularly at the edges of bubbles.

original image

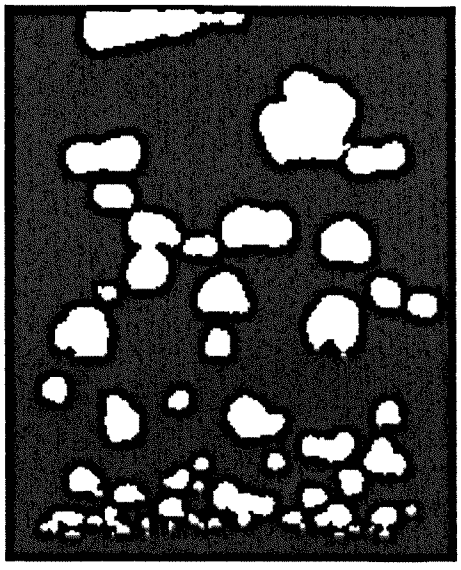

1-bit image: 0.1 thresholding

1-bit image: 0.5 thresholding

1-bit image: 0.8 thresholding

Figure 2.2.7: Snapshot of the bubbling bed as acquired by the image analysis system and the resulting 1-bit images after the binarisation procedure. Images not to scale; actual sizes are 696 pixels (≈655 mm) height x 532 pixels (≈500 mm) width. At threshold of 0.1, the bubbles appear larger and smeared. The distinction of their boundaries is also inaccurate. At threshold of 0.8, the bubbles are smaller while some smaller ones are discounted in the 1-bit image. Threshold at 0.5 is shown to produce the best conversion to 1-bit image.

The developed instrumentation system converted the streaming of monochrome 8-bit raw images into 1-bit processed image data. The threshold value was selected to provide a good distinction between the emulsion phase and the bubble voids with close attention placed on determining the border between the two phases. A range of threshold values was tested for different fluidisation condition to determine the best appropriate value. Ultimately a suitable threshold value has to be applied to a wide range of fluidisation states without compromising the integrity of the task carried out. The constant value of a chosen threshold was shown to work well for the range of freely bubbling regime considered by consistently delivering the desired conversion to 1-bit images.

Connected component analysis of a binary image involves the connected component labelling of the binary value 1 pixels and measuring of the properties of the resulting component regions and some decision-making. All the pixels of an image that have the binary value of 1 and are connected to each other by some path of pixels also with the binary value of 1 are given a unique identifying labelling tag. The label identifies a potential object region. The same applies if the binary value of 0 is being considered otherwise. This operation is carried out by a connected component operator. In short, connected component labelling is a grouping operation. Image analysis often involves processing and converting a pixel from pixel unit to another pixel unit. However, the connected component labelling transforms the image unit from a pixel to a region. A pixel normally has 3 properties: its position, grey-scale and brightness level. A region inherits more properties such as shape, size and other statistical properties: grey-scale and brightness levels of the pixels within that region.

The connected component labelling algorithm deals with grouping all the pixels of the same region and tagging them accordingly. Throughout the years, many algorithms have been developed to carry out such a task for many applications, namely for computer and machine vision systems. Examples could be found in Ronse & Divijver (1984) and Mussio & Padula (1985). The connected component labelling technique is widely used in many industrial and research applications with images often being of several small objects with contrasting background. Examples include finding macroscopic cracks or scratches and dents on surfaces or finding electronic components on printed circuit boards.

The speed at which these operations are carried out varies, but most often a fast or real-time analysis is required. All the algorithms process a row of the image at a time and assign new tag label to the first pixel of each component and attempt to propagate the label of a pixel to its appropriate neighbours. The method at which this propagation is carried out depends on the algorithm.

For this work, a combination of an Iterative and Classical Algorithm was chosen, as they are straightforward to programme and interpret. The Iterative Algorithm is a natural extension for Single Instruction Multiple Data (SIMD) parallel processing (Manohar & Ramapriyan, 1989). The Classical Algorithm is a connected component algorithm for graphs, described in Rosenfeld & Pfaltz (1966). This combined algorithm makes three passes through the image but requires a large global table (matrix array) for recording equivalences, which is not a problem in modern day computers. The first pass assigns each pixel to a unique label. The two remaining passes involve top-down and bottom-up (or left-right) scanning of the image. Top-down scanning initiates the label propagation throughout the image and the bottom-up scanning finishes up the propagation missed by the top-down scan.

This operation proved to be quite computationally intensive but is manageable by current modern computers. The computation time depends on the size of the image under investigation. Therefore, the larger the image size, the longer the computation time. For example, when carrying out the algorithm to calculate bubble population and their respective sizes, the image analysis system sampling rate reduced to a minimum of approximately 12.5 Hz when used to acquire, process and analyse a roughly 300x200 pixel image with ControlLab running on a Pentium III, 766 MHz PC. A compromise has to be reached for an optimum operating setting or condition for this task. As the whole image will not so often be of interest in the analysis, a user manageable Region Of Interest (ROI) setting can be defined. This will also help manage the intensity of computation required of the computer.

Generally in a connected component labelling operation, two binary value 1 pixels, a and b are considered to belong to the same region 'C', if there is a sequence of other binary value 1 pixels (say, $a_0, a_1, \ldots, a_n$) of 'C' where $a_0 = a$ and $a_n = b$, and a_i is a neighbour to a_{i-1} for ($i = 1, \ldots n$). Hence, the definition of a connected component depends on the definition of

neighbour. When the north, east, south and west neighbours of a pixel are considered to be part of its neighbourhood, then the resulting region is 4-connected. When the north, north-east, east, south-east, south, south-west, west and north-west neighbours are considered, this is the 8-connected region. *Figure 2.2.8* shows the definition of 4 and 8 connectivity neighbours around an element of interest, marked with 'X', through which different regions could result.

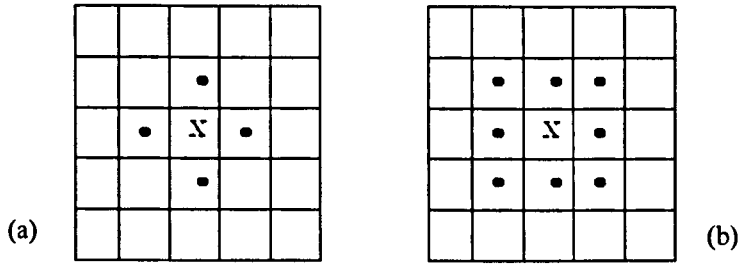

Figure 2.2.8: (a) the 4 connectivity region and b) the 8-connectivity region, based around the centre element, marked 'X'.

(a)

0	1	1	0	1	0	0
0	1	1	0	1	0	1
0	1	1	0	1	0	1
1	0	0	0	1	1	0
1	1	0	0	0	0	0
0	0	1	1	1	1	0
0	1	1	1	0	0	0

(b)

0	1	1	0	4	0	0
0	1	1	0	4	0	5
0	1	1	0	4	0	5
2	0	0	0	4	4	0
2	2	0	0	0	0	0
0	0	3	3	3	3	0
0	3	3	3	0	0	0

(c)

0	1	1	0	2	0	0
0	1	1	0	2	0	2
0	1	1	0	2	0	2
1	0	0	0	2	2	0
1	1	0	0	0	0	0
0	0	1	1	1	1	0
0	1	1	1	0	0	0

Figure 2.2.9: The different regions that could possibly be obtained from the original 1 bit image data in (a) with a 4-connectivity search as in (b) and with an 8-connectivity search as in (c).

Based on the requirement and desired outcome from an analysis, different connectivity complexity is used. For this study, the 8-connectivity neighbourhood search was used, to accurately detect the complex region and boundaries of the bubble void and its interface with the emulsion phase. Sets of diagrams in *Figure 2.2.9* illustrate the difference between

the regions obtained via 4 and 8 connectivity neighbourhood search. With a 4-connectivity neighbourhood search, the diagram in *Figure 2.2.9(b)* was obtained from the original 1-bit image data in *Figure 2.2.9(a)*. Diagram *Figure 2.2.9(c)* shows the regions from an 8-connectivity search, which will result in much fewer but larger regions than if the former was used. The remaining portion of a connected component analysis involves counting the number of regions found and statistically classifying these regions.

The frame grabber and image analysis instrumentation module in ControlLab was programmed to perform all the above-mentioned tasks, executing them to real-time rate and with precision. Then, calibration of the Region Of Interest, ROI has to be carried out on the image of the bed to be analysed. The acquired images from the video camera were first stored in the computer memory buffer where the image data was subsequently retrieved for processing and then analysis. The results of the analysis are transferred either to another module for further manipulation such as for control purposes, for displaying on scopes or for storing in data file for later use. Shown in *Figure 2.2.10* is the operation flow chart of the frame grabber and image analysis module as per acquisition cycle, including initiation and termination of use.

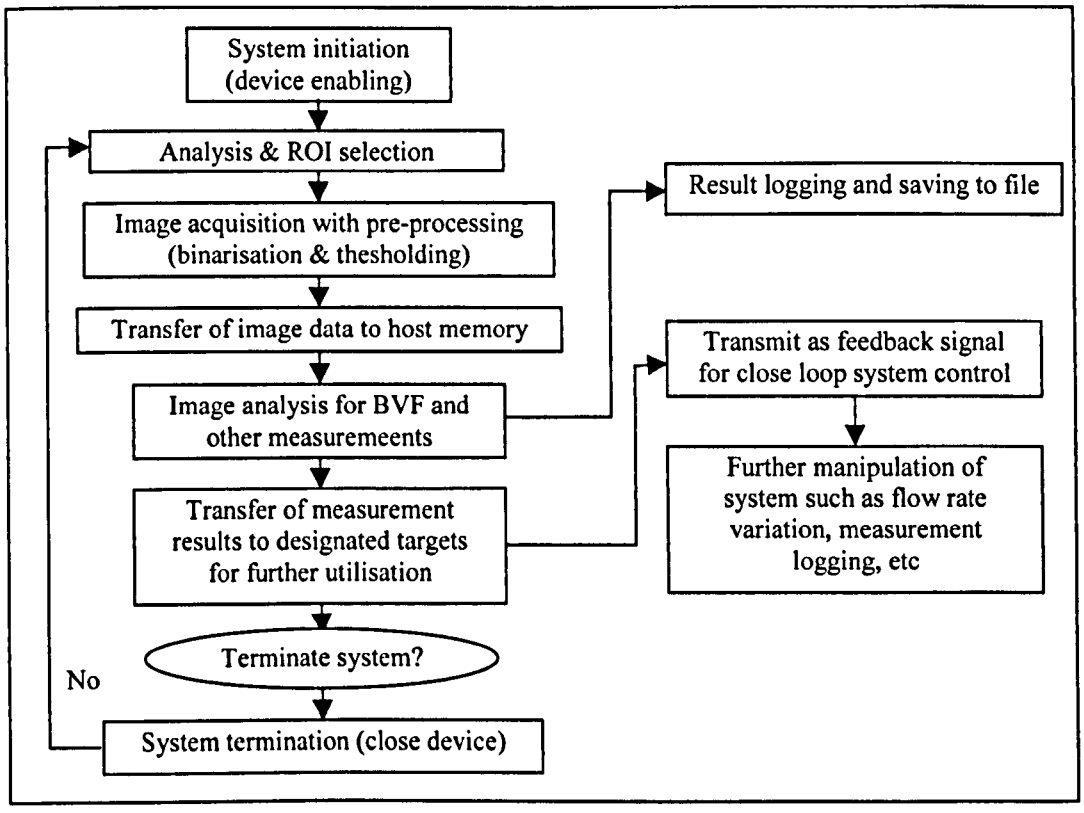

Figure 2.2.10: The operation flow chart of the image analysis instrumentation system module.

2.3 A parameter for characterising the dynamical features of the bubbling process

The capabilities of the instrumentation system via image analysis techniques have allowed the various parameters associated with the existence of bubbles in a bubbling fluidised bed to be investigated. The explicit measurement of the properties of bubbles directly through the transparent planar bed provides an analytical view of how the presence of bubbles qualitatively and quantitatively affect the overall behaviour of the fluidised bed, such as its fluidisation quality.

2.3.1 Parameter selection and discussion

In order to effectively characterise the bubbling process globally, as well as to capture the dynamical behaviour of the bed, a suitable parameter had to be determined. The parameter should explicitly and effectively correspond to the state of the process it was measured at. Its measurements should also be relatively simple to obtain and must be consistent over a range of process conditions. Furthermore, according to Brown & Brue (2001), the minimum sampling frequency required to appropriately investigate the condition of the fluidisation process should be more than approximately 20 Hz to be capable of capturing all the dynamical features and to avoid anti-aliasing of fast dynamics. They showed from their experiments (Brown & Brue, 2001) with pressure measurements that there are no differences in high-frequency spectral content obtained with the sampling rates between 20 and 100 Hz.

Makkawi & Wright (2002b) indicated in their work with electrical capacitance tomography measurements that two important measurement criteria need to be considered and properly chosen while obtaining measurements based on the type of fluidised system. They outlined that optimum recording span for reliable analysis of the solid-gas hydrodynamics ranges between 20 to 100s while the acquisition rate should range between 20 to 100 Hz. The combination of acquisition rate and recording span should be based on the type of fluidised system that is being measured.

The image analysis system has a limited acquisition rate of 25Hz thus requiring that any measurement made to investigate the dynamics of the fluidised system should span for an adequate time period. In *Chapter 3*, *Chapter 4* and *Chapter 5*, measurements were carried out for significantly long time period, extensively more than that recommended by Makkawi and Wright (2002b), ranging between 20 to 60 minutes typically. This compensates for the acquisition rate limitation (25 Hz) of the image analysis system and should pick up all the dynamics of the process including very slow ones.

The obvious parameter obtainable from the system was the measure of the proportion of the bed under investigation occupied by voids associated with bubbles. This measurement was termed the Bubble Void Fraction or BVF. Its acquisition was very easy involving the calculation of the ratio of bright areas in the images associated with bubbles to the total area of interest in the bed. The rate of acquisition was only limited by the image acquisition devices (frame grabber and digital video camera) at 25 Hz. *Figure 2.3.1* shows an example of the BVF measurement time series obtained from a freely bubbling bed fluidised at steady state, 12.8 mm/s above incipient condition.

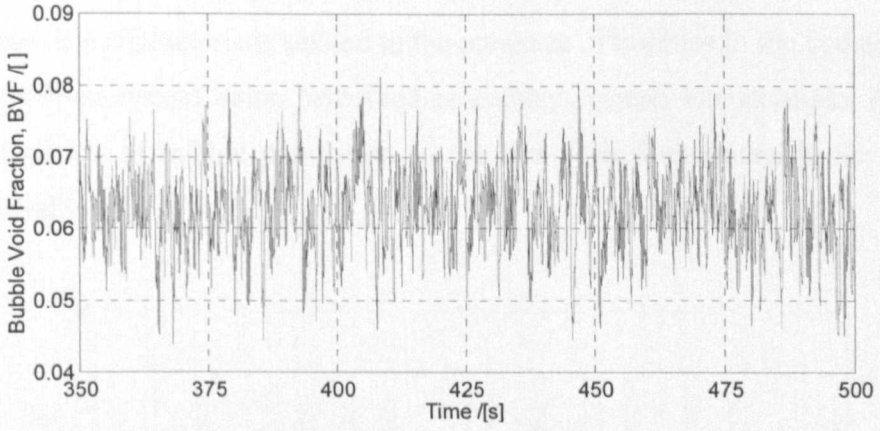

Figure 2.3.1: The BVF time series of an example bubbling bed operation fluidised at a steady state flow rate of 12.8 mm/s above incipient condition.

As BVF is a measure of the proportion of the bed occupied by bubble voids, it has a direct relation to the number of bubbles or packets of excess gas in the bed corresponding to the flow rate above the incipient state, in which there would be no bubbles. By measuring this parameter, many aspects of the bubbles in the bed can be interrogated. First, the magnitude of BVF in the bed has direct relationship to the magnitude of gas in excess introduced into the bed. Secondly, the changes experienced by this parameter with time represent how the

bubble behaviour affects the condition and the overall dynamical behaviour of the bed, which in turn affects the BVF measurement.

The fluctuations in the signal as seen in *Figure 2.3.1* were mainly due to bubble coalescence and division, formation and departure from the bed. Experimentally observed bubble coalescence and division were seen to cause fluctuations in the BVF as coalescence and division did not necessarily conserve the original total void area detectable on the planar bed by the image system. The new bubble after coalescence was larger than the total volume of the original pair while there is a net decrease in bubble volume when a bubble broke-up. There have been similar reports, elsewhere (Grace & Venta, 1973) where expansion of up to 20% and a qualitatively similarity in net volume reduction were observed. The formation of bubbles would increase the BVF value with simultaneously the departure of bubbles reduces the BVF at the same instance. These sorts of sequences in events were indefinitely reflected in the readings by the presence of the fluctuations.

Therefore the BVF measurement is directly associated with the behaviour of bubbles in the bed during the freely bubbling regime of the fluidisation process. The fluctuation in the BVF is an intrinsic characteristic related to the presence of bubbles in the bed and therefore led to the fluidised system being perceived as a noisy system. For example, *Figure 2.3.2* shows the measure of bubble population in the bed with fluctuations in the time series clearly observable.

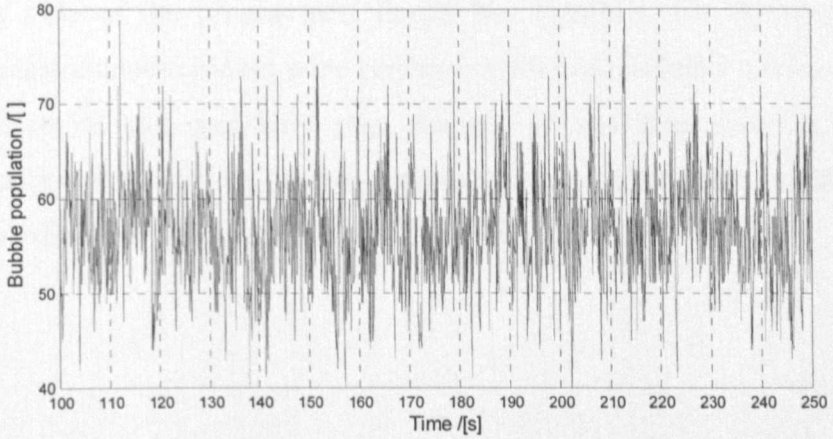

Figure 2.3.2: The time series of bubble population of an example bubbling bed operation fluidised at steady state superficial flow rate of 12.8 mm/s above incipient condition.

The sampling frequency criterion of above 20 Hz for a reliable sampling of the process dynamics suggested by Brown & Brue (2001) and Makkawi & Wright (2002b) further implied that the acquisition of parameters requiring the connected component analysis was not suitable primarily because it could not satisfy this criterion. This meant that several other parameters that were considered, such as the measurement of bubble population and average and maximum bubble size, were therefore unsuitable.

Given what it was able to offer towards the characterisation of the bubbling process, the Bubble Void Fraction, BVF measurement was used. It has been demonstrated that through the means of imaging technique it is possible to appropriately acquire measurements directly linked to activities of bubbles within the planar bed that could offer pointers as to how these bubbles would affect the behaviour of the bed. Tests were subsequently carried out to benchmark the performance and characterise the BVF measurements and are detailed in *Section 2.3.2*.

2.3.2 Signal benchmarking and characterisation

Before the BVF measurement could be competently used, it had to be benchmarked and characterised. Benchmarking of the signal was done to determine the capability and limits of the measurement in detecting changes in the state of the bed, so that it can be used reliably and does not produce ambiguous results. Out of the operating range of the measurement, any results obtained cannot be used confidently to identify the corresponding state of the process and should be discarded. For this purpose, signal benchmarking and characterisation were carried out for two different modes of operation: with steady flow of gas, and with step changes of gas flow into the bed. Signal characterisation involves relating the measurements made to the corresponding source or cause that determines the trend or value in the signal.

2.3.2.1 Steady flow of gas into the bed

The measurement of BVF for the steady state flow of gas into the fluidised bed was carried out over a period of time for several constant flow rates above the quiescent condition. The sensitivity and effectiveness of the measurement in detecting the changes in the content of excess gas in the bed could be assessed in this way, allowing a relationship between BVF and gas flow into the bed to be established. A look-up table of BVF and gas flow was used to provide a mapping of the BVF reading over the whole range of the bubble regime.

The fluctuations in the signal were caused by changes in the proportion of the bubble void that could be seen appearing in the emulsion phase when the bubbles were sufficiently large to span the depth of the bed, allowing illumination through from the back. This was the reason some bubbles were seen to disappear and reappear, although this observation of bubbles was also due to the short-circuiting of gas from a bubble to another higher up in the bed or when bubble void area becomes hidden in the particulate phase. These are considered as minute changes in the measurement and not macroscopic changes experienced by the measurement when the flow of gas into the bed changes.

The results for this are shown in *Figure 2.3.3*. Values shown amidst the graph are the mean of BVF at each flow condition. The BVF measurement resembles a stair-like graph corresponding to step increase in flow into the bed. The changes in the time series with step increment of flow rate indicate that the measure of BVF was effective and robust in its measurement for a range of bubbling condition, despite the presence of fluctuations in the signal. The 95% confidence limits are also shown on the graph for approximately 2.5 s of BVF time series for different bed conditions.

However, the reliability of the measurement gradually deteriorated as the BVF standard deviation increased with flow rate. This is due to the gradually growing fluctuation magnitude caused by the presence of large bubbles and their departure from the bed that also masks out any non bubbling phase associated fluctuations in the BVF such as those from light source fluctuation and hardware electronic noise. These fluctuations are comparatively minute (by several orders of magnitude). Small fluctuations in flow rate (say ± 2.56 mm/s superficial flow) during bubbling were experimentally observed not to cause noticeable change to the state of the bed and the BVF. As the mean BVF sometimes

varied for different repeated measurements made for the same bed condition, the measurement was conventionally taken relative to a datum, in this case, U_{mb}. In this way, the BVF values will correspond to flow supply relative to the datum, therefore minimising (to within the 95% confidence limits of the BVF measurement) the effect of fluctuations of the mean BVF due to U_{mb} fluctuation.

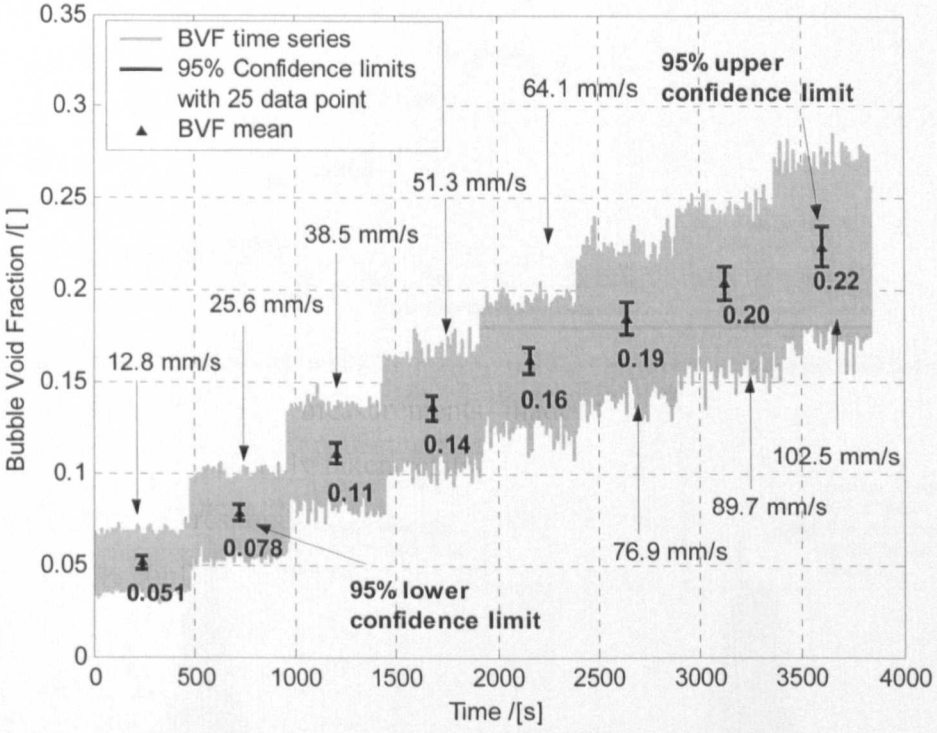

Figure 2.3.3: The results from the benchmarking of the BVF time series over a range of steady state flow rate above quiescent fluidisation. Step-like changes with step increment of flow rate indicate that the parameter could distinctly infer changes in flow rate. The mean of the presented BVF time series (~12,000 data points at 10 Hz sampling) for each flow condition shown amidst the graph describes the increasing trend of the BVF with flow rate. The 95% confidence limits are also shown for a 25 data point BVF time series, which is reasonably consistent for different sets of BVF data for similar bed condition.

Figure 2.3.4 shows the standard deviation of the BVF measurement taken over different flow rates above incipient condition for a period of time. *Figure 2.3.5* shows the histogram of the BVF measurement for two extremes of steady gas flow rates. The spread of the BVF measurements could be approximated well by a normal distribution curve characterised by the distinct maxima peaks at the mean and the symmetrical bell-shaped BVF histogram for each flow condition. With increase in flow, the maxima of the BVF histogram reduced gradually as the distribution of the BVF spread wider complemented by the increase in the standard deviation.

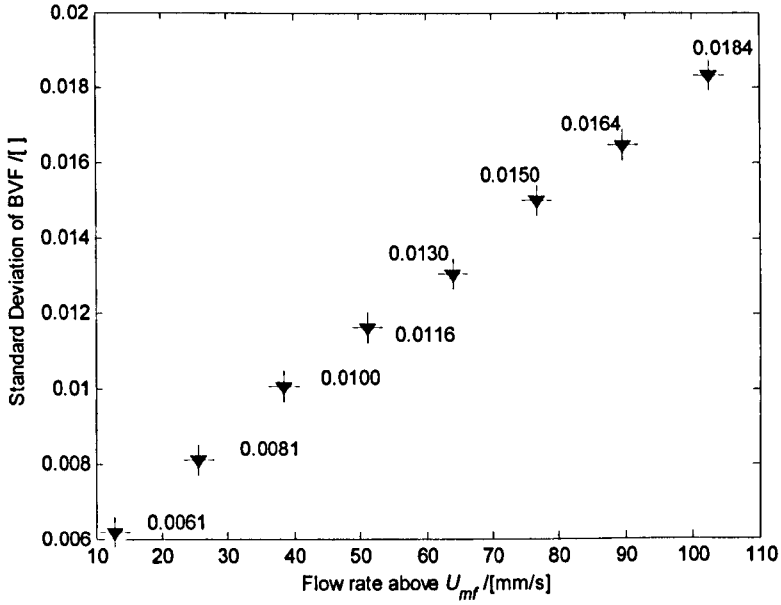

Figure 2.3.4: Standard deviation of BVF for different flow rates above incipient fluidisation.

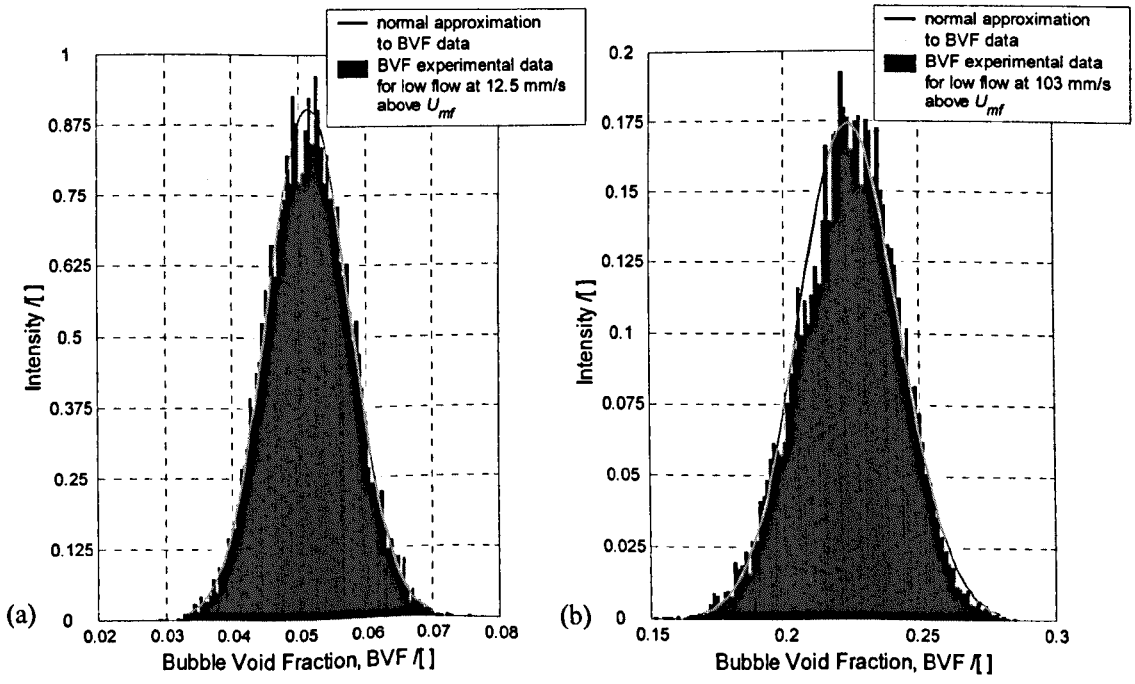

Figure 2.3.5: The histogram of the BVF measurement and the corresponding normal distribution approximation at (a) 12.5 mm/s and (b) 103 mm/s superficial gas flow above U_{mf} with standard deviation of 0.0061 and 0.0184 respectively.

Figure 2.3.6 shows the distribution of the BVF for a range of steady superficial gas flow from 12.5 mm/s to 103 mm/s to demonstrate the trend of spread in BVF measurement with flow.

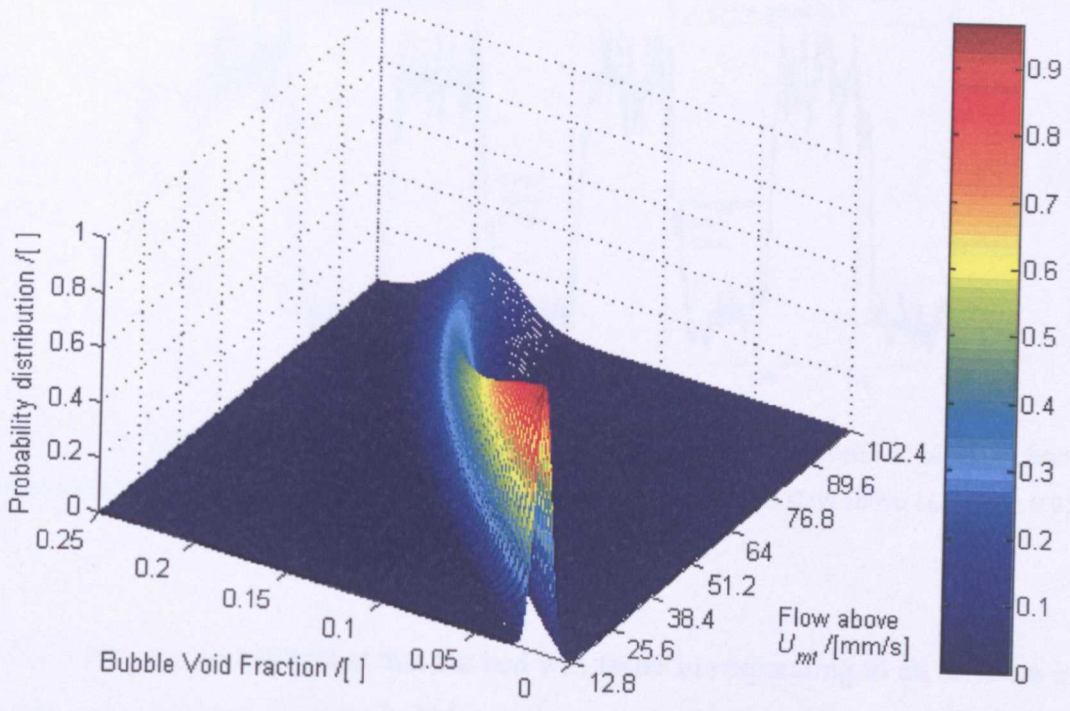

Figure 2.3.6: The figure shows the three dimensional contour plot of BVF against the amount of flow into the bed above U_{mf} with a normal distribution approximation to the spread in measurement of BVF.

2.3.2.2 *Step changes in flow of gas into the bed*

Some of the dynamical features in the bed, such as the transient response of the bed and other features appearing only during dynamic transition in bubbling condition, could only be observed by applying open-loop control to the bed. By varying the flow of gas into the bed at desired manner, usually in the form of a repetitive step change in flow of gas at a range of excitation frequency, the transient effects on the bed could be revealed and the response of the bed characterised by the BVF measurement could be seen in *Figure 2.3.7* and *Figure 2.3.8*. The BVF responded well to the changes in flow demand exhibiting several characteristic features. The most obvious feature as could be observed in *Figure 2.3.7* is the persistent noise or fluctuation in the signal, which is of higher magnitude at higher flow than when the flow is lower.

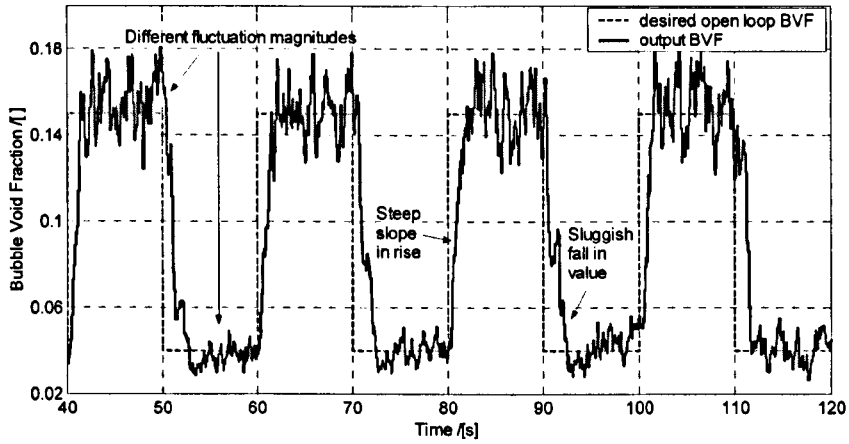

Figure 2.3.7: A typical open-loop signal from the image analysis system with several of its salient features. The graph is for the bed fluidised at 12.8 mm/s to 64.1 mm/s superficial gas flow above U_{mf} with a 0.05 Hz step excitation in the flow supply.

The BVF features also indicated that the bed was faster in responding to an increase in gas flow than to a decrease because bubbles will persist in the bed after the reduction of the flow. There was a transition period after the flow reduction during which the remaining bubbles rose to the bed freeboard before the BVF value reached a steady state condition. A rapid introduction of gas into the bed would quickly generate the corresponding amount of bubbles and sharply increase the BVF. The skewness or hysteresis in the signal due to these phenomena is an example of the bed's non-linear behaviour. Overall, the bed responded slowly to the changes in flow rate compared to the frequency of the noise in its signal as bubbles already present in the bed persist when the flow rate is changed, so the high frequency components (approximately above 0.6 Hz) of the system contribute little to the overall dynamics.

Occasionally, depending on the instantaneous condition of the bed response, undershoot and overshoot in BVF values may occur as shown in the *Figure 2.3.8*. There is also an observable amount of time delay present in the signal whenever the flow changes. The bed only responded a fraction of time after the changes to the flow has been made. Despite being a slow system, the time delay after which the bed responded to change was substantial and has implications when a control system is to be devised around this characteristic behaviour. This will be discussed in *Chapter 8*.

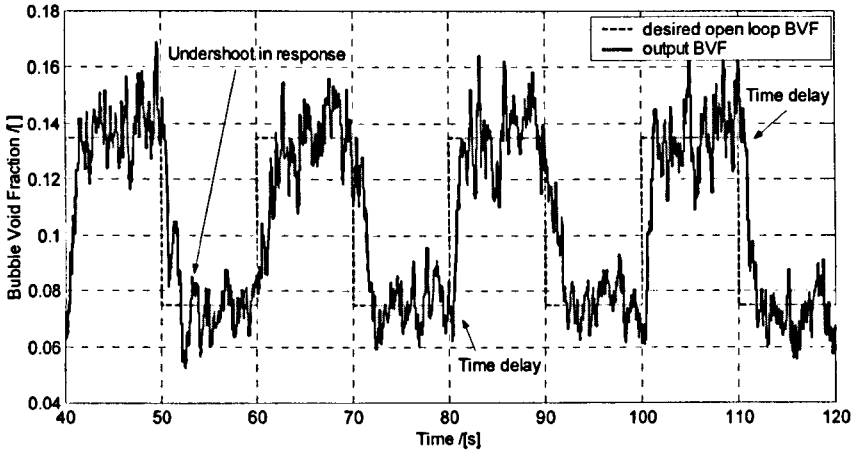

Figure 2.3.8: Figure shows the occasional undershoot and overshoot and presence of time delay in the output signal. The graph is for the bed fluidised at 25.6 mm/s to 51.3 mm/s superficial gas flow above U_{mf} with a 0.05 Hz step excitation in the flow supply.

2.3.3 Experimental errors and image system accuracy benchmarking

Measurement errors are inevitable in any experimental set up. The errors suffered in this system were mainly due to electrical and electronic noise such as those inherent in the frame grabber, video camera as well as the D/C converter card. Noise is unwanted and degrades the quality of signals and data providing meaningless information about the trend in the signal. The noise levels in these devices were very low magnitude (quantum or resolution level of the electronics of the device) disturbances compared to the magnitude of changes in the measurements, therefore negligible in the measurement. The fluctuations in the BVF measurement intrinsic in the system (mentioned earlier in *Section 2.3.1*) were caused by the nature of the measured parameter. Therefore, this fluctuation was not exactly categorised as a typical noise disturbance. However, the fluidised system was considered a noisy system based on this feature with the intention to facilitate the selection of the appropriate technique to study and control the system.

As the measure of BVF in the bed by the image system was also subject to various sources of disturbance, the accuracy of the system must be benchmarked, carried out through several tests. This included the measure of other properties of bubbles, such as bubble size. Since each video pixel contained by default non-zero values even while acquiring a completely dark image, the threshold of 0.1 imposed onto the raw image's 256 grey levels

during the binarisation process gave a benchmark accuracy of up to ±0.00005 for the measure of BVF for this case. Above that threshold value, the BVF is constant at 0 for the same image.

The second test involved measuring the BVF of an acquired image of dark surroundings with a light source (fluorescent backlighting for the planar bed) beaming through a circular opening. The distance between object and camera was approximately 700 mm. The first part of the test measured the BVF at this distance with different image binarisation threshold values of 0.45, 0.5 and 0.55, where repeated measurements were carried out after a time interval to check consistency. This was to evaluate the sensitivity and accuracy as well as the time resolution of the BVF measurement.

The results in *Table 2.3.1* show the statistical characteristics of the BVF measurements at different threshold values. The time series of each BVF measurement contained fluctuations about a mean. It was pointed out in *Section 2.2.5* that the threshold value of 0.5 was most appropriate in most cases in distinguishing areas of bubble voids from the emulsion phase. With an accuracy of ±0.0002, slight deviations of the threshold choice of value did not affect the BVF measure significantly. However, extreme deviations of threshold value (0.3 and 0.7) resulted in significantly different BVF measurements in the test as seen in the BVF means. With a threshold of 0.3, the binarisation of the image resulted in smeared edges between bright and dark region due to the penumbra effect of the light source in the original image. At threshold of 0.7, the circular bright area was smaller in the binarised image, of which, along with the former were inaccurate measurements.

Threshold	Mean	Std Dev	Max	Min	Max-Min	Accuracy
0.30	0.163	30.16e-5	0.165	0.162	0.002964	±0.0015
0.45	0.143	6.07e-5	0.143	0.143	0.000456	±0.0002
0.50	0.142	4.79e-5	0.142	0.142	0.000403	±0.0002
0.55	0.141	4.42e-5	0.142	0.141	0.000368	±0.0002
0.70	0.137	4.01e-5	0.137	0.137	0.000316	±0.0002

Table 2.3.1: A summary of the results from the benchmarking tests carried out on the BVF measurement by the image system.

In the second part of the test, a similar image was acquired from a closer range, approximately 50% of the distance (~ 350 mm) in the first test, and the accuracy of the measurement at each threshold remained at ±0.0002. Time resolution or measurement consistency test showed that the BVF measurement drifted about the mean due to minute variations of intensity of the fluorescent backlighting, but was acceptable given the obtained accuracy. The variations in the light-source intensity were also thought to be responsible in causing fluctuations in the BVF measurements in the tests.

Any form of image distortion due to lens effect in the video camera was also inspected and confidence could be placed where locating the camera on any position of the vertical plane parallel with the planar bed would not cause detectable distortion to the acquired image within the ROI. The test results showed that the image system could be reliably used to measure the properties of bubbles in the planar bed with satisfactory accuracy and consistency.

With the use of the planar bed, certain bubbles with sizes close to the bed thickness (13 mm) will not be accurately measured. When a bubble is smaller than the bed thickness, it does not properly span across the bed thickness to allow proper detection by the image analysis system. Those that are slightly larger will span the bed thickness but would still give an inaccurate indication of size when measured with the image analysis technique described. These bubbles are usually ones close to the distributor although some will manage to rise up the rest of the bed height in isolation and are seen as bubbles that are disappearing and reappearing in the emulsion phase. As this error only occurs when bubbles are reasonably small, their effects on the overall behaviour of the bed are considered small in terms of the dynamical analyses that were involved in the dissertation and will be addressed in the relevant chapters. These small bubbles occupy relatively small portion of the bed (bottom half) and their activities and presence cause only small variations in the BVF of the bed. Therefore, no dedicated corrections were done to compensate for the errors in measurement by the image analysis in this respect.

2.4 Conclusion

A robust and consistent means to characterise the bubbling state of a fluidised system was found in the instrumentation using image analysis techniques. This was implemented on a planar bed with the aim of understanding the bubbling behaviour in the bed in its most explicit and simple form before extension into a more complicated scenario. The development of the instrumentation system to complement the existing experimental rig has been fully described; assessments were then carried out and the Bubble Void Fraction, BVF, was chosen to be the parameter that could effectively characterise the state of the bed. Several other parameters were considered such as the measurement of bubble population, and bubble average and maximum size. However, these parameters were unsuitable mainly due to the problem of down-sampling required in the image analysis system to obtain these parameter making it to fall below the minimum acquisition rate recommended in the literature for reliable measurements.

The BVF measurement has been characterised and the salient features present in the signal at various operation conditions of the bed have been identified. These features become important when the dynamical response behaviour of the bed needs to be understood and a controller is built around these characteristics in order to design a suitable strategy. As it is intrinsically noisy with the presence of time delay and interlaced with non-linear features, a fluidised bed is thought to be a difficult and complex system. However, progress has been made and continues to point towards a better understanding of the system.

The work in this chapter is the milestone to any further work along the line of characterising bubbles as the fundamental determinant of the behaviour of a bubbling fluidised bed in this dissertation. Further studies would be to analyse the data obtained from the system developed here and to develop theories and models based on the basic understanding of the physical behaviour of the bed. The system will from this point forward be the key instrument in the rest of the study of the process. Optimisation and modifications are carried out from time to time and on needed basis to cater to custom requirement of the research; these are detailed in the relevant chapters in the dissertation.

Chapter 3

Assessment of bed fluidisation quality

3.1 Introduction

The fluidisation quality of a bed is highly dependent on the distribution of bubbles and their physical properties in the bed. Ideally, the population of bubbles in the bed must be smallish in size and homogeneously occupy the column of the bed for there to be a good quality of fluidisation (*Chapter 1*). Hence, the understanding of how and why bubbles are distributed in certain ways in the bed as well as what determines the size distribution of bubbles are crucial. For this, a reliable measurement plays the important role of providing the data for the studies of bubbles associated with the quality of the bed. This could be found in the statistical measurements of the bubble size population in the bed and the bubble spatial distribution as well as localised bubble void. The techniques of analysis employed in the study in the chapter were inspired by the work of Werther & Molerus (1973a, 1973b) and Makkawi & Wright (2002a).

3.2 Statistical measurements

The acquisition of the statistical measurements of the bubbling process required the connected component analysis in the instrumentation system (*Section 2.2.5*). This analysis provides information such as the range and distribution of bubble population and sizes in the bed at an instance over a period of time from which the largest bubbles and average bubble sizes in the bed could also be found. When fluidised at a steady state, with excess superficial gas speed of between 12.8 mm/s and 102.5 mm/s above incipient state with continuous increments of 12.8 mm/s after a period of time, the measurements taken of an

example bubbling bed produced a set of results as presented in *Figure 3.2.1* to *Figure 3.2.4.*

Figure 3.2.1 shows the bubble size histogram for different bubbling flow rates into the bed. The bubble size distribution is inherently skewed because there is always a higher population of smaller bubbles. The population distribution profile could be well approximated as a log-normal distribution. The small bubbles are bubbles produced initially at the distributor and the larger ones are artefacts of the interaction and coalescence of these smaller bubbles and are therefore of lower population count. The bubble size axis was plotted on a logarithmic scale to gain higher scaling resolution on the smaller size range while still maintaining a high upper bound of bubble sizes range on the plot.

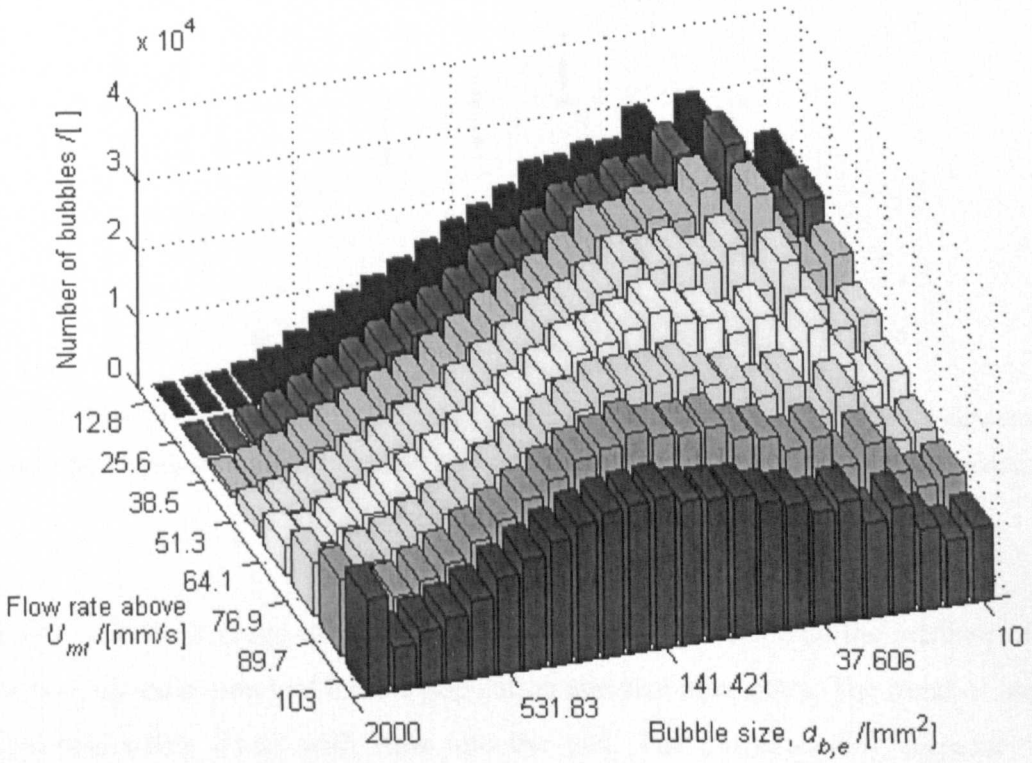

Figure 3.2.1: The histogram of bubble sizes in mm^2 in a bubbling bed fluidised at between 12.8 mm/s and 102.5 mm/s superficial flow above U_{mf} with the increment of 12.8 mm/s very 300 seconds of steady state condition.

At low gas flows, the population distribution of bubbles is skewed towards the lower bound of the size range. As the gas supply is increased, the peak of the steady state

bubbling bubble population histogram gradually shifts towards a higher bubble size value. At 103 mm/s superficial gas velocity above U_{mf}, the distribution is reasonably symmetrical, with a central bubble size of approximately 800 mm^2 ($d_{b,e}$ = 32 mm), except for an extreme peak at the larger size bound. The larger value in bubble size corresponds to an equivalent bubble diameter, $d_{b,e}$ of approximately 120 mm in the bed located at the high extreme of the histogram. The high population of bubbles of this size extreme indicates that severe coalescence occurring at this bubbling condition produced bubbles of some characteristic size, probably associated with transition to a slugging bed.

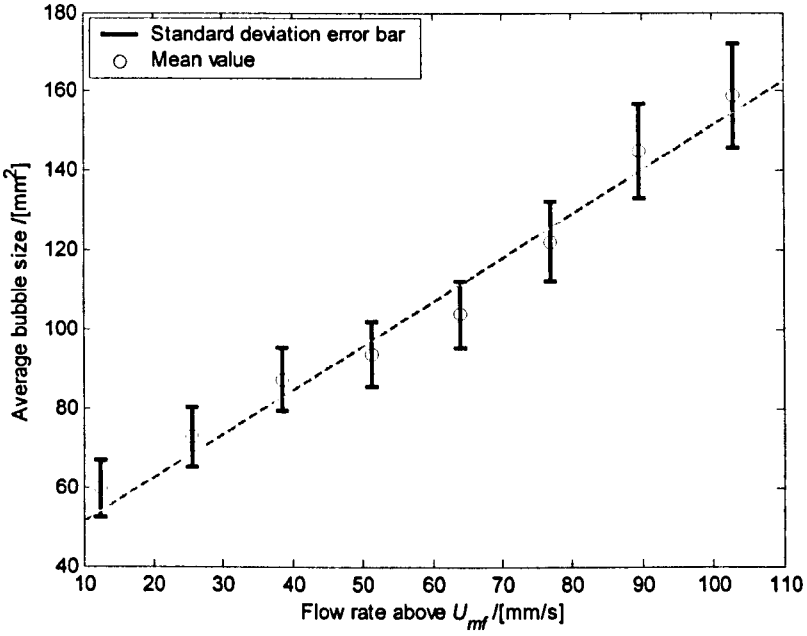

Figure 3.2.2: Time series of the average of bubble sizes in mm^2 in a bubbling bed fluidised at between 12.8 mm/s and 102.5 mm/s superficial flow above U_{mf} with the increment of 12.8 mm/s every 300 seconds in a steady state condition.

In *Figure 3.2.2,* the average of bubble sizes is shown to increase with the increase of flow into the bed, an indication that bubble population and size have risen. The trend of increase appeared reasonably linear with flow into the bed. The corresponding increase in the measure of the largest bubbles present in the bed at each flow condition also appeared approximately linear as can be seen in the graph in *Figure 3.2.3.* This was a product of severe bubble coalescence promoted by a high concentration of bubble population in the bed as more excess gas was introduced into the bed.

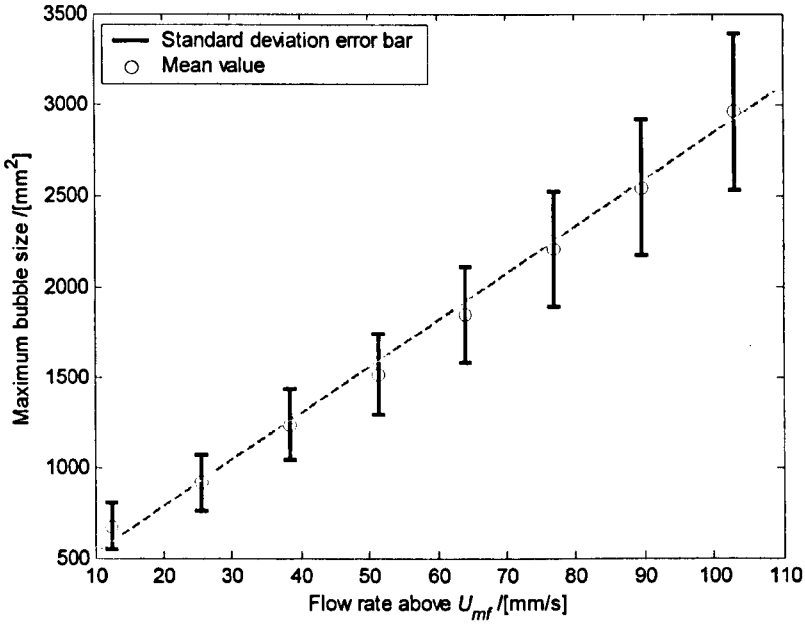

Figure 3.2.3: The time series of the maximum of bubble sizes in mm^2 in a bubbling bed fluidised at between 12.8 mm/s and 102.5 mm/s superficial flow above U_{mf} with the increment of 12.8 mm/s very 300 seconds of steady state condition.

The increase in size of bubbles and the formation of large bubbles due to coalescence have bad implications for the condition of the bed. Large bubbles formed from the vigorous coalescence of bubbles occupy large volumes in the bed column, hence promoting even more coalescence with other smaller or even large bubbles on their way up the bed. This effect reduced the number of bubbles in the bed and is therefore detrimental to the quality of the process. *Figure 3.2.4* shows the average population of bubbles in the bed with respect to the amount of flow issued. Initially above incipient condition, the bubbling bed observed an increase in bubble population with increase in gas flow. However, as more bubbles meant more coalescence in the freely bubbling bed, the population reached a peak at approximately 52 mm/s of superficial gas flow. Thereafter, the bubble population suffers a gradual decline with further introduction of gas as vigorous coalescence creates more large faster bubbles. These bubbles leaves the bed quickly and occasionally exhausting the bed of bubbles by sweeping through the bed and coalescing with other bubbles in their path, leaving few large ones while progressively the supply of bubbles is renewed at the distributor.

The statistical measurement demonstrated that the fluidisation quality during a bubbling process reaches an optimum level with excessive gas supplied above quiescent state. At

this level, bubble population is supposedly at its highest possible in the bed, exhibiting acceptable size ranges in terms of ability for effective phase mixing and heat and mass transfer. Further increase in gas flow degrades the quality of fluidisation with the generation of excessively large fast rising bubbles through coalescence that in turn vigorously plough through the bed coalescing with other bubbles in their path. The effectiveness of the bed for its intended function (e.g. heat exchange, chemical reaction) subsequently suffers.

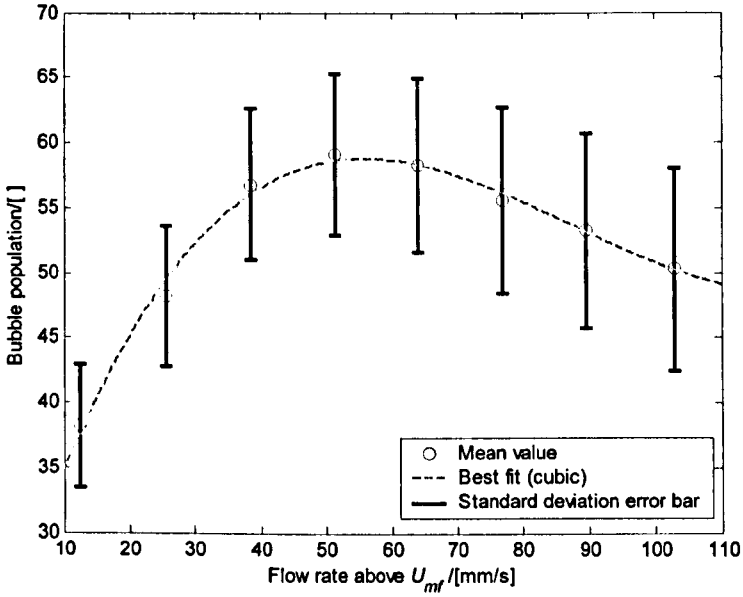

Figure 3.2.4: The average population of bubbles in the bubbling bed fluidised at between 12.8 mm/s and 102.4 mm/s superficial flow above U_{mf} with the increment of 12.8 mm/s very 300 seconds of steady state condition.

3.3 Bubble spatial distribution

The measurement of bubble spatial distribution in the bed (combination of spatial and temporal measurement) provided by the instrumentation system offered an insight into how well bubbles produced at the distributor are subsequently distributed and how they populated the operating column of the bed. This is consistent with the need to gather information on the homogeneity within the bed induced by the presence of bubbles that has direct consequences on the fluidisation quality of the process. The ability to map out the distribution profile of bubbles promotes a better understanding of how bubbles affect the

dynamical behaviour of the bed and support that already obtained about the process from previously described measurements.

Through the accumulation of pixel data from the images of the bubbling bed over a time period, the bubble spatial distribution could be determined. Consecutively acquired images were analysed to distinguish between areas occupied by bubbles or the emulsion phase and by accumulating the pixel value over time, indicate the probability that an area would be occupied by a bubble. In other words, it is similar to obtaining a time-history record of areas in the bed frequent by bubbles and producing a mapping of bubble spatial distribution profile throughout the bed. The following are examples of the bubble spatial distribution in the experimental planar bed over several steady state freely bubbling conditions. The measurement was taken over a 20 minute time period at the acquisition rate of 25 Hz.

Figure 3.3.1 shows the series of resulting contour plots of the bubble spatial distribution in the bed fluidised between 12.8 mm/s to 102.5 mm/s superficial gas flow above U_{mf} (103 mm/s) with a 12.8 mm/s increment in superficial flow velocity. It can be seen that the distribution of bubbles in the bed during bubbling is non-uniform, although upon introduction, they were spatially distributed evenly along the plane of the porous distributor plate. The distributor design is known to play a significant part in influencing how bubbles are produced and distributed. The porous distributor used in this study was shown (*Chapter 2*) to consistently produce bubbles uniformly across its length. This suggests that there is an underlying mechanism that promotes non-uniformity in bubble distribution as they gradually rise up the bed.

The profile of bubble distribution in the planar bed during freely bubbling is such that there is a pair of narrow bands of high concentrations of bubbles along either sides of the bed close to the walls near the distributor that gradually migrate inwards, spreading over the centre of the bed higher up in it. This creates an area of bubble deprivation in the bed centre near the bottom. The tapering of bubble distribution also leaves the regions close to the wall in the upper part of the bed short of presence of bubbles. Although the bubble distribution profile is observed to change with the amount of gas flow into the bed, the overall distinctive profile (two narrow bands near the bottom and a single, wide band at the upper part of the bed, of high bubble concentration regions) is preserved.

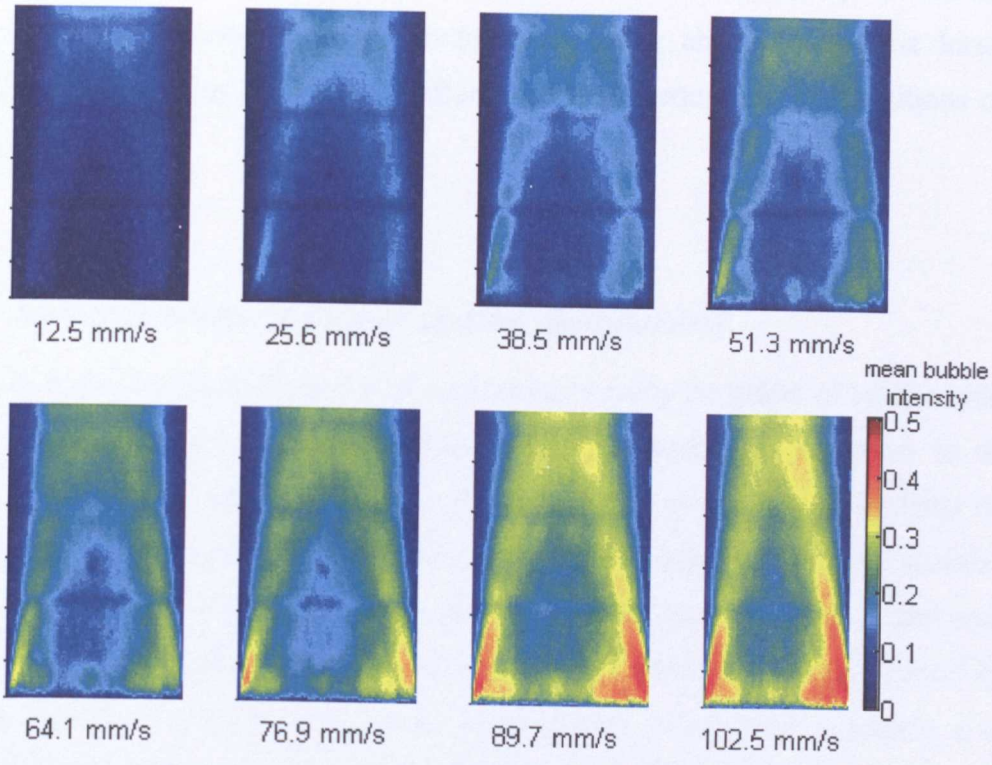

Figure 3.3.1: A series of contour plots of the bubble spatial distribution of an exemplary run of the experimental planar bed fluidised at steady state bubbling regime with excess superficial gas of 12.8 mm/s to 103 mm/s above quiescent condition with 12.8 mm/s increment in flow.

When the flow of gas into the bed is increased, the tapering becomes more pronounced with a higher concentration of bubbles at the centre of the bed occurring closer to the distributor. The narrow bands of high concentration of bubbles near either side of the walls are shorter in height as the tapering pair of bands joins up earlier in the bed. These changes in distribution profile correspond to the shifting of the bubble spatial population into primarily the bed centre column due to the rapid coalescence of bubbles caused by their high concentration, owing to the extreme of excess gas, which quickly creates large bubbles near the centre column of the bed. If the flow is increased further, bubbles would be concentrated at the centre line of the bed throughout its height, except for very close to the distributor where a uniform distribution of bubbles may still persist. This may correspond to the crossing into the slugging regime with large bubbles spanning the width of the bed apparent with the resulting bubble spatial distribution profile.

The natural behaviour of the bubbles is such that there is a tendency for them to migrate towards the centre of the bed due to their interaction with other bubbles and that with the

bed walls. Upon introduction, bubbles formed at the distributor rise up the bed and also come under the influence of their predecessors rising above them. The location of predecessor bubbles has a significant effect on the subsequent lateral positions of these bubbles.

3.3.1 Previous study of bubble spatial distribution

There has been a substantial amount of work done to study the effect of bubble interaction on the spatial distribution of the bubbles and their subsequent successors in the bed, including the work by Grace & Harrison (1968) and that of Werther & Molerus (1973b). Grace & Harrison were among the first to generate systematic quantitative studies on the spatial distribution of bubbles by photographing bubbles in a two-dimensional bed. They proposed a simple coalescence model that attempts to explain the development of the non-uniform distribution of bubbles across the bed that used, as an initial condition, a uniform distribution of bubbles at the distributor. They also suggested that the existence of non-uniform bubble distribution in the bed as being a natural feature that is caused by the presence of wall constraints to movement of bubbles and the lateral movement of bubbles during the coalescence process and therefore associated with the corresponding deprivation of bubbles of the bed region near the walls.

Grace & Harrison's experiments were carried out on a planar bed with a porous plate distributor (6.3 mm thick grade C Porosint) that provided uniform introduction of gas into the bed. They measured the spatial distribution of bubbles by calculating from the acquired images of the bubbling bed the bubble void area at various locations in the bed to obtain bubble frequency and bubble flow distribution in the bed. They then compared their experimental results with their proposed theoretical model. In their model, they divided their fluidised bed into several imaginary equi-sized vertical sections from the distributor to the freeboard. They calculated the probability of the position of a bubble as it rose up the bed and undergone several coalescence processes. The theoretical and experimental results agreed reasonably well in general, which they suggested showed that the non-uniformities in bubble distribution is caused by bubble coalescence and interaction, resulting in bubble concentration peaks to form near the walls and gradually move towards the bed centre.

Grace & Harrison showed that non-uniformities in bubble distribution become more prominent with increase in superficial gas velocity and height above the distributor. The development of non-uniformities could be explained by the lateral motion of coalescing bubbles and the presence of wall constraints restricting bubble movement. They also described the non-uniform bubble distribution as the source of bulk circulation pattern of solids where the observed scenario of solids moving up the centre and down near the walls, which only occurs when the final stage of bubble distribution pattern development, is achieved.

The theories put forward by Werther & Molerus were supported by their measurements of bubble spatial distribution in cylindrical vessels using capacitance probes (Werther & Molerus, 1973a). Werther & Molerus (1973a) described a sensing system based on their design of capacitance probes. Werther & Molerus (1973b) used the system to investigate the bubble spatial distribution in three-dimensional beds under various operating conditions, containing different solids and with different bed dimensions. To obtain the distribution profile, they calculated the local bubble gas flow in the bubbling bed from their capacitive measurements, where the local bubble gas flow

$$Q_{b,L} = v_{b,L,av} f_{b,L,av} \delta_{b,L,av} \tag{3.1}$$

and $v_{b,L,av}$ is the average local bubble rise velocity. $f_{b,L,av}$ is the average local bubble frequency over time period, P and $\delta_{b,L,av}$ is the average local bubble pulses (positive signal duration picked up by capacitance sensor when bubble is detected) over P. In their experiments, the fluidised beds used were fitted with porous plastic or sintered metal plates to produce uniform distribution of gas introduction.

Werther & Molerus concluded that an annulus-type bubble distribution profile near the bed walls was found in all the beds used in their investigation that gradually approached the centre of the bed with height. Tall cylindrical beds were also used in their work and have demonstrated the emergence of a single peak at the centre of these beds at the mark of final bubble distribution development in the transition to slugging beds. With regard to this, Werther & Molerus found that for a given bed diameter, if the bed is not sufficiently tall, the bubble spatial distribution profile would be such that solids will flow down at the walls and also in the centre of the bed, indicating that the final stage of bubble distribution development has not been achieved (*Figure 3.3.2(a)*). On the other hand, if the bed is

sufficiently tall, then solids will flow down only at the wall, as observed in slugging beds (*Figure 3.3.2(b)*).

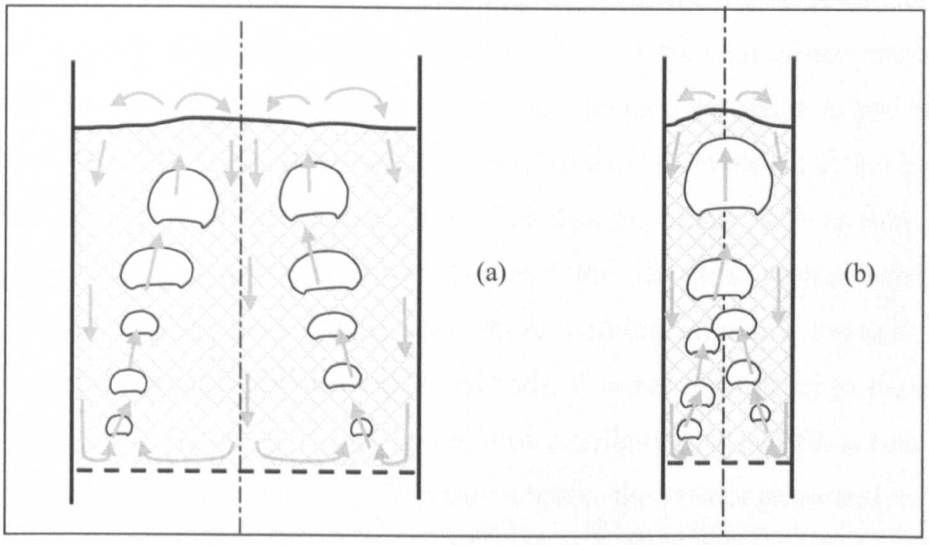

Figure 3.3.2: The bubble preferred path up a bed with consequent solid flow path, indicated by the arrows, (a) in a shallow bed where solids are still able to flow down the middle as well as at the walls, and (b) in a narrow bed where bubbles rise through the middle leaving solids to only flow down only at the walls. (Reproduced from Werther & Molerus, 1973b).

Studies conducted by Rowe et al. (Rowe & Partridge, 1962; Rowe et al., 1965; Rowe, 1971) showed that rising bubbles in fluidised bed cause an upwards drift in the surrounding particles, as well as carrying up solids in their wakes, inducing macroscopic circulation of solids in the bed. This establishes a gross circulation pattern of solids that ascend the bed in areas of high bubble concentration and descend the bed where the bed is deprived of bubbles. The circulation pattern therefore causes, according to Werther & Molerus (1973b), solids to rise in the annulus zone of high bubble concentration, then in the centre and subsequently descend at the wall proximity. Leva (1962), Schügerl (1967) and Potter (1971) reported to have observed these features in their work.

Werther & Molerus went on to propose theories that may explain the causes of non-uniformity of bubble distribution upon formation at the distributor. They were strongly inclined to the idea that the annulus profile of high bubble development was caused by a preferential bubble formation near the walls upon introduction into the bed; this is reflected by the maxima of bubble flow profile in close proximity to the wall at the distributor found in their work.

Werther & Molerus compared their findings with the studies conducted by Grace & Harrison (1968) on bubble development in a two-dimensional bed concluding, from their analysis, that a two-dimensional bed is not a good representation of the three-dimensional bed when investigating bubble spatial distribution. Investigating three-dimensional bed processes by two-dimensional models is inaccurate due to the wall effects imposed by the planar walls. Effects that immediately come to mind include the shape of the bubbles and their rise velocity. The wall effect would have a different geometrical effect compared to that caused by the three-dimensional bed. The data of Grace & Harrison on bubble frequency and distribution of bubble gas flow over the bed cross-section exhibited weak maxima near the wall in contrast to the rather more prominent maxima found in Werther & Molerus's measurements in three-dimensional beds. Werther & Molerus proposed that this could be apparently caused by the initial uniform distribution of bubble across the planar bed distributor. However in Grace & Harrison's work, the results presented in the graphs were all of local bubble frequency against horizontal displacement. They exhibit weak maxima near the wall because the ratio between maximum and minimum local bubble frequency is low. The measure of the mean number of bubbles striking the probe per unit time used in Werther & Molerus (1973b), which is equivalent to the measure of bubble frequency, is compared with that of Grace & Harrison, and they are found to be relatively similar. On the other hand, the larger maxima in local bubble gas flow in Werther & Molerus's work might also be an artefact of the physical presence of the capacitance probe.

Rowe & Masson (1981) investigated the interaction of bubbles with different kinds of probes in gas-fluidised beds. Their earlier work (Rowe & Masson, 1980) showed that a probe could disturb a bubble by attracting it towards the probe, and change its shape and velocity as well as locally inducing their nucleation. Later, they tested numerous probes used and described by many workers by making models, mounting them in fluidised beds and taking X-ray cine-photographs of the interaction of bubbles in the bed with the probes. Rowe & Masson concluded from their data and results that no matter what probe is being used, as long as is it a physical insertion into the fluidised bed it will cause disruption to the natural operation of the process. In addition, this disturbance becomes more prominent if the probe is used in a three-dimensional than in a two-dimensional bed. Therefore, the more prominent maxima of bubble development observed in three-dimensional beds by Werther & Molerus could be attributed to the influence induced by the probe itself that gave rise to formation of bubble around the probe while attracting other bubbles towards it.

However, the more important comparison made between the studies conducted by the two groups of workers is the explanation of the underlying mechanism that promoted non-uniformity in bubble distribution in the bed. Werther & Molerus refuted the suggestion by Grace & Harrison that bubbles are initially introduced uniformly at the porous distributor, claiming that bubble formation was in fact favoured near the walls. However, there was no satisfactory explanation as to why this is so nor is there substantial discussion on their claim. They suggested that the altered packing geometry of the particle layers near the wall in packed beds and liquid-fluidised beds might lead to an increased flow through this region. In addition, they also proposed that the different conditions of friction between the particles and the wall surface and within the fluidised particles in the fluidised bed might favour bubble formation in the vicinity of the walls. This is somewhat unusual as particles are effectively weightless and while suspended when fluidised, friction should not be an important factor.

3.3.2 Geometrical effect as the cause of bubble migration

If two bubbles in a fluidised bed are considered, one of which is located near the wall and the other in the middle of the bed, the one near the wall will either move inwards or maintain its distance from the wall, but the one away from the wall can move inwards, not at all, or also outwards. The wall is a physical constraint not encountered by the bubble in the middle. Therefore, there is a net effect where there is a greater probability that a trailing bubble near the wall to either maintain its lateral position or move inwards if it were to be involved in a coalescence process with a leading bubble placed somewhere closer to the middle to the bed. On the other hand, the bubble in the middle has equal tendency to laterally move to either sides of the bed depending on their interaction with a leading bubble.

By means of a simple simulation conducted in MATLAB (Mathworks Inc.), an illustrative proof of the formation or generation of this natural non-uniformity in the bed is shown here. The simulation started by aligning 100 spheres horizontally at equal distances apart from each other in a vertical column. The spheres were only allowed two degrees of freedom movements – two-dimensional with lateral and vertical translation. A simple and crude attraction law was used to govern the lateral interaction and movement of each

sphere. The spheres were allowed to rise up the column with constant initial vertical velocity component and were liberal to interact laterally with each other. The instantaneous profile of the spheres' lateral concentration in the column was monitored and the plots of the profile at different heights in the column produced consecutively over time are given in *Figure 3.3.3*.

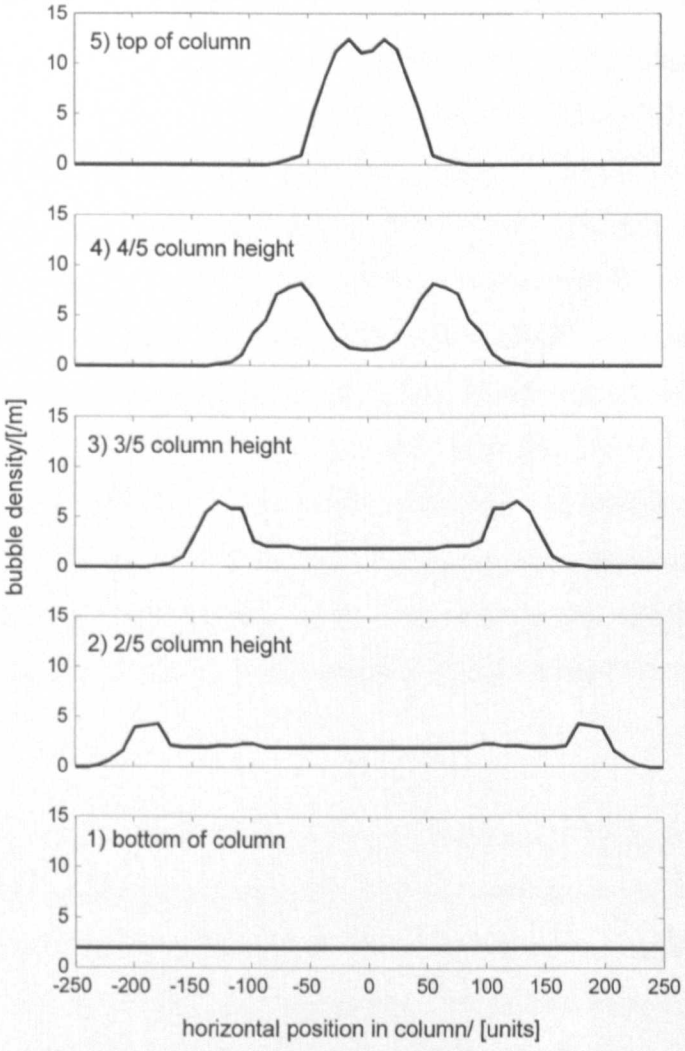

Figure 3.3.3: The sequential plots of the spheres (modelling bubbles) density at different column heights obtained from the simulation of interaction between 100 spheres.

Set off at uniform distribution across the column cross-section, the spheres interacted and gradually formed a bimodal concentration near the lateral ends of the column. As they rose through the column, these peaks gradually moved inwards and increased in magnitude. This shows an increasing sphere concentration around these two areas. The peaks eventually arrived at the centreline of the column, forming a single peak. The above

illustration with the simple simulation supported the view that the change in the spatial distribution profile obtained in this work, in Werther & Molerus and Grace & Harrison is in fact a natural process and is due to geometrical influences. The geometrical effect of the planar bed would also give a much higher measurement of local bubble gas flow than in three-dimensional beds.

This outcome also shows that the suggestion by Werther & Molerus that bubble formation at the distributor is preferred near the vessel walls is unusual. The analysis demonstrated that the underlying mechanism that promoted the region of high concentration of bubble development is a geometrical effect: the location of interacting bubbles and the presence of wall constraint restricting bubble movement. This factor affected the distribution of bubbles when they interact with others and coalesce further up the bed, displacing their region of high population towards the bed centre with height, depriving the areas close to the walls of bubbles and affecting the distribution of subsequent bubbles below. The tapering of bubble distribution away from the walls and the lack of bubbles in the bed centre column near the bottom are caused by interaction of bubbles occurring almost instantly as they are introduced into the bed. To summarise, the spatial distribution of bubbles in the bed plays an important role in governing the quality of the process. Therefore, understanding this leads to fabricating methods to improve it during the control of the process.

In relation to the quality of fluidisation in the bed, the band of high bubble concentration and development implies heterogeneous distribution of bubbles in the bed, upsetting good gas-solid contact and reaction efficiencies. The distribution of bubbles determines the degree of bubble coalescence activities in the bed that in turn determine the bubble size population in the bed. When the flow of gas as bubbles is preferred along a certain path causing bubble concentration to be high, these bubbles are strongly involved in coalescence. The gas associated with these bubbles also spend less time in the bed, with these bubble rising at much higher rate due to their sizes.

Furthermore, the onset of such a distribution would propagate into subsequent deterioration of a good bubble spatial distribution, such that the newly created successive bubbles, strongly influenced by their predecessors above them that are placed closer to the bed centre, tend to migrate to zones of high bubble population. With this, the spatial

distribution of bubbles suffers even greatly as they gradually migrate more and more towards the centre of the bed.

3.4 Measurement of localised bubble void fraction associated with bubbles

Despite having achieved a good spatial distribution of bubbles in the bed, the quality of the process may not necessarily be satisfactory. The quality of fluidisation is also governed by the physical properties of the bubbles existing in the bed. For a good quality, bubbles should be small, which will promote high solid-gas contact and hence, reaction efficiencies, while still acting as a good mixing mechanism. The measurements of such properties in the bed would allow the full assessment of the quality of the bed to be made, coupled with what was known about the spatial distribution of these bubbles.

The subsequent measurement in the instrumentation system involved the measuring of the localised changes of the bubbling state in the bed. The image system detects the changes to localised pixel value of consecutive images, determined by the existence of bubbles. Each image obtained from the bed after having undergone a full image processing procedure consisted of 1-bit energy level. The values of '0' or '1' marked whether a pixel of the image contained bubble void. The changes of this value for each pixel were associated with bubble residency, which is largely affected by the bubble size, shape and population, thus giving a good representation of the state of the bed quality.

In general, upon introduction bubbles are small at the distributor. The existence of bubbles throughout the bed with this characteristic would define a bed with good quality. However, the persistence of bubble coalescence inherent in freely bubbling beds upsets this stable and desired state. Coalescence of these bubbles forms larger ones that travel faster up the bed. These features in a typical freely bubbling bed can be detected using the technique of localised bubbling state changes measurement developed here. The assessment of the bed with this technique allows the degree of fluidisation quality in the bed to be identified. The statistical parameters characterise and classify the measurements where the standard

deviation as well as the frequency of localised changes contain valuable inferences of the quality of the bed.

The rule of thumb for a bed with good quality is to have both the measure of localised standard deviation of bubbling state and the local state switching frequency registering relatively high values in the measurements taken from all locations in the bed. This corresponds to having relatively small bubbles distributed evenly throughout the bed. However, this is difficult and intricate to achieve in a normal freely bubbling bed with the presence of natural bubble interaction, coalescence and size growth with height in the bed. The localised standard deviation and switching frequency measurements would register lower values on parts of the bed where bubble residency is either sparse, due to lack of bubbles or where there are larger bubbles in this sort of beds.

The following demonstrates how the measurements were made on the bed freely bubbling at steady state with excess of gas at 12.8 mm/s superficial flow above incipient condition with increment of 12.8 mm/s of gas for different measurements. These measurements were again cumulative over a period of time (5 minutes), from which mappings of the standard deviation and switching frequency of local states in the bed could be produced as shown in *Figure 3.4.1* and *Figure 3.4.2*.

The series of contour plots in *Figure 3.4.1* demonstrated how the standard deviation of local states in the bed changes with the increase in flow into the bed. At low flow, the upper part of the bed and the pair of narrow vertical bands of high bubble concentration have higher standard deviation of local state changes that corresponds to changes in local states due to the bubbles rising pass these regions. The increase in standard deviation in these regions and the initiation of non-zero standard deviation on other localised regions close to existing ones corresponds to the increase in bubble population as the flow was increased.

These increments in standard deviation values and regions of non-zero standard deviation progressively grew to encompass the whole column of the bed. However, localised regions within the tapered twin-bands of bubble population merging at the bed centre registered relatively higher plateau of values. Although the local standard deviations are reasonably similar in magnitude, physically they were caused by different states in the bed. Near the

bottom of the bed, the narrow bands were populated by small bubbles while near the top centre of the bed much larger and faster bubbles were present; both cases induced vigorous changes in local states in these regions.

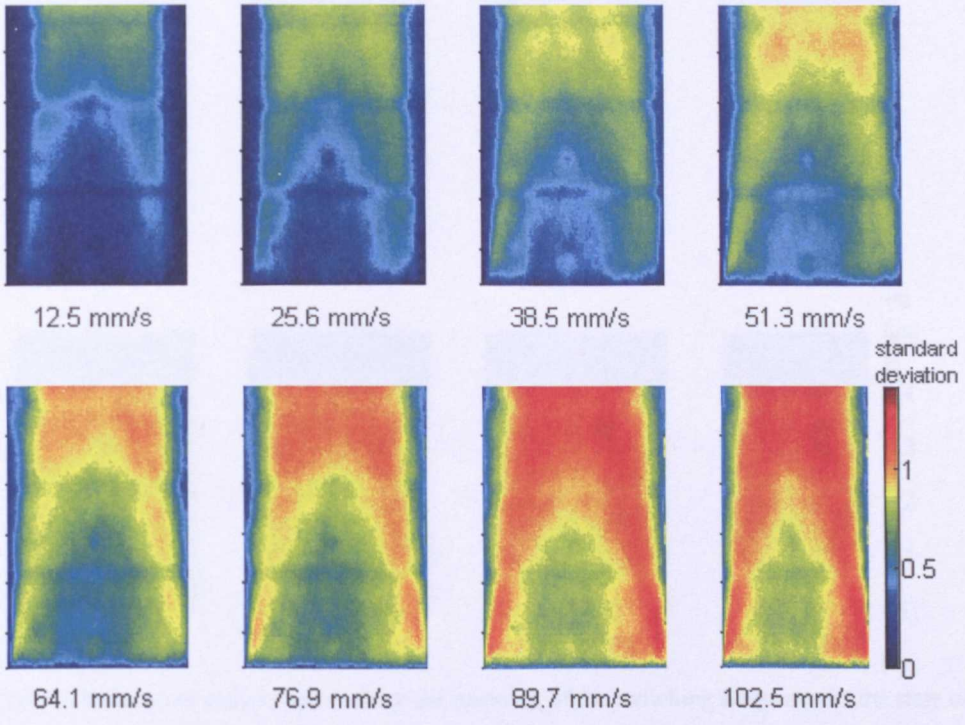

Figure 3.4.1: The series of contour -plots show the mapping of the standard deviation of the local states of the steady state bubbling experimental bed, fluidised at superficial gas of 12.5 to 102.5 mm/s above incipient fluidisation.

Complementing the measure of local state standard deviation, the measurements of local state switching frequency as presented in *Figure 3.4.2* indicates that at low flow rates, local state changes were concentrated mostly near the bottom of the bed corresponding to the rapid introduction of many small bubbles. In the upper part of the bed, local state changes were caused by fast larger bubbles passing through and therefore correspond to lower switching frequencies. As the flow increased, the switching trend as seen for lower flows prevailed and in general the switching frequency in all parts of the bed increased except for the tapered section near the walls. At high flows, very high switching frequencies concentrated at the bed bottom due to the even higher concentration of bubbles that rapidly changed the local states where they formed. Other parts of the bed where there are non-zero switching of local states registered relatively low values corresponding to a smaller population of larger and faster bubbles in residence. Although spatially comprised of

bubbles constantly, the bubbles were large giving less switching of local states compared to when the bubbles were smaller.

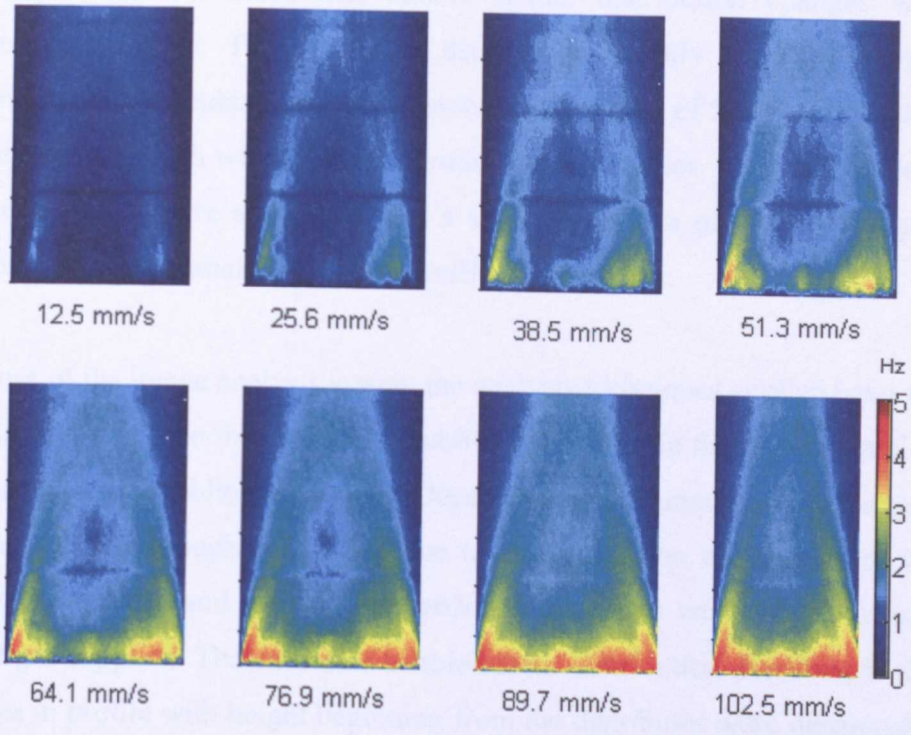

Figure 3.4.2: The series of contour -plots show the mapping of the switching frequency of the state of the selected localised regions (pixels) for a steady state bubbling bed, fluidised at superficial gas of 12.3 mm/s to 102.5 mm/s above incipient fluidisation.

When the contour plots of both the local standard deviation and switching frequency are analysed together, it can be concluded that the fluidisation quality deteriorated with increase in flow rate as well as with height in the bed. The combination of the two types of contour plot shows that although the general local standard deviation in the bed is high, the switching frequency is only high near the bed bottom. This shows the top of the bed has less desirable quality compared to the bottom.

3.5 Conclusion

The laboratory experiments and analysis conducted on a planar gas-fluidised bed described in this chapter have revealed that bubble spatial distribution changes with bubble progression up the bed. The profile of distribution quickly forms a two-peak (two-dimensional bed) or annular (three-dimensional bed) region of high bubble concentration near the distributor, even with uniform introduction of bubbles. This profile slowly tapers inwards to the bed centre and establishes a single peak at a given height signifying the completion of bubble spatial distribution profile development.

With the use of the image analysis system the analysis techniques applied have managed to properly identify the described profile of bubble distribution in the experimental planar bed over different freely bubbling conditions. Depending on the amount of excess gas supplied, the profile changes throughout the bed due to the interaction of bubbles, of which their population, kinematics and physical properties such as size were also influenced by the amount of gas supplied. The causes of bubble spatial distribution alteration in the bed and the changes in profile with height beginning from the distributor were discussed where the studies by previous workers were reviewed. A theoretical simulation further supported the argument that the nature of the migration of bubbles is caused by geometry.

From the obtained results, an estimated best operation bubbling condition for the given experimental bed was approximately at 51.2 mm/s superficial gas flow above incipient fluidisation (103 mm/s) for achieving an optimum quality of fluidisation in every respect considered in the study. The investigation into the prospect of managing bubble distribution in the bed as a means of negotiating a desirable fluidisation quality in a proactive sense was considered and is detailed in *Chapter 8*.

Chapter 4

Resolving bubbling process dynamics with frequency domain techniques

4.1 Introduction

This chapter seeks to describe the study of the bubbling fluidisation process using frequency domain techniques. Frequency domain techniques are known to be a reliable and credible means for identifying the underlying dynamical features that govern the behaviour of a system. Fluidised systems have been studied in this domain previously by many investigators (Fan et al., 1981, 1983; Kaart et al., 1999; Brown & Brue, 2001; Brue & Brown, 2001; Kage et al., 2000). It was used to identify characteristic frequencies of the process as well as to detect regime transitions.

In this chapter, frequency domain techniques are used to analyse the Bubble Void Fraction, BVF, time series measurements obtained for the bed's bubbling process at various operating conditions using the developed image analysis system described in *Chapter 2*. The BVF, which is the measure of the proportion of the bed occupied by void associated with bubbles, has been shown to be effective and suitable for characterising the bubbling regime. Its measurement has direct relationship to the existence and behaviour of bubbles that determines the overall state of the bed and therefore is the key parameter to be analysed for the fundamentals of the process to be understood.

Techniques for the interpretation of the resulting frequency plots of the BVF measurements include the plotting of a frequency spectral graph of the BVF measurements using an adaptation of the Bode diagram. Bode diagrams were used extensively in the study of dynamical systems through which characteristic features of a system's dynamics could be

easily identified. A modified version of this diagram converts the BVF frequency spectral graph to facilitate the characterisation of the measurements so that they can be matched to the measured bed condition.

The final section underlines the prospect of implementing techniques developed here as a diagnostic tool to continuously assess the fluidisation quality, indicating the possibilities of applying it in-situ.

4.2 Frequency domain techniques in fluidisation

4.2.1 Introduction

The frequency domain analysis of time-series measurement of the fluidisation process has been recently used by a number of researchers to characterise and reveal the behaviour of fluidised beds. It has been shown and proven to be a very useful tool in analysing and understanding the dynamical behaviour of the fluidised systems. Johnsson et al. (2000) have shown that the frequency content of the time series data obtained for different fluidisation conditions are very different, although from the time-series data itself, not much distinction could be identified. This serves as a reliable tool to identify the different fluidisation regimes, to characterise the general behaviour of the process itself and also to assist in the effort to generate a set of relationship rules for the scaling of fluidised beds.

Many researchers compared the dominant frequencies of a prototype or scaled model with those of the full-scale version (Brue & Brown., 2001; Newby & Keairns, 1986; Kage et al., 2000). Others used a selected frequency range for comparison (Glicksman et al., 1993; Nicastro & Glicksman, 1984). The measure of pressure fluctuation in the fluidised bed is commonly taken as the characterisation parameter where pressure probes are placed into the side of the bed wall or in the plenum to record pressure signals related to the activities taking place in the fluidisation process. Bi et al. (1995), Musmarra et al. (1995) and Schaaf et al. (1998) have used the time-series data to characterise the behaviour of the bed and have associated pressure fluctuations with pressure waves arising from the bubbling phenomenon. Johnsson et al. (2000), Kage et al. (2000) and Brown & Brue (Brown & Brue, 2001; Brue & Brown, 2001) used the frequency spectra of the pressure signals as an

alternative method to investigate the fluidisation process and conditions. They have identified dominant peaks in the spectra that could be associated with natural phenomena occurring in the bed. Kage et al. (2000) demonstrated that in various freely bubbling beds, the bubble formation and eruption frequency as well as characteristic frequency of the bed could be determined.

In this study, an alternative measurement with the use of image analysis technique was used where a time-series data of the Bubble Void Fraction, BVF, was generated from real-time image acquisition and analysis of the planar bed. The frequency spectral graph of the BVF time-series was subsequently obtained and analysed with frequency domain techniques.

4.2.2 Power spectral density and frequency response transfer function

In the frequency domain analysis, normally the power spectral density (PSD) is used. PSD is defined as the amount of power per unit (density) frequency (spectral) as a function of the frequency. The PSD describes how the power or variance of a time series data is distributed with frequency. Mathematically, it is defined as the Fourier transform of the auto-correlation sequence of the time series data. According to Kay (1981) an equivalent definition of PSD is the squared modulus of the Fourier transform of the time series, scaled by a proper constant term.

Many researchers have used PSD in their research, mainly to interpret the time-series data of pressure fluctuations. Fluidisation region transitions can be identified by a change in the frequency distribution in the power spectra (Lirag & Littman, 1971; Canada et al., 1978; Satija & Fan, 1985; Satija et al., 1985; Johnsson et al., 1995; Svensson et al., 1996a). Johnsson et al. (2000) reviewed the use of frequency domain analysis among other time-series analysis tools and showed that this analysis could identify the different fluidisation regimes. They also plotted the spectra graphs in semi-logarithmic scale to emphasise the fall-off region of the spectra, relating them to the frequency content of the chaotic Lorenz equations and the velocity fluctuations of turbulent pipe-flow.

The response of a linear dynamical system to a sinusoidal input can be described by the system's frequency response. A stable system with the transfer function $G(s)$ excited by a sinusoidal input with unit amplitude at frequency ω will, after its response reaches steady state, exhibit a sinusoidal fashion output at the frequency ω with a magnitude of $A(\omega)$ ($A(\omega) = |G(j\omega)|$) and a phase difference of $\phi(\omega)$ ($\phi(\omega) = \angle G(j\omega)$) from the input. This is the linear characteristic of the system. A frequency response plot could be produced based on information gathered regarding the systems response over a range of excitation frequencies, comprising of a magnitude plot, $A(\omega)$ against ω, and a phase difference plot, $\phi(\omega)$ against ω. The most appropriate method for this study for plotting frequency response plots is discussed in the next section.

Brue & Brown (2001) conducted system identification on several fluidisation conditions via the use of pressure fluctuation signals. In their efforts to identify the dynamic features of the process, they analysed the pressure fluctuation signal via the PSD and the use of logarithmic plots. Logarithmic plots have proven to be a useful way of presenting PSD as they enhance and improve the ability of identifying features in the plot. A well-known logarithmic plot is the Bode diagram commonly used by control engineers. The introduction and implementation of the Bode diagram is also given in the next section.

4.2.3 Bode diagrams and Bode scaled frequency spectra plots

A reasonably good graphical presentation of frequency response data had been an issue studied for a long time until a useful technique was developed by H. W. Bode at Bell Laboratories between 1932 and 1942. This technique is particularly useful for purposes of investigating dynamical systems. It enables the development of good intuition in identifying key features of the dynamical behaviour of a system (Franklin et al., 1994).

The Bode diagram involves plotting the magnitude of the frequency response data using a logarithmic scale while the phase on a linear scale. This enables the plotting of high order frequency response transfer functions by allowing the simple addition of the separate terms in the transfer function. This allows a convenient approximation of the system frequency-response characteristics to dynamical changes.

This is possible as the complex expression expressed in terms of poles and zeros can be written as

$$G(j\omega) = \frac{r_1 e^{j\theta_1} r_2 e^{j\theta_2}}{r_3 e^{j\theta_3} r_4 e^{j\theta_4} r_5 e^{j\theta 5}} \tag{4.1}$$

$$G(j\omega) = \left(\frac{r_1 r_2}{r_3 r_4 r_5}\right) e^{j(\theta_1+\theta_2-\theta_3-\theta_4-\theta_5)} \tag{4.2}$$

From (4.2), the phases of the individual terms are conveniently added together resulting in a composite phase expression, $G(j\omega)$. Since the magnitude of the frequency response transfer function,

$$|G(j\omega)| = \frac{r_1 r_2}{r_3 r_4 r_5} \tag{4.3}$$

imposing a logarithmic operation onto it would give,

$$\log|G(j\omega)| = \log_{10} r_1 + \log_{10} r_2 - \log_{10} r_3 - \log_{10} r_4 - \log_{10} r_5 \tag{4.4}$$

Figure 4.2.1 shows the magnitude and angle of the resulting vector which is made up of the combination of several constituting vectors plotted in a polar plot as an example of applying the postulate given in (4.4).

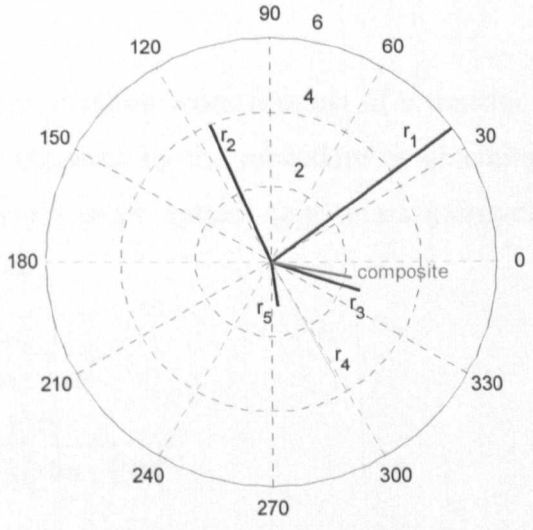

Figure 4.2.1: The polar plot of the individual components of $G(j\omega)$ and the resulting composite plot.

The addition of the logarithms of the individual terms forms the logarithm of the magnitude of the composite expression. Therefore, the Bode diagram typically comprises of two plots; first, the logarithm of the magnitude and the second, the phase, both plotted against the logarithm of frequency (in rad/s or in Hz). The former is a plot of the

magnitude of system's output to input ratio against the corresponding frequency of excitation. The latter plot is the phase angle-frequency plot. This plot shows the phase difference between the output and input at the corresponding frequency of excitation. The magnitude axis is normally scaled to the unit of decibel (dB), via

$$|G|_{dB} = 20\log_{10}(|G|) \tag{4.5}$$

and the phase axis is plotted in degrees (°). The transfer function of a system could be obtained from the Partial Differential Equation (PDE) of the system. As an example, a second order transfer function could be obtained by the following:

$$\begin{aligned} f(t) &= m\ddot{x}(t) + c\dot{x}(t) + k_s x(t) \\ F(s) &= ms^2 X(s) + csX(s) + k_s X(s) \\ \frac{X(s)}{F(s)} &= \frac{1/m}{s^2 + c/m\, s + k_s/m} \end{aligned} \tag{4.6}$$

for a mass-spring-damper system where m is the mass, c is the damping coefficient, k_s is the spring constant, f is the excitation force and x is the displacement. The form in (4.6) is comparable with the standard second order system transfer function shown below

$$G_p(s) = \frac{\lambda\omega_n^2}{s^2 + 2\zeta\omega_n s + \omega_n^2} \tag{4.7}$$

where λ is the Low Frequency Gain, ζ is the damping ratio and ω_n is the undamped natural frequency.

A brief example of a Bode diagram representation of a transfer function of a dynamical system is illustrated accompanied by the procedure of obtaining it. Consider an under-damped (oscillatory) second order system (e.g. mass-spring-damper system) with the following transfer function:

$$\begin{aligned} G_p(s) &= \frac{\lambda\omega_n^2}{s^2 + 2\zeta\omega_n s + \omega_n^2} \\ &= \frac{1(10)}{s^2 + 2(0.3)(10)s + (10)^2} \\ G_p(s) &= \frac{10}{s^2 + 6s + 100} \end{aligned} \tag{4.8}$$

where m is 0.1 kg, k_s is 10 N/m and c is 0.6 Ns/m corresponding to a damping ratio, ζ of 0.3 and an undamped natural frequency, ω_n of 10 rad/s. The resulting step response of the system is shown is *Figure 4.2.2* with approximately 2 overshoots and a settling time of about 1.12 s. The steady-state is 0.1 (0.1 m) for a step input magnitude of 1 (1 N).

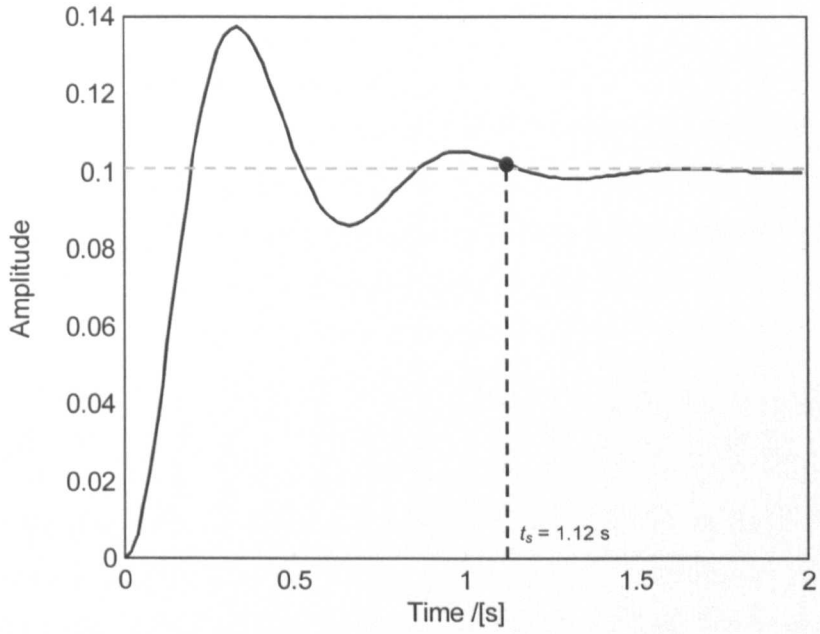

Figure 4.2.2: The step response of the transfer function to a unit input.

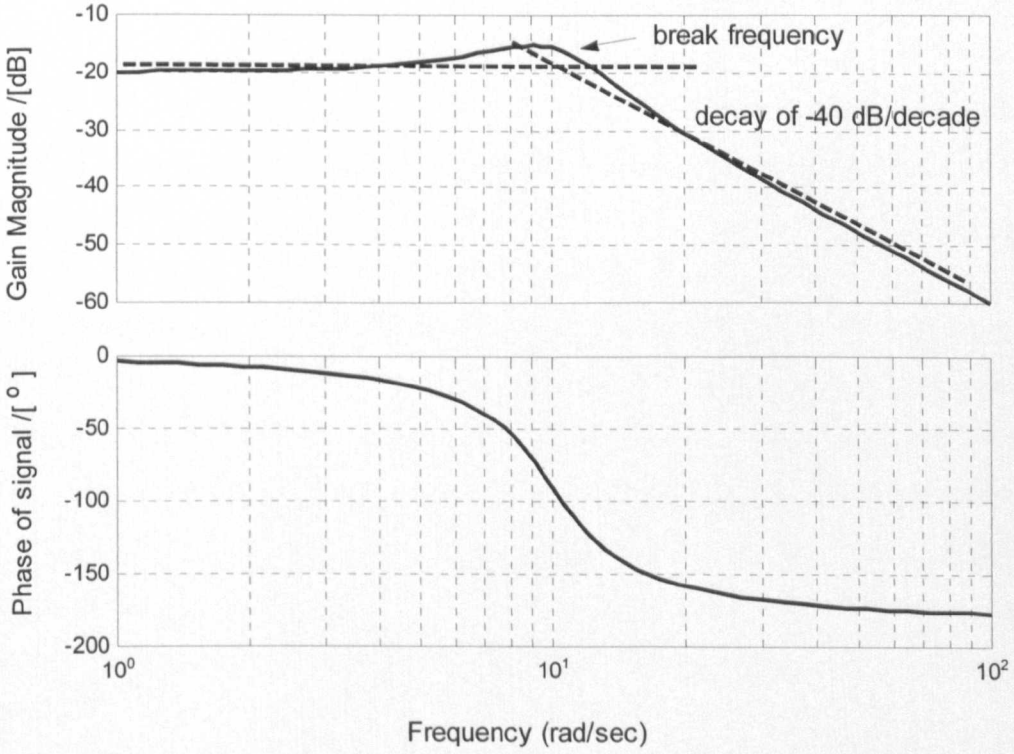

Figure 4.2.3: The Bode diagram for the transfer function in (4.8)

The corresponding Bode diagram is presented in *Figure 4.2.3*. In the magnitude-frequency plot, a peak is an indication of an under-damped system. The break point or change of asymptotic slope around 10 rad/s corresponds to the natural or characteristic frequency of

the system, ω_n. The slope of the asymptote thereafter of –40 dB/decade shows that the system is second order. The Low Frequency Gain (LFG) of –20 dB is the log10 of the ratio of output (= 0.1) to input (step input = 1, see *Figure 4.2.2*) multiplied by factor of 20. The phase-frequency plot starts of from 0°, goes through -90° at approximately 10 rad/s, corresponding to the system's ω_n, and reaches the asymptote of -180° at high frequencies. This is a typical phase-frequency plot for this sort of system.

Throughout the studies that were conducted in the frequency domain, two different aspects of the bubbling bed were looked at. First, a direct analysis in the frequency domain on the output measurement from the image analysis system (i.e. the BVF measurement) was carried out. The time series data was converted into frequency spectral and then scaled into a Bode-scaled diagram (magnitude plot only) by imposing a logarithmic scaling rule on the vertical and horizontal axes. This plot shows the sort of activities occurring, at various frequencies and magnitudes that the BVF measurement contained. Imposing a Bode-scaling on the BVF frequency plot assists in visually enhancing the low frequency band of the plot so that dynamics within this region could be easily studied. This treatment of the frequency spectral graph was used extensively to interpret the frequency plots of the BVF data described in *Section 4.3*. It was also later used in the study carried out in part of *Chapter 6*.

The second aspect involved analysing the dynamical behaviour of the bubbling bed, where a transfer function of the system was extracted from the obtained output and the given input signals of the system. The transfer function is an equation that governs the dynamical behaviour of a system in response to a given input excitation, as introduced earlier in the section (*Section 4.2.3*). From the plot, one could know what to expect of the output from the system for what is given at the input over a range of frequencies. Therefore, there are together two forms of Bode diagrams generated in the studies, appearing in *Chapters 7* and *Chapter 8*.

In *Chapter 7*, the transfer functions are generated that describe the dynamical features of the bubbling process in the experimental bed during steady state freely bubbling mode. The transfer functions were plotted in the form of magnitude against frequency, i.e. a frequency spectral graph on Bode-scaled axes. In the system identification work detailed in *Chapter*

8, transfer functions were obtained from the experimental bed subjected to various modes of flow rate excitation. The transfer functions show how the bed responded to dynamical changes in the input over a whole range of excitation frequencies. The transfer functions were plotted in two types of plots: magnitude against frequency and angular difference (phase) against frequency; these are referred to as Bode diagrams of the dynamical system.

4.3 Interpretation of the bubbling bed operating at various conditions

4.3.1 Interpretation of the bed BVF frequency spectral

A body of procedures and methods that could appropriately interpret the frequency spectral of the BVF measurement is essential to obtain a good understanding of the dynamical behaviour of the bed based on this data. The interpretation of the plots should enable direct inferences to the corresponding physical state and behaviour of the process in the bed that affected the BVF measurements.

Having obtained the time series data of BVF from the experimental bed measured at a given fluidisation condition, a Bode-scaled spectra graph could be plotted and hence an example is shown in *Figure 4.3.1(b)*, with the corresponding time series used to produce it shown adjacent in *Figure 4.3.1(a)*. Generally there is a large amount of fluctuation in the time series signal and this does not allow interpretation of any useful information on the process. However, in *Figure 4.3.1(b)* the plot shows that the BVF time series generally contains a high magnitude of signal changes occurring at low frequencies, from the DC level of 0.02 Hz up to approximately 0.6 Hz. At about 0.7 Hz, referred to in this study as the break frequency, the curve begins to break into a decay in signal magnitude at the roll-off rate of −15 dB/decade.

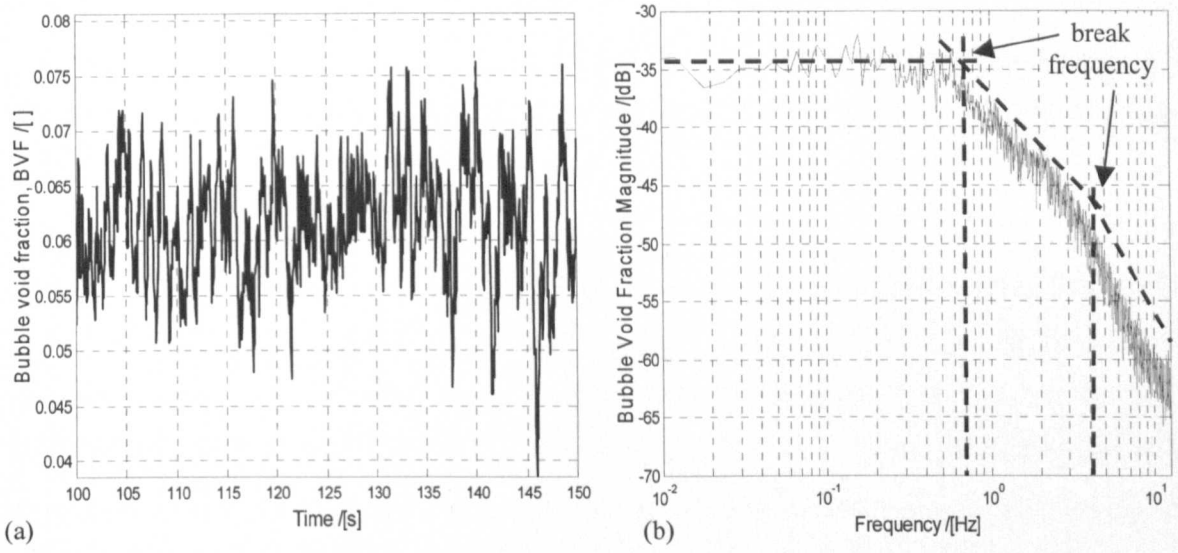

Figure 4.3.1: (a) the time series and (b) the Bode scaled spectra graph of the BVF for the experimental bed fluidised at 12.8 mm/s superficial flow above U_{mf} sampled at 25Hz.

The secondary break at frequency of approximately 4 Hz increases the decay rate to –25 dB/decade, extending up to the Nyquist frequency of 12.5 Hz. As the frequency increases, it could be seen that the spectra graph is gradually swamped with noise. This is a typical phenomenon in the plot and care must therefore be taken when interpreting the features in the plot. The decay of the plot at higher frequencies indicated that the BVF time series contains either gradually fewer signal changes or lower energy changes at those frequencies. Referring to the physical behaviour of the bubbling process in the bed, it means that the behaviour of the bed was dominated by slow changing events covering the lower half of the frequency range under investigation. The slow events were identified as, amongst others, the bubbling activities such as the bubble growth with height and bubble exit rate. Several activities that occurred at a slightly higher frequency level were bubble introduction frequencies, sudden disappearance and reappearance of bubbles while in residence in the bed, and the coalescence of bubbles.

In *Chapter 3*, the time series of the BVF measurement was shown statistically to have a standard deviation resulting from the fluctuation intrinsic to the measurement, which increased with the gas flow rate into the bed. In other words the standard deviation of the BVF is directly governed by the size of the bubbles existing in the bed. It is therefore appropriate to state that the activities or events in the bed associated with the bubbles inherit energy content whose magnitude is highly dependent on the relative sizes of the

bubbles in the bed. In other words, if the bubbles are small then the activities associated with them are a low energy component on the BVF measurement and on the other hand, if these bubbles are larger, the activities they undergo in the bed cause the BVF to have higher magnitude of changes.

It is therefore relevant to imply that the above postulate is also spatially dependent as the extent at which activities in the bed affected the BVF is heavily dependent on the location in the bed where they take place. The natural distribution of bubble sizes in a typical freely bubbling bed is such that smaller bubbles are concentrated near the bottom half of the bed. Starting at the bed distributor, excess gas issuing through the porous medium randomly (uniformly random distribution) generates small bubbles, associated with events that cover the whole range of frequencies (DC to Nyquist). However, it has very small magnitude of BVF change associated with it and therefore contributed small magnitudes (or energy) in the frequency domain.

Depending on the fluidisation condition, bubbles that form at the bottom of the bed interact with one another. This ultimately leads to the coalescence of bubbles and larger sized bubbles gradually populate the bed as the population of smaller bubbles gradually diminishes, as they are converted into larger bubbles. This would continue to occur throughout the height of the bed producing gradually larger bubbles with height. These events affect or change the BVF in the bed to a greater extent than the bubble introduction would. However, they occur at a narrower band of frequencies and hence are associated with a much higher magnitude along that band of frequencies in the BVF spectrum. Other events such as bubble size and shape fluctuations as well as bubble disappearance and reappearance in the emulsion phase contribute to a wide range of frequencies but are associated with low energy contribution to the changes in the BVF signal.

In the upper portion of the bed, bubbles are larger than those in other parts of the bed. Due to their sizes, they rise faster up the bed (Davidson et al., 1977). However, due to their sizes as well, when these bubbles exit the bed, this event is somewhat at a less high frequency, as the exit of these bubbles is gradual rather than instantaneous. Because they are larger, they cause large changes to the BVF measure hence increasing the energy associated with the frequency band at which these changes occur.

Based on the relationship established between the bubbling process in the bed and the BVF measurement, an analysis was carried out. It involved measuring several sets of BVF time series of the bed, extending from the distributor upward to different bed heights, as illustrated by the diagram shown in *Figure 4.3.2*. Normalisation of the measurements was made to the measure of BVF by the division of the total area of the bed (constant dimension) from the total void area obtained from the respectively Region Of Interests, ROIs for all the measurements. The size of each ROI used is listed in *Table 4.3.1*.

ROI	Height of ROI in mm
ROI 1	0 - 25
ROI 2	0 - 115
ROI 3	0 - 185
ROI 4	0 - 325
ROI 5	0 - 465
ROI 6	0 - 650

Table 4.3.1: The ROIs and their sizes used in the experiment carried out during the analysis.

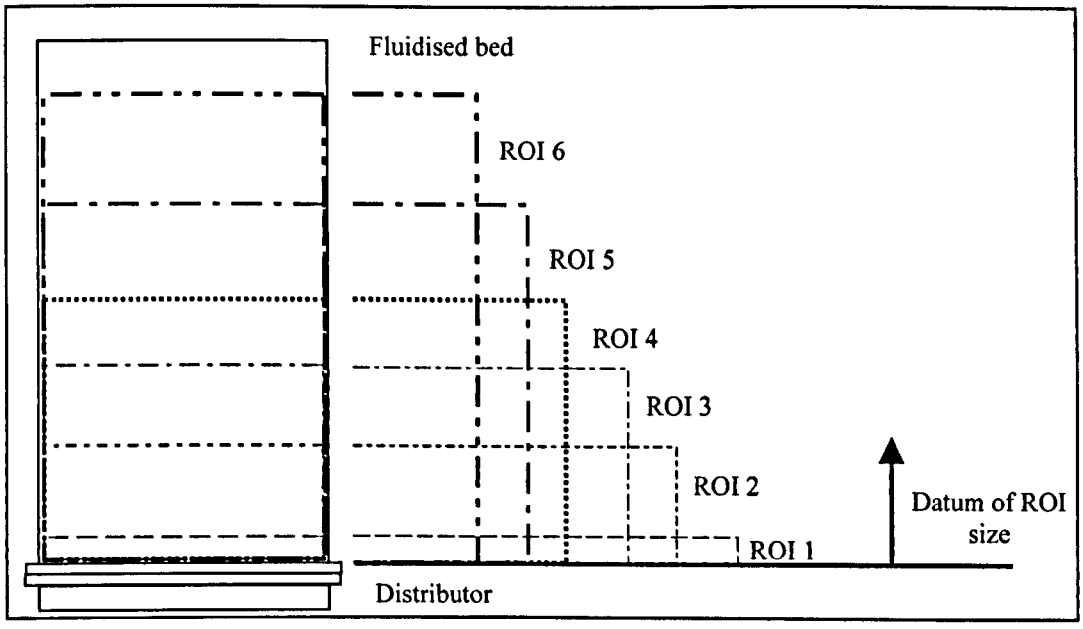

Figure 4.3.2: The diagram illustrates the areas in the bed from which different sets of BVF time series were measured.

The Bode-scaled BVF frequency plots of these measurements are shown in *Figure 4.3.3* for the experimental bed fluidised at 25.6 mm/s superficial flow above U_{mf}. *Figure 4.3.3* shows that the analysis results agree well with the above-presented ideas regarding the

bubbling behaviour in the bed viewed in the frequency domain. Shown relative to other areas in the bed, the frequency content of BVF measurement close to the distributor spans the whole range of frequencies but is of low magnitude. Extending the top end of the ROI higher up the bed shows the corresponding frequency content gradually skews towards the low frequency region as the magnitude of the frequency content elements gradually increase with ROI size.

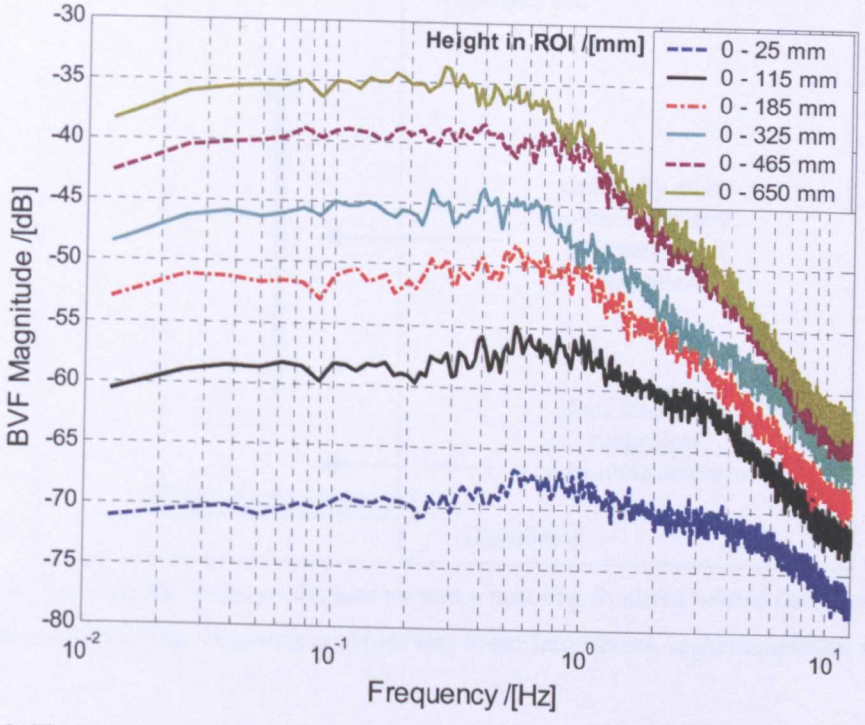

Figure 4.3.3: The Bode scaled spectra graph for BVF time series measured in different areas in the bed, extending from the distributor upward. Measurements were taken from the experimental bed fluidised at 25.6 mm/s above U_{mf}.

The results of this analysis also suggested that the bubbling behaviour in the bed is such that when many small bubbles were first introduced into the bed, the frequency content in the bed consisted of wide bandwidth low magnitude frequency elements. Gradually proceeding up the bed, the high frequency elements were converted or shifted into a lower frequency range seen as a corresponding increase in their magnitudes. This conversion is attributed to the coalescence process where smaller bubbles lower down in the bed, responsible for high frequency events, are gradually merged into larger bubbles further up the bed, that have lower frequency attributes, but are high magnitude events. In all of the measurements, the bottom of the bed was being included in the ROIs. As the energy of the

frequencies associated with this part of the bed is small compared with the rest, their significance in the frequency domain probably appears as noise fluctuations in the resulting BVF Bode-scaled frequency plot on the upper end of the frequency range. With the given description, the natural characteristic of the bubbling fluidised bed can be represented by the diagram in *Figure 4.3.4*.

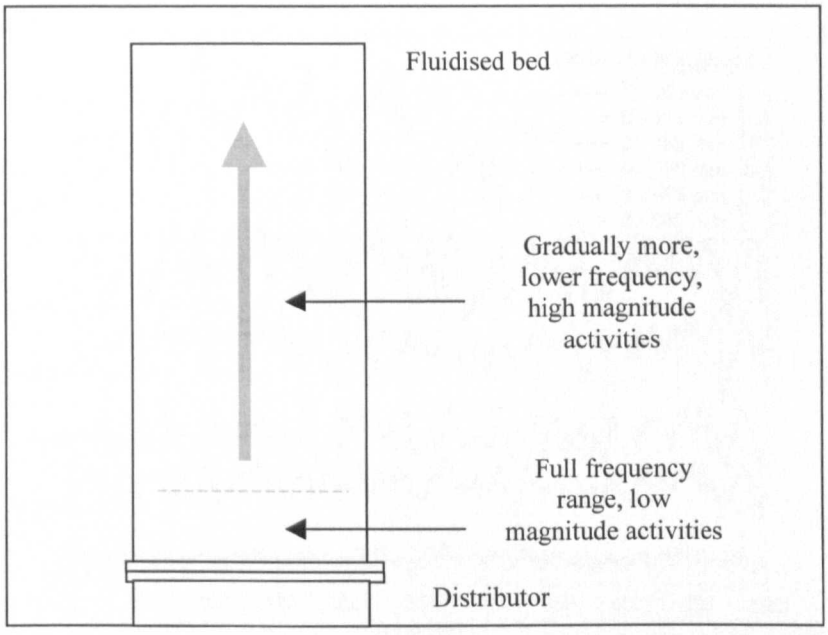

Figure 4.3.4: The diagram illustrates the idea on how a bubbling fluidised behave during steady state condition; converting high frequency activities into lower frequencies, higher amplitude activities.

The decay rate of -15 dB/decade at the first break frequency and a subsequent rate of -25 dB/decade on the second break in the Bode-scaled spectra graph mentioned and shown earlier in *Figure 4.3.3* indicated reduction in BVF signal magnitude or its attenuation at higher frequencies. It does not to have any other dynamical significance such as indicating the order of a dynamical system representing the fluidised bed. This could only be extracted from the proper treatment of Bode diagrams described in the earlier section. The shape of the BVF Bode-scaled spectra plot gives an indication of the nature of changes in values experienced by the BVF measurement such that by interpreting the shape of the plot appropriately, one should be able to infer the condition of the bubbling fluidisation process.

Figure 4.3.5 shows the BVF time series for the different ROI configurations used. Consider the time series of BVF at lower portion of bed and a larger ROI extending up the

top of the bed beginning from the distributor. It can be seen that the fluctuations are different in terms of the mean and standard deviation, factors which reflect how the bubbling activities in the bed influence the frequency content of the BVF and hence the dynamics of the bed. The lowest of BVF values was registered by the ROI set closest to the distributor while the largest was obtained when the ROI extended farthest up the bed.

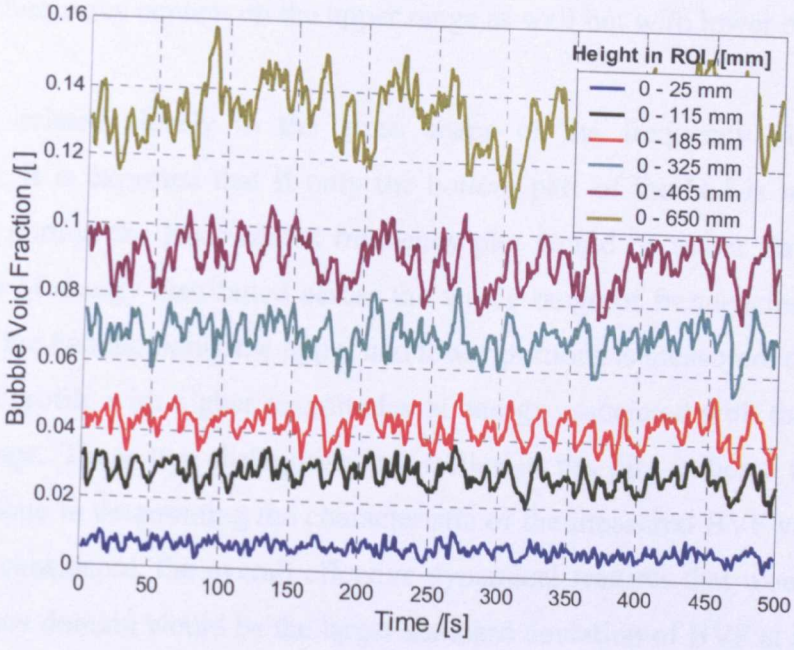

Figure 4.3.5: The time series of the BVF obtained from different ROI sizes extending from the distributor upwards for a freely bubbling bed fluidised at 51.2 mm/s above U_{mf}.

Observed closely, the fluctuations in the BVF for the smallest ROI, ROI 1, contain a wide range excitation frequency including those of upper range, all of which have relatively similar energy content. Comparatively for the larger ROI (ROI 6), the high frequency fluctuations are still observable; however, the fluctuations of the lower frequency range have a much larger magnitude. Due to the relatively much weaker magnitude or energy of changes that the activities at the bottom of the bed had on the BVF measurement compared to those higher up in the bed, their effects are masked by the latter effects. High frequency content is then insignificant compared to the overall BVF measurement. Therefore, the activities of bubbling that occur near the distributor (source of bubble introduction) or at the bottom portion of the bed has a less significant effect on the overall dynamical behaviour of the bed compared to the effects of other activities located gradually further up in the bed.

In *Section 3.4*, it was shown that in the top portion of the bed where the standard deviation of BVF is high, the switching frequency of any localised region in the bed between being in the emulsion phase and a bubble void, is lower compared with the lower portion of the bed; therefore, the consequent BVF measurement in that area has lower frequency content. The lower portion would typically have slightly lower standard deviation but higher switching frequency of localised regions due to the presence of many small bubbles so that the BVF has frequency content on the upper range as well but with lower energy levels.

This finding related closely to the gross shape of the frequency plot of the BVF measurement. It is expected that if only the bottom part of the bed is measured for the BVF, in that portion the Bode-scaled frequency plot would be rather flat with relatively equal amount of energy distributed across the whole range of frequencies. However, if a larger part of the bed including the upper and lower portions is measured, the resulting plot has a skewed profile with higher magnitudes of energy associated with the lower band of frequency range. These two distinguishing profiles in the plot indicate the influence of bubble size alone in determining the characteristic of the measured BVF values. When the whole bed is considered, the overall effective dynamical features that would be picked up in the frequency domain would be the larger standard deviation of BVF at lower switching rates due to activities associated with larger bubbles. The lower standard deviations at higher switching rates associated with smaller bubbles are overshadowed by the latter due to its low energy content.

Having established the proper means of interpreting the frequency plots such that the fundamentals of the process responsible for the features in the plots are identified, fluidisation at different conditions could be studied and the bubbling process be investigated and understood.

4.3.2 The steady state bubbling process at different constant gas supply flow rates

In order to determine if the developed technique could be used to help identify the state in which is a bubbling bed, several tests were carried out on the experimental bed, where the BVF values were measured with the image analysis system for the freely bubbling process at different constant gas flow rates. The experimental bed was fluidised at superficial flow above U_{mf} (≈ 103 mm/s) of 12.8 mm/s, 25.6 mm/s, 51.3 mm/s and 76.9 mm/s. Images of the entire bubbling bed were acquired by the image analysis system at 25 Hz, producing sets of BVF time series over a period of approximately 3600 seconds containing up to 90000 data points.

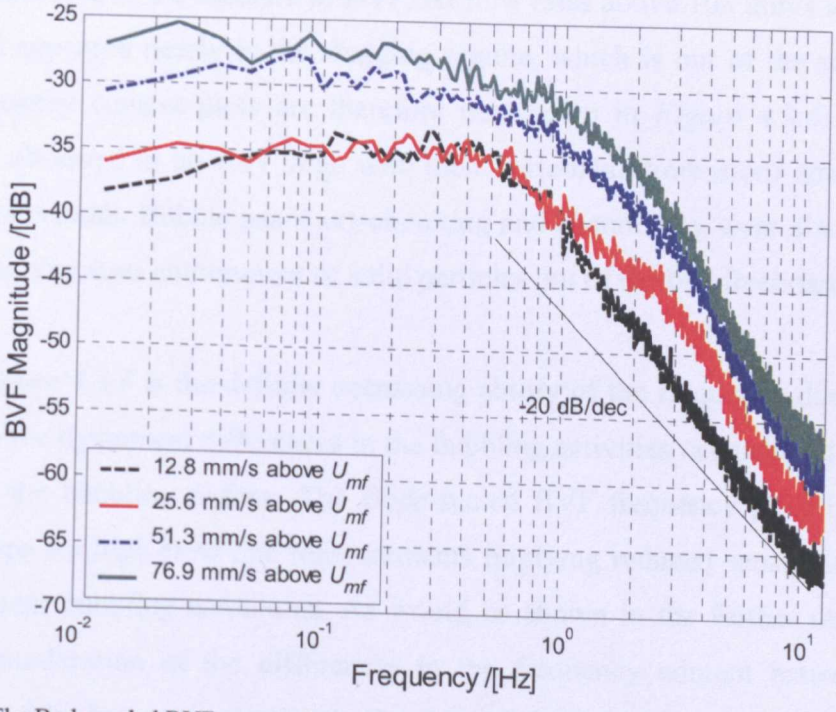

Figure 4.3.6: The Bode scaled BVF spectra for the freely bubbling process in the experimental bed, fluidised at 12.8, 25.6, 51.3 and 76.9 mm/s superficial flow above U_{mf}.

Figure 4.3.6 shows the Bode-scaled frequency plot of the BVF for the listed fluidisation conditions. Generally, the low frequency band of the plot increases with flow rate, indicating increased energy associated with the existence and activity of larger bubbles and bubble populations in the bed. The break frequencies and rate of roll-offs are generally similar for all the plots, although the break frequency became slightly less distinguishable above superficial flow of 51.3 mm/s above the incipient state.

At the lowest fluidisation flow rate, 12.8 mm/s above U_{mf}, the frequency plot has significantly different shape and characteristics from the rest of the plots. At this flow rate, the bed was very close to its incipient state and bubbles of small sizes were seen to form at the distributor. As the bubbles rose up the bed, many experienced disappearance and reappearance in the emulsion phase. Also, a majority of the bubbles rose through the height of the bed without undergoing coalescence.

Between fluidisation at 25.6 mm/s and 76.9 mm/s above U_{mf}, the bubbling process was reasonably similar, with rapid formation of many small bubbles at the distributor, which quickly coalesced into larger bubbles along the height of the bed. Bubble disappearance and reappearance, as observed for lower flow rates could still be seen in the bed, but had a somewhat lesser role in the measure of BVF. At flow rates above 103 mm/s above U_{mf}, the bubbling bed appeared nearly in the slugging regime, which is out of the scope of study and the frequency content plots are therefore not shown in *Figure 4.3.6.* The bubbles formed were observed to be very large with their horizontal dimensions spanning almost across the bed breadth. Bubble gas short-circuiting and channelling were also taking place causing further vigorous entrainment of solid particles out of the bed freeboard.

Evident in *Figure 4.3.6* is the definite decreasing ability of the frequency domain analysis to distinguish the dynamical differences in the bubbling activities occurring at much higher flow rates in the bubbling regime. The Bode-scaled BVF frequency plots become more similar in shape for high flow rate measurements implying reduced sensitivity to identify plots of different bubbling conditions. As would be shown in the further sections of the chapter, the moderation of the differences in the frequency content between different bubbling flow rates has some relation to the state of the bubble spatial distribution in the bed.

4.3.3 The influence of bed height on the bed dynamics

The overall bed dynamics vary with the height of the bed, a factor that determines the nature of bubble behaviour over the whole bed from the distributor up to the freeboard. Therefore, the BVF frequency content of a portion of the bed of a given height could be different from that of the same or different portion of another bed with a similar or different given height. In order to investigate this, three different bed heights have been used to explore the frequency content of the bubbling bed with different geometries. The planar bed heights of 700, 350 and 180 mm were used, with all the beds fluidised at an excess of 51.3 mm/s of gas superficial velocity above the respective bed U_{mf}. The BVF in the beds was measured and subsequently analysed in the frequency domain.

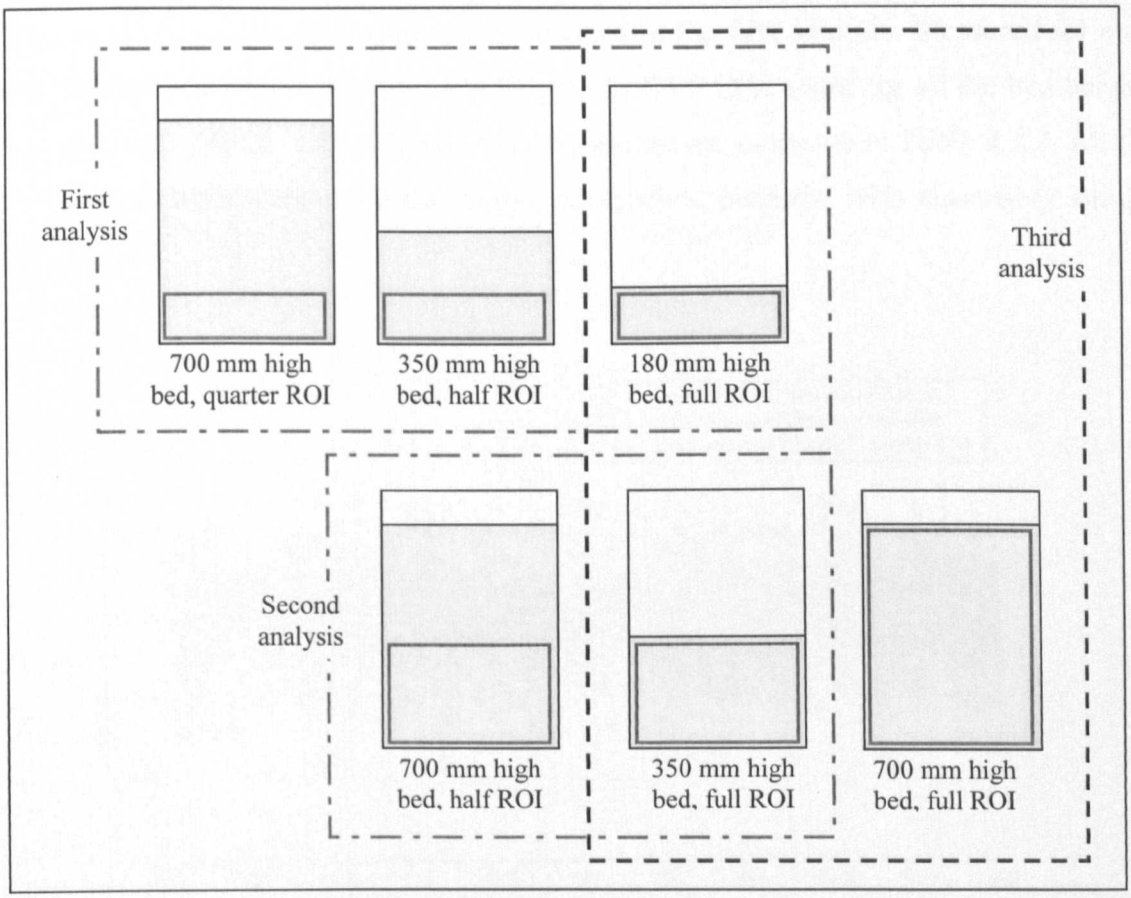

Figure 4.3.7: The diagram shows the bed heights studied and the size of the ROIs used in the first, second and third analysis respectively.

Three different analyses were considered. The first was the study of the frequency content of the BVF in the lower quarter portion of the 700-mm tall bed for beds with different heights and the second looked at the frequency content of the BVF in the lower half

portion of the 700-mm tall bed for beds with different heights. In the third analysis, the BVF frequency content over the whole bed of heights 180, 350 and 700 mm were compared. The diagrams in *Figure 4.3.7* illustrate the experiments carried out. The analyses were done by varying the vertical size of the ROI of the image analysis system, all extending upwards beginning from the distributor. For full-size ROI acquisition of BVF, the upper limit of the ROI was placed below the lower bound of the freeboard height fluctuation.

4.3.3.1 Frequency content of similar ROI (from distributor to 180 mm high) of beds of different heights (first analysis)

Figure 4.3.8 shows the BVF time series obtained in the first analysis. Measured for only from the distributor up to 180 mm bed height, the BVF time series for all the bed heights were relatively similar with their statistical measurement as shown in *Table 4.3.2*. All the BVF measurements exhibit similar degree of standard deviation with reasonably similar BVF means.

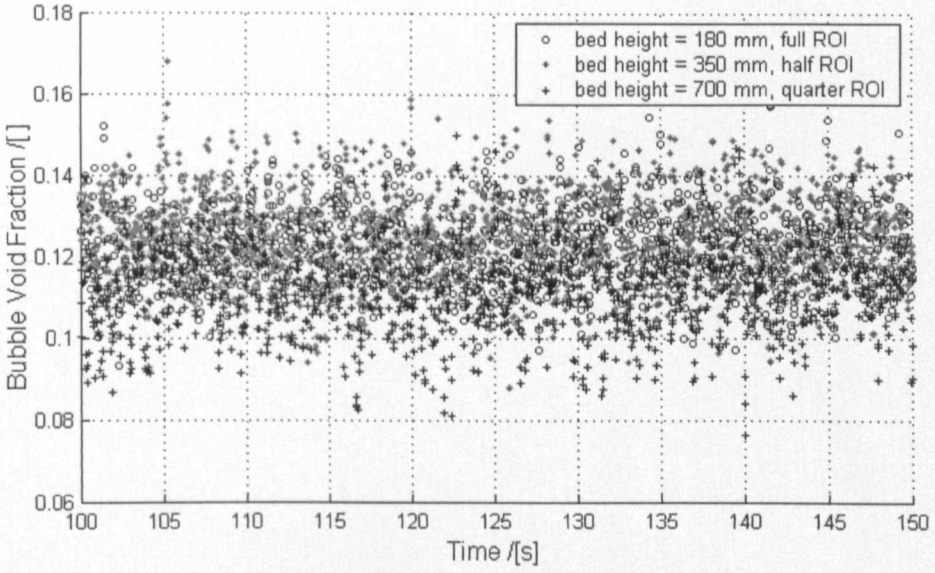

Figure 4.3.8: The BVF time series for the bed with different heights obtained for the first analysis where the BVF measurements were reasonably similar.

Bed height / [mm]	BVF mean	BVF standard deviation
180 (full ROI)	0.120	0.010
350 (half ROI)	0.122	0.012
700 (quarter ROI)	0.114	0.012

Table 4.3.2: The BVF mean and standard deviation (to 3 and 2 significant figures respectively) obtained from the distributor to 180 mm from distributor for the respective bed heights.

However, their respective BVF frequency contents were distinctively different. Presented in *Figure 4.3.9*, the Bode-scaled BVF frequency plot of the bed with the height of 180 mm has a level frequency content energy from the DC range up to approximately 2 Hz where the energy decayed at higher frequencies. The bed with the height of 350 mm recorded a slightly higher frequency energy content up to approximately 1 Hz then exhibited a mild peak up to 2 Hz, thereafter the plot decayed rapidly to conform with the decay fashion of the shallower bed (180 mm bed height) at around 3 Hz. The BVF frequency content of the bubbling process of the 700 mm-tall bed has a level energy content from the DC range up to approximately 0.2 Hz where a broad band peak developed. This plot then decays to again conform with the decay trend of the 180 mm high bed at 3 Hz.

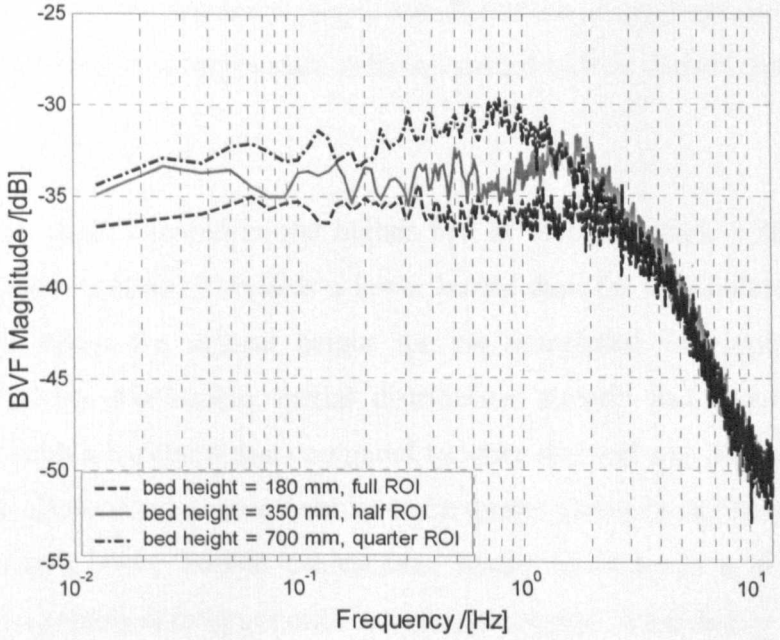

Figure 4.3.9: The Bode-scaled BVF frequency plots for beds with different heights obtained for the first analysis.

The results from the analysis demonstrate that the same region of the bed experienced changes in its dynamical behaviour as an effect of the global changes of dynamical behaviour throughout the bed when the height of the bed was altered. The break frequency changed from 2 Hz down to approximately 0.9 Hz as the bed height increased from 180 to 700 mm. A broad peak also developed. This fashion of change reflects the gradual enhancement of lower frequency activities in the bed with the increase of bed height, attribute to the interaction and the coalescence of bubbles.

Referring back to work in *Section 3.3.2*, the above-described occurrence can be related to the influence of bed height, or more accurately the bed aspect ratio, through the spatial distribution of bubbles in the bed, where the migration of regions of high bubble concentration from close to the bed walls near the distributor to the bed centre higher in the bed has been experimentally observed. The influence of bed geometry, directly determined by the change of bed height in this study is such that with a shallow bed (180 mm high), the interaction of bubbles, although it has a similar trend to that seen in higher beds, fell short of completing the final stage of migration, which is the merging of the two narrow bands of high bubble concentration regions in the bed centre at a critical bed height, due to insufficient bed height. The resulting BVF frequency content, already exhibiting the transfer of energy to lower frequency range, was due to the interaction and coalescence of bubbles that the bed could accommodate with the spatial bubble distribution profile at that bed height.

Similar behaviour was observed in the higher bed at 350 mm high, with slightly more shifted BVF frequency content towards a lower bound than for the shallow bed. The bed height was still below the critical height for the completed development of bubble migration profile, but the bubble spatial distribution already had much more tapered regions of high bubble concentration compared to when the bed was more swallow at 180 mm. This height allowed successive bubbles to be drawn closer to the bed centre than the shallow bed causing more bubble coalescence hence resulting in a farther extent of conversion of small bubbles to larger ones in that same region of the bed.

When it was 700 mm tall, the bed height exceeds the critical height required for the final stage of bubble migration profile to develop, hence the merging of the narrow bands of high bubble concentration in the bed could be seen as the spatial distribution of bubbles

tapered significantly to the centre of the bed. Consequently, bubbles were more concentrated causing successively produced bubbles to interact and coalesce more readily throughout the bed, even in the same lower portion of the bed considered in the earlier two cases, giving much higher energy content of the BVF around the lower frequency bound as seen in the figure.

Figure 4.3.10 shows the mesh plot of the bubble spatial distribution in the bed with the height of 350 mm fluidised at 51.3 mm/s above U_{mf}. The final stage of bubble migration profile was not achieved, indicated by the twin maxima of bubble concentration band at the top of the bed, both of which have undergone a tapered distortion towards the bed centre but did not merge. The critical height at which the merging of the bands was experimentally observed to be much higher than 350 mm (it was estimated to be 450 to 550 mm) from the distributor but no quantitative reasoning for this could be suggested at this point of study leaving it as a topic of interest for future studies.

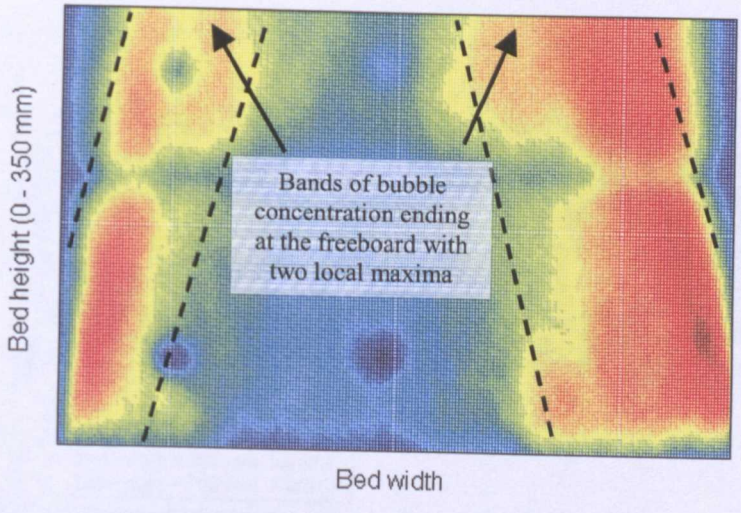

Figure 4.3.10: The mesh plot of the bubble spatial distribution acquired from a 350 mm deep bed fluidised at 51.2 mm/s superficial flow above U_{mf}. It can be seen that the twin maxima of bubble concentration remain to exist at the top of the bed for the given bed height.

4.3.3.2 *Frequency content of similar ROI (from distributor to 350 mm high) of beds of different heights (second analysis)*

Figure 4.3.11 shows the time series of BVF obtained from the beds in the second analysis. The measure of BVF on the lower half portion of the beds of heights 700 mm and 350 mm are different with the taller bed registering a lower mean of BVF values. The statistics of the BVF measurements are shown in *Table 4.3.3*. The standard deviations for the 350 mm high bed with full ROI and that of the 700 mm high bed with half ROI appeared similar.

Bed height / [mm]	BVF mean	BVF standard deviation
350 (full ROI)	0.142	0.010
700 (half ROI)	0.107	0.010

Table 4.3.3: The BVF mean and standard deviation (to 3 and 2 significant figures respectively) obtained for lower half portion of the beds from the distributor to 350 mm above the distributor for the respective bed heights.

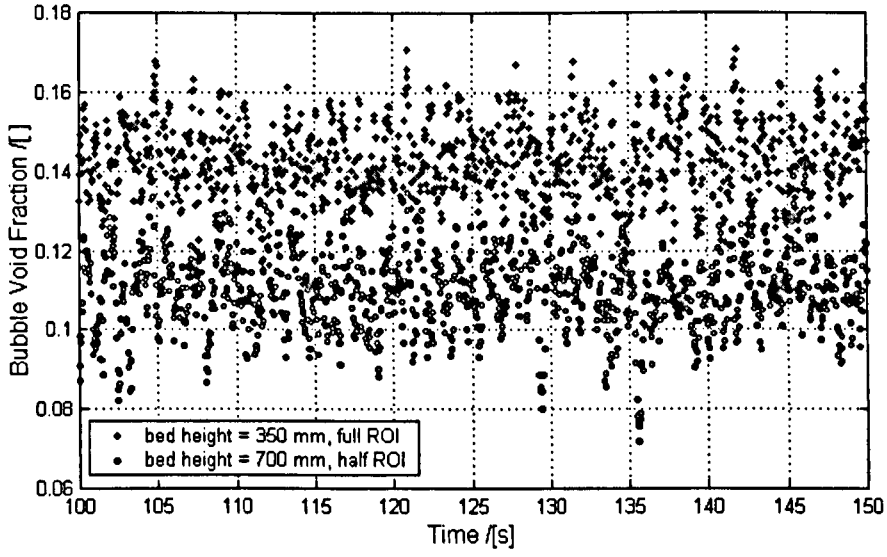

Figure 4.3.11: The BVF time series for beds of different heights obtained for the second analysis. The measurements were significantly different with the 350 mm tall bed having higher BVF values.

Shown in *Figure 4.3.12*, the Bode-scaled BVF frequency content from the 350 mm bed with full ROI is comparable with that of the half ROI acquisition of the 700 mm-high bed. Both of the plots exhibit level energy content from the DC range up to approximately 0.9 Hz where they decay in energy with increase in frequency after the break frequency.

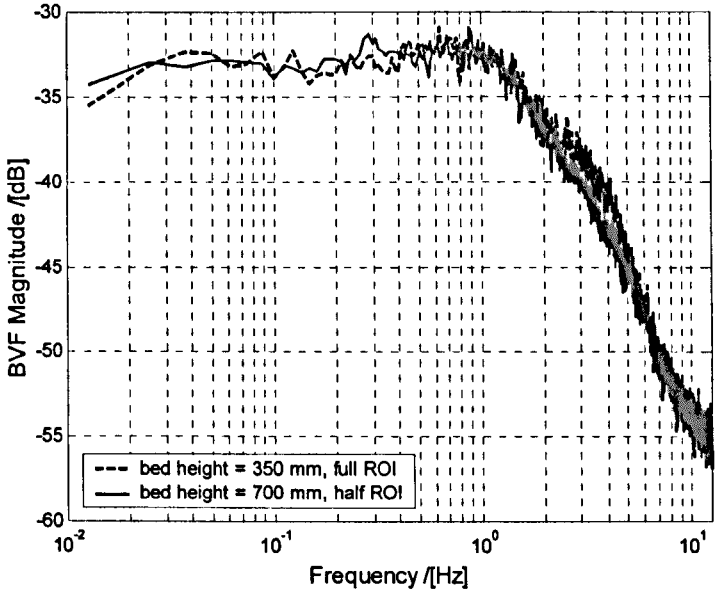

Figure 4.3.12: The Bode-scaled BVF frequency plots for beds with different heights obtained for the second analysis.

When similar portions of the beds were measured, they had comparable BVF frequency content, indicating that the dynamics of the bed in that region were similar. As they were obtained for beds of different heights, at first instance the results appeared almost contrary to those in the first analysis. However, a logical reason is that the bottom part of the bed is significantly more sensitive to changes in the bed height, reflected by the alteration of the dynamical behaviour of bubbles in that area in conjunction with the alteration of bubbling dynamics over the whole of the bed. The bottom part of the bed coincides with the regions where the bubble spatial distribution is subjected to vigorous modification with height.

The bottom of the bed, especially near the distributor, is particularly sensitive to the arrangement or distribution of bubbles higher up in the bed, as the lateral migration of bubbles at the bottom of the bed is determined by their interaction with the bubbles placed higher in the bed. This sensitivity however, is moderated with position in the bed, such that the increase of bed height after a certain critical limit does not noticeably alter the dynamics of the bubbling process on the portion of the bed below that critical height. The increase in height only allows further modification of the frequency content to continue above that critical point with the occurrence of more subsequent coalescence. The consequent change in frequency content due to activities in this region of the bed (from the critical height upwards) is superimposed onto the frequency content of portion below the critical height, if this area is considered in the ROI of the BVF measurement as well.

4.3.3.3 *Frequency content of the full ROI of beds of different heights (third analysis)*

To support this explanation, the third analysis was therefore devised. The BVF frequency content obtained for the bed with the height of 700 mm at full ROI were compared with that of the 350 mm and 180 mm tall beds both also with full ROI acquisition of BVF. *Figure 4.3.13* presents the time series of all three obtained BVF measurements in the analysis. The mean and standard deviation of the BVF measurements are listed in *Table 4.3.4*. The BVF mean of the 180 mm high bed is slightly lower than the other two beds while the 700 mm bed had a larger standard deviation of BVF.

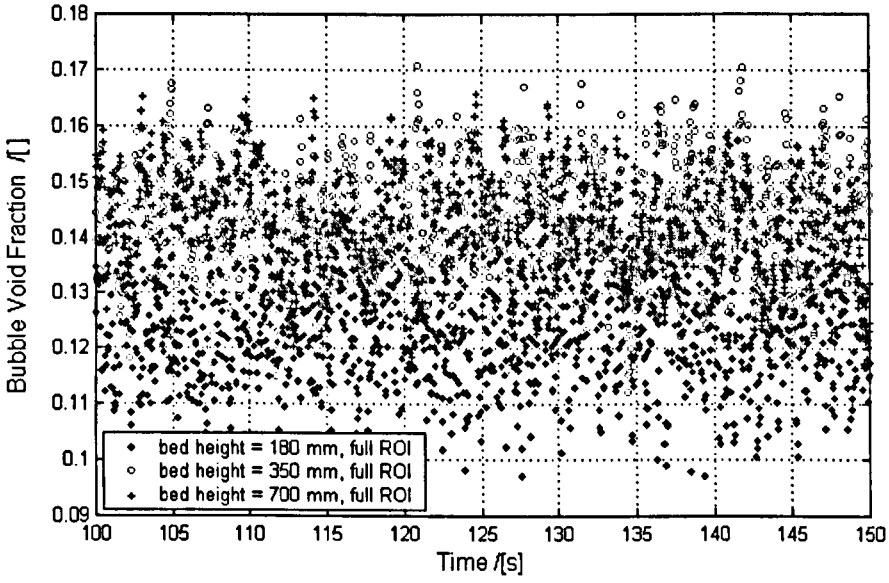

Figure 4.3.13: The BVF time series for beds of different heights obtained for the third analysis.

Bed height / [mm]	BVF mean	BVF standard deviation
180 (full ROI)	0.120	0.010
350 (full ROI)	0.142	0.010
700 (full ROI)	0.142	0.012

Table 4.3.4: The BVF mean and standard deviation (to 3 and 2 significant figures respectively) obtained for three different bed heights all with full ROIs.

In the frequency domain, all the BVF measurements, seen in *Figure 4.3.14*, are different such that the shallow bed was shown to have the highest break frequency at approximately 2 Hz, from an initial level content of energy over the lower band of frequencies. The 350 mm bed exhibits a slightly higher level low frequency energy content breaking at about 0.9 Hz while the 700 mm bed decayed off at the break frequency of 0.3 Hz with comparatively the highest low frequency magnitudes.

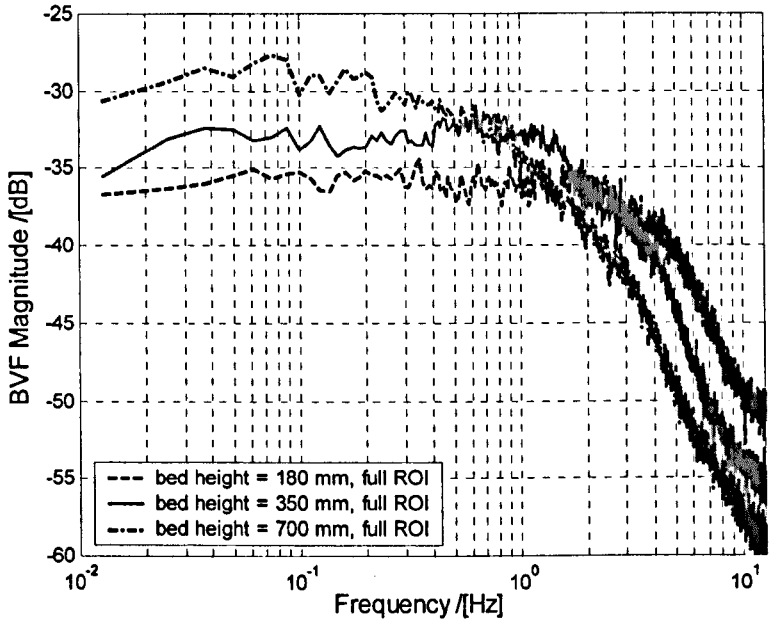

Figure 4.3.14: The Bode-scaled BVF frequency plots for beds with different heights obtained for the third analysis.

The results from the analysis appear to support the proposed explanation given in conjunction with the observation done in the second analysis. As the bed height was increased from 180 mm to 350 mm and then finally to 700 mm, the break frequency reduced while the low frequency range magnitudes gradually increased. This was the result of bubble interaction that affected the bubble spatial distribution in the bed, which is essential in governing the interaction of successive bubbles and hence the bubbling dynamics of the bed. At the bed height of 180 mm, the modification of bubble distribution profile was at an early stage and would be subjected to more modifications with the extension of bed height to 350 mm.

Experimental observations suggested that its height at 350 mm was reasonably close to the critical value, which is the reason its Bode-scaled BVF frequency plot has close

resemblance to that of the 700 mm tall bed - a height at which the bed would have already achieved the final stage of bubble distribution profile. The higher energy content towards the lower frequency band for the 700 mm tall bed suggested the integration of more high magnitude low frequency events such as those associated with further coalescence of bubbles above the critical height. Any further bubbling activities in the bed above the critical height only affected and modified the dynamics of the bed there, leaving the rest of the bed relatively unaffected dynamically.

A deduction is that the bed height has to exceed the critical height for the complete bubble spatial distribution profile modification to be achieved, otherwise the extent of flow into the bed appears to be the determinant of the state of the modification. At low flow where bubbles are small and scarcely populate the bed, there are only moderate bubble interactions and coalescences; therefore the consequent bubble spatial distribution profile modification is under-developed. At higher flow rates, bubbles are larger and more densely populate the bed with significant bubble interaction and coalescence taking place modifying the distribution profile such that with the given bed height, complete modification could be achieved.

Therefore, referring back to *Figure 4.3.6*, the Bode-scaled BVF frequency plots for the lower flow rates such as those at 12.8 and 25.6 mm/s are significantly different from each other as well as with the higher flow rates. However, at higher flow rates beginning at 51.3 mm/s onwards, the shape of the plots are relatively similar with only subtle differences associated with the changes in the bubbling activities occurring above the critical height as the flow further increases.

4.3.4 The influence of fluidisation abnormality on the bed dynamics

An abnormality occurring in a regular freely bubbling process leads to a possible regime change that affects the dynamics of the bed. Abnormality is associated with a change in the behaviour of bubbles in the bed in the ways of their interaction and coalescence normally expected in a typical freely bubbling bed. To simulate this during a freely bubbling process, the single nozzle at the centre of the bed distributor was allowed to issue additional gas into the bed in excess of that issued through the porous distributor.

The simulation was done by having the single nozzle and the porous plate distributor plenum connected to the similar air supply such that the single nozzle initially issued on average the same flow into the bed as the porous plate. From initial freely bubbling condition, the nozzle flow was increased so that more of the total gas supply was issued into the bed through the nozzle.

The stream of bubbles from the nozzle acted as an attraction to which other bubbles issued successively from the nozzle as well as elsewhere in the bed are attracted. The effect was a more pronounced concentration of bubbles at the centre of the bed compared to the profile of bubble distribution of a freely bubbling bed, replicating a localised defluidisation situation near the walls of the bed. A large degree of bubble coalescence and short-circuiting took place and the overall dynamics of the bed totally altered. The measure of BVF for this was logged, the time series and corresponding Bode scaled BVF spectra plots are shown in *Figure 4.3.15*.

The BVF time series shown in *Figure 4.3.15(a)* for both the cases gave the BVF mean and standard deviation as shown in *Table 4.3.5*. Shown in *Figure 4.3.15(b)*, the Bode-scaled BVF frequency plot for the abnormal bed is different from that of the normal bed. It has slightly higher energy over the low frequency range, decaying slightly later than the normal bed at approximately 0.6 Hz instead of at 0.4 Hz. The two plots coincide close to about 4 Hz. The higher break frequency for the abnormal bed suggested quicker bubbling dynamics probably because of the faster travelling larger bubbles and the more rapid bubble coalescence occurring.

Tests	BVF mean	BVF standard deviation
Normal bubbling bed	0.062	0.0057
Abnormal bubbling bed	0.059	0.0076

Table 4.3.5: A summary of the BVF mean and standard deviation (to 2 significant figures) of the normal and abnormal bubbling bed, both fluidised above incipient condition at 25.6 mm/s superficial flow.

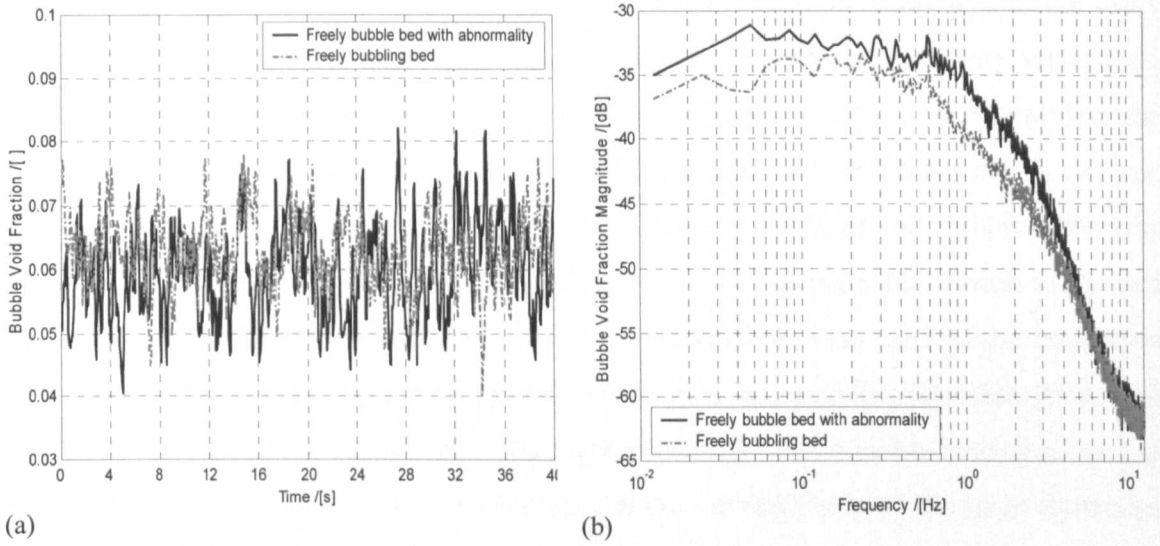

Figure 4.3.15: (a) the time series of BVF and (b) the Bode scaled spectra plot for the bed normally bubbling and with abnormality present, both cases with a total flow rate of 25.6 mm/s above U_{mf}.

The test shows that this technique could detect a change in the bubbling dynamics of the bed caused by an internal change of bed properties with a constant gas flow into the bed. However, the differences in the two plots shown in *Figure 4.3.15(b)* are subtle and may not be readily detected if the abnormality was milder. This is again probably the artefact of the type of characterisation measurement used, i.e. measuring the BVF using the imaging analysis technique.

4.4 Other applications of frequency domain techniques in the study of fluidisation

With the proper procedures and methods established for the interpretation of the BVF frequency domain plots, the identification of the essential dynamical features in the plots allowed the fundamental physical behaviour of the bed associated with the presence of bubbles to be corresponded to the instantaneous state of the process. There is great potential for the techniques to be a useful tool to assess the condition of the fluidisation process in relation to the process quality. Distinct features in the plot represent certain characteristics unique to a process condition and when implemented in-situ, changes to the desired process state can be detected with this technique in real-time and the appropriate action can be taken when this takes place.

However, there are also other forms of applying frequency domain techniques to the study of the fluidisation process with the fundamental aim of understanding the underlying dynamics. *Chapter 5* shows how the frequency domain technique is used to validate the dynamical similitude of the experimental bed with the simulated bubbling bed developed in the research. A simulation and modelling programme of the bubbling fluidised bed was developed and a means to verify its ability to replicate the experimental version of the bed was required. For this reason, the frequency domain analysis was used in the validation work where the frequency content of the BVF time series obtained from the simulation was compared with that of the experiment. The method proved to be a viable analytical tool as already being used by other researcher for comparing the similitude of the hydrodynamics of the model and prototype beds (Brue & Brown, 2001).

In *Chapter 6* and *Chapter 7*, the study of the dynamical behaviour of a simple or idealised bed as well as the development of a theoretical model of the bubbling process conducted mostly in the frequency domain, has applied knowledge conceived in this chapter. *Chapter 8* describes the system identification study carried out on the experimental bed via the use of Bode diagrams on the frequency response of the bed subjected to various modes of excitation. Through this, the bed transfer functions for various system identification tests were obtained, its dynamical behaviour studied and subsequently, controls of the bed could be designed based on this data.

4.5 Conclusion

The implementation of frequency domain analysis methods on the study of the bubbling regime carried out on the measure of BVF from a planar bed has been described. Techniques and procedures to appropriately interpret the frequency plots have been established with the adaptation of the Bode diagram and the Bode-scaled frequency plot, shown to be useful tools in enhancing the ability to identify the dynamical features in the plots. The frequency domain analysis demonstrated that the differences in dynamical behaviour of the bed at different conditions that may not be readily detected via statistical measurements of the BVF time series could be significantly identified and distinguished.
The technique was used to study the dynamics of the bubbling process at different flow rates into the bed as well as for beds with different geometry and briefly, on the changes in

the bed fluidisation regime due to abnormality during normal operation. The technique was shown to be able to detect the differences of bed dynamics for these conditions. The salient features in the frequency plots corresponded to the physical behaviour in the bed associated with the activities of the bubbles, helping to describe the fundamental workings of the bed. Through the studies carried out, the bed was described as a dynamic mechanism through which low energy full-bandwidth activities introduced into the bed at the distributor are gradually converted into high energy activities of lower frequency range in nature via coalescence and bubble size growth.

The bubbling activities that affected the overall dynamical behaviour of the bed inferred by the measure of BVF were also shown to be flow rate as well as spatially dependent. A critical bed height was identified as a crucial criterion in determining the development of the bubble distribution profile in freely bubbling beds, which, if the bed height exceeded, would create a condition of relatively constant bed dynamical behaviour for portion of the bed below that critical height. Activities occurring above the critical height would be an added effect to the overall dynamics of the bed without imposing the rest of the bed to any further significant dynamical changes. There were significant changes in bed dynamics with an increase of flow from close to incipient condition but this gradually moderates after certain critical bubbling flow.

Chapter 5

The simulated bubbling fluidised bed

5.1 Introduction

A two-dimensional fluidised bed sensing and monitoring instrument using image analysis techniques was developed and detailed in *Chapter 2* for the characterisation, monitoring and control of bubbling fluidisation of a gas-solid fluidised system. To support empirical findings and facilitate safe pre-experimental test runs, a software version was developed in the MATLAB environment. This chapter describes the formulation and development of the simulation of the bubbling fluidised bed, detailing the simulation engine and the bubble interaction model used. This software allows operating conditions such as bed dimensions, fluidisation characteristics, flow rate settings and bubble interaction models to be varied. The simulation uses kinematic laws to regulate bubble motion and interaction in the bed. This allows the adaptation of the well-known and widely applied Clift & Grace model of bubble interaction (Clift & Grace, 1970, 1971a, 1971b) in the simulation.

The simulated version of the bubbling fluidised bed helped to save a large amount of experimental time and prevented any unnecessary wear and tear or even damages to the experimental equipment. It also provided a convenient environment to try out, test and run methods and ideas before bringing them to the experimental rig. It also provided a virtual environment within which certain effects or parameters of the process could be investigated without the influence of other parameters that are not important or that make analysis difficult.

The ability to replicate the experimental version of the bed acts as a mechanism to gauge the extent to which the process is understood. It enables the identification of the key

features in the fluidisation process and how their presence affects the working of the process.

5.2 Introduction to MATLAB and SIMULINK

MATLAB, a software package developed by The MathWorks Inc., is a graphic orientated, dynamic numeric mathematical solver. MATLAB also includes the SIMULINK toolbox package, which is a programme for modelling, simulating and analysing dynamic systems. SIMULINK, like MATLAB, is graphic orientated, and the user can construct the dynamic system by dragging and linking the appropriate block functions. The dynamic nature of SIMULINK enables it to solve systems with differential equations efficiently. It supports linear and non-linear systems, modelled in continuous time, sampled time, or a hybrid of the two. SIMULINK can be used to investigate the behaviour of a wide range of real-world dynamic systems, such as electrical circuits, shock absorbers, brake systems, and many other electrical, mechanical, and thermodynamic systems. SIMULINK consists of a comprehensive block library of sinks, sources, linear and non-linear components, and connectors. New customised functions could also be written by the user using the 'S-function' building block. This feature was used to tailor the simulation engine in the SIMULINK environment, as explained in the following section.

5.3 Development of simulation engine and bubbling bed model

5.3.1 Simulation engine

5.3.1.1 Simulation programme

For this study, SIMULINK was used to execute and regulate the simulation. An S-function block function was used to link the MATLAB scripts (*.m files) that contain the codes for the bubbling bed simulation engine. A separate script regulated the bubble interaction model. *Figure 5.3.1* shows a snapshot of the simulation programme along with an image of the bubbling bed in operation.

The simulated bed was always assumed to be incipiently fluidised when there was no supply of gas surplus. The simulated bubbling bed was designed to simulate the dynamics and behaviour of a group B powder bed of the Geldart powder classification (Geldart, 1973). Introduction of more gas into the system results in the formation of bubbles at the distributor. A porous plate distributor was simulated by allowing bubbles to form randomly with uniform distribution across the bed width. Bubbles were produced within a certain given range of sizes also in a uniformly random distribution probability. The default bed geometry was similar to that of the experimental bed: 710mm tall, 500mm wide, and 13 mm deep. In some simulations, the bed height could be adjusted to simulate a tall bed.

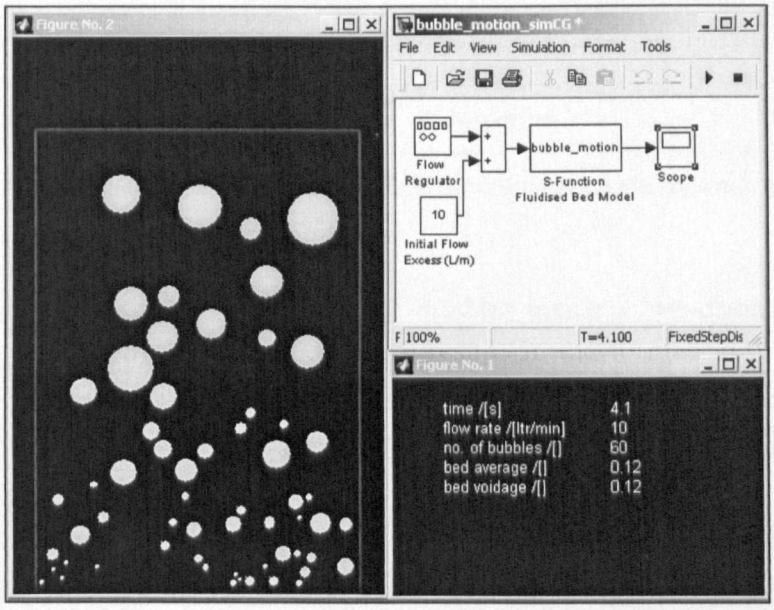

Figure 5.3.1: The snapshot of the MATLAB and SIMULINK toolbox simulation interface accompanied by an animated simulation of the bubbling bed.

The simulation engine simulated the bed using kinematic laws to describe the motion of the bubbles. Displacement, velocity and acceleration properties governed the dynamic motion and position of every bubble created in the bed. The programme simulated each bubble from introduction into the bed until its expulsion from the freeboard. The bubbles were modelled as circles in a gas-solid fluidised bed, facilitating simulation and computation efforts. These bubbles maintained constant circular geometry throughout the simulation. Other researchers (Miwa et al., 1967; Korte et al., 2001) also simulated bubbles with circular shapes in their work. The circular shape was crucial during bubble interaction and coalescence, as the simulation engine required the information of the location of the

bubble roof or nose, void and wake. Therefore, a bubble was modelled by a circle constituted by the bubble void and wake as shown in *Figure 5.3.2*. The void is an area clear of particles and the wake is an area of particle collection at the bottom of the bubble, an artefact of the interaction between gas and particles.

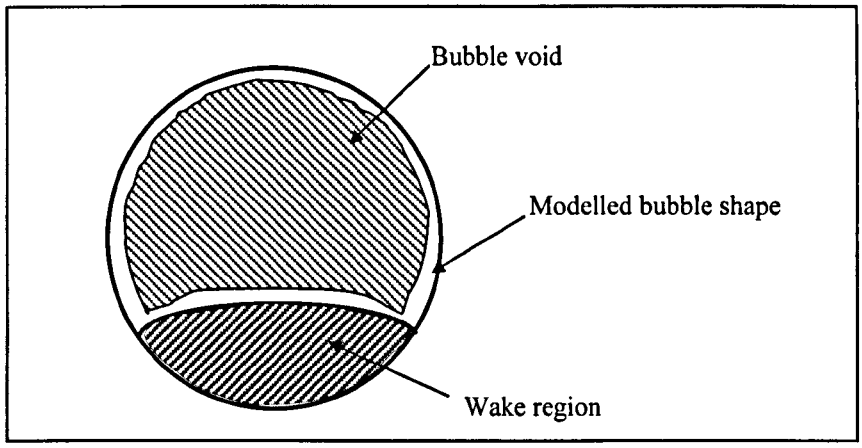

Figure 5.3.2: The modelled bubble circular shape with its constituents, the void and wake.

Pyle & Harrison (1967) worked on the rise of bubbles inside a two-dimensional bed and produced an empirical relationship between bubble rise rate, v_b and bubble projected area, A_b via

$$v_b = 15.9 A_b^{1/4} \quad \text{[cm/s]} \tag{5.1}$$

The mean velocities of single bubbles analysed in the authors' experiments agreed with (5.1) to within 1% although instantaneous velocities varied widely about this mean. Clift & Grace used (5.1) to calculate the isolated rise velocity. From the work of Rowe & Partridge (1962) and Toei et al. (1965), Clift & Grace assumed that the bubble particle wake occupies approximately 24% of the enclosing circle. The authors reported that the assumption predicted the mean radius of the circumscribing circle over a complete range of bubble sizes used to within approximately 8% when compared to the measurements made on films of isolated bubbles from their equipment.

As approximately 75% of the modelled bubble area is occupied by the bubble void or bubble projected area, the relationship between bubble rise velocity, v_b and modelled bubble diameter, d_{bm} in (5.1) becomes

$$v_b = 1.39\sqrt{d_{bm}} \quad \text{[m/s]} \tag{5.2}$$

Davies & Taylor (1950) described the rise velocity of isolated bubble in their work with air bubbles in nitrobenzene and water. Based on the principles of pressure equilibrium, which made the top surface of the bubble spherical, they related the rate of rise of single bubble to the radius of curvature at the nose of the bubbles, r_{bn}

$$v_b = K_b\sqrt{gr_{bn}} \tag{5.3}$$

with K_b found to be typically 0.67 for gas bubbles in liquids. Davies & Taylor's work has been proven to be fundamentally sound when relating the rate of rise of air bubbles in liquid to the pressure distribution around the front of the bubble determined by the size of its spherical front. Based on their work, other researchers have empirically determined values for the coefficient K_b correlated with the different ways of measuring the bubble diameter in fluidised beds. A common way is to take the diameter of the sphere having the same volume as the spherical cap bubble, $d_{b,ev}$ and relating that to its rise velocity such that

$$v_b = K_b\sqrt{gd_{b,ev}}$$

With this, there is an exhaustive list of K_b values for different fluidised systems as shown in Kunii & Levenspiel (1969). These vary between 0.57 and 0.85.

For a two-dimensional bed, the K_b value was empirically determined to be 0.5 by Stewart (1968). Therefore, relating v_b to r_{bn} produces

$$v_b = 0.5\sqrt{gr_{bn}} \tag{5.4}$$

The relationships of bubble rise velocity with some bubble size parameter were generated from empirical data that are scattered in nature, due to the periodic changes in the bubble shape, as reported by Toei et al. (1969) and the variations in the lateral position of the bubbles of up to 20% of the bubble radius. Although the instantaneous bubble velocity may vary significantly, the mean velocity agrees closely with the derived relationships. Due to the difficulty to accurately determine the value for the K_b coefficient empirically, the differences in the treatment of bubble rise rate used in the simulation in (5.2) and that of (5.4) was assumed acceptable.

5.3.1.2 *Relationship between bubble cloud and void in bubble model structure*

In a two-dimensional bed, the excess gas introduced into the bed clears a portion of the bubble of particles, referred to as a void, while concealing the remaining portion in an area known as the cloud. The cloud is the boundary defining a bubble that encloses the volume of gas associated with the bubble. In the cloud, the gas forms a vortex that flows upwards through the void at the centre of the bubble that offers negligible resistance, then circulates around the sides of the bubble due to a stagnation point at the bubble nose. The persistence of the vortex and hence the existence of the bubble is due to the positive feedback effect created by the evacuation of the area in the emulsion phase from particles such that more gas would flow through and continuously vacating the bubble rise path of particles.

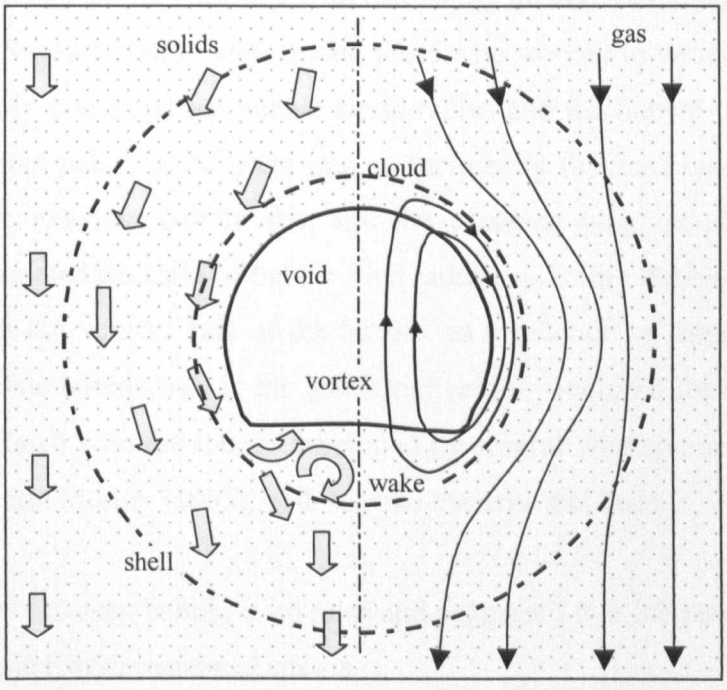

Figure 5.3.3: The diagram shows the structure and flow around a bubble in a fluidised bed, with the terminology used to describe the different parts of the bubbles.

When the gas in a bubble rises faster than the interstitial gas flow, the flow field forms a closed streamline around the bubble and the gas becomes divided into two phases inside and outside the closed streamline. The presence of the bubble disrupts the flow field in the emulsion phase such that an expanded shell of particles exists that encloses the bubble and the area within the emulsion phase affected by the presence of the bubble. The void fraction within the shell is considerably higher than in the rest of the emulsion phase

remote from the bubble, undisturbed by the presence of the bubble. The shell of a bubble is much larger than the bubble and was observed by Yates et al. (1994). Relative to the bubble, solids are pushed aside, running along the side of the bubble, then some are either circulated in the wake region of the bubble (Rowe et al., 1964) or left behind in the path of the bubble (Rowe et al., 1964). *Figure 5.3.3* shows the description of the structure of a typical bubble in a fluidised bed with several of the standard terms used throughout this dissertation.

In the planar bed, the proportion of bubble void occupying the enclosing circle is bubble size dependent and therefore flow rate dependent. Typically for a small bubble, a larger proportion of the gas that constitutes that bubble would be 'hidden' in its cloud, hence making the bubble void appear smaller. When the bubble is larger, more of the gas in the bubble becomes visible as the void area with less being 'hidden' in the bubble cloud. Rowe et al. (1964) and Stewart (1968) were among those who worked to verify this observation. They independently compared the bubble cloud radius and the bubble void radius. Rowe and Stewart injected pulses of NO_2 gas into an incipiently fluidised two-dimensional bed and observed the resulting bubble size and the accompanying cloud surrounding the bubble. They correlated the ratio of bubble void radius, r_{bv} to the bubble cloud radius, r_{bc}, both measured on the vertical axis of the bubble, as a function of the ratio of the rising velocity of an isolate bubble, $v_{b\infty}$ to the interstitial velocity required for incipient state v_{mf}. These were correlated with the theory developed by several workers; amongst them were Davidson (1961) and Murray (1965), both for two-dimensional beds.

Davidson's theory assumes bubble is circular and suggested that the ratio of bubble cloud to void radius in the two-dimensional case is

$$\frac{r_{bc}}{r_{bv}} = \left[\frac{(\alpha_b + 1)}{(\alpha_b - 1)}\right]^{1/2} \tag{5.5}$$

where $\alpha_b = v_{b\infty}/v_{mf}$. While Davidson's theory appeared simple to implement, it was shown that it overestimated the actual penetrations. Murray came forth with a more accurate but more cumbersome theory to use, taking into account of the gas momentum and therefore bubble shape, hence proposing that

$$\frac{S^2 + 1/2S}{S^2 - 1} = \alpha_b \tag{5.6}$$

where $S = r_{bc}/r_{bv}$. The relationships established in (5.5) and (5.6) plotted in *Figure 5.3.4* demonstrated good agreement between the respective proposed relationships.

The graph in *Figure 5.3.4* has appeared in numerous references (Rowe et al., 1964; Stewart, 1968), but in order to illustrate more clearly the relationship between cloud and void ratio with flow rate, *Figure 5.3.5* is produced. The plot in *Figure 5.3.5* implies that the ratio of bubble void volume to the total gas volume constituting the bubble increases with bubble size, supporting the observation presented earlier regarding bubble void size variation with bubble size. The variation of void with bubble size in the simulation was shown not to significantly affect the estimation of bubble rise velocity, hence for simplification and ease of computation, the coefficient in (5.2) can be constant for all bubble sizes. A maximum variation of up to 12% was reported, however, the dynamical behaviour of the simulated bubbling process due to variation in determining bubble rise velocity was not significantly affected.

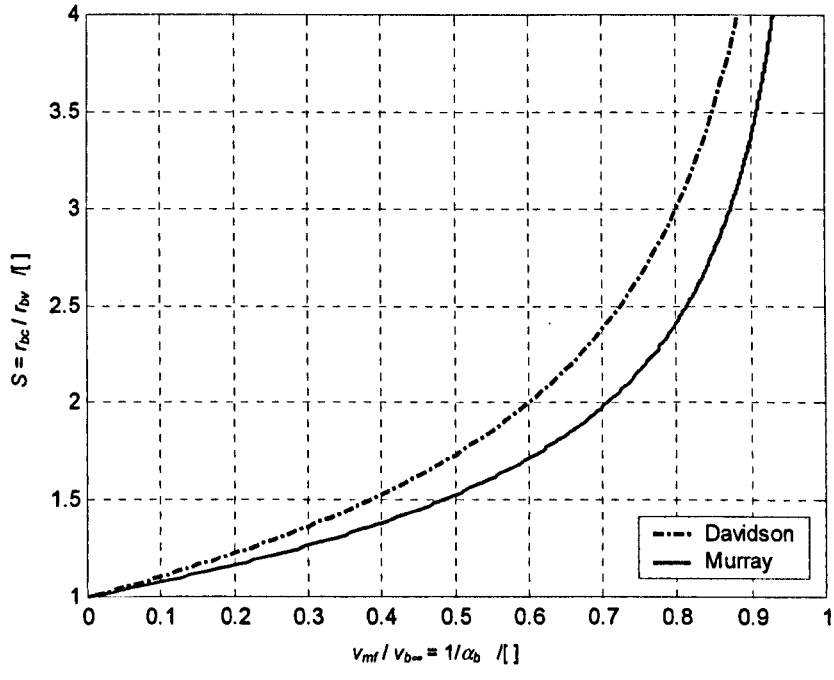

Figure 5.3.4: The graphs are of the Davidson and Murray's model of r_{bc}/r_{bv} plotted against $v_{mf}/v_{b\infty}$

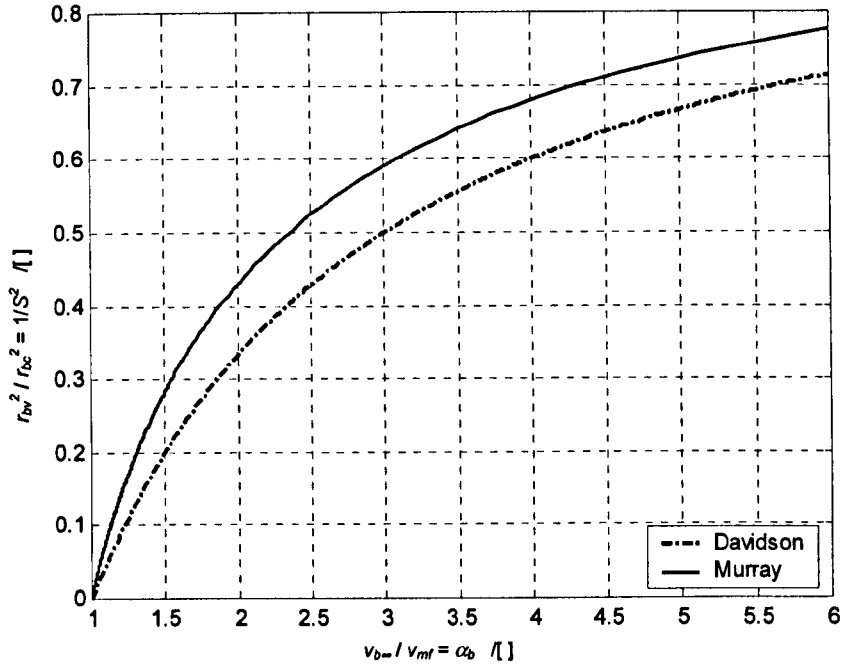

Figure 5.3.5: The plots show the relationship between r_{bv}^2/r_{bc}^2 and $v_{b\infty}/v_{mf}$ for the Davidson and Murray theoretical models for two-dimensional beds.

Figure 5.3.6 shows the modified version of the bubble model defined in the simulation. The modelled circle with diameter, d_{bm} was constituted by the bubble void and wake similar to previous model shown in *Figure 5.3.2*. In addition, as the bubble void area varies with bubble size, the remaining part of the circle where the 'hidden' gas resides was the bubble cloud. The treatment of varying the bubble void area with bubble size was essential as will be shown in *Section 5.4* for the characterisation of the process.

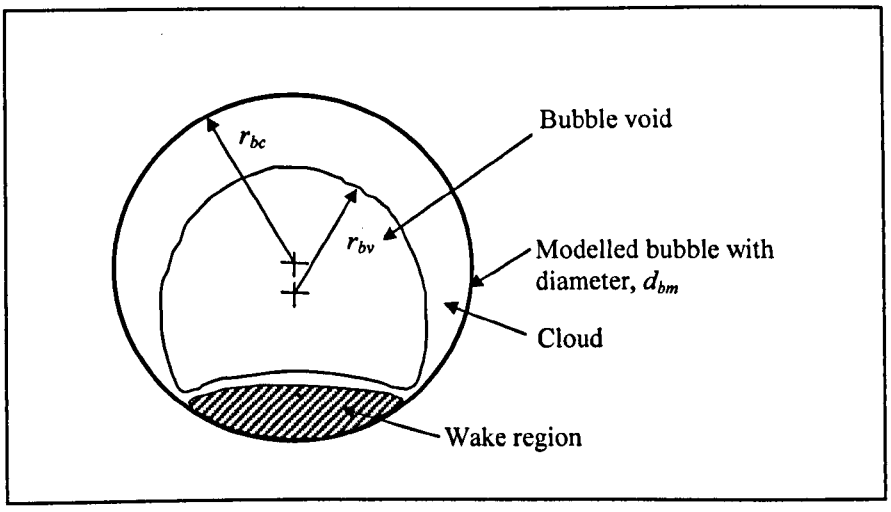

Figure 5.3.6: Assumed bubble model used in the simulation

5.3.1.3 *Bubble growth and coalescence*

Typically, bubbles in fluidised systems expand when they rise up the bed. Bubble expansion with height in the bed was also simulated with the relationship between bubble diameter, d_b and height above the distributor, h_b given by the empirical relationship derived by Kunii et al. (1967) for two-dimensional beds. The estimation of bubble diameter with height due to growth based on the work by Kunii et al. gives

$$d_b = d_{bi} + 0.0034 h_b \tag{5.7}$$

with d_{bi} as the bubble initial diameter where for simplicity, the empirical relationship was assumed to be linear. The consequences of this linear approximation of bubble growth was experimentally justified and considered acceptable. (5.7) was not explicitly expressed in Kunii et al. (1967).

When a bubble was introduced into the bed, it was assumed to only possess a vertical velocity component with magnitude corresponding to its instantaneous size. The exit of a bubble from the bed freeboard was assumed to be gradual up to the point when the bubble centre coincided with the freeboard height. Thereafter, the bubble instantaneously exits the bed by the next time step. The bubble shape does not change in the simulation regardless of circumstances; however, in real fluidised beds bubbles are more circular when small and elliptical when large. They also experience elongation just before coalescing with leading bubbles, or flattening just before coalescing with trailing bubbles (Toei et al., 1967; Shichi et al., 1968; Clift & Grace, 1970). Therefore, there will be differences in the bubble interaction behaviour in the simulation compared to the real world.

In the simulation of bubble coalescence, the centres of the coalescing pair of bubbles need to be within 80-90% of the sum of their radii. Technically, the bubbles would appear to be overlapping each other but visually as well as dynamically this situation portrays a realistic coalescence process. This condition allows the simulated coalescence process to take place over a time interval of several time steps, initiating the moment the bubbles are at distance equals to the sum of their radii from each other. This is a rather more realistic dynamical behaviour compared to when the process was assumed to take place within one time step which is the conventional approach used by other researchers (Miwa et al., 1972; Korte et al., 2001). Their approach assumes that the coalescence process takes place instantaneously upon initiation with bubble edge contact and is completed at the next time step.

Farrokhalaee (1979) proposed the relationship in (5.8) to estimate the time from bubble wake entry to the completion of the coalescence process.

$$t_c = \frac{R1^2}{0.8 v_{b\infty 1} R2}\left\{\left[1-\left(\frac{R2}{R1}\right)^2\right]-0.67\right\} \tag{5.8}$$

where $v_{b\infty 1}$ was the rise velocity of the leading bubble in isolation. (5.8) assumes that the trailing bubble is drawn into the leading bubble by the circulation of the particulate phase in the wake of the leading bubble at a characteristic velocity proportional to $v_{b\infty 1}$. (5.8) was found to be consistent with available results for both two- and three-dimensional bubbles.

As there was no clear indication in the literature of what *R1* and *R2* actually represent in terms of the bubble radius, it was assumed they are the interacting bubbles' cloud radii, consistent with the parameter of the modelled bubble in the simulation. This would still give a reasonably good approximation. The emphasis was not to obtain the correct relationship from (5.8), but only to adequately estimate the order of coalescence time the simulation had to replicate. The analysis with (5.8) produced a mesh plot shown in *Figure 5.3.7* for two interacting bubbles of sizes *R1* and *R2* ranging between 0.01 to 0.07 m. This analysis reassured that the steps taken to account for bubble coalescence time in the simulation was reasonable compared to when a unit time step process duration was used.

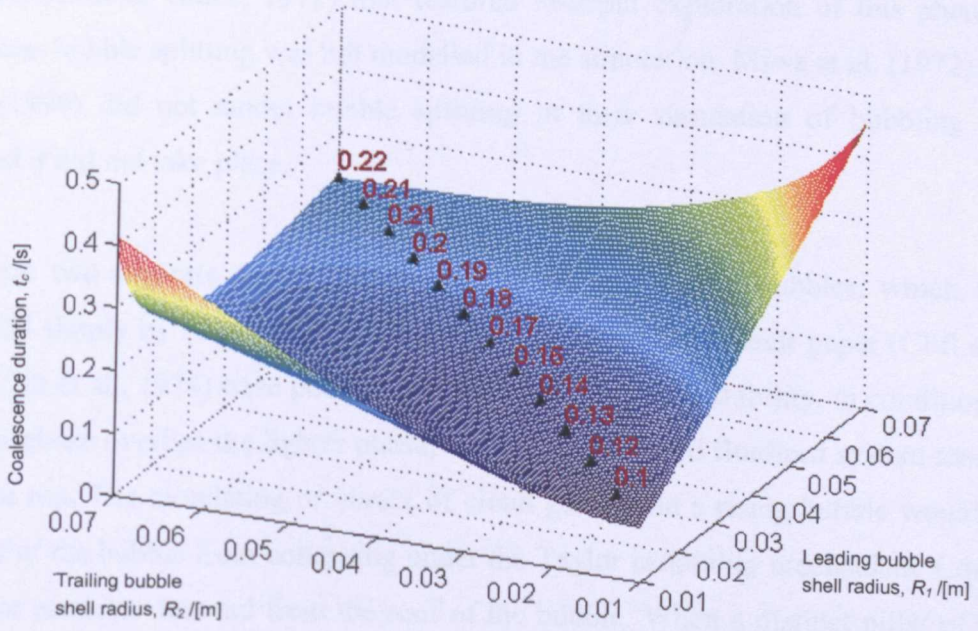

Figure 5.3.7: The estimate of coalescence time involving trailing and leading bubbles of different size (cloud radius) combinations as proposed by Farrokhalaee (1979)

The newly formed bubble, product of the coalescence process, was assumed to have the diameter of a circle with the equivalent area of the total area of the two coalescing bubbles. There have been studies (Clift, 1970; Grace, 1971; Grace & Venta, 1973) on the size of the bubble void resulting from the coalescence of two bubbles, stating that there will be an increase of between 10% to 20% of the total size of the two bubbles. The total volume growth typically reaches 20%-30% during coalescence and reduces by about 10% in the final stages of coalescence. The magnitude of this size increase can not be properly explained by hydrostatic pressure change and there are yet adequate theoretical attempts to explain these changes. In the simulation, the centre of the new bubble from coalescence of two bubbles was assumed to coincide with the centre of the leading bubble. This accounted for the 'jump' in the new bubble height as the trailing bubble accelerated towards the leading bubble during the coalescence process, projecting its portion of gas further up the bed, hence forming a higher roof position for the new bubble.

5.3.1.4 Bubbling features not modelled in the simulation

When a bubble becomes unstable and cannot maintain its shape, the bubble splits or breaks into multiple children bubbles. This is still not properly understood and there is limited literature (Clift & Grace, 1972) that featured in-depth exploration of this phenomenon. Therefore, bubble splitting was not modelled in the simulation. Miwa et al. (1972) and Lim et al. (1990) did not model bubble splitting in their simulation of bubbling bed and assumed it did not take place.

There are two separate causes that mechanise the splitting of bubbles, which could be identified simply by the location of initiation. Clift & Grace in their paper (Clift & Grace, 1972; Clift et al., 1974) have pointed out that due to Taylor instability, in conditions where a denser phase overlies the lighter phase, bubbles in gas-solid fluidised system tend to split from the top. The circulating or vortex of cloud gas within a rising bubble would prevent the roof of the bubble from collapsing under the Taylor instability mechanism. Commonly, pillars of particles descend from the roof of the bubble. When a distinct pillar of particles reaches the bottom of the bubble before the root of the pillar is swept around to the bubble equator, bubble splitting will initiate producing two children of equal or different sizes.

A second mechanism of splitting with which bubbles split from the rear could also occur in the bed and is due to the entrance effect or pulsation of gas to form bubbles. With sufficient momentum, the wake particles penetrate the bubble and reach the roof, hence splitting the bubble from the rear. This phenomenon could be readily observed in the experimental planar bed during the pulsation of gas into the bed to generate single bubbles, with an incipiently fluidised emulsion phase.

The re-coalescence of children bubbles, which often occur almost instantly after the splitting of a parent bubble, was observed by Rowe et al. (1964). Harrison et al. (1961) suggested that the rate of bubble splitting in fluidised beds is dependent on the gas velocity inside the bubble which could probably explain an expected higher rate of bubble splitting in planar beds (Judd, 1965). Bubble splitting gives rise to smaller bubbles and therefore directly resulting in a maximum bubble size in the planar bed. Bubble splitting was not modelled in the simulation currently and might therefore affect the dynamical comparison of the simulation with the experimental bed.

Other activities taking place in a real bubbling fluidised bed include bubble shape and size fluctuations, disappearance and reappearance and slugging. In a bubbling bed, a bubble would experience both size and shape fluctuations due to vortex shedding or periodic wake growth (Rowe & Partridge, 1962) as well as other local influences of the emulsion phase. This effect was not possible in the simulated bed. In addition, the extent a bubble void is visible in the bed also fluctuates time to time depending on its size. This phenomenon typically involves bubble of the smaller size range. As it travels up the bed, exchange of gas between it and the emulsion phase fluctuates in quantity such that the bubble appears to disappear or dissolve into the emulsion phase where in actual case it still exist. In another instance, there might be a fluctuation of increased influx of gas into that bubble, increasing its size hence rendering it more visible spanning across the depth of the two-dimensional bed. This phenomenon again could not be modelled properly with the lack of knowledge and hence, did not occur in the simulation. Slugging of bubbles was also not modelled and simulated in the simulation. Slugging behaviour of bubbles is the subsequent regime of fluidisation with high flow rates and is therefore not possible to simulate as the Clift & Grace bubble interaction model was designed to operate within the freely bubbling regime.

5.3.2 Bubbling bed – bubble interaction model

The Clift & Grace bubble interaction model has been applied in the simulation to simulate the behaviour of bubble in a two-dimensional gas-solid fluidised bed. Clift & Grace's work in 1970 and 1971 (Clift & Grace, 1970, 1971a, 1971b) was based on potential flow theories. Rowe & Partridge (1962) showed that the motion or flow field outside the bubble and wake could be approximated well by potential flow around a cylinder or sphere, and therefore this representation was used in Clift & Grace's model. Clift & Grace also assumed that vorticity is confined to the particle wake regions, which completed the circle or sphere of which the bubble void forms the cap. The model basically assumes the emulsion phase as a porous medium, such that the coupling of interaction between the solid and the gas is removed. The flow field around the modelled circles (or cylinders) is the flow pattern of the interaction between the objects through the surrounding medium.

The interaction model devised is a mechanistic approach using kinematics to calculate the bubble trajectory and dynamic properties. The model assumes that there is a flow field generated around each bubble, which affects the rise velocity and trajectory of other nearby bubbles. The flow field was assumed to exist around a Davidson bubble model as shown in *Figure 5.3.8*.

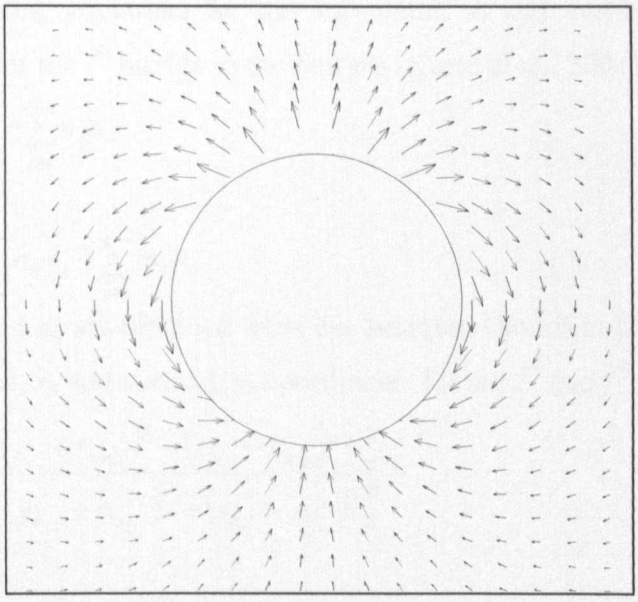

Figure 5.3.8: The flow pattern of motion around the modelled two-dimensional bubbles based on potential flow theory after Davidson (1961). The arrows illustrate the velocity of the dense phase relative to the bubble.

Clift & Grace postulated that the velocity of a bubble may be approximated by adding the velocity of the continuous phase at the position of the nose of the bubble if it were absent to its rise velocity in isolation. The velocity component in the continuous phase is assumed to be the linear combination of the velocities caused by all other bubbles present in the bed. The model also assumes that all gas in excess of that necessary to maintain the incipient fluidisation state flows through the emulsion phase as bubbles. This concept was applied to the coalescence of two bubbles on a common vertical line (Clift & Grace, 1971a) and later to the coalescence of two bubbles vertically displaced with horizontal offset (Clift & Grace, 1971b).

The model of Clift & Grace is simple and does not require extreme computational efforts. Clift & Grace (1971b) formulated a set of governing equations for the model to operate in the two-dimensional beds as well as a set for three-dimensional beds that calculates explicitly the velocity components for all the bubbles in the bed. The model agrees well with experimentally observed bubble interaction and behaviour from the authors' work and by other workers. Korte et al. (2001) compared the bubble size prediction by the model with a bubble-size relationship for Geldart-B powders reported in the literature by Darton et al. (1977).

Clift & Grace governing equations for the horizontal, u_i and vertical, v_i instantaneous velocity components for the i^{th} bubble in the bed are (Korte et al., 2001)

$$u_i = \sum_{j \neq i} m_{ij} v_j - \sum_{j \neq i} n_{ij} u_j \tag{5.9}$$

and

$$v_i = v_{b\infty,i} + \sum_{j \neq i} n_{ij} v_j + \sum_{j \neq i} m_{ij} u_j \tag{5.10}$$

The coefficients m_{ij} and n_{ij} are obtained from the assumed Davidson flow pattern around a bubble, with horizontal, x_b and vertical, y_b coordinates for the i^{th} and j^{th} bubbles where

$$n_{ij} = \frac{\left[\left(y_{b,i} - y_{b,j} + r_{bm,i}\right)^2 - \left(x_{b,i} - x_{b,j}\right)^2\right] r_{bm,j}^2}{\left[\left(y_{b,i} - y_{b,j} + r_{bm,i}\right)^2 + \left(x_{b,i} - x_{b,j}\right)^2\right]^2} \tag{5.11}$$

and

$$m_{ij} = \frac{2\left(y_{b,i} - y_{b,j} + r_{bm,i}\right)\left(x_{b,i} - x_{b,j}\right) r_{bm,j}^2}{\left[\left(y_{b,i} - y_{b,j} + r_{bm,i}\right)^2 + \left(x_{b,i} - x_{b,j}\right)^2\right]^2} \tag{5.12}$$

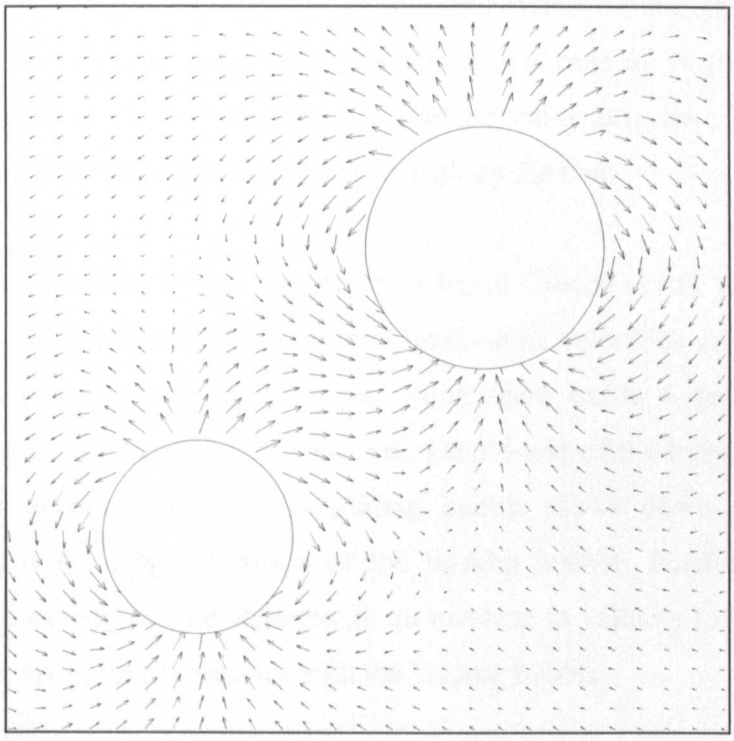

Figure 5.3.9: The flow pattern around two interacting bubbles based on potential flow theory. The arrows indicate the velocity of the dense phase relative to the bubbles.

Implementing the model, the simulation calculated for each modelled bubble, its effective velocity components from its isolated rise rate and the velocity components influence from other bubbles above and below it. This resulted in a flow field pattern as illustrated in *Figure 5.3.9* for two interacting bubbles.

Assessments on the performance of the model in predicting bubble kinematics behaviour showed considerable similarities to reality. Instances of comparison between simulated bubble behaviour with reality are available from the authors in their publications as well as various other studies that have implemented the Clift & Grace bubble interaction model (Korte et al., 2001; Rafailidis & Clift, 1991). Observations of such similarities, particularly several of the prominent bubble interaction behaviours were also witnessed in this study. For example, the sequences of events of how a larger bubble pushes aside a smaller bubble not directly above it and passes through without coalescing, as described by Clift & Grace (1970, 1971b) and Korte et al. (2001), also occurred in the simulation. Should the smaller bubble be more vertically aligned above the larger bubble, then coalescence could perhaps occur. The former observation demonstrates the influence of the flow field around the larger bubble on other nearby bubbles, tending to push aside smaller bubbles in its path.

However, this may not necessarily apply to all fluidised system where typically, for larger group B particles, coalescence could occur for the similar case of vertical alignment of bubbles as the gas tend to flow directly through the emulsion phase, short-circuiting between nearby bubbles providing a less resistive path up the bed.

Consistent with observation and that reported by Clift & Grace (1970), when two similar sized bubbles are rising at the same horizontal level, their velocities are expected to be slightly less than their rise rate in isolation, while there exists a horizontal velocity component tending to keep them apart. However, should one of the bubbles fall back, an unstable situation occurs such that the trailing bubble slows down and then shifts horizontally towards the lateral position of the leading bubble. Positioned behind the leading bubble, the trailing bubble experiences an increase in velocity towards the rear of the leading bubble, and then coalescence with the leading bubble.

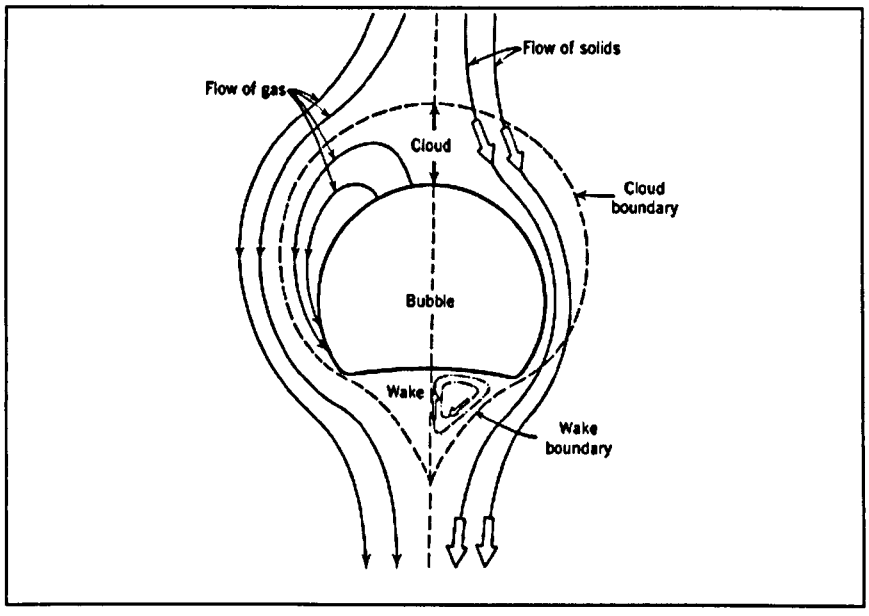

Figure 5.3.10: The Murray's bubble model. Source: Kunii & Levenspiel (1969).

In their validation study, Clift & Grace (1971b) indicated that the model sometimes underestimates the velocity of the trailing bubble when it was directly under and in the wake of the leading bubble, as the model theory assumed the wake particles have similar velocity as the bubble. The discrepancy suggested the presence of a trailing vortex pair in the particle wake, which is consistent with Rowe & Partridge (1962) and Reuter (1966).

The trailing vortex pair in the wake region could be seen in Murray's bubble model (Murray, 1965) shown in *Figure 5.3.10.*

Figure 5.3.11 shows the modelling variables and parameters used to model the bubbles and regulate bubble interactions. In the simulation, each bubble was treated as an object with properties such as horizontal and vertical components of velocity and position and diameter. After each time step, the simulation and model modified the properties of each bubble present in the bed while removing those exiting the bed and assigning properties to new ones created at the distributor. These property elements were then updated before the next round of computation was executed.

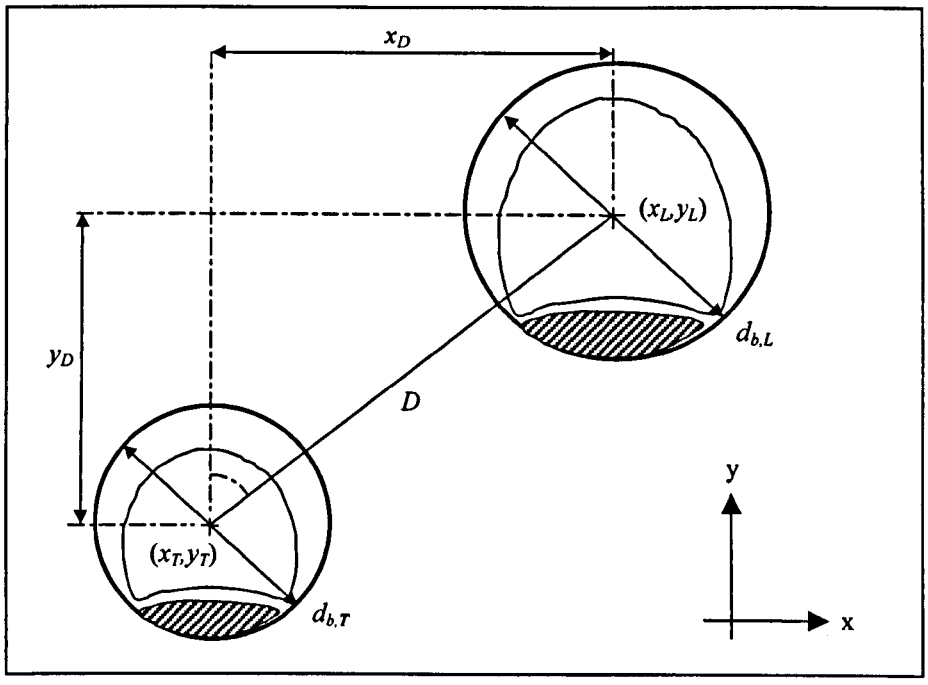

Figure 5.3.11: Two interacting bubbles as modelled in the simulation for the two-dimensional bed. All the simulation parameters and variables are also shown.

In the simulation, the kinematics properties of each individual bubble were a combination of the effects by all other bubbles surrounding the bubble in question. Principally, the Clift & Grace bubble interaction model worked for coalescence two- and three-dimensional bubble pair. Clift & Grace (1971b) suggested that the model could be applied to cases with multiple bubbles as in the modelling of a bubbling bed hence, it has been adopted in this simulation.

To determine the velocity of a bubble, the simulation classifies the population of bubble surrounding the bubble in question into two classes: a group with their vertical position above the bubble in question and another group of bubbles positioned below. Based on the model, different sets of equations, derived from the potential flow theory, were used to calculate the combined effect of the bubbles in the group on the overall kinematics properties of the bubble in question.

Therefore, in an instance of the interaction computation, a bubble in question, b_n, may have an i^{th} bubble, b_i, below it. In this case, b_n is the leading bubble and b_i is the trailing bubble, allowing the algorithm of the interaction model to work accordingly. The opposite order is also true with b_n now being the trailing bubble. In situations where two or more bubbles are at similar elevation in the bed, the surrounding bubbles are considered being slightly on top of b_n and the algorithm again works accordingly.

5.4 Bed characterisation technique and measured parameters

Similar to the experimental bed, the state of bubbling in the simulated bed was estimated from the fraction of the region of interest of the bed occupied by the bubble voids. As the simulated bed was a replication of the experiment, the same image analysis technique was used to diagnose the state of the bubbling process. Frames of the simulated bed within a defined Region Of Interest, ROI, were acquired at each simulation time step, analysed and the proportion of the bed occupied by bubble voids, termed the Bubble Void Fraction (BVF), was measured and recorded. The time series of BVF was then analysed to infer the corresponding bubbling condition.

In the simulation, the bubbles comprising of the bubble cloud, void and wake as shown in *Figure 5.3.6*, were modelled as circles with areas proportional to their diameter squared (d_{bm}^2). The entire modelled circle was visible in the bed and this implies that the portion of the circle supposedly containing the opaque wake region was also computed in the measurement of BVF as well. The circles representing the bubbles in the simulation enable the kinematics in the bed to be properly modelled, but are not the same as the actual voids that can be observed and that are measured in the experiments. Typically, the bubble voids are not circular, but rather have a cap-like shape or a variation of that. Therefore, when

compared to the experimental bed, the direct measurement of the circles in the simulation would incur errors of significant proportions. This can be eliminated by applying a correction factor on the BVF. Termed the f_{BVF}, it was imposed on the measurement of BVF in the simulation, guided by several criteria.

The f_{BVF} factor can be found by comparing the time series of BVF for the simulation and experimental measurements. By adjusting the appropriate value of the f_{BVF}, the same volume of the bed will be occupied by bubble voids in the simulation and in the experiment, such that the time series would have the same mean and standard deviation. In another words, the f_{BVF} was estimated by minimising the difference between the mean and standard deviation of the time series of BVF in the experiments and the simulation. This has the effect of shifting the curve of the frequency content of the simulated bed on the magnitude axis without affecting its dynamics.

It must therefore be emphasised that f_{BVF} was not a fitting parameter. It was used to correct the measured BVF in the simulation such that it would be consistent with that of the experimental measurement on the same fluidisation condition i.e. corrected so that the similar parameter is measured. The f_{BVF} served to only take the relevant portion (void area) of the total modelled circle as a valid contribution to the BVF in the bed.

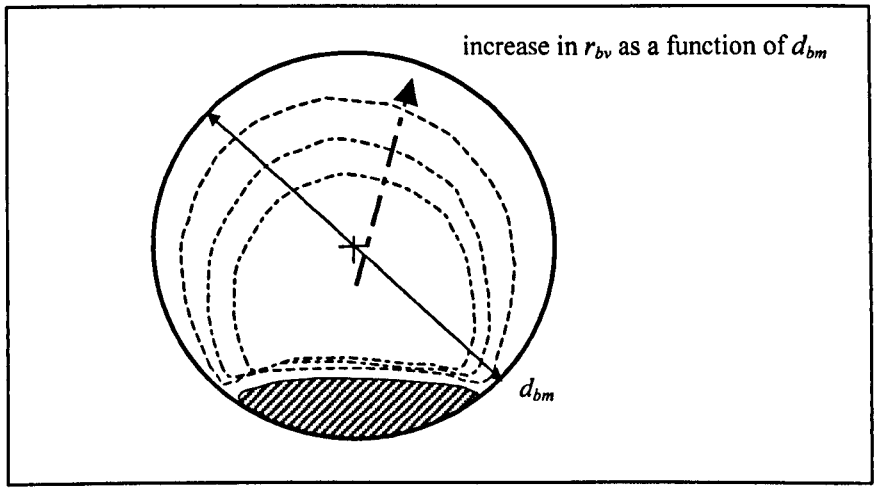

Figure 5.4.1: The variability of the bubble void area depending on bubble size as modelled in the simulation. f_{BVF} was used to determine the ratio of the modelled bubble circular area that would consist of the void area.

In Clift & Grace (1970), it was assumed that typically the bubble void occupied approximately 75% of the enclosing modelled circle, with the remaining part being the

wake. This gave the f_{BVF} a default value of 0.75. As discussed earlier in the chapter, the proportion of bubble void area compared to the volume of gas that constitutes a bubble is size dependent: the larger the bubble size, the larger the bubble void area compared with the cloud. A smaller bubble has a smaller void area as a higher proportion of its gas is hidden in the cloud area. Furthermore, dependence of bubble void on bubble size implies that f_{BVF} value would vary with flow rate. A lower value was expected as the bubbles are generally of the smaller size range when the gas flow rate was lower. *Figure 5.4.1* illustrates the variation of bubble void area as the bubble size changes, hence affecting the value of f_{BVF} needed to provide comparable similarity between the simulation and experimental measurement of BVF. However, proper values of f_{BVF} for a fluidisation condition will be validated in *Section 5.5*.

f_{BVF} was used to determine the bubble void area instead of applying the relationship established by Davidson (1961) and Murray (1965) between bubble cloud, r_{bc} and void, r_{bv} radii. This was because there was no direct relationship between the bubble cloud radius, r_{bc} and the corresponding bubble void radius, r_{bv}, such that a confident inference of bubble void area based on the bubble modelled diameter could be established. As there is inadequate understanding and data to validate the relationship between bubble void and size, the f_{BVF} was used. f_{BVF} was not directly applied to individual bubbles; rather it imposed a global correction factor on the measurement of BVF.

The method of determining the appropriate f_{BVF} value was by comparing the BVF time series and spectra graph for the simulated and experimental measurements at the same fluidisation condition, from which a suitable f_{BVF} could be found that allowed the sets of measurements to coincide. The complete application of the above-mentioned technique is demonstrated in the next section (*Section 5.5*).

Figure 5.4.2 illustrates several possible sets of BVF values if the f_{BVF} was not properly used. Large deviations from the experimental BVF measurements could be seen when no f_{BVF} or a default value of 0.75 was used for the simulated bed bubbling at excess gas of 25.6 mm/s above U_{mf}. However, with a f_{BVF} of 0.43, the simulated BVF measurements compared well with the experimental measurements.

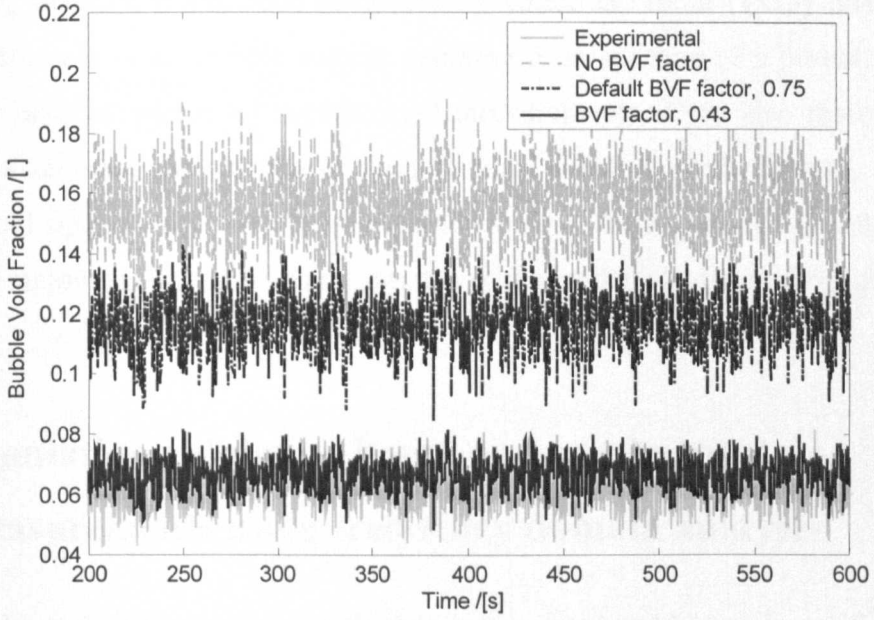

Figure 5.4.2: The plots show examples of how the different f_{BVF} used could affect the BVF time series from simulation as compared to the experimental measurement.

Simplifications in the simulated bed affected the measurement of BVF. Some unmodelled events in the bed such as the bubbles' disappearance and reappearance would affect the dynamical measurement of BVF. Changes and fluctuations in bubble shape and size would also affect the BVF in the bed in the similar way. Also, slugging bubbles are slower and therefore the effect of these bubbles on the BVF value lasts longer. However, slugs were not modelled in the simulated bed and this might cause some discrepancies when the bed is fluidised close to the regime of transition to slugging.

The extent of which these simplifications individually affected the simulated BVF measurements is not known and can only be collectively assessed via comparison with the experimental BVF measurements. This triggered a separate school of thoughts and is addressed in detail in *Chapter 6*, where the concept of an idealised bed condition was devised to investigate the effects of these events individually on the overall dynamics of the bubbling process.

Bubble splitting was also not modelled in the simulated bed. In a bubbling bed, certain bubbles split due to instability and other effects. Some re-coalesce immediately after splitting. This might affect the overall dynamical behaviour of bubbles in the bed. However, to certain extent, it should not have affected the BVF measurements

significantly, although it has been suggested by Grace & Venta (1973) that there is a significant decrease of net bubble volume resulting from splitting of a parent bubble, but this has not been supported by experimental measurements. They also thought that the extent of the decrease was erratically variable from event to event. Instead, splitting of bubbles would significantly affect bubble population and if this parameter of the bubbling process was measured, large deviation from that of the realistic bed would result.

5.5 Simulation validation based on experimental measurements using frequency domain analysis

For the results and measurements acquired from the simulated bed to be confidently used to investigate the behaviour and dynamic features of the bubbling fluidised bed, some form of validation of the simulation against the experimental results needs to be conducted. This section describes the methods carried out in the frequency domain, as well as analysis of the time series with statistical techniques and the assessment of the transient response characteristic of the simulated bed.

In the first stage of validation, the simulated bed was used to simulate the normal freely bubbling bed (steady state) for comparison with the experimental measurements in the frequency domain and for time series congruency. Statistical measures were then used to further support the validation process. The final validation stage involved testing the simulated bed on transient responses comparable to those of the experimental bed. The ability of the simulated bed to appropriately replicate the transient response is crucial, especially when the simulated bed was used in the analysis of how the bubbling bed dynamics affected the measured parameters. Therefore, this part of validation assesses the extent to which the simulated bed was able to capture the important dynamical characteristics of the experimental bed.

5.5.1 Freely bubbling bed

Both versions of the beds were subjected to flow of fluidising gas of 25.6 mm/s, 51.2 mm/s and 76.8 mm/s superficial flow above U_{mf} (approximately 103 mm/s). For both beds, the bubble void fraction, BVF was measured at 25 Hz for about 60 min producing approximately 100,000 data points.

For frequency domain, as discussed in Chapter 4, the Bode scaled diagram of BVF was produced from the frequency spectra graph. Frequency domain analysis produces a frequency spectra graph that represents the magnitude (or energy) of the activities occurring in the bed affecting the BVF at varies frequencies. There are several parameters that need to be adjusted so that the simulation could properly replicate the experimental bed. These parameters are not fitting parameters that are used simply to make the simulation behave more desirably, but to link the simulation to factors in the experimental bed. These parameters were measured from the experimental bed and are:

- bubble maximum initial diameter, $d_{bi,max}$
- bubble minimum initial diameter, $d_{bi,min}$
- bubble void fraction factor, f_{BVF}

The first two parameters are self-explanatory. They represent the range of bubble initial size upon introduction into the bed at the distributor. Their values vary with flow rate and presumably $d_{bi,max}$ increases with flow rate. These values were obtained from the calculation of bubble sizes in the images of the experimental bed. The third parameter is used so that so that during the calculation of BVF from every individual bubble, only a fraction of the bubble simulated as a circular shape is taken as the bubble void area (the other fraction occupied by opaque wake). Refer to *Section 5.4* for more details.

Re-iterating on selection of f_{BVF} value, it is obtained by comparing the time series of both the simulated and experimental bed. The time series of the simulated bed needs to be statistically similar to that of the experiment within reasonable accuracy. However, this must not compromise other aspects of similarities, particular the dynamical similarities of the beds (frequency domain). Therefore a value of f_{BVF} may only be suitable for only a range of different fluidisation conditions. The results from rigorous tests and simulations of the bubbling bed are as presented below.

5.5.1.1 *Freely bubbling bed at 25.6 mm/s superficial flow above incipient condition*

Based on the comparison of time series between the experiment and simulation measurements of BVF, the suitable measured parameter values obtained from the experiment used in the simulation are:

- $d_{bi,max} = 20$
- $d_{bi,min} = 6$
- $f_{BVF} = 0.42$

Figure 5.5.1 shows the time series of the BVF of both the beds fluidised at 25.6 mm/s superficial flow above incipient condition with the chosen f_{BVF} value. The statistical measures (accurate to 2 significant numbers) of the time series that determined the chosen f_{BVF} value are shown in *Table 5.5.1*.

	Mean	Standard Deviation	Max	Min
Simulation	0.067	0.0047	0.085	0.047
Experiment	0.062	0.0057	0.084	0.037

Table 5.5.1: Table summarises the statistical measure of BVF (to two significant figures) of the simulated and experimental beds fluidised at 25.6 mm/s superficial flow above U_{mf}.

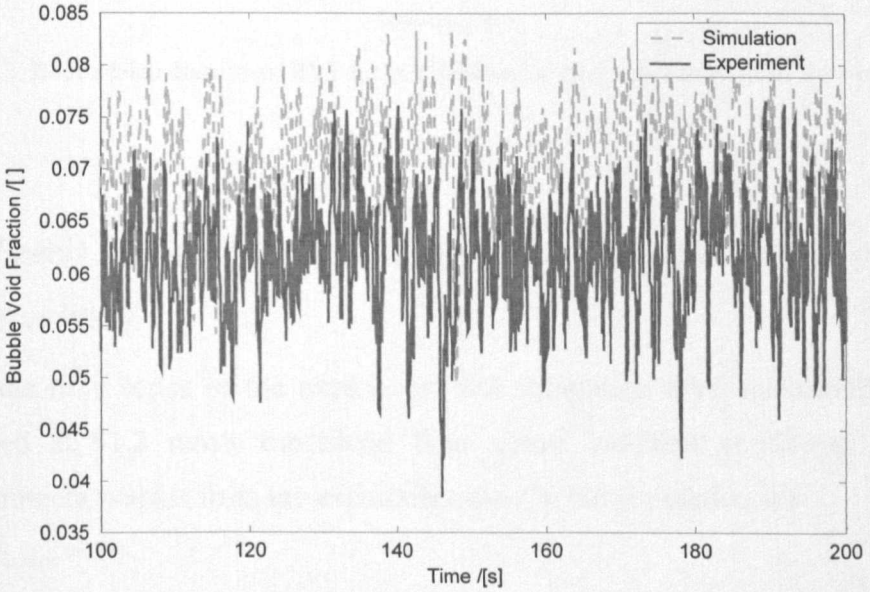

Figure 5.5.1: Time series of BVF for bed fluidised at 25.6 mm/s superficial flow above U_{mf}.

Figure 5.5.2 shows Bode-scaled frequency plot of BVF for beds fluidised at 25.6 mm/s above incipient condition. The plots show generally good agreement from the Low Frequency Gain, LFG or DC level up to about 2 Hz where similarity starts to deteriorate with frequency. Both the plots have similar break frequencies at approximately 7 Hz. The differences at high frequency will not significantly affect the dynamical similarity of the beds as the magnitude associated with the activities occurring at frequencies in this range are small, hence they would have a negligible affect on the overall dynamics of the bed.

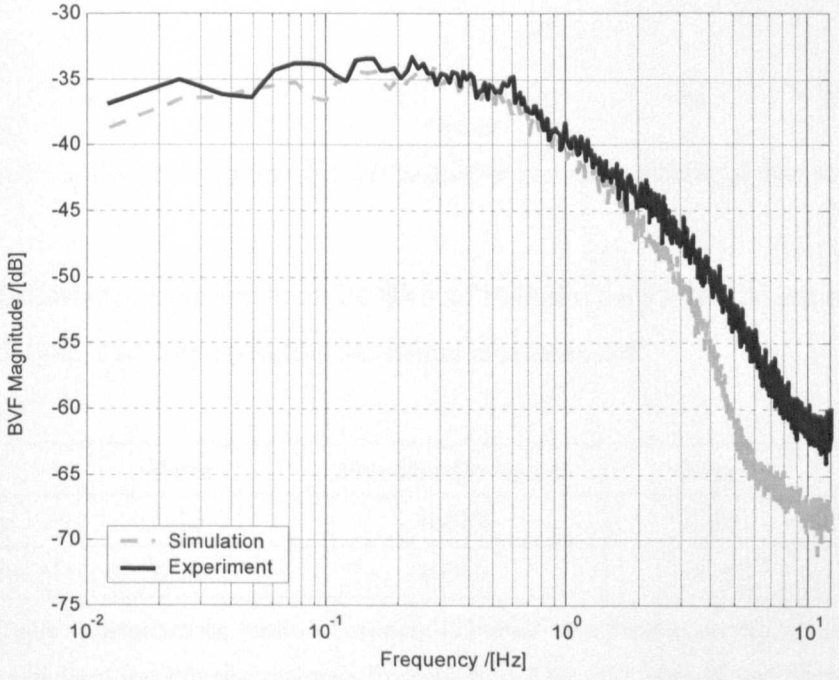

Figure 5.5.2: Bode scaled diagram of BVF for bed fluidised at 25.6 mm/s superficial flow above U_{mf}.

5.5.1.2 *Freely bubbling bed at 51.2 mm/s superficial flow above incipient condition*

Comparing the time series of the experiment and simulation BVF measurements of the beds fluidised at 51.2 mm/s superficial flow above incipient condition, the chosen measured parameter values from the experiment used in the simulation are:

- $d_{bi,max} = 30$
- $d_{bi,min} = 6$
- $f_{BVF} = 0.75$

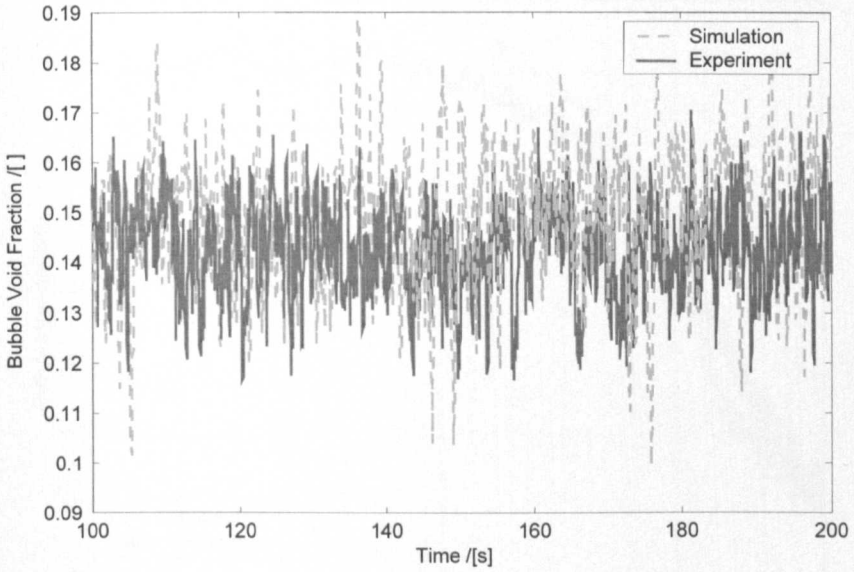

Figure 5.5.3: Time series of BVF for bed fluidised at 51.2 mm/s superficial flow above U_{mf}.

Figure 5.5.3 shows the time series of the BVF of both the beds with the chosen f_{BVF} of 0.75 for the simulation. The corresponding statistical measures are:

	Mean	Standard Deviation	Max	Min
Simulation	0.15	0.013	0.20	0.089
Experiment	0.14	0.010	0.18	0.096

Table 5.5.2: Table summarises the statistical measure of bubble void fraction (to two significant figures) of the simulated and experimental beds fluidised at 51.2 mm/s superficial flow above U_{mf}.

Figure 5.5.4 shows Bode-scaled frequency plot of BVF for bed fluidised at 51.2 mm/s superficial flow above incipient condition. The plots again show generally good agreement. However, there is a broadband peak in the simulation frequency content plot beginning from approximately 0.2 Hz slowly decaying to rejoin the decaying path of that of the experiment. The congruency of the LFG or DC level of the plots is again reasonably good. There are also some slight improvements seen on the congruency of the plots at higher frequency. Overall, the performance of the simulated bubbling bed deteriorated slightly compared to when the flow rate of gas is lower, although at this point, it still gives reasonable replication of its real world counterpart.

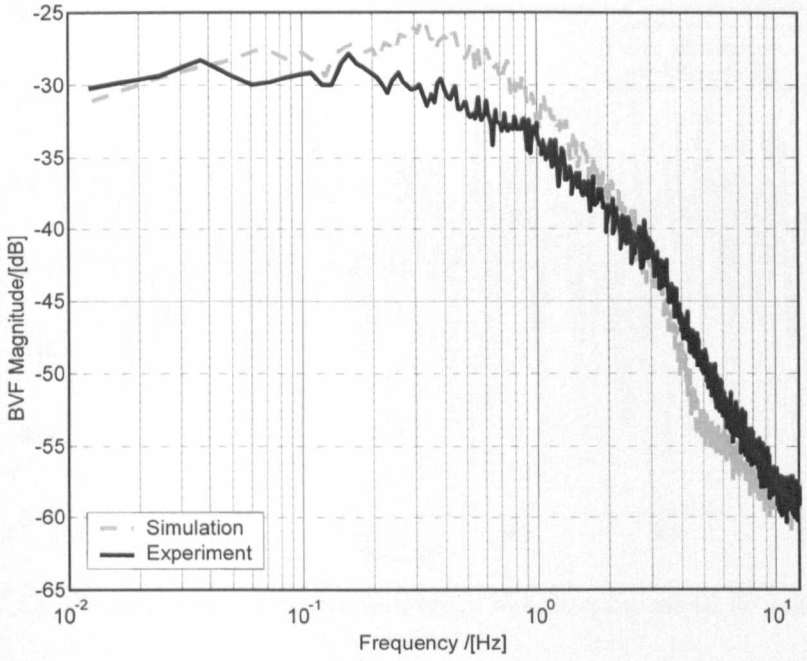

Figure 5.5.4: Bode scaled diagram of BVF for bed fluidised at 51.2 mm/s superficial flow above U_{mf}.

5.5.1.3 *Freely bubbling bed at 76.8 mm/s superficial flow above incipient condition*

The measured parameter values from the experiment used in the simulation obtained from the comparison of BVF time series from both beds are:

- $d_{bi,max} = 30$
- $d_{bi,min} = 6$
- $f_{BVF} = 0.75$

Figure 5.5.5 shows the time series of the BVF of both the beds, with the simulated bed using the f_{BVF} of 0.75. The corresponding statistical measures are as shown in *Table 5.5.3*.

	Mean	Standard Deviation	Max	Min
Simulation	0.174	0.0166	0.230	0.0903
Experiment	0.189	0.0128	0.239	0.123

Table 5.5.3: Table summarises the statistical measure of bubble void fraction (to three significant figures) of the simulated and experimental beds fluidised at 76.8 mm/s superficial flow above U_{mf}.

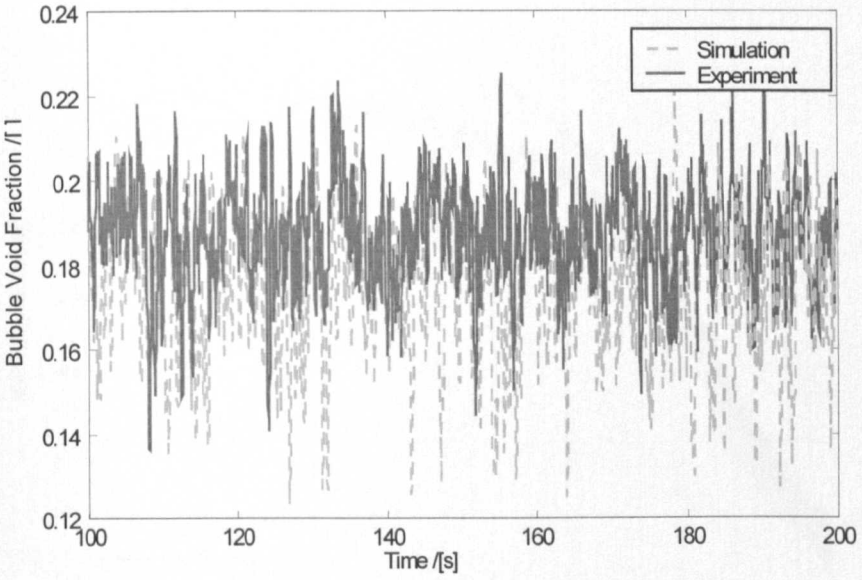

Figure 5.5.5: Time series of BVF for bed fluidised at 76.8 mm/s superficial flow above U_{mf}.

Figure 5.5.6 shows Bode-scaled frequency plot of BVF for bed fluidised at 76.8 mm/s superficial flow above incipient condition. At this point of fluidisation condition, the bubbling in both beds was vigorous with large bubbles being produced and the bed was probably close to transition into the slugging regime. Bubble spatial distribution is poor with bubbles generally congregating toward the centre of the beds. Despite these features there is still good agreement between the experiment and the simulation as shown in *Figure 5.5.6*. Similar to conditions of fluidisation with 51.2 mm/s superficial flow excess gas into the bed (*Figure 5.5.4*), the DC levels of the plots are the same, with a broadband peak present on the simulated plot from 0.2 Hz onwards and decaying slowly toward that of the experimental.

The broadband peak has been a significant factor affecting the similarity of the beds. Its causes have been looked into resulting in several suggestions. Clift and Grace's bubble interaction model, which has been used throughout all the simulations, is predominately designed to calculate the interaction between two bubbles. However, it is not designed to work in regimes of fluidisation other than that of freely bubbling state. This suggests that at a high flow rate where regime change is or has already occurred, the model will fail to properly govern the bubbles in the bed.

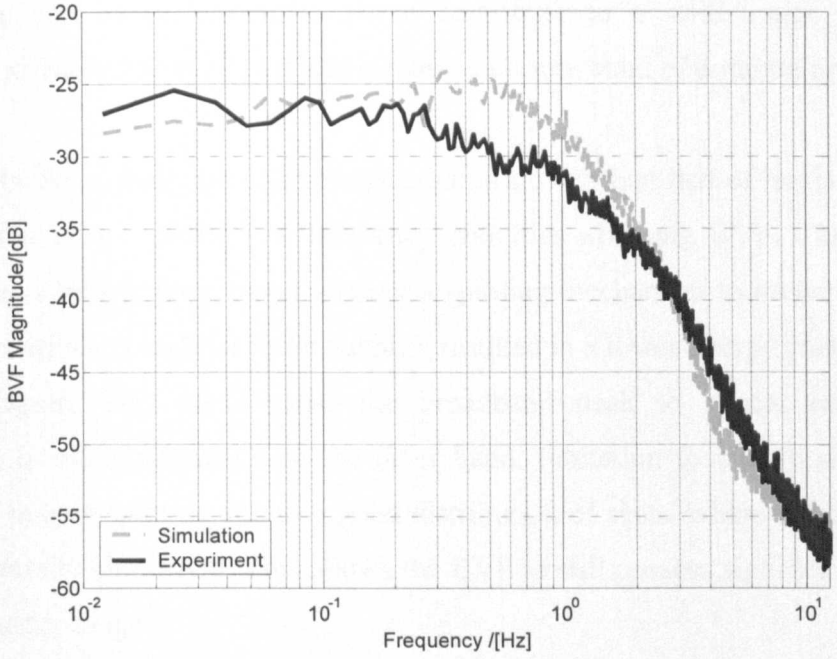

Figure 5.5.6: Bode scaled diagram of BVF for bed fluidised at 76.8 mm/s superficial flow above U_{mf}.

The slugging of bubbles, as observed in the simulation, contributes to a narrower band of frequencies and this suggests higher frequency strength over a particular frequency band, observed as a wide bandwidth peak in the plot. Small bubbles that are formed at the distributor rapidly coalesce and form large bubbles close to the bottom of the bed, resulting in a small population of bubbles with dominating size and rise rate over the remaining height of the bed. Due to their sizes, their effects are of high strength and significant on the measurement of BVF.

The simulation does not simulate bubble splitting. Although its effect could be neglected at lower flow rates, where BVF is not significantly different from that of the experiments when bubbles do not split, at higher flow rates however, there will be a limit to the maximum size that a bubble could have. The limit is set by the splitting mechanism where bubble of certain size could not withhold and succumb to splitting into smaller bubbles. The knock-on effect would be the limiting of the maximum possible bubble rise velocity. Although observation by Geldart suggested that there are no limit to bubble size in group B powder fluidised beds (Geldart, 1973), Geldart indicated that in some case where given sufficient bed height, bubbles were allowed to reach a maximum size due to bubble instability as predicted by the theory proposed by Harrison et al. (1961). Bubble splitting in the experimental bed limits the bubble maximum stable size, resulting in more varied

bubble sizes and hence velocities. These contribute to a wide range of frequency components affecting the BVF, without creating a narrow band of dominating elements.

For smaller bubbles, their rate of size expansion is slower than that of larger ones. Bubble size expansion is one of the low frequency activities affecting BVF. Therefore in the simulation, as a bubble grew larger without a splitting mechanism to moderate it, the rate of expansion, which is high for these bubbles, resulted in a lower energy content in the low frequency region. This could cause the broadband peak to appear relatively more pronounced. In the experiments on the other hand, limitation to bubble size due to the existence of bubble splitting allows a good distribution of sizes, where bubbles of smaller size are not totally eliminated. This allows the BVF to still possess significant strength for its low frequency range.

5.5.2 Transient response to change in gas flow rates in the freely bubbling regime

Several tests involving continuous alteration of the gas flow rate into the bed in a periodic manner were carried out. The simulated bed was tested to investigate whether it could behave similarly to the experimental bed to dynamic changes and its capability in replicating transient response. The evaluation of the similitude of both beds is based on whether the simulated bed could reproduce a similar transient response to the experimental bed in terms of the rise and fall rates, steady-state levels and other salient features that are characteristic of the BVF measurement obtained from the image analysis technique.

The beds, initially bubbling above U_{mf} (≈ 95 mm/s superficial gas velocity in this study), were subjected to step change in flow rate at a frequency of 0.05 Hz (an excitation rate tested to be suitable to effectively interrogate the bed dynamics). Three ranges of step changes in flow rates were looked at covering, (i) lower flow rate range, (ii) upper flow rate range, and (iii) full flow rate range within the freely bubbling regime. These three tests allow the response characteristics of the beds to be assessed for a range of condition changes over the bubbling range. The results are presented in *Figure 5.5.7* to *Figure 5.5.9*. An additional test was carried out by subjecting both beds to a higher frequency of flow rate excitation, where the result can be found in *Figure 5.5.10*.

As shown in *Figure 5.5.7*, when there was a step change at 0.05 Hz from 8 mm/s to 36 mm/s superficial flow above U_{mf}, the BVF changed between about 0.05 to 0.12. The noise or fluctuation present in both time series appears comparable. The rise and fall rates of the signals agree as well. In the second test, the BVF switches between 0.12 and 0.18 with high fluctuation on these steady state values for both beds. The results presented in *Figure 5.5.8* show good congruency in their transient response to step changes between 33 mm/s and 74 mm/s above quiescent fluidisation.

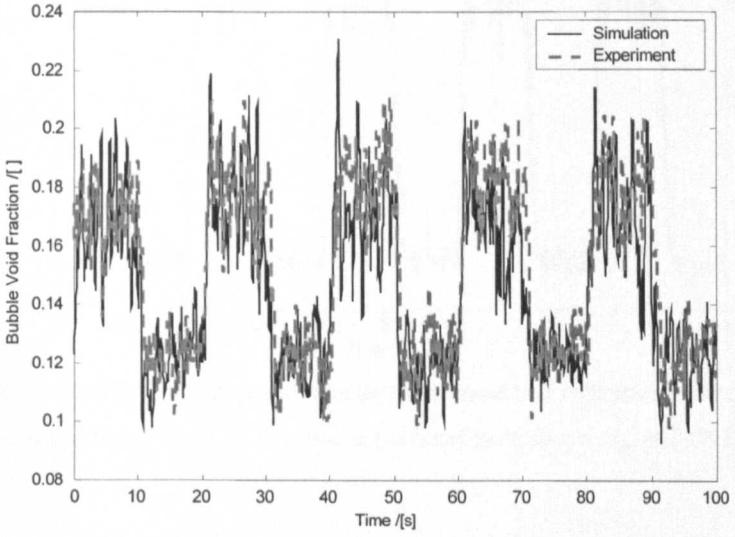

Figure 5.5.7: The time series of BVF for experimental and simulated bed with transient response to flow rate step change from 8 mm/s to 36 mm/s above U_{mf} at 0.05 Hz.

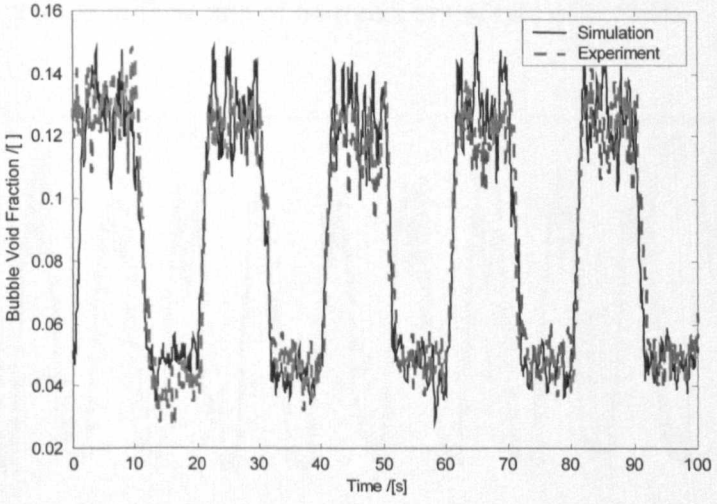

Figure 5.5.8: The time series of BVF for experimental and simulated bed with transient response to flow rate step change from 33 mm/s to 74 mm/s superficial flow above U_{mf} at 0.05 Hz.

Changing the flow rate over full range from 7 mm/s to 86 mm/s in excess gas, the simulated bed continued to maintain good reproduction of the experimental bed, except for a slightly larger magnitude of fluctuation of BVF at the upper limit of the flow rate than that of the experimental measurement. *Figure 5.5.9* shows the results of the comparison.

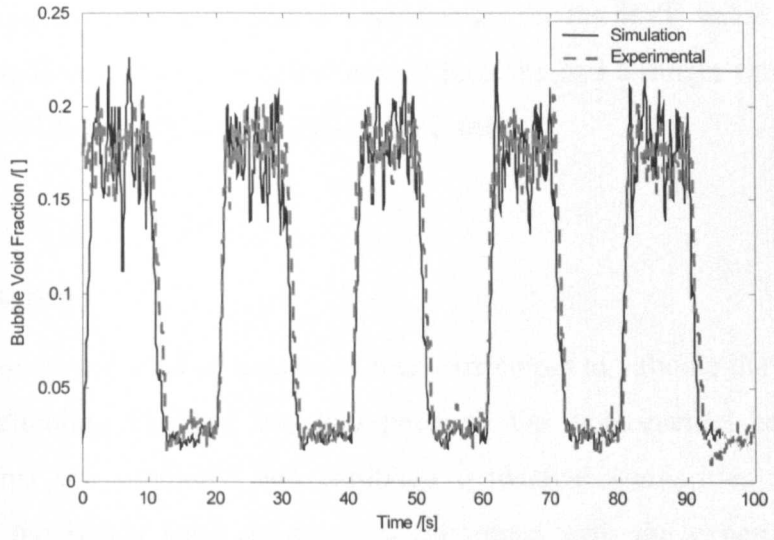

Figure 5.5.9: The time series of BVF for experimental and simulated bed with transient response to flow rate step change from 7 mm/s to 86 mm/s superficial flow above U_{mf} at 0.05 Hz.

The transient response capability of the simulated bed was also tested at a much higher excitation frequency, giving the results shown in *Figure 5.5.10*. The experimental and simulated beds were initially fluidised at 8 mm/s superficial flow above incipient state then subjected to a step change in flow rate of 64 mm/s at the rate of 0.15 Hz.

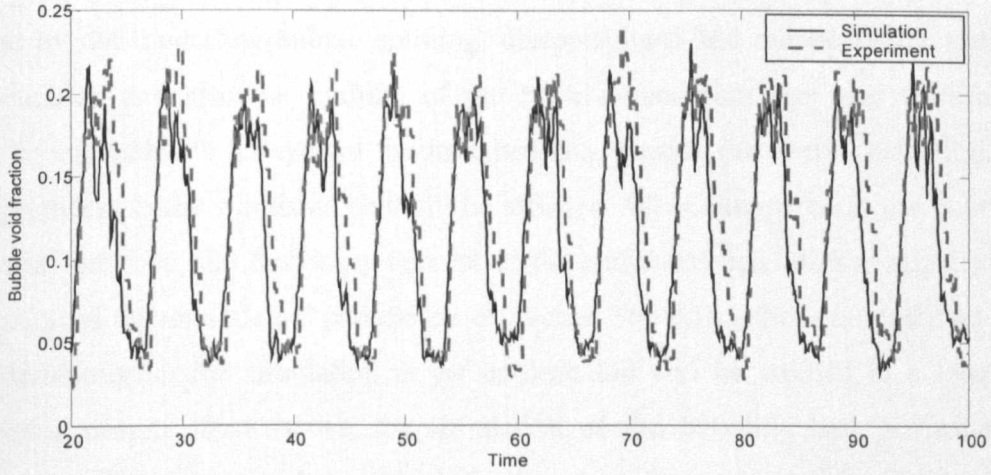

Figure 5.5.10: The time series of BVF for experimental and simulated bed with transient response to flow rate step change from 8 mm/s to 72 mm/s superficial flow above U_{mf} at 0.15 Hz

It can be seen from the figure above (*Figure 5.5.10*), that the simulated bed could not completely reproduce the transient response of the experimental bed. However, it was still able to reach reasonable upper and lower steady state values as well as keep up with the rise rate as that for the experimental bed. The simulated bed could not properly replicate the fall behaviour of the BVF value when the gas supply reduces at the tested excitation frequency. The simulated bed predicted a swifter fall in the BVF value when the flow supply was stepped down while in actual case it took the bed a longer time to exhaust of bubbles and therefore a much sluggish fall in BVF value.

5.5.3 Discussion

An exhaustive study and a list of tests have been carried out to validate the performance of the simulated bubbling fluidised bed in replicating the experimental bed. It has been demonstrated that the simulated bed exhibited dynamical similarities in its bubbling process during the steady state condition as compared with the experimental bed, by analysis in the frequency domain. The similarity differs slightly (by maximum of about 5 dB and is flow rate dependent) with fluidisation condition and the general trend suggested that the similitude deteriorates on both extremes of the bubbling regime, i.e. close to quiescent and slugging states where the Clift & Grace bubble interaction model does not apply well.

Apart from that, there are several other factors that have been suggested to account for the lack of similarities on other grounds during the comparison with the experimental bed. It is clear that by not modelling bubble splitting, disappearance and reappearance, shape and size fluctuation and also the limiting of the bubble maximum size and therefore rise velocity (if applicable to the type of fluidised bed considered), the overall behaviour of the bubbling process in the simulated bed will be affected. When compared to the bubbling in the experimental bed, the frequency content of the simulated beds differs slightly due to the omission of the unmodelled parameters or events. The effect these unmodelled factors have individually on the simulation is yet unclear and will be studied in a later stage. Nevertheless despite these issues, the simulation of the bubbling bed performed well overall in closely replicating the real bed. Furthermore, the presence of non-linearities in the experimental bed such as the regime changes close to U_{mf} as well as the transition to

slugging behaviour complicates modelling efforts and simply allows more differences to come in between the simulated and experimental bed.

The transient response of the simulated bed to step excitation, as compared to the experimental bed, is generally acceptable. A good agreement could be obtained between the two versions of the bed especially at low frequency of excitation. However, at a higher excitation frequency, the simulated bed could not model the fall in BVF value properly, due to a phenomenon that could not be modelled in the simulated bed: when the flow rate is abruptly reduced, the supply of gas is disturbed and becomes discontinuous, causing the bed suspension to collapse under its own weight and as a consequence, some bubbles are dissolved into the defluidised emulsion phase. The larger the magnitude of reduction, the larger the shock suffered by the bed, and as a consequence, the smooth fluidisation condition could not be maintained causing temporary localised defluidisation in parts of the bed.

However, there was a portion of the bubble population, normally located in the mid-height of the bed, that would instead form several bands of bubble void spanning across the bed horizontal cross-section rising slower than the bubbles would in isolation up the remaining height of the bed. The formation of the rows of bubbles caused a much slower evacuation of bubble voids from the bed during the step transition of flow reduction and this resulted in a much slower rate of transient response of the experimental bed. Due to modelling limitations, this phenomenon was not picked up by the simulated bed. This phenomenon could have caused the hysteresis effect that is intrinsic in the transient response of the real system.

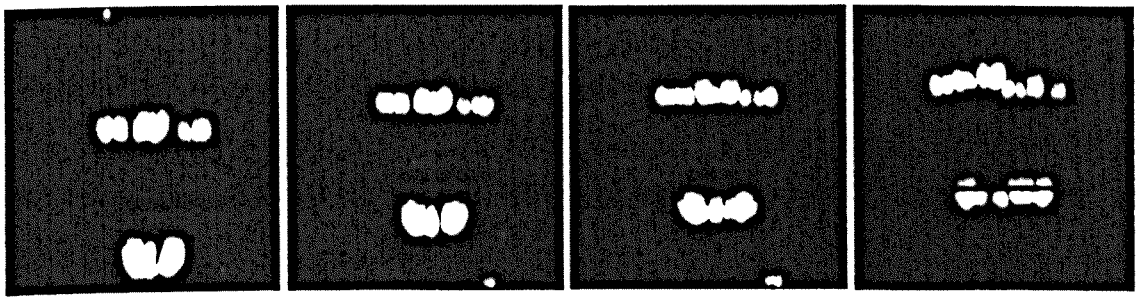

Figure 5.5.11: Sequential snapshots (left to right) of the experimental fluidised bed showing the lining up of a band of single bubbles (children) caused by the breaking up of a single bubble (parent) introduced at intervals by a solenoid valve. This simulates the phenomenon where single bubbles form horizontal bands of slower moving bubbles when the flow supply is reduced abruptly.

The objective of the development of the simulated bed has been from the beginning to maintain simplicity and only to model the main and major events in the bubbling process, and this has so far been successfully carried out. The validation results suggest that the simulated bed performs reasonably well both in the steady state as well as the transient mode in replicating the experimental bed.

5.6 Conclusion

A simulation programme was developed in the MATLAB environment to simulate a bubbling fluidised bed. An object-orientated interfacing with SIMULINK toolbox enabled studies to be carried out efficiently and conveniently. The simulation engine regulated the bubbles modelled in the bed using kinematics laws. The Clift & Grace bubble interaction model was used to govern the dynamical behaviour of the bubbles. Experimental support and robust theoretical background based on potential flow knowledge have popularised this model among many researchers in their work.

The application of this theory to replicating the bubbling fluidisation process has been validated via the frequency domain against the experimental counterpart of the simulated bed. It is inherent that many simplifications and assumptions of the reality are present in the simulation. Unmistakably, systematic errors and deviations would stem from these treatments. However, it has been shown and assessment carried out that sufficient details were embedded into the core of the simulation such that replication of the reality is satisfactory.

This study acknowledged the fact that the extent at which the different events and phenomena individually affected the overall behaviour of the bubbling process is not known and that it can only be collectively assessed via comparison with the experimental measurements.

Chapter 6

Idealised bubbling fluidisation process

6.1 Introduction

The activities of these bubbles determine the state of the bed. In the control of the fluidisation process, good fluidisation quality is often associated with a state where there is a high density of bubbles of relatively small size in the bed. This provides good mixing while maintaining excellent conversion efficiency between the solid and gas phase. This is also an ideal condition for good heat transfer. Good fluidisation quality is very important in all processes and requires control.

If the presence of these small bubbles can be maintained throughout the bed, then the good quality in a bed will be preserved; however, in real beds the natural phenomenon of bubble interaction and consequently bubble coalescence eliminate the existence of small bubbles particularly in parts away from the distributor. The growth of bubbles as they rise up the bed also contributes to bubbles of larger sizes in the bed.

In order to impose the appropriate control to achieve the desired condition in the bed, a reference process condition must first be established. A reference in the form of an example or an idealised bubbling bed enables the bed quality of the controlled bed to be compared and assessed. However, as its name suggests, an idealised bubbling bed is a bed condition that no real beds can fully achieve. The effort in controlling the process would go into as closely approaching these idealised conditions as possible.

The establishment of the idealised bubbling bed and subsequently other more complicated beds that gradually approach realistic conditions would enhance the understanding of the bubbling fluidisation process and certainly in the interpretation of the dynamics

characteristics of real beds in the frequency domain, of which some fundamental knowledge have already been established in *Chapter 4*.

6.2 Defining the idealised bubbling bed

To achieve an ideal fluidisation quality while maintaining good mixing characteristics of the bed, the bed should not have large bubbles, and they would be totally suppressed if bubble interaction and coalescence do not take place. Bubble growth with height is also undesirable. Therefore, with these criteria, an idealised or reference bubbling bed was conceived.

In the idealised bubbling bed, small bubbles formed at the distributor rise up the bed with velocities proportional to the square root of their respective characteristic diameters without any form of influence on or interaction with any other bubbles. The bubbles are assumed to retain their original rise path at fixed size and velocity regardless of possibilities that there are any other bubbles in their rise paths. In such case, there will be scenarios where bubbles of a larger size overtake those of smaller sizes during their rise. Hence, the resulting bubble overlapping, which is a norm when their lateral positions coincide, would be unrealistic in real vessels. However, this is maintained for the sake of conceptualisation of the idealistic operation of the bed. The introduction of a bubble into the idealised bed should be at random in both the size and lateral location, simulating the characteristic of bubble generation by a porous plate distributor.

To lay down the fundamental characteristics and behaviour of an idealised bubbling bed, the simulated bed developed for the research as described in *Chapter 5* was used, with modifications made to the simulation accordingly. The use of a simulated bed in this study allowed the effects of the processes in the bed that upset the fluidisation quality to be isolated and studied separately, so that their respective individual influences could be identified. The simulated planar bed had the same dimensions (710 mm tall, 500 mm wide, 13 mm deep) as its experimental equivalent with a porous plate distributor. Bubbles were formed from introduction of gas in excess of incipient condition. Upon formation at the distributor, the bubbles rose until the bed freeboard and thereafter, removed from the simulation. The step frequency for all the simulations was 25 Hz. Other simulation

parameters were similar to that used in the simulations carried out and validated with experimental data shown in *Chapter 5*. Frames of images of the simulated bed covered by the Region Of Interest, ROI which included the distributor up to very close to the freeboard such that a leaving bubble would exit the ROI gradually. Image analysis was carried out on these images to measure the Bubble Void Fraction, BVF, in the bed.

Studies carried out based on simulation compromised on having various simplification of the real bubbling fluidised bed because it is impossible to completely model reality. Consistent with details in *Chapter 5*, several assumptions and simplifications were made to the simulated bubbling bed. Amongst the most significant are, that bubble splitting was assumed not to take place as it is difficult to model and simulate. The bubbles were also assumed to have circular shapes throughout the simulation, with a correction for the discrepancy between the size of the bubble, defined by the cloud and the size of the visible void. At the distributor, bubbles were randomly generated at each time step in both size (of certain range) and lateral position to simulate a porous plate distributor.

A simulation of the idealised bubbling bed where all the extra processes (e.g. bubble interaction, coalescence and splitting) were disabled was carried out and its Bode-scaled BVF frequency plot is presented in *Figure 6.2.1* for an idealised bed bubbling at 25.6 mm/s superficial gas above U_{mf}. In comparison with a typical Bode-scaled BVF frequency plot obtained from a normal bubbling bed (*Section 6.3*), the plot shown for the idealised bed exhibits several discrete features. Most apparent is the existence of only one rate of decay of –20 dB/decade at high frequency. There exists a uniform distribution of energy at low frequencies below the break frequency (approximately 0.4 Hz). This implies that the prohibition of bubble growth, interaction and coalescence in the idealised bed has affected the shape of the plot and hence the overall dynamical behaviour of the bed. The differences in the idealised bed plot compared to that of a normal bubbling bed will be discussed in *Section 6.3*. The phase plot is not available because the Bode-scaled BVF plot is essentially a log-log frequency spectral plot and is not an input output comparison of a dynamical system.

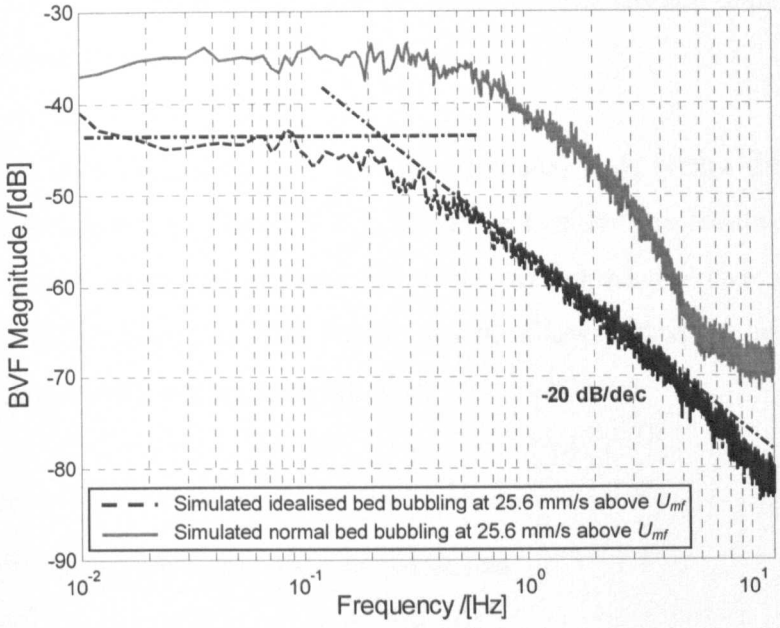

Figure 6.2.1: A typical Bode-scaled BVF frequency plot of a idealised and normal bubbling bed fluidised at 25.6 mm/s superficial gas above U_{mf}.

6.3 The processes complicating the idealised bed

In the idealised bed, which is the bed at its simplest form, bubbles nucleate at the bottom and move up it independently of one another. In reality, the bed closest approaches this state just above the point of minimum fluidisation and deviates with increased excess gas as the process is complicated by other processes, of which three of the most prominent are:

- the increase in bubble size with distance from the distributor;
- the movement of bubbles owing to the influence of others;
- the coalescence of bubbles.

These processes cause the quality of fluidisation in a bubbling bed to deteriorate and therefore it is important that their effects are identified and included in an overall dynamical model of the bed. With one or more of these effects absent, the bubbling behaviour in an idealised bed could be observed and studied and their influences found. The creation of small bubbles that do not grow in size and do not interact nor coalesce would enable the characteristic of the resulting BVF for an idealised fluidisation to be studied. Subsequently with the effects of the other processes included individually, a gradually more realistic bed can be studied after having identified those characterising an

idealised bed. The additional processes can be separately studied and understood, and their effects on the process quality known.

The Bode-scaled BVF frequency plots for two simulated beds where different processes were deployed are shown in *Figure 6.3.1*, alongside that for the idealised and a normal freely bubbling simulated bed. Simulations were performed for two different sets of circumstances: the idealised bed with bubble growth allowed; and the idealised bed with bubble growth and bubble coalescence allowed.

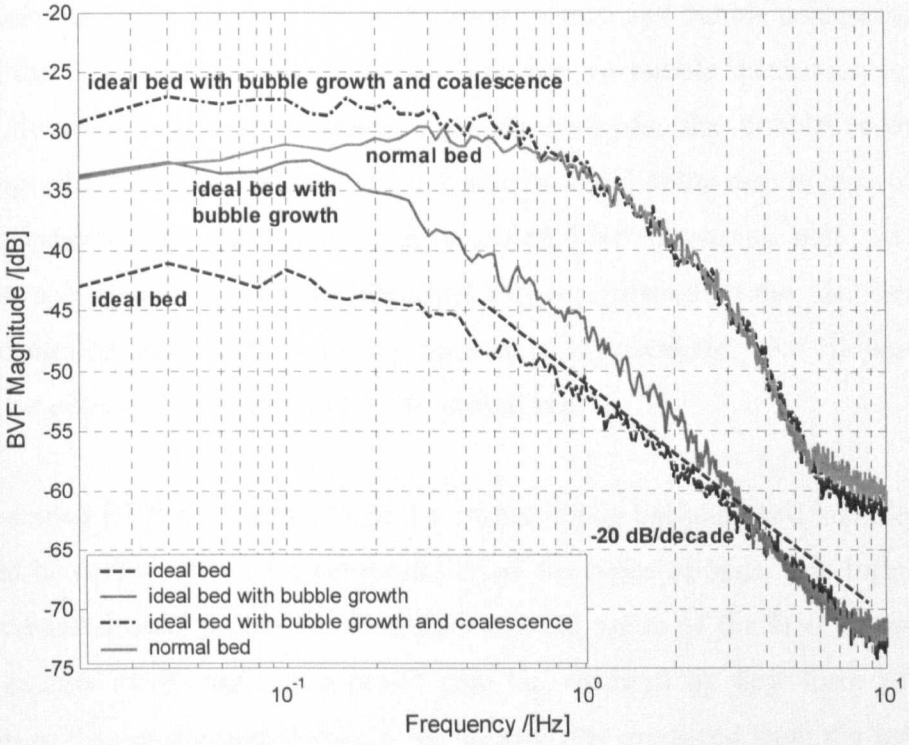

Figure 6.3.1: The Bode-scaled BVF frequency plots of the idealised bed and the derivation of idealised bed with bubble growth, bubble interaction and bubble coalescence. The plot for the normal freely bubbling bed is also included. All the beds were fluidised at 25.6 mm/s superficial flow above U_{mf}.

The size increase of bubbles in the simulation was determined by the empirical relationship due to Kunii et al. (1967) shown in (5.7), such that the diameter increase is linearly proportional with risen height. Bubble interaction was based on the interaction model developed by Clift & Grace (1970, 1971, 1972). Bubble coalescence was governed by the mechanism already detailed in *Chapter 5*, where the process takes place over several time steps based on the properties of the coalescing bubble pair.

The resulting BVF plot for the idealised bed with bubble growth has higher energy in the low frequency band than the idealised bed owing to the frequencies associated with the growth of the bubbles being added to the signal at relatively low frequencies. The discrepancy between the two plots tapers off with increase in frequency. The consequential increase in energy for ranges of frequencies higher than that associated with bubble growth activities was partly the contribution of the harmonic frequencies accompanying some fundamental frequencies of activities in the bed, nevertheless the significance of this feature in the frequency plots is not paramount.

In the simulation of the idealised bed with bubble growth and bubble coalescence, bubbles formed at the distributor rose vertically as there was no bubble interaction to shift them laterally. However, when their lateral positions coincide, the bubbles coalesce upon overlapping. The newly formed bubble has a volume equal to the sum of the volume of the coalescing bubble pair. The resulting Bode-scaled BVF frequency plot has an overall increase in energy over the whole frequency range compared to the idealised bed with more concentrated on the low frequency band up to approximately 0.6 Hz where the plot decays in the similar fashion as that for the normal bed.

The Bode-scaled BVF frequency plot of the normal freely bubbling bed included in *Figure 6.3.1* could be considered as the composite of all the types of beds. The influence of the listed processes spreads across the frequency content range of the BVF measurement at different extents producing a composite plot not dictated by any form of arithmetic summation of the constituting elements but rather a plot produced from the influence of a composite of the processes acting as a whole.

Overall, the plot of the normal bed is similar to that of the idealised bed with bubble coalescence. However, it has a much lower energy around the low frequency region compared to the amount of energy for the idealised bed allowing for bubble growth. Due to the bubble interaction and coalescence process and other activities some of which directly and indirectly derived from the two processes, the normal bed Bode plot has significant amount of energy on the intermediate frequency band. Some of the energy content in this region was also generated by the effect of bubbles leaving the bed.

6.4 Relating the different approaches to dynamical modelling of the fluidised system

As shown in *Chapter 4*, the Bode-scaled BVF frequency content plots revealed much of how the bubbling activities in the bed were observable dynamically via the BVF measure. However, it did not directly disclose the governing dynamics of the bubbling process that determine the frequency content of bubble activities occurring in the bed obtained from the measure of BVF. This can be resolved by treating the fluidised bed as a dynamical system.

There are several methods for modelling the bed as a dynamic system. Model 1 is through system identification that leads towards generation of models for control as shown in *Chapter 8*. The whole fluidised bed is treated as a system with the valve position regulating the flow being the input and the BVF as the output. Model 2 is a modelling method that considers the gas flow rate into the plenum before the distributor as the system input and the measure of BVF that characterises the state of the bed as the output. The dynamical system comprises of both the distributor and the bed.

A third model separates the distributor from the bed, models them individually and treats them as separate entities that affect the overall dynamical behaviour of the fluidised system. This prevents the influence of any other parts of the fluidised system, the distributor in particular, from interfering with the capture of the behaviour of solely the bubbling process. With the flow of gas into the bed plenum remaining constant at steady state bubbling, some of the introduced gas nucleate into packets of gas associated with as bubbles, while some fluidise the bed in the emulsion phase. Taking the input as the time series of introduction of gas bubbles into the bed and the BVF measurement as the output, Model 3 allows the fundamental physical behaviour in a bubbling bed to be studied, investigating the effect of bubble introduction and interaction on the dynamics of the bed without the interference of the dynamics of other sub-systems. This modelling technique is described in detail in *Chapter 7*.

Figure 6.4.1 summarises the scope of each modelling method for the dynamic aspects of the bubbling bed. It shows the portion of the system that was modelled, either as a whole or as isolated components. All of the methods are different in terms of the starting point.

Therefore in this section, certain issues must first be made clear. The first issue is with regards to the treatment of input. In system identification, the input into the plant was taken to be the voltage signal dictating the position of the valve controlling the flow rate into the bed. It determines the amount of flow supplied into the bed.

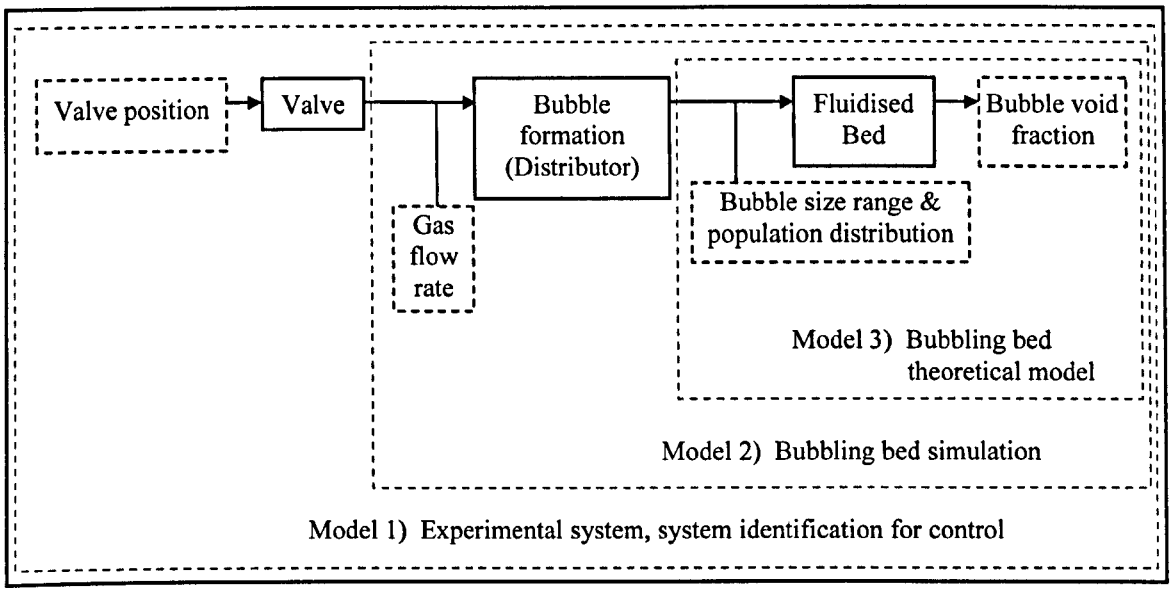

Figure 6.4.1: A summary of the scope of which each modelling method undertakes in modelling the dynamic aspects of the bubbling bed, clearly marked by the boundaries encompassing sub-sets of the entire system.

Brue & Brown (2001) in their effort to dynamically model their fluidised bed based on pressure fluctuation data used an unusual assumption that the input to the process (treated as a dynamical system) was all the activities that were occurring in the bed, which included bubble formation, rise and eruption, and was assumed to contain a frequency content similar to white noise (uniformly distributed energy across the investigated frequencies). Through that assumption, they concluded that a pair and in some occasion three second order transfer functions operating together was a probable representation of the process dynamics without proper physical correlation to the model's dynamic parameters such as natural frequency and damping ratio. This illustrates the practical and difficult problems in appropriately deriving a model to represent the dynamics of the process.

For the theoretical model of the bubbling bed (*Chapter 7*) derived from the description of bubbles expanding in the bed, the input was the time-series of area (volume per unit bed thickness) of gas introduced as bubbles per unit time, A_{gb} into the bed at the distributor. This parameter is consistent with the output signal, BVF, which is also essentially two-

dimensional. However, this parameter was only appropriately measurable in the simulation and not possible on the experimental rig due to the use of a porous distributor at the present configuration, but it might be possible with an orifice distributor.

The indirect measurement of the introduction of gas as bubbles at the distributor using the image analysis system (measuring changes in BVF near the distributor) would not give an appropriate measurement required in the formulation of the model. The frequency content of gas flow into the bed as bubbles measured using the image analysis system produced the graph shown in *Figure 6.4.2*, which is very similar to that of white noise. It is shown later in *Section 6.5*, that the frequency content of the time series of A_{gb}, required to properly fabricate the model and was measured directly at each simulation time step when the bubbles are produced, is indeed very different.

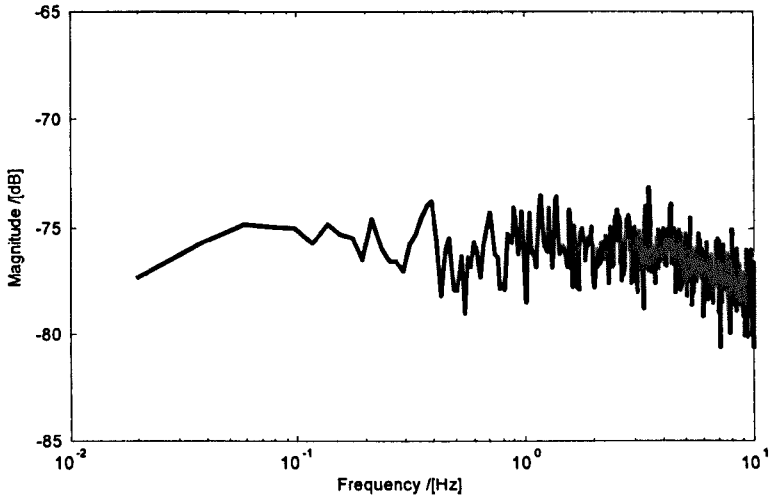

Figure 6.4.2: The frequency content of A_{gb} measured using the image analysis system acquiring images with a very thin slice of ROI at the distributor. The obtained measurement is not a true representation to the actual dynamics of bubble introduction at the distributor.

The modelling of the bubbling process by looking at how individual bubbles affected the BVF in the bed was carried out without taking notice of any prior knowledge of the overall dynamics of the bed. Rather, the bubbles were modelled based on what were known would happen to bubbles introduced at the distributor and rose up the bed (*Chapter 7*). Therefore, this does not include the effect of the distributor and hence characterises the bubbling process alone. However, in the control of the process, the effect of the distributor also plays an important role in the dynamics of the bed. Therefore, it shows that although the

theoretical dynamic model of expanding bubble found is a good description of the bubbling fluidisation process, it falls short of being able to be directly used in the design of controllers. *Figure 6.4.3* illustrates the topography of where the input information was acquired in the different treatments discussed above.

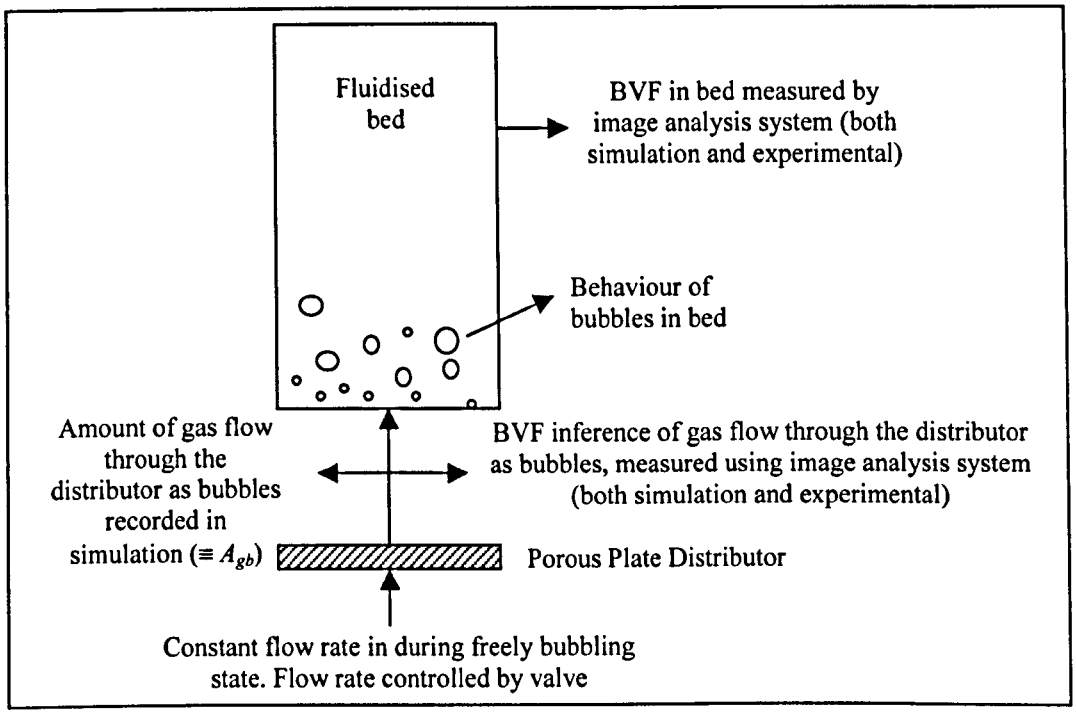

Figure 6.4.3: The relationship between the different methods of acquiring the input and output measurement.

6.5 The influence of gas input into plenum on the bubbling behaviour of the bed

It is evident that the normal bubbling bed significantly deviates from the idealised fluidisation condition due to the presence of bubble interaction and coalescence, as well as other processes that are promoted by the increase in gas supplied into the bed. The consequence of this not only affected the fluidisation quality of the bed, but to the extent that the whole dynamics of the bed is completely altered.

From a dynamical viewpoint, as the gas supply intensifies the input into the bed (introduction of gas as bubbles) changes in terms of its frequency content. The fluidised bed viewed as a dynamical system, also changes dynamically due to internal processes like

interaction and coalescence, whose presence is flow intensity dependent. These changes are therefore explicitly observable in the frequency content of the system output - the BVF. In other words, the change in the fluidisation condition due to the change in the flow intensity into the bed plenum, affects the input into the bubbling bed (introduction of gas as bubbles), the transfer function (the governing dynamics of the bed), and therefore the output response of the fluidised system.

At low flow rate close to the incipient condition, bubbles are sparsely generated resulting in an input signal (A_{gb}) with a wide range of frequency content. At low gas flow rate, the bubbles are introduced into the bed at generally low frequencies. The time-series of BVF mostly consisted of zero values with occasional non-zero BVF values lasting for as long as the nucleated bubbles remained in the bed. *Figure 6.5.1(a)* shows the time series of BVF at low gas flow. However with an increase in the bubbling flow rate, bubbles are more intensely formed at the distributor. This phenomenon produces a frequency content of input with more energy skewed towards the mid and high frequency region. At a much higher gas flow, there were no instances where there were no bubbles in the bed. The fluctuations in the BVF depended on the flow rate of gas where fluctuations of higher frequencies and energy occurred with high flow rates. *Figure 6.5.1(b)* shows this condition in the BVF time-series.

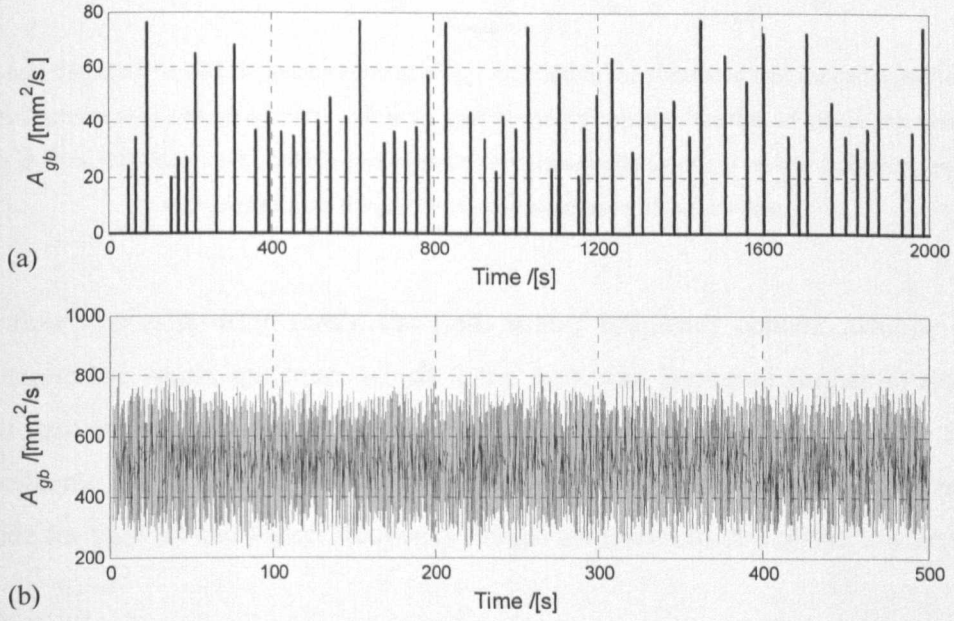

Figure 6.5.1: The time series of A_{gb} for (a) low (0.00256 mm/s) and (b) high (25.6 mm/s) superficial flow above U_{mf} obtained from simulations.

In the simulation of bubbling beds, the introduction of bubbles was dependent on the flow rate. The frequency of introduction was proportional to the magnitude of the gas above U_{mf}. As the flow rate increased, the introduction of bubbles in the simulation was carried out at a higher frequency to maintain a constant average flow rate over time. This introduced a much higher frequency randomness into the bed. With the loss of low frequency inducing activities of bubbles introduction, the increase in the energy of the frequency plot was not as significant for the low frequency range compared to the rest of the frequency range at higher flow rates. The two extreme plots can be seen in *Figure 6.5.2*, with other plots for intermediate flow rates.

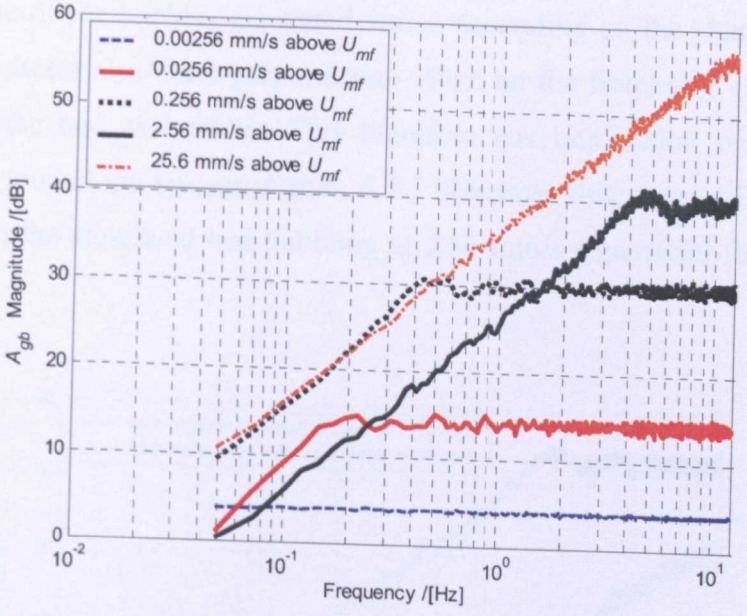

Figure 6.5.2: The Bode-scaled frequency content of A_{gb} supplied to the simulated bed for different flow rates. The plots demonstrated a lower increase in low frequency energy content than that of higher frequency with increase in flow rate because the bubble generation activity gradually loses out on low frequency inducing activities as high frequency elements increase with flow rate.

At low flow rate of 0.00256 mm/s, the Bode scaled frequency content exhibits a level profile across the whole spectrum, which if the flow was increased further in excess of incipient state, began to transform into a somewhat skewed profile, gradually more towards the enhancement of the mid and high frequency band. There was more increase in magnitude for the mid and higher frequency ranges compared to that of the low frequency band.

These changes in the frequency content of the measure of A_{gb} (the input signal for the modelled dynamical system) show the change in bubble introduction dynamics, indications of non-linear characteristics. The alteration of the amount of flow into the bed plenum modified the dynamics of bubble generation and was caused by the porous distributor, demonstrating that non-linearity was intrinsic to the use of this type of distributor. It may be suggested that the distributor converts the constant flow of gas into the distributor to random elements, associated with bubbles. More and more high frequency randomness was generated as the flow rate into the distributor increases, resulting in a plot with a lifted high frequency band as shown in *Figure 6.5.2* for high flow rates.

The range of size of the bubbles generated varies depending on the characteristics of the distributor. This factor also has a preponderate effect on the frequency content of the gas introduced into the bed as bubbles. This therefore has implication on the rest of the dynamical behaviour of the system. *Figure 6.5.3* illustrates this using different distributor characteristics on the simulated bed bubbling at 2.56 mm/s superficial flow above U_{mf} in both cases.

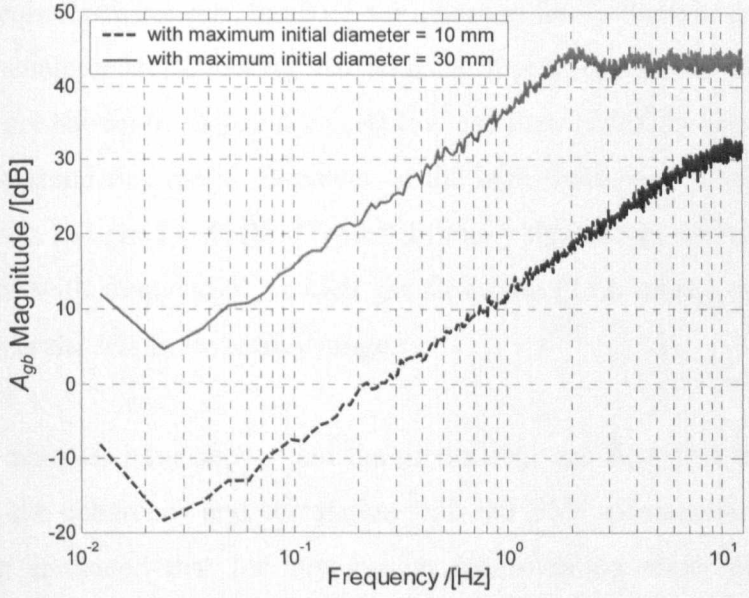

Figure 6.5.3: The frequency content of A_{gb} into the bed as bubbles for the simulated idealised bubbling bed fluidised at the same flow rate (2.56 mm/s superficial flow above U_{mf}) but having different type of distributors installed respectively.

The range of bubble sizes generated at the distributor in a normal bubbling bed was expected to change with flow rate as shown in *Figure 6.5.2*, however, it was assumed

constant for the idealised bed. The nature of the changes in size range in the normal bed is unclear in the present study but reasons of conservation and early rapid coalescence at the distributor were suggested as probable causes of the changes.

6.6 The measure of input-output coherency

In order to obtain the transfer function of the dynamical system, the input and output of the system must have a good coherency. A common term that was used in the system identification study, coherence is a measure of how well the output is correlated to the input, where a value of one marks a good coherency and zero none. The coherence measure offers a guideline as to the best frequency range over which any system identification should be carried out for the system. In system identification, if the coherence between the input and the output is not sound, the obtained transfer function which is suppose to be a representation of the dynamics of the system will not be an accurate one.

The calculated coherence between the BVF for a normal freely (bubble growth with height, interaction and coalescence) bubbling bed with the input, A_{gb}, at two extremes of steady state flow rates are shown in *Figure 6.6.1*. At low gas flow (0.00256 mm/s), the coherence was good at low frequency range. However, at the high frequency range of the spectrum, the coherence was not good (which is typical in many dynamical system signified by the fall in coherence with frequency). At high gas flow rate (25.6 mm/s), the coherence was generally bad over the whole frequency range.

The coherency analyses have shown that the increase of gas flow into the plenum caused deterioration to the coherency and correlation with the BVF measurement. The coherence analyses further indicated that for any system identification study carried out on the fluidisation process, the excitation frequency should also contain low frequency band elements to ensure a good coherence and correlation between the input and output of the system across majority of the frequency range under investigation. However, it is difficult to ensure a good coherency between the input and output at higher band of frequencies, indicated by the deterioration of coherency at higher frequencies in both the plots shown in

Figure 6.6.1. The sudden increase in coherency at approximately 9 Hz does not have any dynamical significance and is related to high frequency noise disturbance.

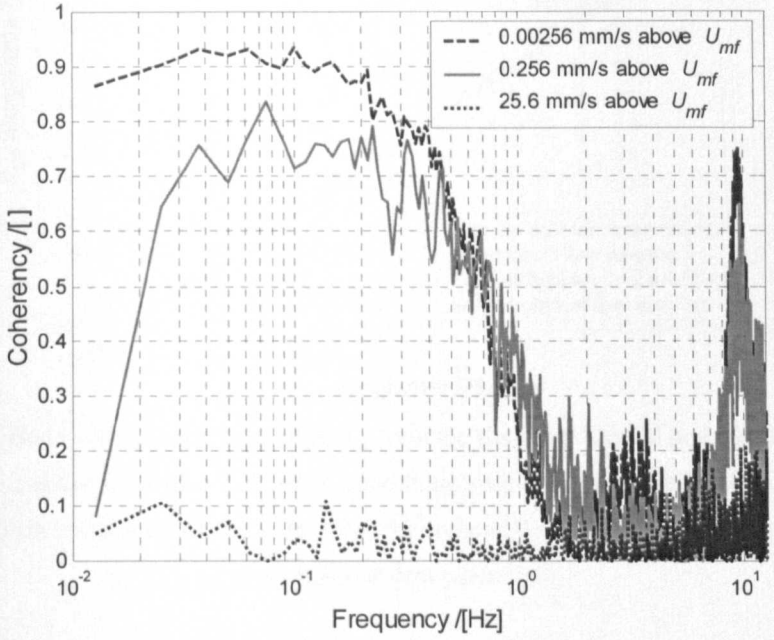

Figure 6.6.1: The graph of coherence between the BVF with A_{gb} for (a) low gas flow rate, 0.00256 mm/s, (b) low gas flow rate, 0.256 mm/s and (c) high gas low rate, 25.6 mm/s superficial flow above U_{mf} obtained from a simulated normal freely bubbling bed.

Superimposing a logarithmic swept sine wave variation to the initially constant flow into the plenum provided low frequency excitations that would improve the coherency at these frequencies. However, it was difficult and seemingly impossible to improve the coherency for higher frequencies, typically above approximately 0.5 Hz. This is dynamically realistic in a system such as this where it is inherently a slow and delayed system and will not properly respond to high frequency excitations. Although the improvement technique is more relevantly required for bubbling at higher flows, application to lower flows as well would guarantee accountability in any coherency issues. The area of gas bubbles introduced per unit time, A_{gb}, into the simulated bed using this strategy resulted in a Bode-scaled frequency plot presented in *Figure 6.6.2.*

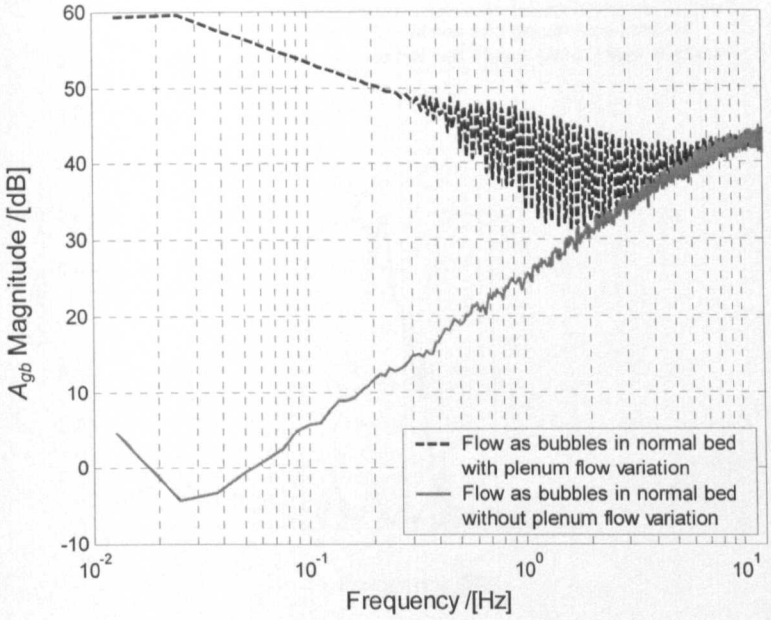

Figure 6.6.2: The Bode-scaled frequency plot of A_{gb} from the simulated normal bed bubbling at a superficial flow of 25.6 mm/s above U_{mf} with a 7.68 mm/s logarithmic swept sine wave variation in flow into plenum from 0.01 to 10 Hz excitation frequency. Included for comparison is the corresponding plot without the superimposed flow excitation.

It can be seen that there are intermittent fluctuations in the frequency content from 0.3 Hz onwards, corresponding to the local minima of the waveform, which contain relatively lower energy than the local maxima. Although problems associated with this may not be immediately apparent, a more conservative approach could be taken to overcome this with the use of a uniformly random variation in flow superimposed on the initially constant flow into the bed plenum. The nature of randomness in the variation could prevent the distinct intermittent fluctuations from appearing in the energy content of the input, A_{gb}.

Conducted tests gave a good coherency measure for the simulated normal bed bubbling at flow rate of 25.6 mm/s with a 7.68 mm/s logarithmic swept sine wave variation in the plenum flow excited from 0.01 to 10 Hz. A_{gb}, was measured to obtain the frequency plot and it could be seen that the low frequency end of the plot has been lifted significantly, although, gradually decaying in magnitude with frequency running up to the Nyquist frequency. This frequency content profile gave a much desirable coherency with the BVF measurement as shown in *Figure 6.6.3*.

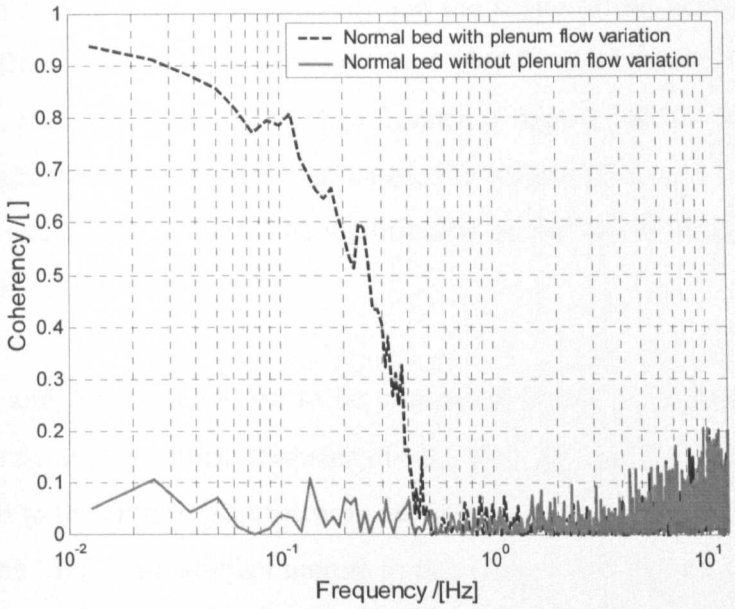

Figure 6.6.3: The improved coherency between the BVF and A_{gb} measurement for the simulated normal bed bubbling at 25.6 mm/s superficial flow above U_{mf} with a 7.68 mm/s logarithmic swept sine wave variation in plenum flow with 0.01 to 10 Hz excitation frequency.

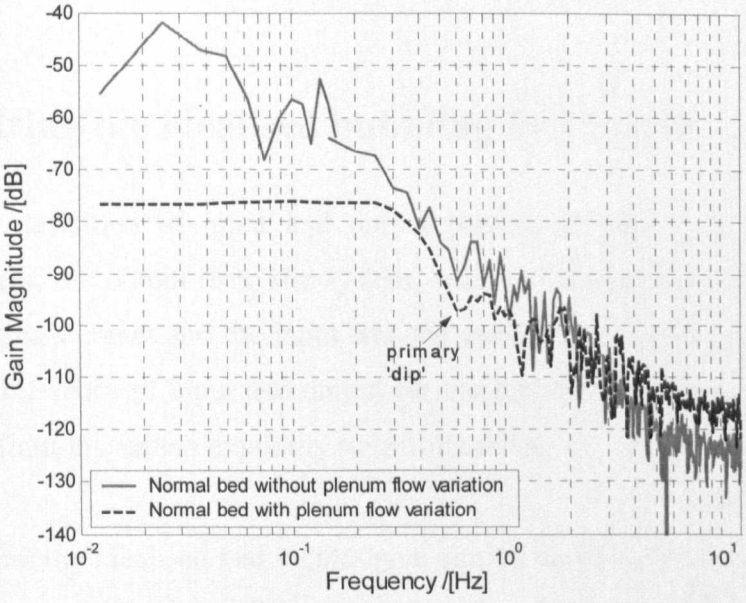

Figure 6.6.4: The transfer function of the simulated normal bed bubbling at 25.6 mm/s superficial flow above U_{mf} with a 7.68 mm/s logarithmic swept sine wave variation in plenum flow from 0.01 to 10 Hz excitation frequency.

The improved coherence achieved with this approach enabled the actual transfer function of the bubbling process to be obtained, which dictated the behaviour of the bubbling process at various excitation frequencies. The transfer function presented as a Bode gain

plot is shown in *Figure 6.6.4*. It is apparent that the shape of the actual transfer function Bode plot is different from the initially obtained plot for the bed without flow variation into the plenum, particularly around the low frequency region. Due to the lack of desirable coherence at higher frequencies for both cases, the shapes of the plots at that region of frequencies are reasonably similar. The significance of the salient features in the plots is discussed in detail in the *Section 6.7*.

If *Figure 6.6.3* and *Figure 6.6.4* are to be compared, it can be seen that the coherency begin to deteriorate after the break frequency (≈ 0.2 Hz). The continuous drop in coherency is closely related to the drop in gain towards the formation of the primary 'dip' as shown in *Figure 6.6.4*. The 'dip' is an artefact unique to this system and therefore this suggests that correspondingly, the drop in coherency is an artificial feature caused by the coincidental of bubble exit and introduction (see *Section 6.7*). This is a very similar case to where a typical dynamical system operating close to its resonant frequency will witness a sudden and large shift in the phase between the input and output signals.

6.7 Acquiring the idealised bubbling bed transfer function

Reiterating the definition of input and output parameter while treating the bed as a dynamical system, the output from the system, which characterised the system response, was the BVF measurement and the input was the area of gas bubbles introduced per unit time, A_{gb}. Any reference of input and output for the rest of the chapter would refer to the above given definitions, unless explicitly stated otherwise.

It is apparent that the idealised bed would have similar issues as the normal bed with the flow into its plenum as for its realistic counterpart i.e. the deterioration of low frequency range energy that is detrimental to the coherency with the output from it. The improvement technique was therefore required to account for the loss of low frequency elements in the input so that the input and output of the idealised bed could be brought to a better agreement of coherency. The Bode-scaled BVF frequency plots for the idealisedised bed for various flow conditions that would be expected with and without the application of the improvement technique are shown in *Figure 6.7.1*. Comparatively, the BVF frequency plots for the idealised bed when the improvement technique was employed are of higher

energy magnitude than before the improvement was implemented. Apart from that, the intermittent 'dips' in the plots are also more prominent for all fluidisation conditions especially for those of higher flow rates. The rate of decay in all the plots remained similar at –20 dB/decade.

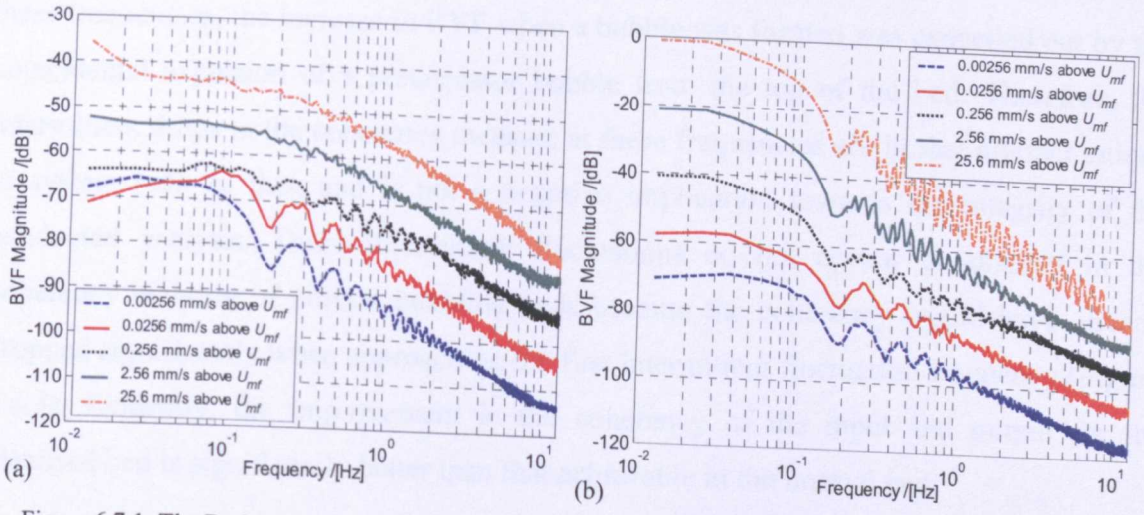

Figure 6.7.1: The Bode-scaled BVF frequency plots are shown for the simulated idealised bed bubbling at different flow conditions (a) without and (b) with the plenum flow variation to improve on coherency.

The improvement technique allowed the actual transfer function of the bubbling behaviour of the idealised bed to be obtained. The coherency between the input and output of the idealised bed at different bubbling conditions with and without the improvement measure undertaken are presented in *Figure 6.7.2*.

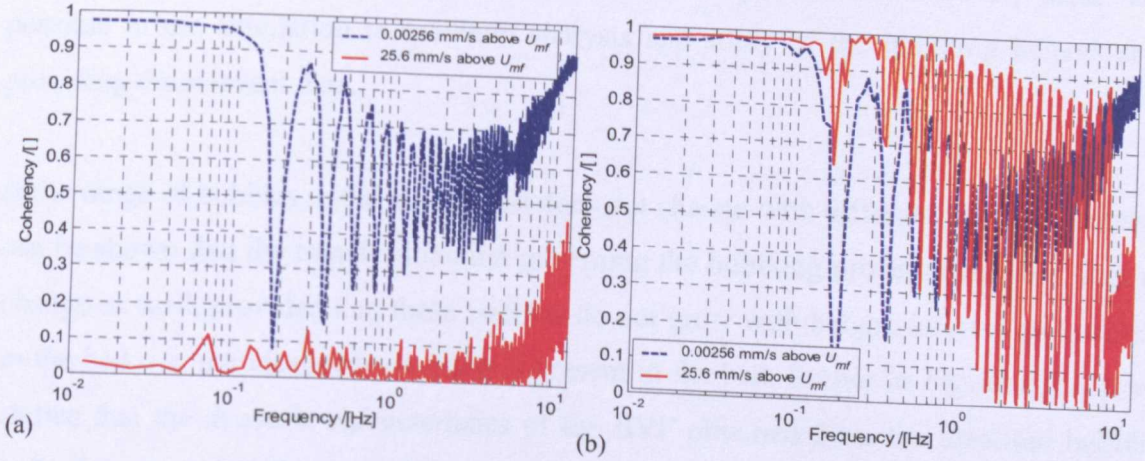

Figure 6.7.2: The coherency between the BVF and A_{gb} measurement for the simulated idealised bed bubbling at different flow conditions (a) without and (b) with the plenum flow variation to improve on coherency.

The points in the intermittent frequencies where the coherence was comparatively worse correspond to the anti-resonance frequencies identified earlier in both the input and output frequency content of the bubbling beds. At these frequencies, the output and the input were not well correlated because an input of energy (bubble introduction) into the system was not complemented by a supposed increase in energy in the output (BVF). It was because at these frequencies, the increase in BVF when a bubble was formed was cancelled out by the coincidental expulsion of a predecessor bubble from the top of the bed. Therefore, the intermittent drops in the coherency measure at these frequencies are in fact artefact unique to system such as this, and is not a negative implication towards the integrity of the conducted analysis. These intermittent fluctuations do not appear as distinct in the coherency measure of normal bubbling beds because the coherency would have already dropped significantly when approaching the first intermittent fluctuation frequency (*Figure 6.6.3*). Evidently, the improvement in the coherency of the input and output for the idealised bed is significantly better than that achievable in the normal bed.

At very low flow rates above the incipient condition, nucleated bubbles were of very small sizes; in fact, most were smaller than the thickness of the planar bed. However, their existence was taken into account in the BVF measurement in the simulation to enable proper study of the bubbling process. This allowed for every bubble generated to be accounted for in the measure of A_{gb}. The measure of BVF and other parameters at very low flow rate conditions (0.00256 to 2.56 mm/s superficial gas flow above U_{mf} into plenum) are apparently physically difficult to measure in the experiments. However, these were possible in the simulation to facilitate analysis and study of the bubbling behaviour by providing the relevant data.

If the range of bubbles initial size issued does not change with different flow conditions, it can be shown that the transfer function governing the bubbling process dynamics does not change as well, provided that these bubbles do not grow with height, interact and coalesce in the bed; i.e. the idealised condition is present in the bed. Earlier in *Figure 6.7.1*, it was shown that the dynamic characteristics of the BVF obtained from the idealised bubbling bed changes with flow condition. These changes were due to dynamical changes experienced only by the measure of A_{gb} when flow supply changes as shown previously in *Figure 6.5.2*. The transfer functions obtained from the idealised bed's input-output measurements at various flow conditions are shown in *Figure 6.7.3*.

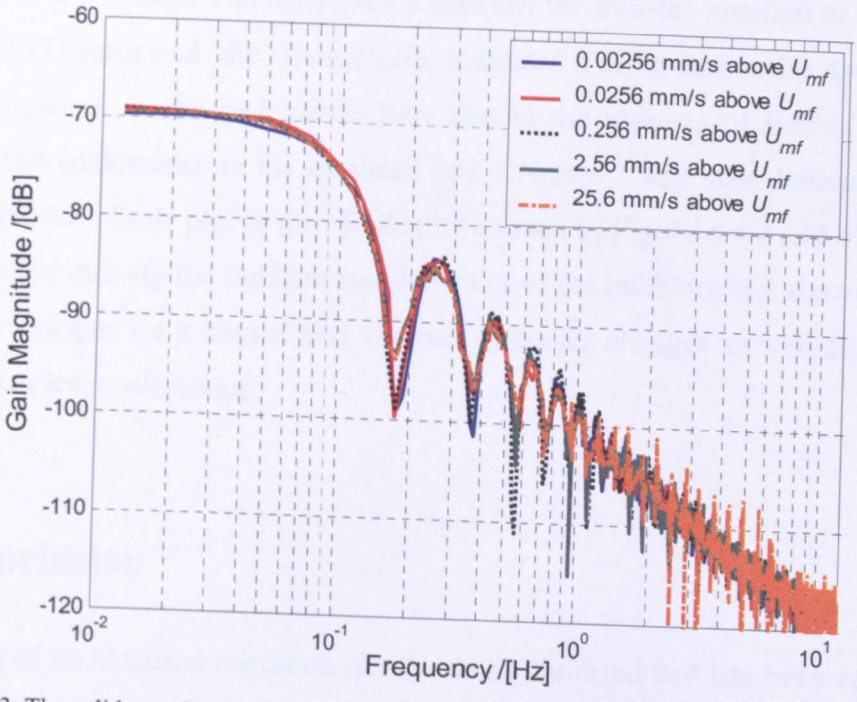

Figure 6.7.3: The valid transfer functions of the bubbling process in the idealised bed bubbling at various flow conditions. Logarithmic swept sine wave variation was introduced in addition to the flow into the plenum.

It can be clearly seen that the transfer function of the bubbling process in the idealised bed did not change with the increase of amount of flow introduced into the bed through the plenum, implying that the governing dynamics did not change over a range of flow rates. A logarithmic swept sine wave variation to the flow was used to improve the coherency between the output and input in order to obtain the legitimate corresponding transfer function. The obtained transfer function of the bubbling process in the idealised bed presents itself as being an unconventionally encountered transfer function of a dynamical system. Apart from having a typically encountered level low frequency gain, LFG and a decay at the rate of –20 dB/decade (typical characteristic of first order dynamic systems) occurring after a distinguishable break frequency, the plot has in addition, intermittent 'dips' or anti-resonances, commencing after the break frequency, which was caused by the coincidences of bubble exit and introduction.

For the case of the normal bed, the transfer function obtained for the bubbling process, such as that shown in *Figure 6.6.4*, is considerably different from that of the idealised bed (*Figure 6.7.3*), although there are significant extent of resemblance between them; the level

LFG, the presence of intermittent 'dips' after the break frequency, and an approximate roll-off rate of –20 dB/decade. The discrepancy between the transfer function of the two beds, in terms of LFG value and 'dip' frequencies, indicated a difference in the dynamics of the bubbling behaviour in the bed, particularly due to the absence of bubble size growth, interaction and coalescence in the idealised bed. *Chapter 7* will later demonstrate the use of transfer function Bode plot or gain Bode plot as seen in *Figure 6.6.4* and *Figure 6.7.3* to characterise and identify the fundamental dynamics of the bubbling bed showing that when flow supply changes for a normal bed, the bed dynamics changes as well due to effect of bubble growth and coalescence.

6.8 Conclusion

The concept of an idealised condition in a bubbling fluidised bed has been conceived and its properties and characteristics have been established. It was pointed out that the fluidised system could be separated into two portions allowing the constitutive components to be studied individually without the influence of others. A fluidised bed comprising of first the distributor, takes in gas supply from the plenum and through its dynamical characteristics introduces gas into the bed as two phases: the fluidising gas of the emulsion phase, and packets of gas nucleating as bubbles when the supply of gas exceeds that required for incipient fluidisation.

The dynamics of introduction of gas as bubbles is shown to change with the amount of flow into the plenum indicating first contact with source of non-linearity. Thereafter, without the presence of bubble size growth due to height in bed, bubble interaction and coalescence, which are non-linear features in normal beds, the idealised bed remains in a state of linearity with the existence of many minute bubbles throughout the whole column of the bed. The dynamics of the bubbling process of a bed in an idealised state was subsequently shown, via the obtained transfer functions, to be similar for different fluidisation conditions. This suggests that the bed in its idealised state will remain as a linear system.

Chapter 7

Dynamical modelling of bubbling fluidisation process

7.1 Introduction

The fundamental physical behaviour of a bubbling fluidised bed is shown in this chapter to be sufficiently well modelled using a relationship found commonly in the field of digital electronics. This modelling method assumes a fluidised bed is a temporary store of gas in which an introduced packet of gas referred to as a bubble resides for a given amount of time determined by its physical properties before leaving at the freeboard. Extending from a simple case with a single bubble in the bed, the process of a freely bubbling bed was investigated and the model was able to capture the fundamental physical features that determined the overall dynamical behaviour of the bubbling process.

It is necessary to relate the transfer function (i.e. G(s) = BVF (output)/A_{gb} (input)) obtained through measurements of the bubbling process to some form of mathematical expression, through which could be achieved by a suitable transfer function model that best-describes its governing dynamics. The model was essential to impose a mathematical description that facilitates the study of the fundamental dynamics of the process such that, through the devised conceptual idealised bed condition (*Chapter 6*), important underlying dynamic features could be isolated and studied in greater depths. This will lead towards a better understanding of first, the basic process and then the fluidised system as a whole. This will ultimately lead to a knowledge-based design of controllers specific to the process.

7.2 Bubbling bed as a temporary storage of gas

It has been demonstrated (*Section 6.7*) that the appropriate treatment of the input allowed a coherent transfer function of the bubbling process to be obtained. The transfer functions obtained for various flow conditions are shown to be similar for when the bed was idealised in *Figure 6.7.3*. The features in the plots, especially the 'dips' or anti-resonances, have significant implications that relate to the dynamical behaviour of the process. To simplify discussion, consider the transfer function for the idealised bed bubbling at 0.256 mm/s above incipient condition, which is reproduced in *Figure 7.2.1*

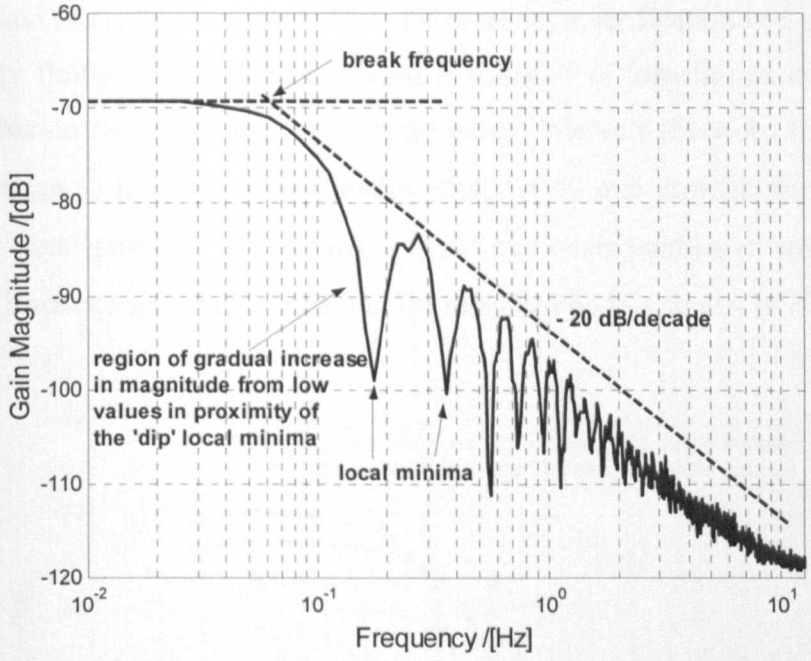

Figure 7.2.1: The transfer functions of the bubbling process in the idealised bed bubbling at 0.256 mm/s above incipient conditions. Logarithmic swept sine wave variation was introduced in addition to the flow into the plenum.

The decay rate of -20 dB/decade in the plot after the break frequency indicated an integrating effect in the transfer function that terminated at the break frequency to form a level LFG, presumably due to the limit in the minimum of size of bubble present in the bed. The frequencies where the intermittent 'dips' occurred on the plot were found to correspond to the residence times of bubbles of size range generated in the bed and the accompanying harmonic frequencies. The 'dips' were caused by anti-resonance within the bed in response to the introduction of bubbles at some frequency just as when some bubbles were leaving at the freeboard. When this takes place, a relatively small change in

the overall BVF in the bed was registered so that there was a low level of energy associated with the frequencies at which the events took place, hence the 'dips' seen. The local minima of the 'dips' was obtained when a bubble of a certain size was leaving the bed just when another of the similar size was introduced at the distributor, of which that bubble would also be the largest in the size range present in the bed. The coincidences of entry and exit of bubbles of other similar sizes also resulted in lower frequency magnitudes in the plot but were associated with frequencies with higher magnitudes located on either sides in proximity of the local minima.

When the idealised bed is issued with a different amount of gas pulsation into the bed, the transfer function of the bed will alter. With this in mind, a verification was carried out with the incipiently fluidised idealised bed being introduced at logarithmic swept (for more dynamic excitation coverage over lower frequencies) intervals (between 0.01 and 10 Hz) with pulses of gas to produce single bubbles of $d_{b,e} \approx 40$ mm through the central nozzle. The resulting Bode gain plot, in comparison to the plot when bubbles of size, $d_{b,e} \approx 80$ mm in equivalent diameter were introduced into the idealised bed, is shown in *Figure 7.2.2)*.

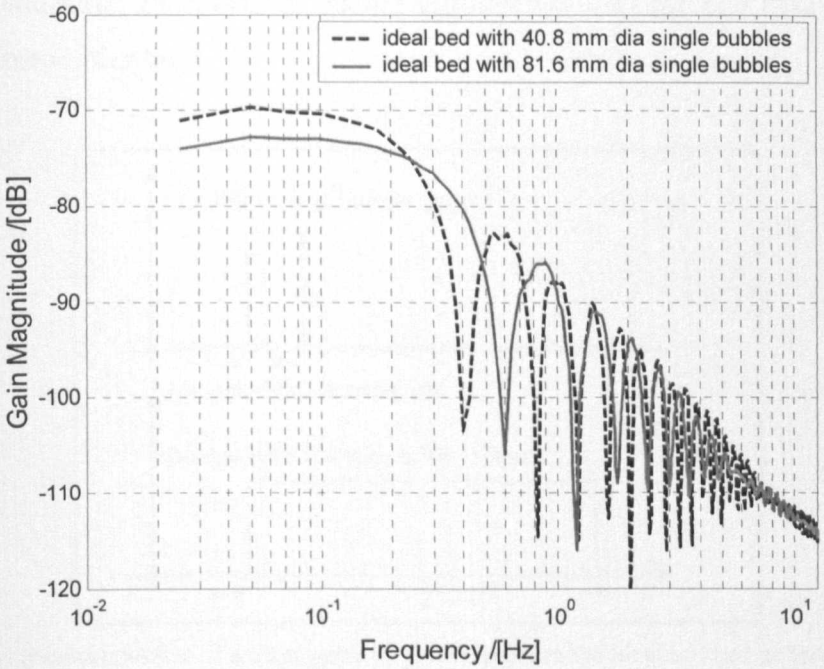

Figure 7.2.2: The Bode gain plots of the idealised bed issued with streams of single bubbles at logarithmic swept intervals 0.01 to 10 Hz with bubbles of equivalent diameter, $d_{b,e} \approx 40$ mm and 80 mm.

The introduction of a packet of gas at the distributor in excess of that needed to incipiently fluidise the bed leads to the nucleation of a void observable in the planar bed. This is associated with the presence of a bubble that would be in residence in the bed for a period of time before expulsion at the bed freeboard. The duration of its residence in the bed is primarily governed by its size. The issuing of a bubble takes a fraction of time. On the other hand, the presence of the nucleated bubble in the bed affects the homogeneity of the particulate fluidised phase for as long as that bubble is in residence in the bed, lasting typically for a few seconds. The presence of the bubble is shown by the measure of non-zero BVF values for that duration. This sequence of events suggests that a simple model of the bed is that it acts as a temporary store of the excess gas introduced into it, where the packet of gas bubble issued into the bed is stored in the bed for the period of time the bubble takes to rise to the freeboard.

This sort of behaviour can be dynamically modelled by a transfer function equation derived in the *s*-domain (Laplace Transform). This sort of system where the output signal resulting from an impulsive input is held at a constant level for a specified time closely resembles a zero-order hold system, which is widely met in the field of digital electronics. *Figure 7.2.3* illustrates the event of bubble introduction into the bed that resembles the function of a zero-order-hold.

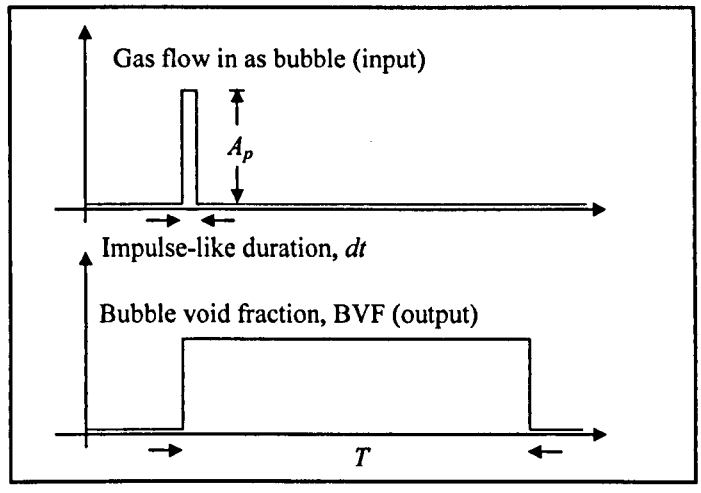

Figure 7.2.3: The introduction of a short pulse of gas bubble into the idealised bed as the input and the corresponding output BVF signal of which the non-zero value was held for a period of time until the bubble exits the bed

7.3 Theoretical model for single bubbles

Assuming the fluidised bed as being a temporary store of gas and adopting the concept of zero-order-hold system, a theoretical model has been developed for the bed with the presence of a single bubble. The transfer function of the theoretical model was validated by comparison to the transfer function of the simulated bubbling fluidised bed. Investigation was carried out firstly with a very simple case of a single bubble in the fluidised bed as described in this section, directly applying the formulated theory to obtain the system transfer function. Progress from this then allowed more complicated situations to be investigated such as having multiple bubbles in the bed, with consideration of the effects of bubble interaction, and coalescence.

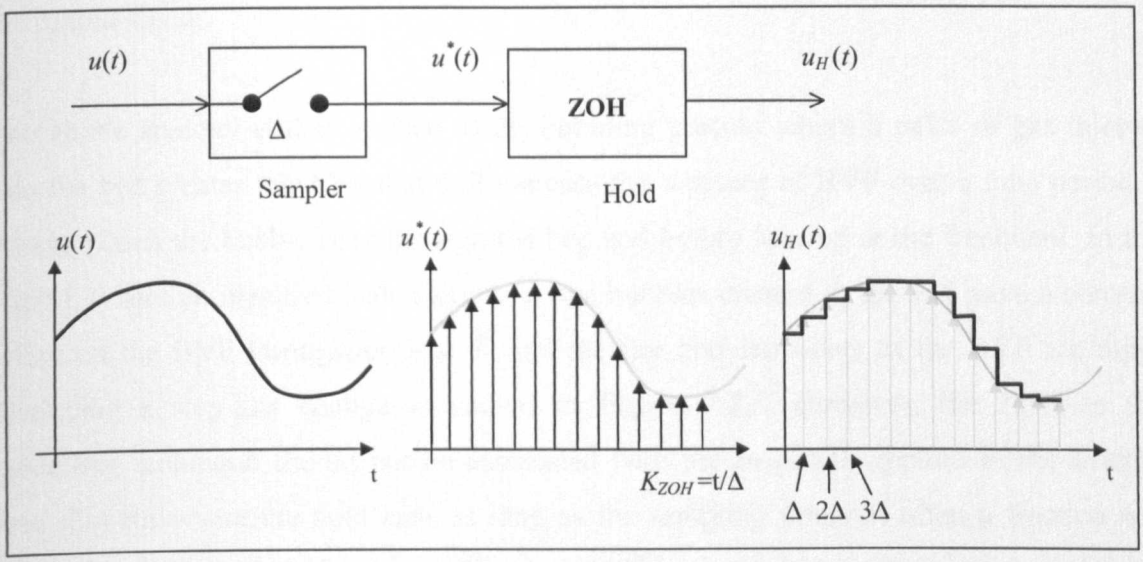

Figure 7.3.1: The block diagram of the zero-order-hold function in digital electronics and the resulting signals.

In digital electronics where time is discrete, when an impulse signal is introduced as the input, the zero-order-hold (ZOH) maintains the signal over a pre-determined time, which is the sampling interval Δ, before the signal changes to the initial value in the output or take on the next given value at the input. The term zero order refers to a zero-order polynomial (a constant value) that is used to extrapolate between the sampling intervals to allow the value of the last sample to be retained until the next sample is ordered. This results in a staircase-like signal as shown below in *Figure 7.3.1.*

Instead of describing the ZOH in the time domain, it is preferable to work in the *s*-domain using the Laplace transfer function, when modelling using dynamics techniques. Applying the Laplace transform, with zero initial conditions, results in:

$$u_H(s) = \mathrm{L}[u_H(t)] = \sum_{K=0}^{\infty} u(K_{ZOH}\Delta) e^{-K\Delta s} \frac{1}{s}\left[1 - e^{-\Delta s}\right]$$
$$= u^*(s) \cdot \frac{1}{s}\left[1 - e^{-\Delta s}\right] \tag{7.1}$$

Therefore, the transfer function of the ZOH is:

$$H_{ZOH}(s) = \frac{u_H(s)}{u^*(s)} = \frac{1}{s}\left[1 - e^{-\Delta s}\right] \tag{7.2}$$

where $u_H(s)$ is the output and $u^*(s)$ is the input. The ZOH can be described as an integrator that is only effective for a time period Δ, and resets at each sampling instant. Its impulse response is similar to the rectangular signal of duration *T*, shown in *Figure 7.2.3* earlier for the output signal.

The above analogy is thus applied to the bubbling process where a pulse of gas injected into the bed creates a bubble that will increase the measure of BVF over a time period, *T* during which the bubble rises through the bed and before leaving at the freeboard. In this regard, where an idealised bed is assumed, the bubbles created in the bed have a constant effect on the BVF throughout time *T*, and the rise and fall times of the BVF are rapid, producing a step-like change as shown in *Figure 7.2.3*. However, the ZOH in this modelling technique should not be associated with the treatment applied in the discrete time domain where the hold lasts as long as the sampling interval, often a fraction of a second. Instead, the hold lasts for as long as a bubble remains in the bed, which could span several seconds.

Therefore, the effect of a pulse of gas issued into the bed as bubble on the BVF could be modelled with the transfer function, similar in form to (7.2), as shown below

$$G(s) = \frac{K_{b,ZOH}}{s}\left(1 - e^{-Ts}\right) \tag{7.3}$$

where $K_{b,ZOH}$ is a constant related to the bubble size. *Figure 7.3.2* shows time series of an example that illustrates the effects on the BVF when a continuous stream of gas pulses were introduced into the bed based on the transfer function (7.3).

In the example, the gas pulses were 0.1 s apart and the bubble residence time in the bed, T was 1 s. It could be seen that after 1 s, the BVF levels off with any additional gas pulses given, as a bubble leaves the bed with every new bubble introduced after the time period of 1 s. The amplitudes of the BVF and the gas pulse were arbitrary.

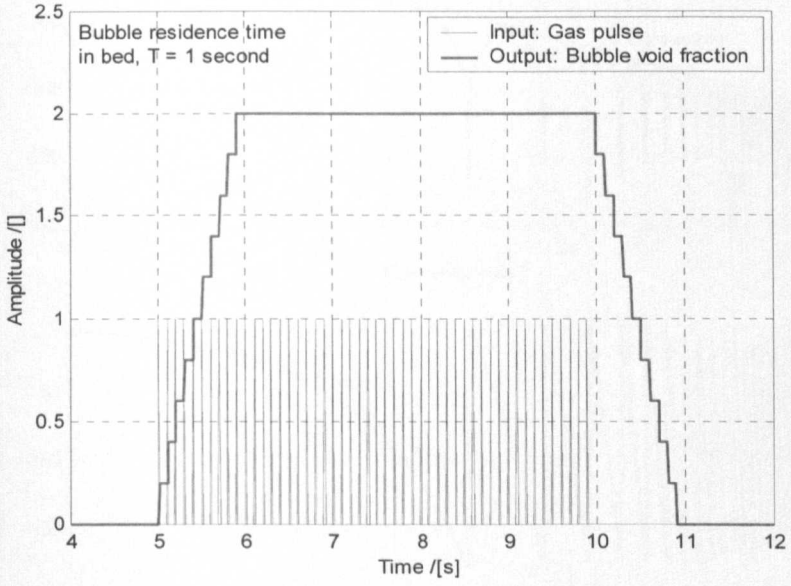

Figure 7.3.2: The effect on the bubble void fraction when a stream of continuous gas pulses were introduced into the bed, based on the transfer function in (7.3).

Simplifying (7.3) in the frequency domain, we have

$$G(j\omega)=\frac{K_{b,ZOH}}{j\omega}(1-\cos(\omega T)+i\sin(\omega T)) \tag{7.4}$$

The magnitude of $G(j\omega)$ can be determined from

$$\begin{aligned}|G(j\omega)| &= \frac{K_{b,ZOH}}{\omega}\left(1+\cos^2(\omega T)-2\cos(\omega T)+\sin^2(\omega T)\right)^{\frac{1}{2}} \\ &= \frac{K_{b,ZOH}}{\omega}\left(2(1-\cos(\omega T))^{\frac{1}{2}}\right) \\ |G(j\omega)| &= \frac{K_{b,ZOH}\sqrt{2}}{\omega}(1-\cos(\omega T))^{\frac{1}{2}}\end{aligned} \tag{7.5}$$

The Bode diagram of the transfer function in (7.3) shown in *Figure 7.3.3* demonstrates that the theoretical model exhibits strong resemblance to the transfer function of the idealised bed from the simulation, with all the characteristic features present in the plot. The phase part of the Bode diagram is also included to show the phase difference between the input and output at the various frequencies under investigation. The decaying trend in the phase

plot is characteristic of a dynamical system containing elements of time delay. The Bode diagram of the theoretical model predicts the magnitude and input-output phase difference of the bubbling process, i.e. the changes of BVF with A_{gb}, at various frequencies.

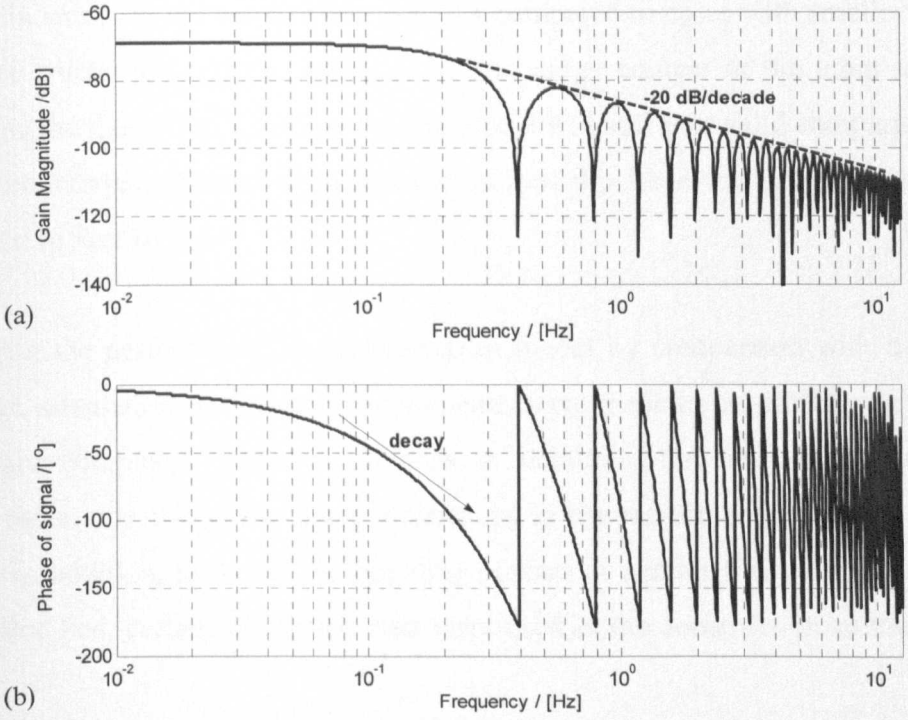

Figure 7.3.3: The bode diagram of the idealised bed with the introduction of single bubbles ($d_{b,e} \approx 40$ mm) at logarithmic swept frequency of 0.01 to 10 Hz modelled by the transfer function in (7.3). The phase plot is left wrapped so that the sudden shift of 180° and the frequencies at which the shift occur can be seen.

For small angles ($\omega \to 0$)

$$\cos(\omega T) \approx 1 - \frac{\omega^2 T^2}{2}$$

The LFG of the theoretical model transfer function is obtainable from (7.5) where the magnitude of $G(j\omega)$ at $\omega \to 0$ is given by

$$\left|G(j\omega)\right|_{\omega \to 0} \approx \frac{K_{b,ZOH}\sqrt{2}}{\omega}\left(\frac{\omega T}{\sqrt{2}}\right) = K_{b,ZOH} T \tag{7.6}$$

It can be seen that the theoretical model suggests that the LFG of the bed is dependent on two factors, which directly relate to the size of the bubble. For a given LFG value, a larger bubble meant a large $K_{b,ZOH}$ value but the value of T will become smaller as larger bubble rises faster. Also, it can be observed in *Figure 7.2.2* that the Bode plot of the idealised bed with smaller single bubbles has relatively higher magnitudes than when larger bubbles were introduced. This does not contradict the above argument, but rather implies that the

relationship between $K_{b,ZOH}$ and T is not linear. The idealised bed exhibits stronger BVF (output) frequency energy content when larger single bubbles were introduced. The corresponding energy content of the input signal, which is the measure of the area of gas bubbles introduced per unit time, A_{gb}, was also higher, therefore proportionally resulting in a lower gain values in the transfer function plot compared to cases with smaller bubbles. It is therefore crucial to study the influence of the energy content of the input signal when constructing the theoretical model so that the model will still be a valid comparison with its simulated counterpart. A detailed explanation of how this issue was dealt with in the study is addressed in *Section 7.4*.

In validating the performance of the theoretical model by comparison with its simulated counterpart, simulation and modelling parameters were made to be similar where possible. As they are completely different methods in obtaining the bed steady-state transfer function, there will always be slight differences in the results observable in their Bode diagrams. In addition, to model the bubbling process at similar fluidisation conditions as the simulated bed, certain simulation data were used in the construction of the theoretical model.

The introduction of single bubbles into the idealised bed with increasing frequency resulted in the formation of a stream of single bubbles when the introduction interval was shorter than the single bubble residence time. However, this did not affect the dynamical treatment of the analysis because in the idealised bed, single bubbles in the stream did not coalesce and interact with each other. However, the scenario would be different if a second single bubble (regardless of size) was introduced simultaneously alongside the first stream creating a second stream of single bubbles. The simulation of the idealised bed with a stream of single bubbles introduced at logarithmic swept frequency of 0.01 to 10 Hz was conducted such that the input signal (A_{gb}) covers the range of excitation frequency similar to the theoretical model. The single bubbles were kept at a constant size of $d_{b,e} \approx 40$ mm by administering a pulse of gas into the centre of the bed through the single nozzle. Similar conditions were replicated in the parameters required in the theoretical model, particularly the bubble size and bubble introduction rate. The results from the two methods of obtaining the transfer function of the idealised bed with single bubble stream are shown in *Figure 7.3.4* in the form of Bode plots.

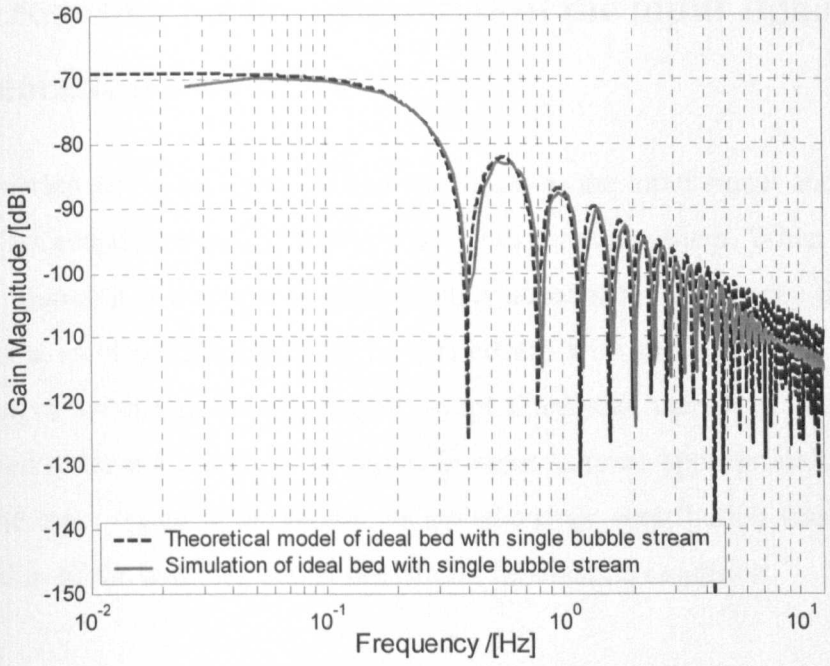

Figure 7.3.4: The comparison of the Bode plots for the idealised bed with a stream of single bubbles ($d_{b,e} \approx$ 40 mm) introduced at logarithmic swept frequency of 0.01 Hz to 10 Hz obtained from the simulation and the theoretical model in (7.3)

It can be seen that the Bode plots from the two methods are very similar indicating that the theoretical model appropriately describes the transfer function of the idealised bed with single bubbles. In other words, the theoretical model has been successfully implemented to describe the governing dynamics of the bubbling process in this simple case. There are minor discrepancies between the plots due to the different approaches to obtaining the transfer functions. It can be seen that the consistency of the oscillating profile in the simulated transfer function plot gradually decreases with frequency. This was apparently caused by the deterioration of the coherency in the simulation input-output data in this frequency region, already shown earlier in *Figure 6.7.2(a)*. However, due to the much lower magnitude of the gain at higher frequencies, the differences in the plots, i.e. the difference in dynamics at higher frequencies, can be neglected. Similarly, this could also be deduced for all the plots produced in future, let it be Bode-scaled BVF plot or transfer function Bode plots.

7.4 Accounting for the magnitude of the input signal in the theoretical model

The introduction of bubbles into the bed was taken as the input signal and in a dynamical sense, this act constitutes adding energy into the dynamical system. When constructing the theoretical model, it is essential to appropriately account for the energy that was given at the input if a valid comparison is to be carried out with the simulated bed. During the construction of the model, the logarithmic swept sinusoidal interval of bubble introduction was assumed to have a unity energy input. In order to more appropriately account for the effect of the input signal in the model, its actual energy contribution was calculated from the simulation of the bubbling bed at the similar fluidisation condition.

Figure 7.4.1 shows the time series of the area of gas bubbles introduced per unit time, A_{gb}, (input) obtained from simulating introduction of single bubbles into the bed. The signal resembled an impulse signal (triangular shape) and the magnitude of the signal was the energy of change experienced by the input signal, which indicates that:

$$\left|A_{gb}\right| = (impulse\ amplitude)(impulse\ duration) * 0.5 \tag{7.7}$$

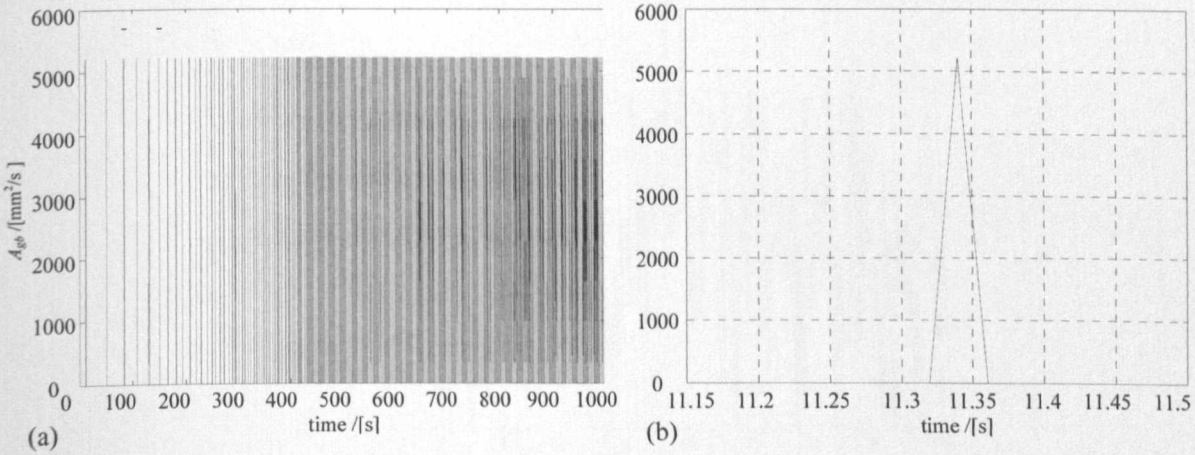

Figure 7.4.1: (a) the time series of A_{gb} that produced single bubbles in the simulated fluidised bed (bubble size $d_{b,e} \approx 80$ mm). The input was in logarithmic swept sinusoidal intervals. (b) the zoomed-in view of the input signal indicating a resemblance to an impulse signal.

The impulse duration was the simulation time step (0.04s). A transfer function denoted by $G(s)$ in the s-transform is derived by dividing the input signal from the output signal of a dynamical system via

$$G(s) = \frac{output}{input}$$

The relationship implies that by removing the effect of the input signal (which includes its energy content), the transfer function that defines the dynamics of the system at various frequencies should be obtainable from the output. Therefore accordingly, the input magnitude or energy should be removed from the Bode gain plot of the theoretical model to obtain the final correct form, which will be at the same decibel (dB) level as the simulated bed Bode gain plot achievable by the shifting of the whole theoretical model plot vertically.

However, with multiple bubbles, as found in normal bubbling beds, the A_{gb} will be of a slightly different nature. As multiple bubbles were introduced at approximately the same instance, it was difficult to determine the magnitude of the signal that was associated with the introduction of a certain bubble into the bed as could be seen in *Figure 7.4.2* for A_{gb}.

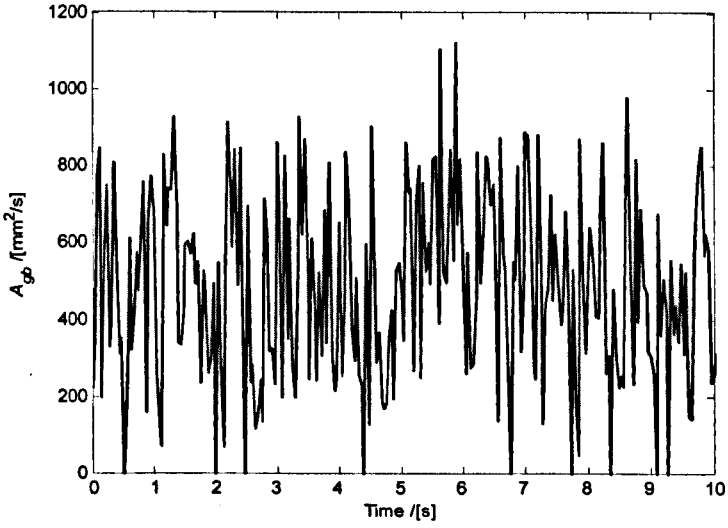

Figure 7.4.2: The time series of A_{gb} that produced multiple bubbles in a freely bubbling simulated bed fluidised at 25.6 mm/s above U_{mf} with randomly uniform excitation to flow rate of ±20 mm/s.

To obtain the best estimate of the energy of change experienced by the input signal, the average magnitude of change in signal was used. Therefore,

$$|A_{gb}| = standard\ deviation(A_{gb}) * signal\ period\ before\ next\ change * 0.5 \qquad (7.8)$$

for a randomly uniform excited input signal. '*Signal period before next change*' was the simulation time step (0.04s). Similarly, this magnitude should be subtracted from the Bode gain plot of the theoretical model to vertically shift the whole plot downwards. All the Bode diagrams of freely bubbling beds would have the theoretical model plot moved by approximately −15 to −20 dB to have them in the similar dB level as the simulated bubbling bed plots. The implemented improvement resulted in the difference in the dB level reduced to a minimum of several decibels as can be seen in *Section 7.5*, *Section 7.6* and *Section 7.7*.

7.5 Idealised bed with bubble size growth with height

At some point in the study, it is appropriate to account for bubble size growth when bubbles rise up the idealised bed. This is an initial approach to fabricating a gradually more realistic bed than the idealised version. The expansion of bubble in the bed can be approximated from the time series of BVF when a single bubble is issued into it. *Figure 7.5.1* shows the experimentally obtained average of BVF measurement from periodic injections of a single bubble with initial size at the distributor of approximately 140 mm in equivalent diameter. Incurring an initial BVF value of 0.04, the bubble rose from the distributor as it grew, increasing the BVF value gradually to the final value of approximately 0.06 before exiting.

Applying a second order polynomial approximation resulted in an estimated bubble expansion equation that agrees well with empirical data as shown by the graph in *Figure 7.5.1*. Therefore, it was accepted as a general assumption that the expansion of all the bubbles created, single or multiple, in the bed could be approximated using a second order polynomial such that,

$$BVF(t) = c_1 t^2 + c_2 t + c_3 \tag{7.9}$$

where c_1, c_2 and c_3 are coefficients governing the bubble expansion. In the simulated bubbling bed, the empirical relationship of bubble size growth in a freely bubbling planar bed suggested by Kunii et al. (1967) was used. For simplicity, the empirical relationship was assumed to be linear where

$$d_b = d_{bi} + 0.034 h_b \tag{7.10}$$

with d_{bi} as the bubble initial diameter and h_b the height of bubble in the bed over the distributor. This relationship led to an approximate quadratic increase in BVF with the corresponding change in height. In the simulation of the idealised bed with expanding single bubbles, (7.10) was also used to determine expansion of the bubbles.

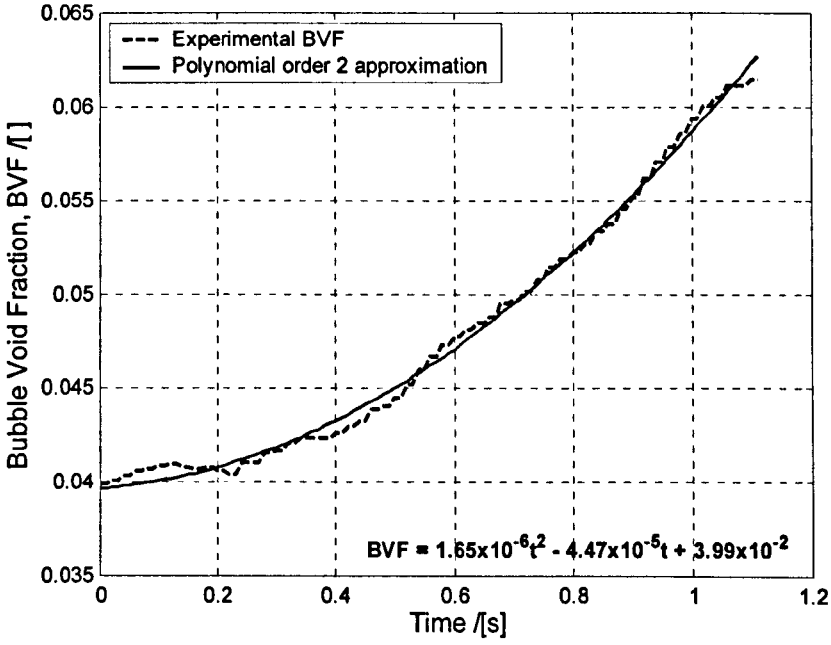

Figure 7.5.1: The time series of BVF obtained from the experimental bed with a single bubble and the corresponding approximation made by a second order polynomial equation model.

For bubbles with different diameters, the influence on the void fraction varies, where the relationship between BVF of the bed and time is shown in *Figure 7.5.2*. The increase of bubble diameter with height subsequently leads to the increase of bubble rise velocity resulting in a bubble spending less time in the bed than if the bubble diameter remains constant. The values of bubble residence time in the bed, T were obtained from the data used to produce *Figure 7.5.2*. Bubble residence time was calculated the moment the bubble was introduced into the bed until the instant just before it left the bed.

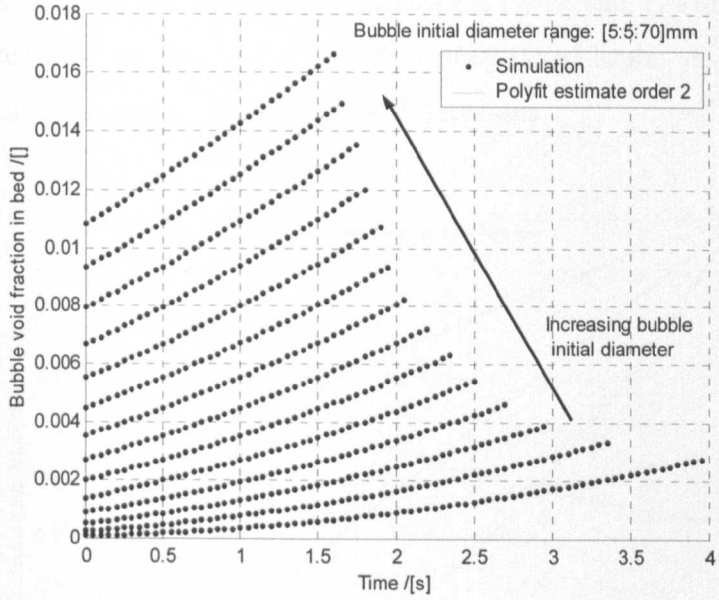

Figure 7.5.2: The data gathered for the BVF in bed over time for a range of bubble initial diameters. The polynomial fit was used to estimate coefficients c_1, c_2 and c_3.

Figure 7.5.3 shows the variation of the residence time of bubbles in the bed of different initial size ranging from 5 to 70 mm in equivalent diameter. The residence time of these bubbles is affected by their growth with height in the bed and it can be seen that the relationship between initial size and residence time is not linear.

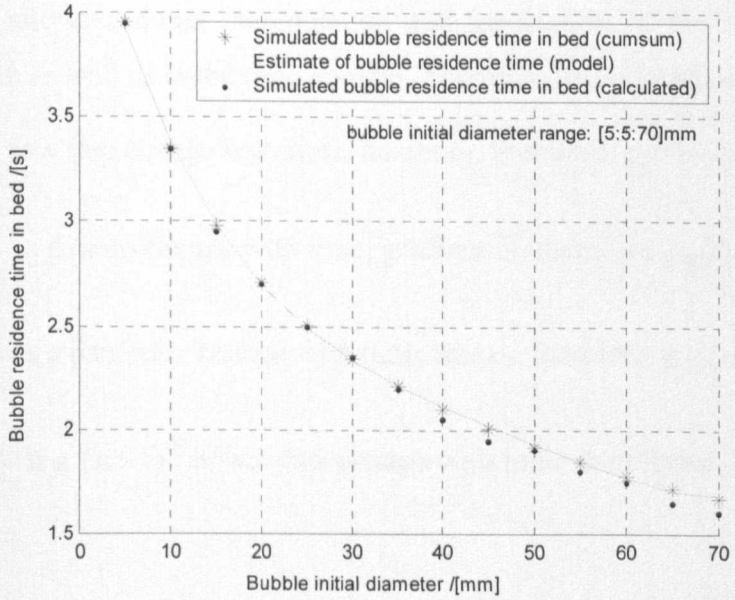

Figure 7.5.3: The bubble residence time in the bed depending on their respective initial diameter.

The relationships between each of the coefficients c_1, c_2, c_3 and T with the bubble initial diameters are presented in *Figure 7.5.4*, with a normalised scale. As the bubble initial diameter increases, c_1, c_2 and c_3 increase while T decreases.

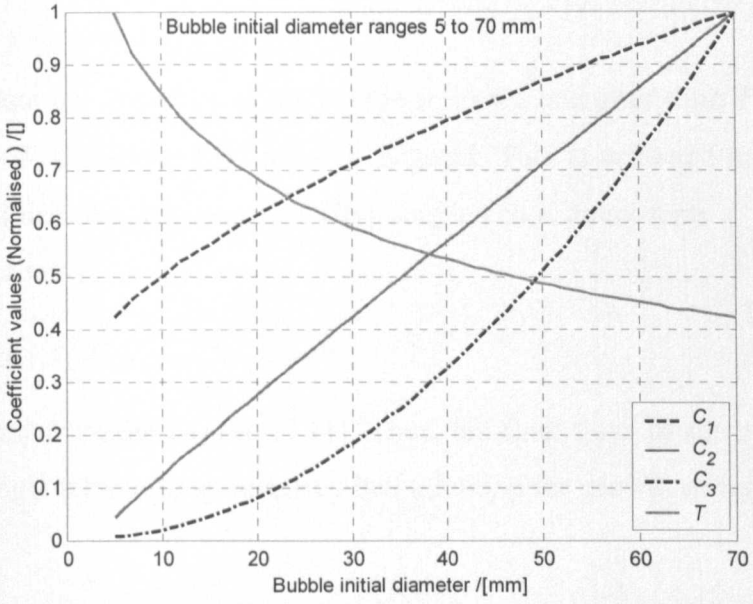

Figure 7.5.4: The relationship between coefficients c_1, c_2, c_3 and T with bubble initial diameter, normalised with respect to their respective maximum values to aid visualisation.

It is convenient in this study to express the relationship in (7.9) in the form a Laplace transform. This allows a direct manipulation and association of the relationship in the frequency domain as well as in the time domain. Therefore, from Laplace transform tables:

$G_1(s)=\frac{c_1}{s}$ is a step change with time, height c_1, therefore $g_1(t)=c_1$

$G_2(s)=\frac{c_2}{s^2}$ is a ramp change with time, gradient c_2, therefore $g_2(t)=c_2 t$

$G_3(s)=\frac{c_3}{s^3}$ is a parabolic change with time, rate c_3, therefore $g_3(t)=\frac{1}{2}c_2 t^2$

$G_n(s)=\frac{c_n}{s^n}$ is a $(n-1)^{\text{th}}$ power-law change with time, therefore $g_n(t)=\frac{1}{(n-1)!}c_n t^{n-1}$

By adding these as appropriate, any desired variation in $g(t)$ can be produced. For example to model the growth with time of a bubble whose size varies according to: $g(t) = 5 + 3t + 10t^2$ requires the transfer function for the parabolic + ramp + constant variation in bubble size given by

$$G(s)=\frac{5}{s}+\frac{3}{s^2}+\frac{10}{s^3}=\frac{c_1}{s}+\frac{c_2}{s^2}+\frac{c_3}{s^3} \tag{7.11}$$

In order to simulate the departure of the bubble from the bed after time T seconds so that $g(t) = 0$ for $t \geq T$, the above $G(s)$ must be negated. This is achieved via subtraction of appropriate multiples of components of $G(s)$ coupled to a delay term e^{-Ts}. In general, to make, $g(t) = 0$ for $t \geq T$,

$$\frac{c_n}{s^n}\left(1+sT+\frac{(sT)^2}{2!}+\ldots+\frac{(sT)^{n-1}}{(n-1)!}\right)e^{-sT} \tag{7.12}$$

must be subtracted from the $G(s)$ in (7.11). Thus, the final form of the modified transfer function for a single bubble in an idealised bed allowing for growth of bubble with height is

$$G(s)=\left(\frac{c_1}{s}+\frac{c_2}{s^2}+\frac{c_3}{s^3}\right)-e^{-sT}\left[\left(\frac{c_1}{s}+\frac{c_2}{s^2}+\frac{c_3}{s^3}\right)+sT\left(\frac{c_2}{s^2}+\frac{c_3}{s^3}\right)+\frac{(sT)^2}{2!}\left(\frac{c_3}{s^3}\right)\right] \tag{7.13}$$

This will deliver the measure of BVF due to bubble size change where

$$g(t)=\begin{cases} c_1+c_2t+\frac{1}{2}c_3t^2 & \text{for } t \leq T \\ 0 & \text{for } t > T \end{cases}$$

Having derived the modified transfer function of the theoretical model for the idealised bed allowing for bubble growth, the resulting Bode diagram can be generated and an example is shown in *Figure 7.5.5*. The Bode plot of the transfer function for the simulated idealised bed with growing single bubbles and that of the original theoretical model of the idealised bed (7.3) are included for comparison. In all cases, single bubbles of approximately 40 mm in equivalent diameter were introduced into the idealised bed.

It can be seen that the modified model (7.13) agrees well with the transfer function of the simulated idealised bed allowing for growth in the single bubbles, except for some discrepancy at higher frequencies above 3 Hz. At these frequencies, the magnitudes are relatively small compared to the rest of the portion of the plot making that region of frequency more susceptible to noise disturbance. Hence, the significance of these discrepancies can be neglected. It can also be seen that (7.13) predicts the primary 'dip' to

be located at a higher frequency than the original model without bubble growth. The higher frequency 'dip' corresponds to faster bubbles rising in the bed due to their size expansion.

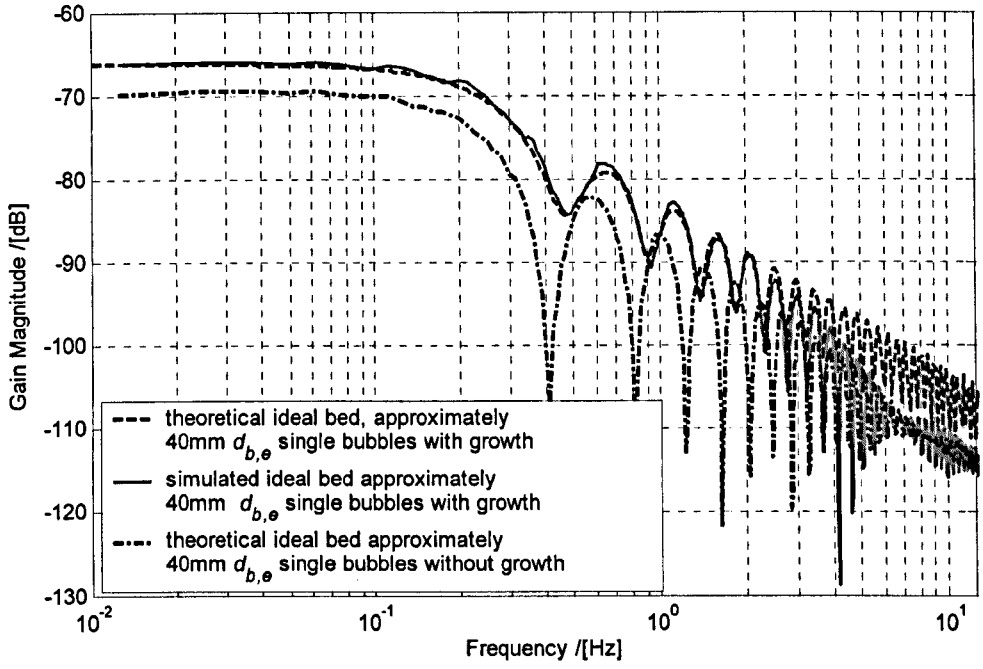

Figure 7.5.5: The Bode diagram of the modified theoretical model allowing for growth in bubble size due to height in the bed (initial bubble equivalent diameter ≈ 40 mm). The Bode diagrams of the simulated bed allowing for bubble expansion and that of the original theoretical model are also included.

As a consequence of expansion, the 'dips' are also more moderate than the narrow and sharp 'dips' seen for the original model (7.3). This is because the bubbles grow as they rise and so their departure will cause a larger drop (change) in the BVF compared to the simultaneous increase in BVF caused by introduction of bubbles (with the smaller initial size). This will result in a higher energy for the BVF measurement at these coincidental frequencies of bubble entry and exit compared to if bubbles do not grow and therefore resulted in the moderation of the 'dips'. The overall Bode plot of (7.13) was also lifted higher in magnitude compared to that of the original model due to the higher value of BVF caused by larger expanded single bubbles. Depending on the size of the single bubbles, the 'dips' and other features will shift accordingly, based on the given values of c_1, c_2, c_3 and T, compared to their original model counterparts.

7.6 Extension to multiple bubbles condition

To proceed with the study of creating a more realistic bed from the basics of the idealised scenario, the theoretical model was extended to one for a freely bubbling bed. An intermittent development stage is crucial in assuring an appropriate transition from idealised to realistic, whereby the idealised bed was subjected to introduction of multiple bubbles. This involved developing a method to generate a composite transfer function, which would then describe the combined effect of introducing two streams of bubbles (instead of one). The algebraic form of the transfer function (Laplace transform) allows the formation of the composite transfer function model by means of simple addition of individual models formulated based on (7.13).

Two single bubbles of different sizes were introduced at different lateral locations simultaneously at logarithmic swept intervals between consecutive bubbles on each stream. This was first conducted in the simulated bed and an attempt was made to replicate this with modifications and improvements made to the method to produce the composite theoretical model. Bubbles were allowed to grow with height. Several improvements needed to be made to the computation method to take into account the average effect that the two bubbles would have in the theoretical model. First, a weighting factor was used to determine the contribution of each of the single bubble, relating to its size, on the transfer function of the model. As a bubble void area determines the BVF in the bed, the characteristic diameter of the bubble has a square effect on the BVF measurement. Therefore, for a bubble with diameter d_{b1}, the weighting factor for the bubble's contribution to the overall BVF is

$$W_{b,1} = \frac{{d_{b1}}^2}{({d_{b1}}^2 + {d_{b2}}^2)} \tag{7.14}$$

and a similar expression applies accordingly to the second bubble with characteristic diameter d_{b2}. $W_{b,1}$ and $W_{b,2}$ were used to determine the relative contribution of the input magnitude (A_{gb}) and for the gain and phase of the theoretical transfer function of each bubble stream to the overall behaviour of the bed.

To calculate the overall gain and phase values of the Bode diagram over the frequency range the following were carried out

Overall transfer function gain = $\left|W_{b,1}G_{b_1} + W_{b,2}G_{b_2}\right|$

Overall transfer function phase = $\angle(W_{b,1}G_{b_1} + W_{b,2}G_{b_2})$

Figure 7.6.1 shows the gain and phase of the transfer function Bode diagram from the simulation and theoretical model for two single bubble streams of 0.15 l/m ($d_{b,e} \approx 60$ mm) and 0.2 l/m ($d_{b,e} \approx 80$ mm) introduced simultaneously at logarithmic swept frequency from 0.01 Hz to 10 Hz into the bed.

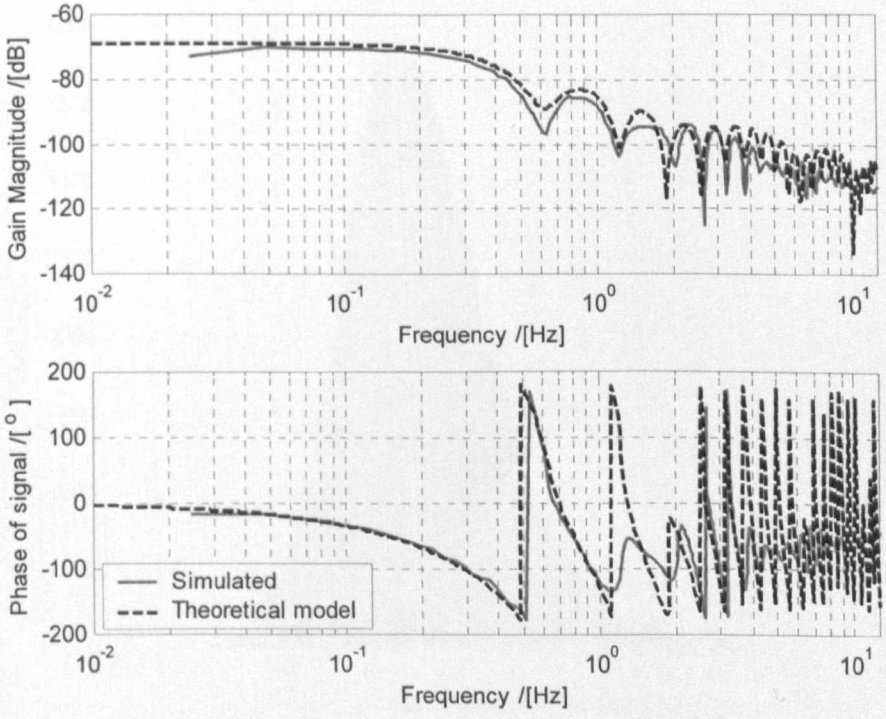

Figure 7.6.1: The Bode diagram for the simulated bed and the theoretical model for a bed with two simultaneous single bubbles introduced at logarithmic intervals.

The technique used to incorporate the effect of two transfer functions of the theoretical model (initially made to model only a single bubble stream) is shown to work well. The divergence of the phase plots is not important after the primary 'dip' frequency. Again the negligible difference in dB level between the simulation and the theory were due to unaccounted causes such as dynamics that were not modelled. The development of the methods established to model multiple bubbles was then extended further to apply to when the bed was freely bubbling where bubble interaction and coalescence were taking place.

7.7 Extension of theory to a normal freely bubbling bed

The techniques applied to the modelling of two simultaneous single bubble streams in the bed were used to model a normal freely bubbling fluidised bed. Several modifications were necessary to realistically replicate closely the behaviour of bubbles in a normal bubbling bed where bubbles are free to interact and coalesce as they rise. The main objective of this effort was to ensure that dominant dynamical features that determine the overall behaviour of the bubbling process were captured in the model. The ability to do so shows that a substantial understanding of the fundamentals of the process has been achieved.

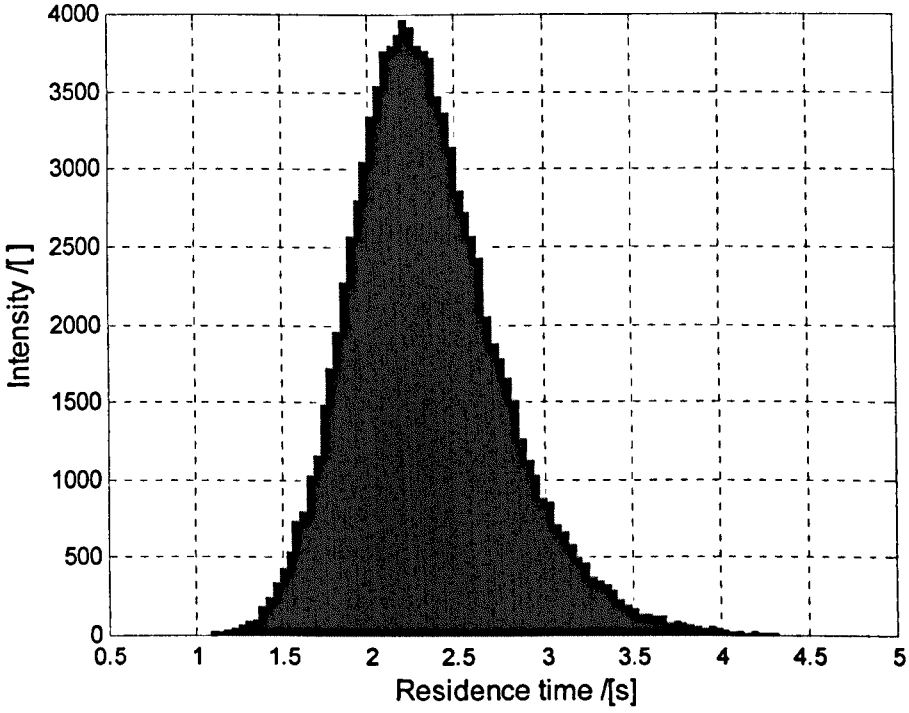

Figure 7.7.1: The histogram of bubble residence time for a total of 100, 000 bubbles generated in the simulated bubbling bed fluidised at 25.6 mm/s superficial gas flow above U_{mf} with a uniformly random excitation of flow into plenum of ±20.5 mm/s.

When a bubble is introduced into the bed, isolated from any effects and interactions, it rises steadily up the bed, spending time T in the bed. In a bubbling bed, where the single bubbles are free to interact and coalesce with other bubbles, their residence times could be significantly reduced. There would be a distribution of possible residence time associated with a bubble of a specific size, ranging from the maximum amount of time, corresponding to the rise of an isolated bubble, to a minimum duration associated with a bubble that has undergone one or a number of coalescence processes with other bubbles, forming a larger,

faster bubble. An example of the bubble residence time distribution for bubbles generated (~ 100, 000 bubbles) in a simulated normal bubbling bed fluidised at 25.6 mm/s superficial gas flow above U_{mf} with a uniformly random excitation of flow into plenum of ±20.5 mm/s is shown in *Figure 7.7.1*. The distribution of bubble residence time in the bed gives an indication of the probability of a bubble of a specific size spending a given amount of time in the bed relative to the other bubbles.

There was also a range of bubble initial sizes, associated with a distribution function governing their production at the porous plate distributor in the normal freely bubbling bed for a given fluidisation condition. An example of this distribution of bubble initial size is shown in *Figure 7.7.2* for bubbles generated in a simulated normal bubbling bed fluidised at 25.6 mm/s superficial gas flow above U_{mf} with a uniformly random variation (to improve input-output signal coherency) of flow into the plenum of ±20.5 mm/s.

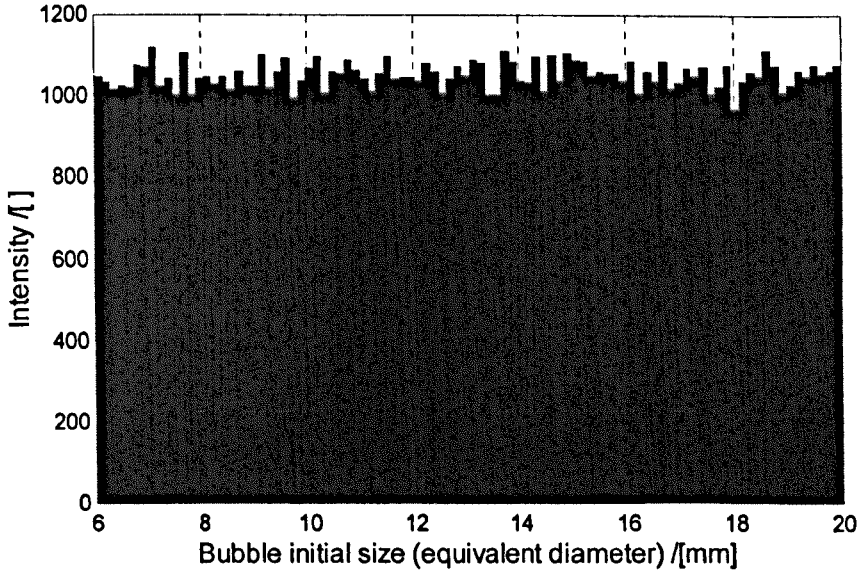

Figure 7.7.2: The histogram of bubble initial size distribution produced at the distributor of the simulated bubbling bed fluidised at 25.6 mm/s superficial gas flow above U_{mf} with a uniformly random excitation of flow into plenum of ±20.5 mm/s

The consequence of bubble interaction and coalescence is not only the modification of bubble residence time but also the rate of bubble size expansion from the point of coalescence onwards, i.e. the modification of the coefficients c_1, c_2 *and* c_3. *Figure 7.7.3* illustrates this point. This phenomenon can be observed in a bed of height, H_{bed} when two single bubbles b_1 and b_2 coalesce at height, $h_{1,2}$, creating a new larger bubble, $b_{1,2}$ of size

$d_{b1,2}$ that will expand at a different rate to its two parent bubbles, approximated by the new set of coefficients $c_{1_{1,2}}, c_{2_{1,2}}, c_{3_{1,2}}$. This bubble will rise up the bed at a faster rate for the remaining part of the bed height, ($H_{bed} - h_{1,2}$). The bubble could be involved in further coalescence with other bubbles for the rest of its residence in the bed, in which case would subsequently create an even larger bubble. This simple illustration points out that bubble interaction and coalescence modify the overall transfer function of a bed derived from the composite of models for isolated single bubbles (7.13) with the use of appropriate values of bubble growth coefficients, residence time and probability weighting function. The models based on (7.13) for each of the bubbles then constitute the composite transfer function model by means of their simple addition in their algebraic form.

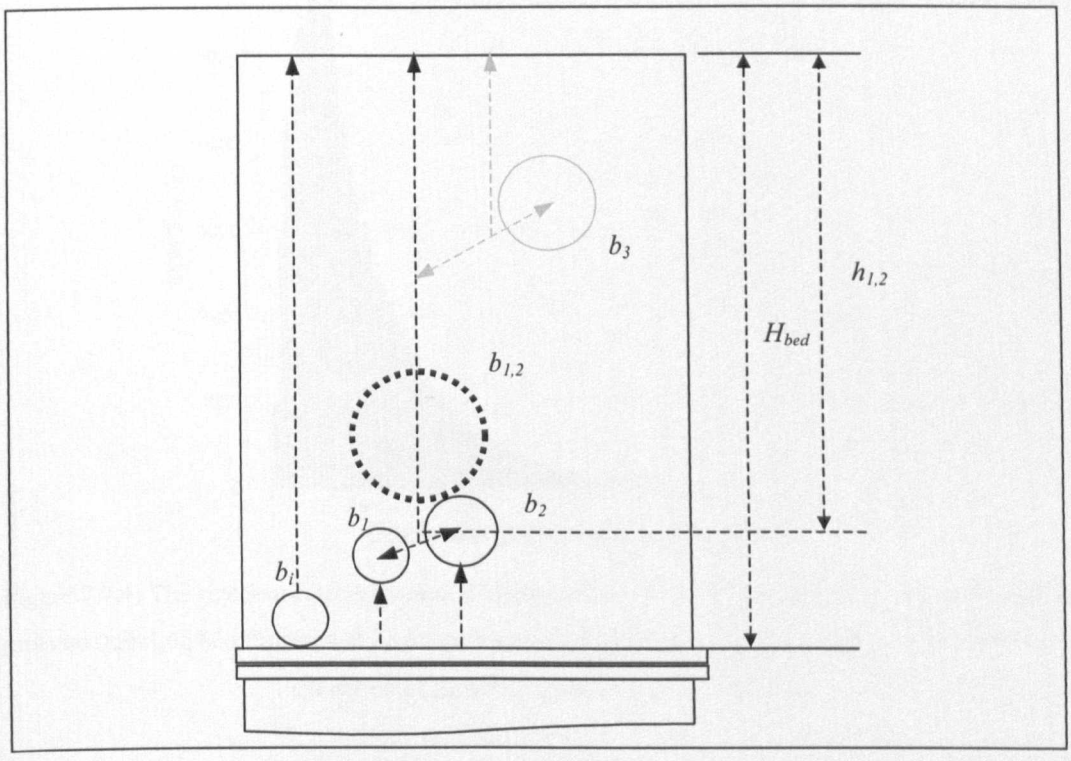

Figure 7.7.3: The consequence of a single bubble involving in a coalescence process with another bubble should it not rise isolated in a bed of height, H_{bed}. In the coalescence between bubbles b_1 and b_2, new larger bubble $b_{1,2}$ is formed. Bubble b_3 represents a potential for further coalescence of bubble $b_{1,2}$ as it rises through the remaining part of the bed.

To account for the effect of bubble coalescence in normal bubbling beds, the composite transfer function requires the information on the distribution of bubble sizes of the population of bubbles existing in the bed. Similar to the bubble residence time distribution, a moderately large sample (~ 100, 000 was used where even larger samples produced

essentially similar distribution profiles) of bubbles would be adequate to allow the model to properly estimate the overall behaviour of the bubbling process in a normal bubbling bed at a given condition. The exact choice of sample population is not critical as the simulation of the bubbling bed conducted to obtain the set of information of the model will produced the transfer function that should correspondingly match the theoretical model plot if it is properly constructed using this information. *Figure 7.7.4* shows the type of distribution encountered in sizes of bubbles in a typical normal bubbling bed. In this case, the bed was fluidised at 25.6 mm/s superficial gas flow above U_{mf} with a uniformly random excitation of flow into plenum of ±20.5 mm/s.

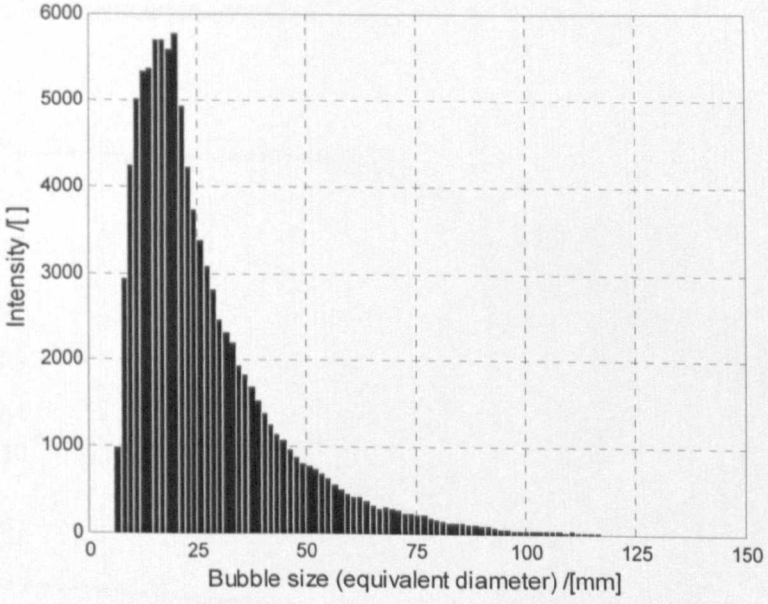

Figure 7.7.4: The size (equivalent diameter) histogram of a total of 100, 000 bubbles populating the simulated bubbling bed fluidised at 25.6 mm/s superficial gas flow above U_{mf} with a uniformly random excitation of flow into plenum of ±20.5 mm/s.

To emphasise, the transfer function in (7.13) describes the dynamics of bubbling in the bed caused by a single bubble introduced at various frequencies. The distribution of bubble residence time and size were required where a probability approach was applied to estimate the effect of each bubble in the bed on the overall dynamics of the normally bubbling bed (composite transfer function of the model). Bubbles of different sizes created at the distributor and through coalescence expand at different rates, which could be modelled using coefficients c_1, c_2 and c_3 (*Section 7.5*). The distribution of bubble size population describes the sizes of bubbles and their population in the bed and hence sets of

coefficients c_1, c_2 and c_3 are created to model the expansion of these bubbles, each set fitted into one theoretical model (7.13). The bubble residence time is then needed and therefore this creates a range of possible combination of T associated with a given set of expansion coefficients (for one bubble size). The T value ranges from the largest possible when a particular bubble rises in isolation to the smallest value found in the distribution of T obtained from the simulation for the similar fluidisation condition. In terms of the dynamical system treatment of the whole investigation, the treatment can be preserved as there was no alteration of the input going into the system for the case with normal bubbling beds compared to the previous study. The only difference is that the existence of bubbles of sizes other than those produced at the distributor has to be included to take into account the effect of bubble coalescence (creating larger bubbles not created at the distributor).

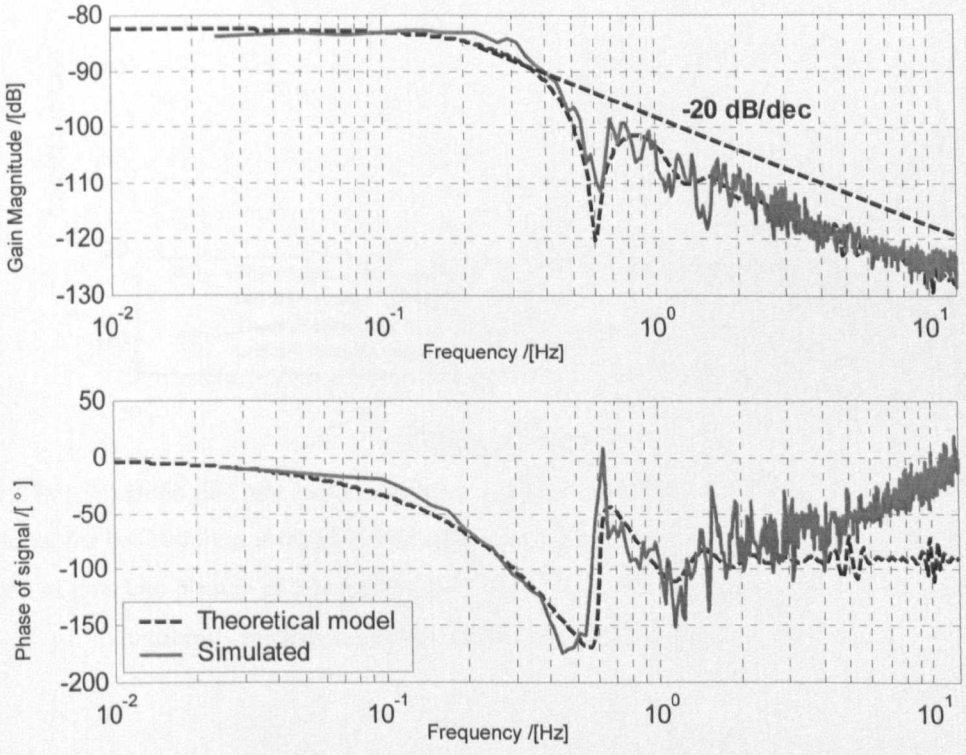

Figure 7.7.5: The Bode diagram comparing the constructed theoretical model with the transfer function of the simulated normal freely bubbling bed fluidised at 25.6 mm/s superficial gas flow above U_{mf} with a uniformly random excitation of flow into plenum of ±20.5 mm/s. The difference in the phase plots at high frequency is negligible because the magnitude (see gain Bode plot) is small.

In *Figure 7.7.5*, a Bode diagram shows the comparison between the transfer function of the simulated bubbling bed and the constructed theoretical model replicating the bubbling process at 25.6 mm/s superficial gas flow above U_{mf} with a uniformly random excitation of

flow into plenum of ±20.5 mm/s. It can be seen that both plots agree well suggesting that the theoretical model has been appropriately constructed to replicate the dynamical behaviour of a freely bubbling process in a normal bed. The primary 'dips' were seen to coincide at the similar locations above the break frequencies, which take place at similar low frequency gain levels. The phase plots also coincide up to the vicinity of the primary 'dips' with the decay trend characteristic of a system with time delay feature. Thereafter, the consequence of differences in the plots is not significant and therefore neglected.

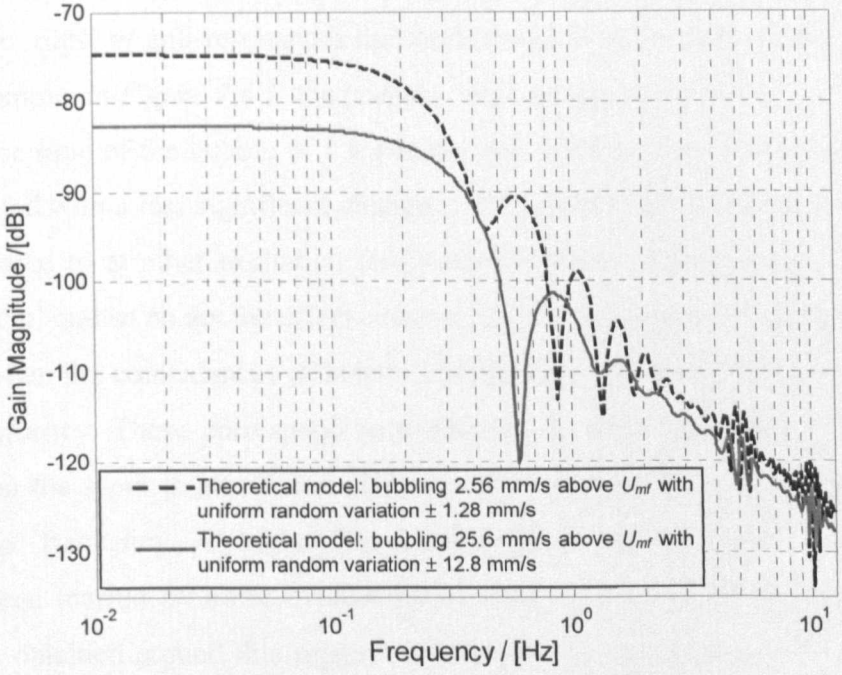

Figure 7.7.6: The Bode gain plot comparing the constructed theoretical models for two different flow condition for the bed bubbling at (a) 12.8 mm/s superficial gas flow above U_{mf} with a uniformly random excitation of flow into plenum of ±20.5 mm/s and (b) 2.56 mm/s superficial gas flow above U_{mf} with a uniformly random excitation of flow into plenum of ±1.28 mm/s.

The resulting composite transfer function of the model demonstrated that these effects caused non-linearity in the system where the transfer function of the overall behaviour of a normal freely bubbling bed changes with different operating conditions, i.e. different flow rates. *Figure 7.7.6* shows the differences in the transfer functions for models of the normal freely bubbling bed operating at different conditions: (a) fluidised at 25.6 mm/s superficial flow with uniformly random variation in flow into plenum at ± 20.5 mm/s and (b) fluidised at 2.56 mm/s superficial flow with uniformly random variation in flow into plenum at ± 1.28 mm/s. It can be seen that the Bode gain plot for the lower flow condition has higher

LFG, as expected, and the primary 'dip' is placed at a lower frequency that for the higher flow rate, which again is as expected. Bubbles stay longer in the bed because they are generally smaller when the flow is lower.

7.8 General discussion

The gain Bode plot is an indication of how much the output (BVF) of the bubbling bed at steady-state conditions would change for a given input. All the gain Bode plots exhibit characteristic 'dips' or anti-resonances that correspond to the residence of a bubble in the bed. For example, in *Figure 7.6.1*, the primary 'dip' at approximately 0.55 Hz corresponds to a residence time of the bubble of 1.8 s in the bed. At this 'dip' frequency, there is less gain associated with a less significant change in BVF value with the same amount of input given compared to at other excitation frequencies (bubble introduction). The subsequent secondary 'dip' and so on are the effect of harmonics in the frequency domain computation as well as when the coincidences of bubble introduction and exit occur at multiples of the primary frequency. These correspond to a decrease in gain value and consequently the output, when the input is introduced at frequency multiples of 2, 3, 4 and so on of the primary 'dip' frequency. At higher frequencies, the coherency between the output and input has been marred by noise evident on the noisy plot seen at this frequency range. Information obtained around this region of frequency is unreliable and therefore must be discounted.

The extent of the 'dip' magnitude is bubble size dependent. In brief, the larger the bubble the deeper the 'dip' will appear. In an idealised fluidised bed where bubble rise without expansion, the resulting transfer function would have a very sharp and narrow decrease in gain, corresponding to a negligible change in the BVF when bubble introduction frequency corresponds to the residence time of the bubble of that size in the bed. In other words, when a bubble is introduced the same instance the bubble of the same size is leaving the bed, there is an insignificant change, if any, to the BVF (output). However in a real fluidised bed, where bubbles expand with height, the 'dip' magnitude is moderated because with a larger sized bubble leaving at the top of the bed at the same instance when a bubble of the smaller size is introduced at the bottom, the BVF value is still affected quite significantly.

The smaller the bubble, the more it will expand in the bed of height, H_b and when a bubble is larger, the degree of expansion it experiences would not be as much, as it rises faster up the bed having less time to experience the same degree of expansion than if it was to stay longer in the bed. *Figure 7.8.1* better puts this point across. Simulated single large bubbles are introduced into an idealised bed of height 710 mm. In the first case, the bubble cannot expand and the gain plot has sharp and narrow 'dips'. When the bubble is allowed to expand, the 'dips' are moderated by the expansion effect. Also, the 'dips' are located at slightly higher frequencies, indicating bubbles travel faster. The transfer function for the case of single bubbles rising in a taller bed (2000mm) has a much lower primary 'dip' frequency of approximately 2.5 Hz, resulting from the bubble spending much longer time in the bed. In addition, the 'dips' appear to be less severe. This shows the degree of expansion is so significant such that a much larger bubble is produced at the top of the bed, hence greatly affecting the BVF value as it leaves the bed even when its timing coincides with bubbles being introduced at the bottom.

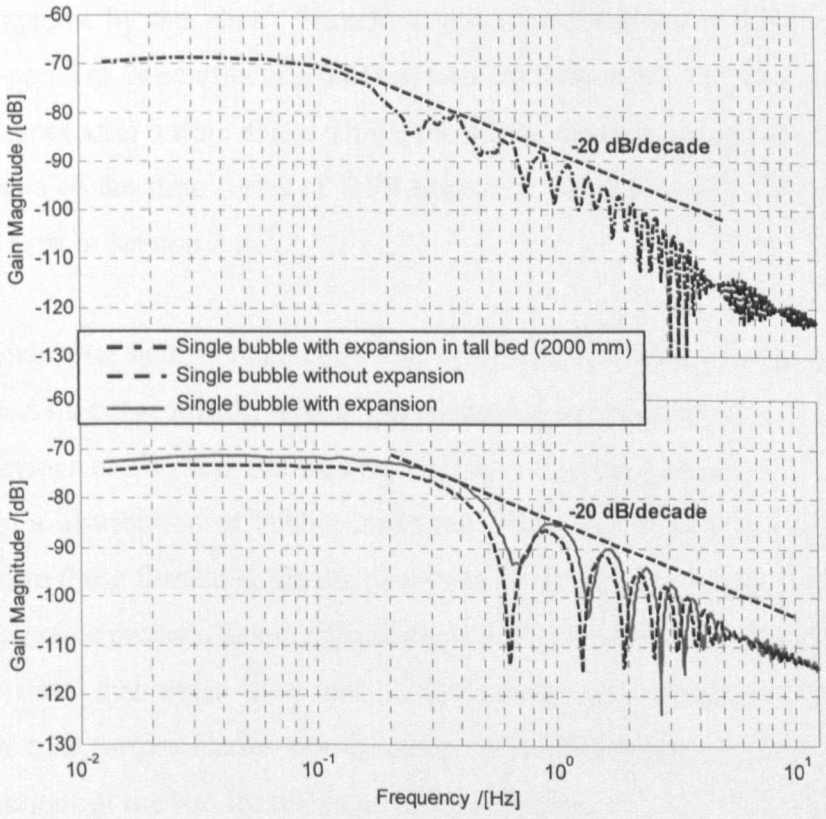

Figure 7.8.1: The gain Bode plots of the transfer functions of single bubbles in a bed allowing and not allowing for expansion as well as for single bubbles rising in a taller bed. All the bubbles produced have similar initial equivalent diameter ≈ 80 mm. Results are from simulated beds.

The gain and phase Bode plots obtained for the simulated bubbling beds are rather 'noisy', particularly at high frequencies, which is common in many dynamical systems. This was also due to the computation process carried out when obtaining the transfer function from time series data. At higher frequencies, noise domination of the plot is inevitable due to the corresponding lower energy content in the output. The noise was also due to the degradation of the input-output coherency, which is impossible to improve at high frequency. Although shown earlier in *Section 6.6* the coherency can be improved by introducing a random or logarithmic swept excitation of flow on top of the constant flow into the bed plenum to provide sufficient level of low frequency energy into the input, it is slightly more difficult to improve the coherency at higher frequencies.

The decay of the phase plots, examples of which could be seen in Bode diagrams such as in *Figure 7.3.3(b)* and *Figure 7.7.5(b)*, characterises the presence of time delay in the behaviour of steadily bubbling beds. The time delay in this case carries a different meaning and corresponds to the residence time of bubbles in the bed, also reflected in the gain plot of the Bode diagrams by the 'dips'. Therefore, this time delay has a different dynamical significant compared to those affecting other dynamical system where typically, the system responds to an input after a time delay. This typical time delay is similar to the time delay identified in some of the time series of BVF measured experimentally when varying the flow rapidly as seen in *Section 2.3.2.2.*

It has been shown that bubble interaction and coalescence modify the bubble residence time in the bed. As a consequence, new larger bubbles are formed thereby modifying their expansion behaviour as the new bubbles rise for the remaining height of the bed. These have resulted in a distribution of bubble residence time, associated with each bubble, for sizes ranging from those formed at the distributor to those formed on other parts of the bed due to the coalescence process. These effects modify the simple relationship of bubble size and residence time that exist in a bed with isolated non-interacting bubbles. This modification in turn further causes non-linearity in fluidised systems thus changing the dynamical behaviour of the bed for different flow conditions.

For normal freely bubbling beds with lower gas flows, those of which Bode plots are shown in *Figure 7.8.2* and *Figure 7.8.3*, it can be seen that the 'dips' in the simulated bed gain plots do not coincide at the same frequency as that for the theoretical model. With the

primary 'dip' located at approximately 0.5 Hz (*Figure 7.8.2*), at a fraction higher frequency than that of the simulated bed, the theory predicted the bed was dominated by bubbles rising through the bed, spending approximately 2 s in the bed. This is an overestimation of that found in the simulation where the true dominating event was an approximate 2.5 s (0.4 Hz 'dip') of residence time for most bubbles travelling through the bed.

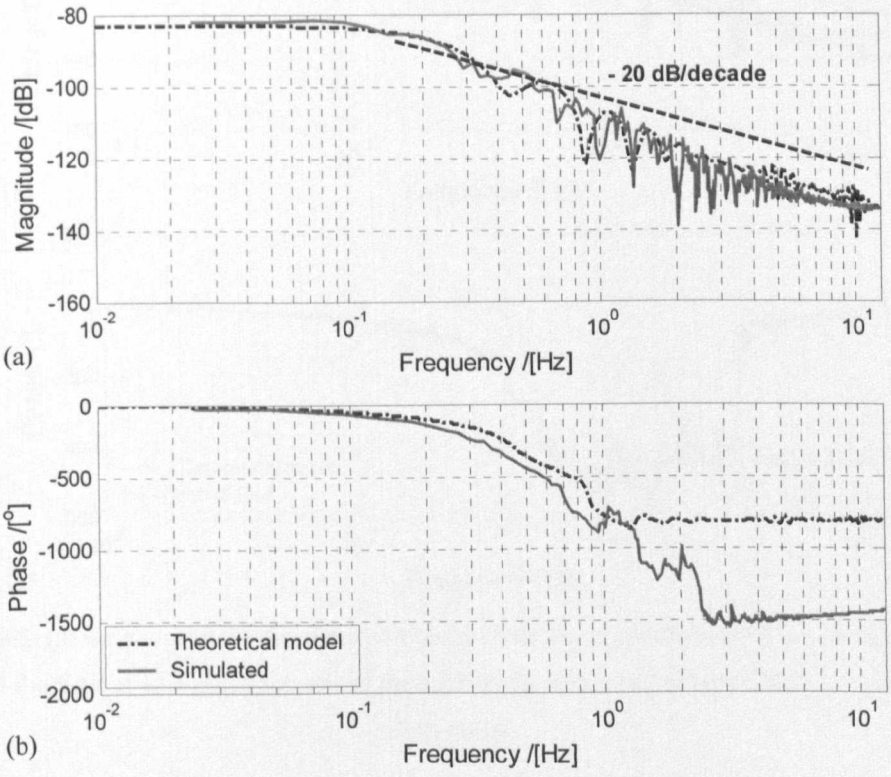

Figure 7.8.2: (a) the gain and (b) the phase plot of the Bode diagram obtained for the simulated freely bubbling bed fluidised at 2.56 mm/s superficial flow about U_{mf} with a uniformly random variation in flow of ±1.28 mm/s.

The similar can be said about the difference in the plots shown in *Figure 7.8.3*. Here, the theoretical model again overestimated the 'dip' frequency predicting that generally bubbles travel faster than the actual case observed in the simulation. This is because while the theoretical model performed well for fluidisation at a high flow rate (e.g. in *Figure 7.7.5*), it failed to agree with the simulated bed for lower flow rate conditions. In a freely bubbling bed, there will be a distribution of bubble residence time associated with every bubble size produced at the distributor or through coalescence (or even division, although is not modelled here). The profile of bubble residence time distribution for the range of bubbles

depends on the fluidisation condition. *Figure 7.8.4* and *Figure 7.8.5* shows the difference of bubble residence time distribution of bubbles formed at the bed distributor for low and high flow conditions respectively.

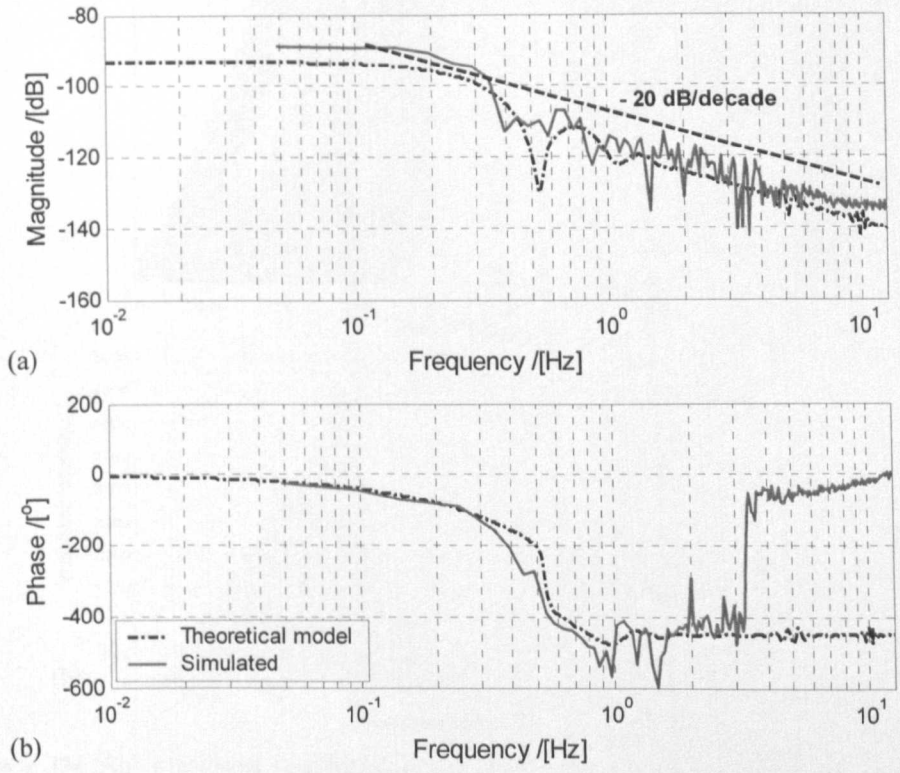

Figure 7.8.3: (a) the gain and (b) the phase plot of the Bode diagram obtained for the simulated freely bubbling bed fluidised at 12.8 mm/s superficial flow about U_{mf} with a uniformly random variation in flow of ±5.13 mm/s.

When comparing the figures, it can be seen that at a lower flow rate (*Figure 7.8.4(a)*), the distribution of residence time associated with each bubble size is unique and different compared to the others. When the flow supply increases, due to the bubble interaction and coalescence processes that gradually swarm the entire bed, bubbles created in the bed have gradually more similar residence time distribution profiles. Therefore, at a higher flow rate it can be seen in *Figure 7.8.5(a)* that the distribution for each bubble becomes reasonably identical with the distribution for other bubbles.

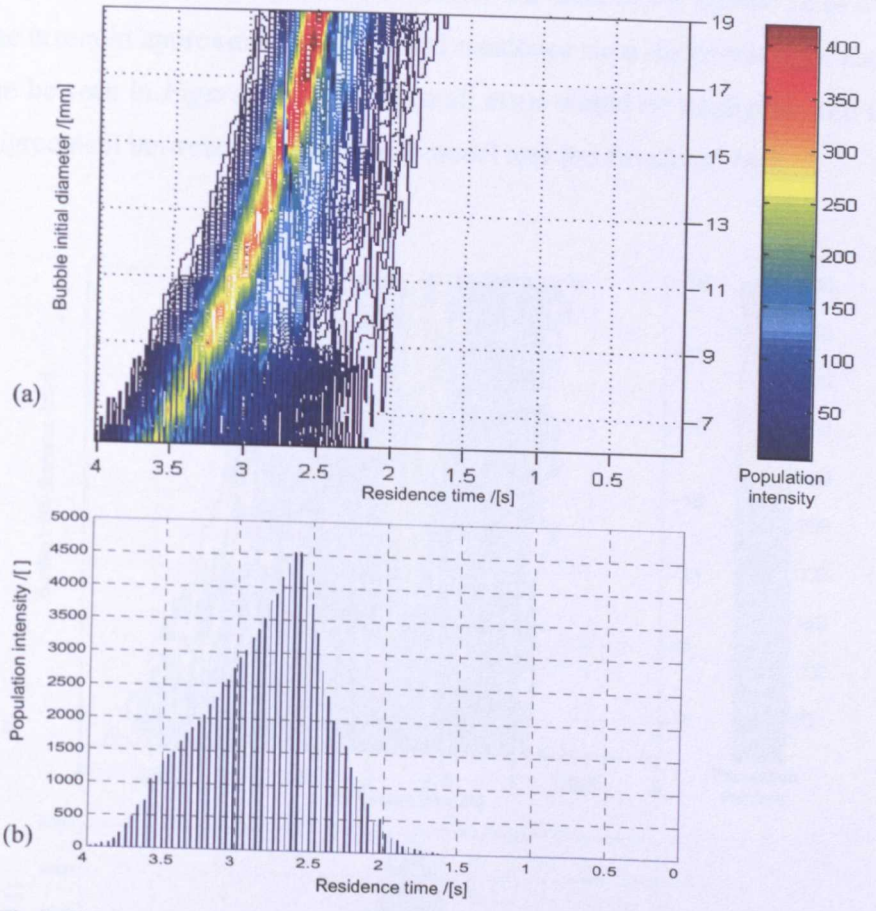

Figure 7.8.4: The bubble residence time for bubbles produced at the distributor for the simulated bubbling bed fluidised at 2.56 mm/s superficial flow above U_{mf} with uniformly random variation of flow at ±1.28 mm/s, (b) the global or cumulative bubble residence time distribution used in the theoretical model.

For simplicity, the construction of the theoretical model assumed a global residence time distribution for all the bubbles produced in the bed (initial sizes as well as sizes of products of coalescence) shown in *Figure 7.8.4(b)* and *Figure 7.8.5(b)*. When a global or overall distribution of residence time is taken for the bubbling process at low flow rate, it becomes an inaccurate approximation of residence time probability for certain bubble sizes, especially for ones with smaller size range. As can be seen in *Figure 7.8.4*, a small bubble would be assumed to have a much higher probability of rising up the bed at a higher pace based on the global distribution than what it actually would have. Therefore, from *Figure 7.8.2* and *Figure 7.8.3*, it is logical why the theoretical model estimated that most bubbles in the bed would spend shorter time in the bed while it is not the actual case in the simulated version. When most of the bubble population is being inaccurately treated in this manner, the misplacement of the location of the 'dips' would result. However for a bed

with higher flow rate, assuming a global distribution for each of the bubble sizes would not result in large errors in approximating the actual residence time distribution for each of the bubble as can be seen in *Figure 7.8.5*. The overall error would be negligible and therefore allow good agreement between the theoretical model and the simulated bed.

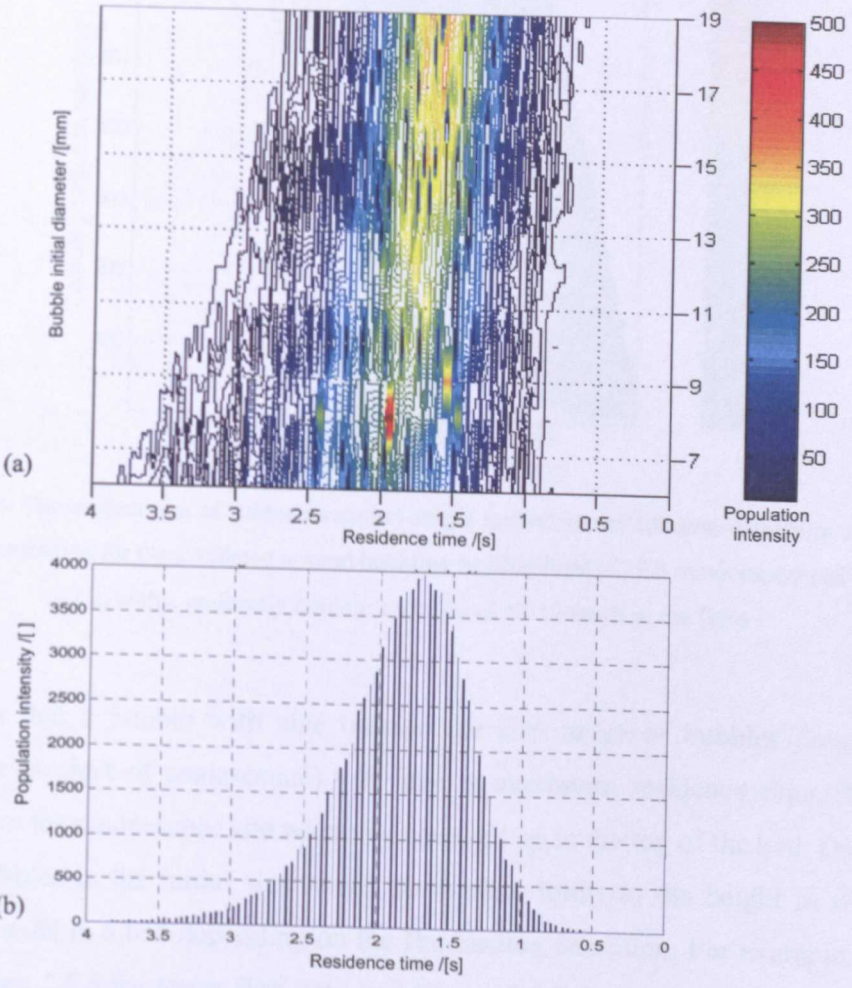

Figure 7.8.5: (a) the bubble residence time for bubbles produced at the distributor for the simulated bubbling bed fluidised at 25.6 mm/s superficial flow above U_{mf} with uniformly random variation of flow at ±12.8 mm/s, (b) the global or cumulative bubble residence time distribution used in the theoretical model.

From the data of bubble population recorded for several fluidisation conditions on the simulated bed, plots given in *Figure 7.8.6* and *Figure 7.8.7* show the likelihood of the locations in the bed for the existence of a bubble of certain size. Bubbles with initial sizes that form at the bed distributor either merge into larger bubbles immediately or rise through a certain height before their size population diminishes gradually owing to the

coalescence process. Bubbles of gradually larger sizes, on the other hand, are being created with progressive height above the distributor due to the process of coalescence.

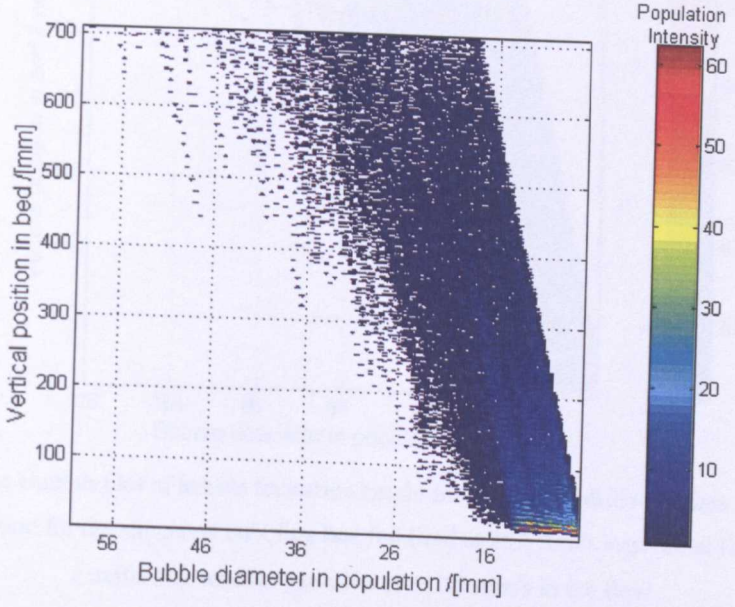

Figure 7.8.6: The contour plot of bubble formation height for bubbles of different sizes from the bubble population distribution for the simulated normal bubbling bed fluidised at 12.8 mm/s superficial flow above U_{mf} with a uniformly random variation of ±5.12 mm/s in the flow.

This implies that a bubble with size outside the size range of bubbles created at the distributor (a product of coalescence) will have a maximum residence time, if rising in isolation, from the coalescence site where it is created up to the top of the bed. On the other hand, for bubbles in the initial size range, there were limits to the height in which they were able to exist in a bed depending on the fluidisation condition. For example, referring again to *Figure 7.8.6* for lower flow rate and *Figure 7.8.7* for higher flow rate conditions, it could be seen that at lower flow rate, bubble of size approximately 16 mm in equivalent diameter could exist in the bed up to about the height of 500 mm above the distributor while at a much higher flow rate, bubble of that similar size could only exist at heights below the 350 mm mark. The coalescence process that constantly takes place in the bed diminishes the number of smaller bubbles to form large bubbles and the locations where these events take place could well be treated as the 'virtual' bed height for some of these bubbles.

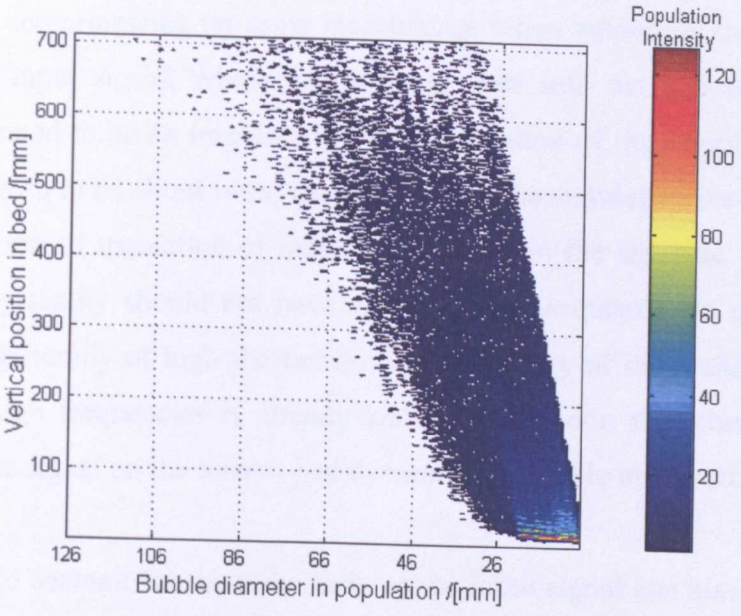

Figure 7.8.7: The contour plot of bubble formation height for bubbles of different sizes from the bubble population distribution for the simulated bubbling bed fluidised at 25.6 mm/s superficial flow above U_{mf} with a uniformly random variation of ±20.5 mm/s in the flow.

The primary 'dip' in the Bode plots of both the transfer function of the simulated bed and the theoretical model of the bubbling process indicates the approximate frequency at which most of the bubbles in the bed leaves (inferring the dominant residence time of bubbles). There will be situations where occasionally large bubbles were created unavoidably in the bed of generally smaller sized population of bubbles. The bed dynamics should still be represented by approximately the dominant residence time of the other smaller bubbles because of the magnitude of their population, although large bubbles contribute significantly toward the overall bed dynamics as well because of size factor. This greatly affects the overall bubbling behaviour in the bed and is thought to be mostly associated with the residence time of the smaller bubbles in any bubble population distribution (initially created at the distributor or from coalescence) in the bed. The primary 'dip' is also an indication of the efficiency of the bubbling process (gas-solid contact) and subsequently the quality of the fluidisation process. It could be suggested that the deterioration of the fluidisation quality in a process is shown by the primary 'dip' placed at higher frequency with narrower and deeper 'dip'. Demonstrated in *Figure 7.7.6* via the simulated bed, the Bode gain plot has a narrower and higher frequency primary 'dip' when the flow supply is higher and the simulated bed is bubbling more violently. This is hypothetical at this stage and of course is subject of great interest for further studies.

The studies carried out were strictly on the basis of improving the understanding of the process, therefore compromising on some inaccuracies when modelling the fluidised bed. For example, the input signal, which was the gas flow into the bed as bubbles, was optimistically assumed to be an impulse signal. The duration of the impulse signal in the simulation was shown to be about twice the time step of the simulation for all the bubbles, indicating some form of truncation of reality carried out in the analysis. This relaxation towards replicating reality should not have significant consequences as the effect of an impulse signal is generally of high frequency. The coherency of input and output for the bubbling bed at high frequencies is already known to be poor, therefore rendering the effect of an impulse signal on the overall bed dynamics negligible in this study.

The method used to account for the magnitude of the input signal has managed to correct the differences in the obtained Bode plots for the theoretical model compared to that of the simulation bringing about a reduction in discrepancy to a minimum of approximately 2 dB, which could be negligible caused by unaccounted sources such as unmodelled process dynamics.

It appeared to be difficult to properly present the phase plot on the Bode diagram, when considering what a correct plot would look like after the primary 'dip' frequency. This was largely due to the bad coherency between the input and output at high frequency. In some cases after the primary 'dip', the phase plot progressed to develop periodic harmonic oscillations for the rest of the frequencies. In some other cases, there was a step change in the phase around the primary 'dip' proceeding to periodic step changes at every subsequent 'dip' frequency. Addressing the issue became essential to mitigate the significance of any features in both the gain and phase plot of the Bode diagram almost immediately after, the very most, the secondary 'dip' frequency. The rule of thumb was clearly that any Bode diagram generated to describe the bubbling process contains reliable information for all considered frequencies below that of the secondary 'dip' frequency.

7.9 Comparison of theory with experimental bed

In order to validate the study carried out thus far with the simulated bed to develop the theoretical model, comparison should also be made with the experimental bed when possible. The earlier parts of the study materialised from purely concepts conceived theoretically and backed by simulated version of the system. No experimental justification was directly achievable on every aspect of the study although it has been possible to make justification of a few points, mainly regarding the fundamentals of the study.

It is not possible to measure the input of gas into the bed as bubbles at the distributor, so direct comparison cannot be made for the normal freely bubbling case. Furthermore, in obtaining the transfer function of introducing single bubble into the bed at different frequencies as done in *Section 7.3*, the use of the simulated idealised bed in which streams of single bubbles existed without interacting and coalescing allowed a comparison with the corresponding theoretical model constructed to replicate exactly this. This is again not possible in the experimental bed.

However, with the case of single bubbles, experimental comparison could be carried out and conclusion was drawn from the obtained results. In the experiment, the fluidised bed was kept at quiescent state while single bubbles with gas volume of approximately 0.2 l/m producing a bubble void of approximately 82 mm equivalent diameter were injected into the bed at an interval of 7.2 s through the centre single nozzle. These bubbles rise in isolation and do not coalesce. The similar condition was repeated in the simulated bed and then replicated in the theoretical model.

The results are presented as gain Bode plots in the diagram shown in *Figure 7.9.1*. It can be seen that the experimental bed, the simulated bed, and the theoretical model agreed very well. The simulated bed also picked up some of the more microscopic details of the behaviour of the bed with single bubble produced at fixed interval seen also on the gain plot for the experimental bed. To produce the theoretical model gain plot a logarithmic swept sinusoidal input was still required in order to generate the transfer function for that range of frequency considered.

Drawing a conclusion, the above comparison clearly shows that the simulated bed and theoretical model have been successfully developed and used to confidently predict the behaviour of the fluidised bed with single bubbles rising through it, giving information regarding the size and residence time of the bubbles. A future consideration would be to fabricate a new experimental bed of which the input of gas through the bed distributor could be measured either directly or through inference. Subsequently, experimental transfer function and its Bode plot could be obtained and compared with the simulated and theoretical model results.

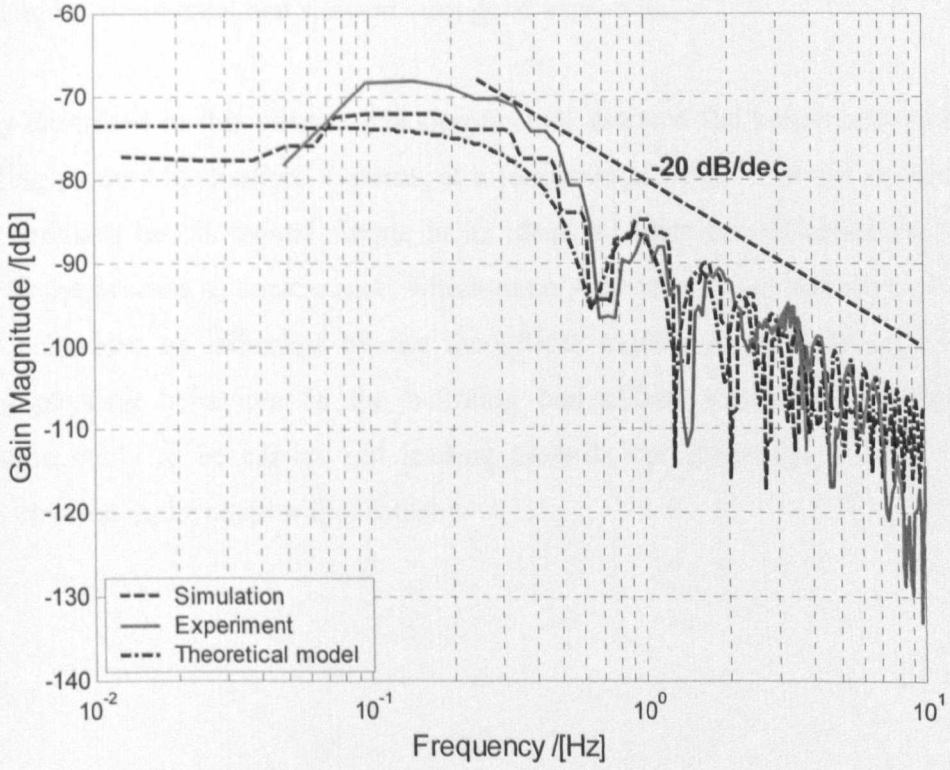

Figure 7.9.1: The agreement between the experimental bed, simulated bed and theoretical model for a fluidised bed with single bubble of diameter approximately 82 mm introduced at fixed intervals of 7.2s such that no coalescence was present in the experimental bed.

7.10 Conclusion

A theoretical model was derived to dynamically model the behaviour of bubbling in the idealised bed with single bubbles, which was gradually transformed into its realistic counterpart where multiple bubbles present in the bed were allow to grow with height, interact and coalesce; features of non-linearity dominant in affecting the overall dynamics of a normal bed. The model was shown to satisfactorily agree with experimentally validated simulated bubbling bed results where their corresponding Bode diagrams were used as form of comparison. In the case of bubbling with single bubbles, the model, simulated and experimental bed showed very good agreement.

The study described in this chapter has significantly assisted the better understanding of the bubbling process in fluidised systems, at a fundamental level. It could be said that the bubbling fluidised bed is indeed simple in its idealised form but complicated and made complex by the process of coalescence, which mainly governs the overall dynamics of the bubbling behaviour as indicated by the theoretical model. A good perception of the governing physical behaviour in the bubbling bed allows a more competent system identification study to be carried out leading towards the design of suitable controller strategies covered in the chapter that follows.

Chapter 8

System identification and control of bubbling fluidised beds

8.1 Introduction

The proper control of a bubbling fluidised bed requires a comprehensive understanding of the dynamical behaviour of the system. The preceding chapters addressed this requirement, of which through to *Chapter 6*, significant progress has been made in acquiring knowledge of the fundamental workings of the bubbling process. The nature and consequences of the existence of bubbles and the influence of their behaviour within the vessel have tremendous effect on the overall dynamics of the fluidised bed. These features determine how the bed behaves at a given supply of gas as well as the response of the bed to various types of changes the supply was subjected to.

Conventionally, the fluidised system is perceived to be a difficult and complex system to understand and therefore consequently to control desirably as well. However, the research conducted so far has pointed to somewhat contrary views. It was demonstrated in *Chapter 6* that very close to quiescent condition, the fluidised bed behaves linearly, only to gradually deteriorate into non-linearity with increase in gas supply so that sufficient bubbles enter the bed that they interact and consequently coalesce. These activities upset the linear relationship of bubble size and residence time.

This penultimate chapter covers the remaining issues left unanswered in this research encompassing the system identification of the fluidised system leading towards attempts to control the process initially with conventional linear controller strategies followed the by benchmarking of the implementation of adaptive control methods. The controllers were

implemented to maintain the bubbling condition in the bed, as well as to adjust it to the desired state. The objective of these approaches to control was to determine the extent the dynamics of the process that has been understood when the controllers are designed and implemented. The controllability assessment would lead to further refinement on the understanding of the bubbling process.

However, the ultimate aim of controlling this process is to establish a good composition of bubbles in the bed such that a good degree of fluidisation quality can be preserved. Controlling the extent of bubbling within the bed would only partially satisfy this criterion. The spatial distribution of the population of bubbles at any operating condition plays a crucial role to also promote such quality. Therefore, the last section in this chapter describes an alternative method of controlling the bubbling process such that it directly affects the distribution of bubbles, shaping the distribution profile into one that nurtures good fluidisation quality.

8.2 System identification

8.2.1 Introduction

System identification is a process of determining the transfer function or obtaining a mathematical description for the dynamic characteristics of a system or its sub-system by means of practical tests. This process requires the introduction of some input signal to the system under investigation and the corresponding system output signal is used along with the input signal to identify the relationship between them from which a model can be constructed and the unknown system parameters can be estimated. Conventionally, step or sinusoidal as well as other waveforms are used to excite the system over a range of frequencies to obtain a full analysis of the system response over the range of operating conditions. Stochastic methods could also be used where random excitation is exerted on the input and cross-correlation calculations can be used to determine system dynamics from the input and the measured output. To implement this on the bubbling fluidised system, the experimental arrangement described in *Chapter 2* was used with the image analysis system to measure the Bubble Void Fraction, BVF of the bubbling phase in the planar bed.

System identification can be carried out via several methods: time domain, frequency domain, and statistical approaches. This study explores the dynamical response of the bubbling bed to perturbations induced by its input over a range of excitation frequencies mainly by time domain approaches with the use of frequency domain techniques for analysing the resulting system identification transfer functions in the form of Bode diagrams.

The product of system identification in the form of transfer functions could then be used to further supplement the understanding of the bubbling fluidisation regime where previous models was constructed to describe the bubbling behaviour in the bed at steady state condition (*Chapter 7*). Here the knowledge of the dynamical response, which concerns with the transient behaviour of the bubbling bed before settling to steady state condition, has been explored.

8.2.2 Linear approximation to process dynamics (and assessment of approximation robustness)

Prior to the approach of any system identification on the bubbling process, the open-loop BVF signal from the image analysis system was observed and assessed. It was found to be possible to linearly approximate the dynamical response of the bubbling process through the BVF measurement from the bed by subjecting it to various transient changes in bubbling conditions, although the extensive signal characterisation and benchmarking in *Section 2.3.2* have identified salient features in the BVF signal that are characteristics of complex process dynamics. This kept analysis simple and directly avoiding complicated details that otherwise required to be dealt with in a non-linear sense, which requires non-linear system identification techniques. Again, the desire in this study was to preserve simplicity and only study the process in its most fundamental level.

This treatment was applied through the whole process of system identification using standard linear methods. The input to the dynamical system, which is the amount of gas flow into the bed plenum was subjected to a logarithmic swept sinusoidal and square wave variation sweeping through excitation frequency of between 0.001 Hz and 2 Hz. The upper limit of the excitation frequency was kept relatively low as the actuator, i.e. the valve-

servomotor coupling system controlling the flow of gas, has limited physical functionality. Apart from that, the variation rate of gas flow above this frequency caused minute bubbling changes in the bed and would therefore contain negligible dynamical significance. The flow of gas into the plenum was brought through a series of different variations within the bubbling regime so that the dynamical transient response of the bed over its full bubbling regime operating range could be interrogated. The system identification analysis would produce a transfer function for each test presentable in the form of a Bode diagram.

8.2.3 Distinction of the system identification study from studies conducted in *Chapter 7*

The product of system identification conducted on the fluidised system is a mathematical expression in the form of a transfer function that describes the dynamical response of the planar bed to perturbations in the flow supplied to the bed at various frequencies. The response of the bed, which includes both the transient and steady state values of the BVF measured by the image analysis system, provides the information about the dynamical characteristic of the bubbling bed at various operating conditions. The obtained transfer function enhances the understanding of why the bubbling bed behave a certain way to a perturbation in the flow supply where the parameters in the transfer function reflect the dynamical properties of the bed responding to that perturbation.

The study of system identification therefore differs from the study conducted in *Chapter 7* where dynamical models, also in the form of transfer functions, were produced. The work in *Chapter 7* involved constructing a theoretical model that describes the dynamics of the bubbling behaviour in the bed that affects its overall behaviour at steady freely bubbling conditions. The model was derived initially for the simple single bubble case and gradually built into a complicated model that took into account bubble interaction and coalescence present in normal freely bubbling process. The obtained transfer functions are meant to describe the fundamental features of bubble existence in the bed and are not directly control-purpose driven nor are they directly applicable to designing controller tactics. However, the models give an insight and some ideas of what requirements must be considered when designing a controller.

Therefore care must be exercised when making interpretation and analysing the two different versions of transfer function obtained from work done in *Chapter 7* and this chapter. In many ways, both versions of the transfer function may have resemblance in certain cases but the obvious distinctive features are the intermittent 'dips' observable on the theoretical model transfer function in *Chapter 7*.

8.2.4 System identification results

8.2.4.1 System response signal characterisation

The salient features in the BVF signal from a typical open-loop transient changes to the bubbling condition and already mentioned in *Chapter 2* are shown again in *Figure 8.2.1* to emphasise their importance in effecting the dynamics of the bed.

The difference in fluctuation magnitudes at different flow conditions and the presence of hysteresis during rise and fall of the BVF signal are evidences of non-linearity in the system. The increase in BVF fluctuation with increase in flow correspond to the increase in bubbling activity indicating a change in the dynamics of steady state bubbling behaviour. The change in the rate of rise and fall of the BVF signal was caused by a change in the dynamics of the bed in its response to transient flow supply.

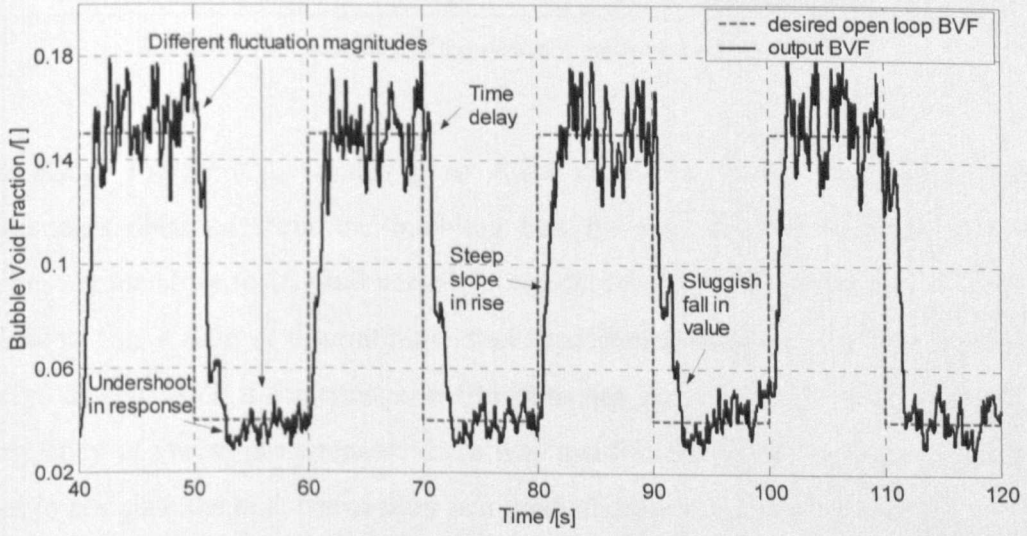

Figure 8.2.1: The typical open-loop BVF signal measured of the bubbling process in a planar bed using the image analysis system. The salient features in the time series are pointed out and labelled accordingly.

Although fluidised beds are generally regarded as a slow response system, the presence of a slight delay is evident. It took the bed a short time before fully responding to changes in the supply of flow noticeable in the response signal (BVF). Time delays have major implications, particularly in the control of such a system.

8.2.4.2 Dynamical response of the bubbling bed to various modes of excitation

The gas supply was brought through a step variation of different degrees with a logarithmic swept frequency variation from 0.01 Hz to 2 Hz. *Table 8.2.1* summarises the tests conducted in the system identification of the process.

Test type	Test	Description (mm/s superficial flow)
Small range variation	1	~U_{mf} to 25.6 mm/s above ~U_{mf}
	2	25.6 mm/s to 51.3 mm/s above ~U_{mf}
	3	51.3 mm/s to 76.9 mm/s above ~U_{mf}
	4	76.9 mm/s to 103 mm/s above ~U_{mf}
Intermediate range variation	5	~U_{mf} to 51.3 mm/s above ~U_{mf}
	6	25.6 mm/s to 76.9 mm/s above ~U_{mf}
	7	51.3 mm/s to 103 mm/s above ~U_{mf}
Full range variation	8	~U_{mf} to 103 mm/s above ~U_{mf}

Table 8.2.1: A summary of the system identification tests carried out.

Figure 8.2.2, *Figure 8.2.3* and *Figure 8.2.4* show the typical results of the BVF measurements obtained from the bubbling bed for two distinct conditions: variations involving regime close to U_{mf} and variations amidst totally bubbling state. It could be seen that close to U_{mf}, a state of discontinuity was experienced where no bubbles were present, registered as zero BVF if the change in flow was not sufficiently large (*Figure 8.2.2*). As the frequency of variation increased, there was insufficient supply of gas to nucleate into bubbles to populate the bed, hence seen as a gradual drop in the average BVF.

This however, would be different if more gas was allowed into the bed (more than the initial 25.6 mm/s) as the upper limit of the step variation as shown in *Figure 8.2.3*. Due to

the high gas flow and the high frequency of variation in the flow, there were always some bubbles present in the bed.

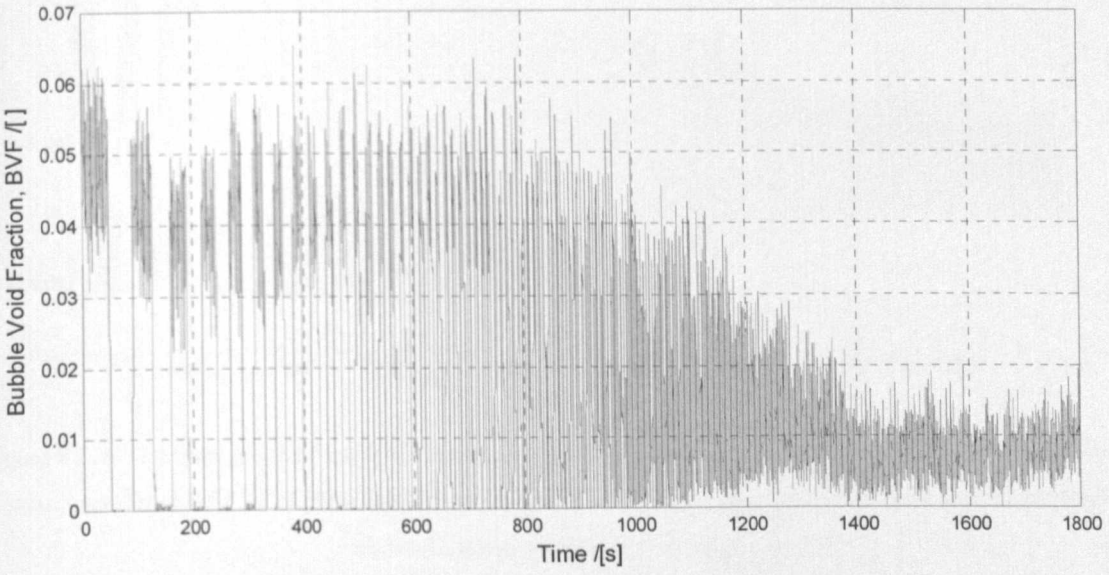

Figure 8.2.2: The time series of the BVF in response to the system identification test of logarithmic-swept square wave from 0.01 to 2 Hz for the bed at gas supply of between ~U_{mf} and 25.6 mm/s superficial flow above U_{mf} over a duration of 1800 s.

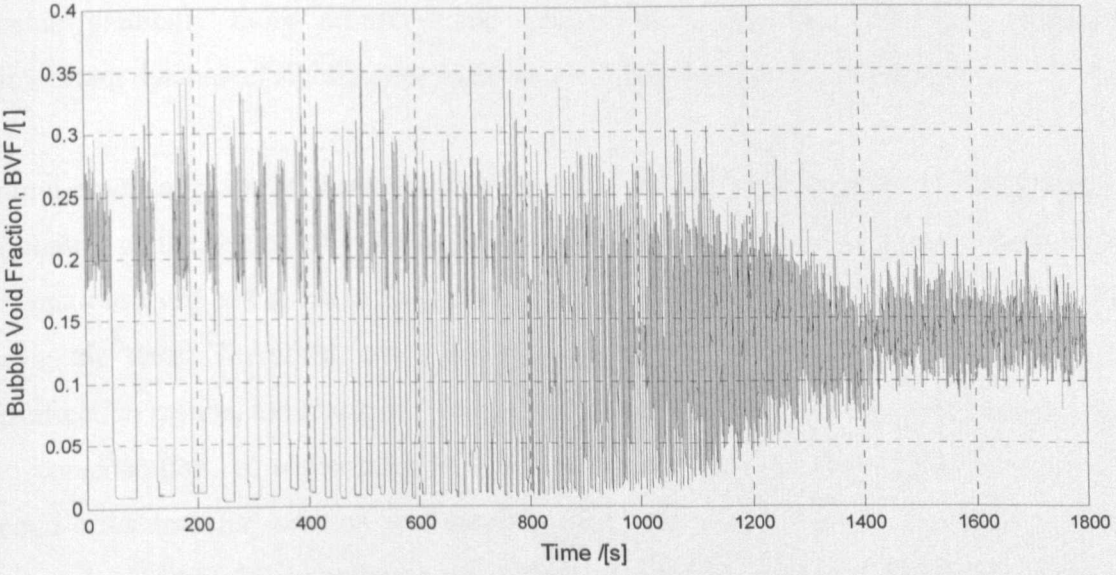

Figure 8.2.3: The time series of the BVF in response to the system identification test of logarithmic-swept square wave from 0.01 to 2 Hz for the bed at gas supply of between ~U_{mf} and 103 mm/s superficial flow above U_{mf} over a duration of 1800 s.

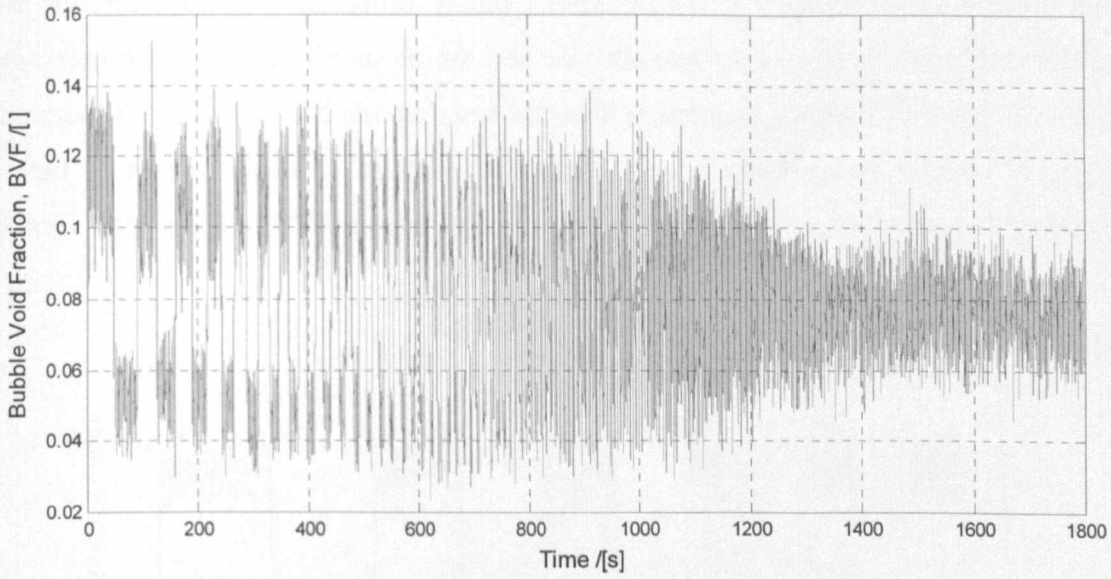

Figure 8.2.4: The time series of the BVF in response to the system identification test of logarithmic-swept square wave from 0.01 to 2 Hz for the bed at gas supply of between 25.6 and 51.3 mm/s superficial flow above U_{mf} over a duration of 1800 s.

On the other hand, variations where the bounds were within the bubbling regime saw a more symmetrical response of the bed registered in the BVF measurement. However, it can be seen on all three figures (*Figure 8.2.2* to *Figure 8.2.4*) that the response of the bed became gradually more arbitrary and noisy with increasing frequency, containing unimportant dynamical significance as far as the control of the bed is concern.

From a practical point of view, the flow should not have to be frequently adjusted during the control of the degree of bubbling because the bandwidth of condition variation in the bed was observed not to reach frequencies as high as 2Hz, as being imposed on the flow during the tests. Therefore, when estimating transfer function models for the system identification results, the range of 0.01 Hz and 0.6 Hz of the frequency response was taken into consideration, corresponding to test data from time 0 to approximately 1400 s. A second order transfer function was assumed where the Output-Error estimator technique was used in MATLAB to estimate the suitable transfer function parameters to model the experimental data. The estimator compares the measured output with the predicted output from the model and then makes the appropriate adjustment to the model to minimise the subsequent error between them.

The successes of the estimation varied where shown in *Figure 8.2.5*, a good model estimation was achieved for when the bed was varying between two bubbling states. On the other hand, *Figure 8.2.6* shows a less accurate estimation of model obtained for the bed excited to regime close to its quiescent state. The model appears unable to properly describe the change of BVF measurement when the bed is close to its quiescent condition.

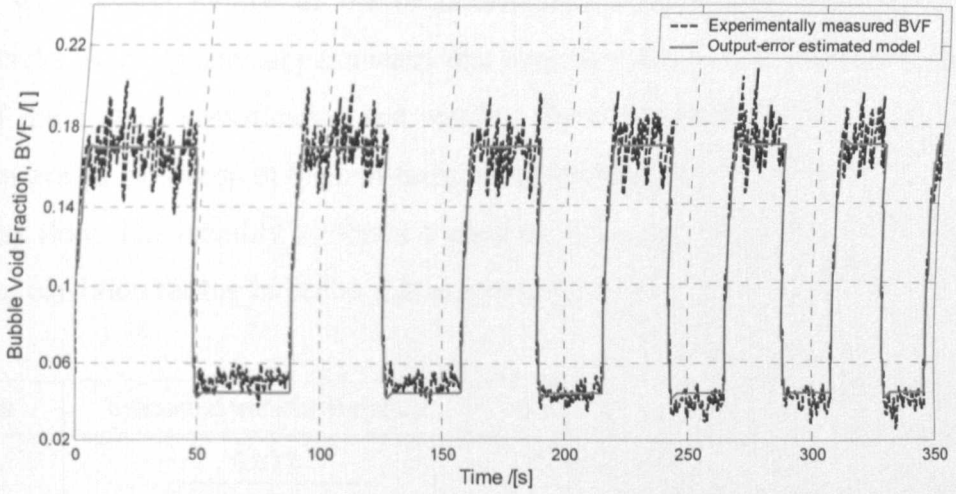

Figure 8.2.5: The time series of BVF in response to the system identification test of logarithmic-swept square wave from 0.01 Hz to 0.6 Hz for the bed at gas supply of between 51.3 and 103 mm/s superficial flow above U_{mf} over a duration of 1400 s. The success of estimating a model using the Output-Error estimator resulted in a well fitted plot.

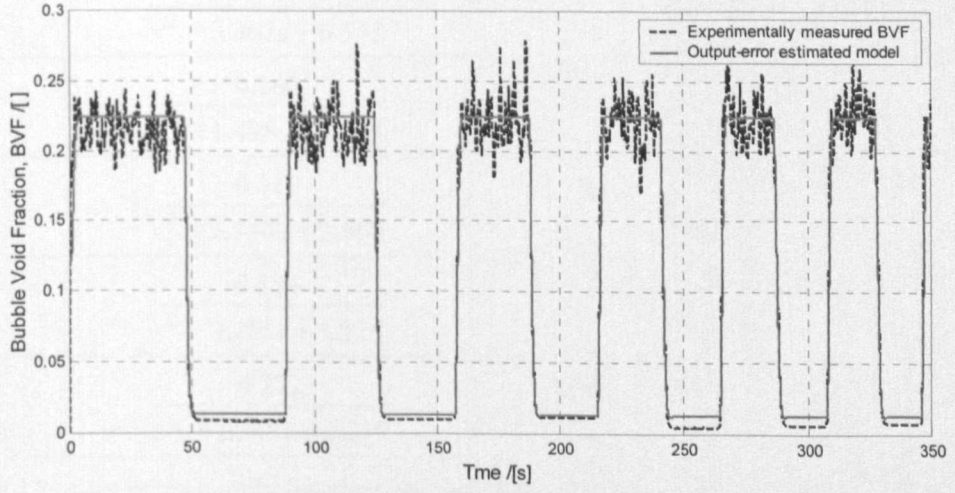

Figure 8.2.6: The time series of BVF in response to the system identification test of logarithmic-swept square wave from 0.01 Hz to 0.6 Hz for the bed at gas supply of between ~ U_{mf} and 103 mm/s superficial flow above U_{mf} over a duration of 1400 s. The fitted model was not accurately estimated using the Output-Error estimator.

A second order transfer function model was chosen to represent the estimated dynamics of the system identification results. The model takes the form

$$\frac{\lambda\omega_n^2}{s^2+2\zeta\omega_n s+\omega_n^2} \tag{8.1}$$

where λ is the low frequency gain, ζ the damping ratio and ω_n the natural or characteristic frequency. The Output-Error estimator adjusts these parameters to get the best-fit of the model with respect to that of the measurements obtained from the tests. *Table 8.2.2* presents the list of dynamical parameters that constitute the transfer functions estimated for each of the system identification test results. The differences in each of these transfer functions are an indication of the non-linearity of the bubbling process response to changes in the gas flow. The inability to obtain a good estimate for the process when close to the quiescent condition further indicates this nature in the bed.

Test	Estimated transfer function	LFG, λ	ζ	ω_n
1	$\frac{0.077}{s^2+0.892s+0.531}$	0.144	0.61	0.73
2	$\frac{0.284}{s^2+1.960s+1.942}$	0.146	0.70	1.39
3	$\frac{0.354}{s^2+2.945s+3.793}$	0.094	0.75	1.95
4	$\frac{0.403}{s^2+3.807s+6.545}$	0.061	0.74	2.56
5	$\frac{0.160}{s^2+1.498s+1.170}$	0.137	0.69	1.08
6	$\frac{0.319}{s^2+2.334s+2.564}$	0.124	0.73	1.60
7	$\frac{0.354}{s^2+3.151s+4.526}$	0.079	0.74	2.13
8	$\frac{0.222}{s^2+2.346s+2.239}$	0.099	0.78	1.50

Table 8.2.2: A list of the transfer functions and their constituting dynamical parameters estimated for the system identification tests.

Figure 8.2.7 compares the value of damping ratio, ζ, for the tests and there were reasonably small variations. ζ, in this case, does not have direct physical meaning correlating it to the dynamics of the system under investigation. However, the tests conceded distinctly different values of natural frequency, ω_n as can be seen in *Figure 8.2.8*. A pattern of variation could be observed where in the first set of tests (Test 1 to 4) involving small changes in flow, ω_n increased with the lower limit of the test variation.

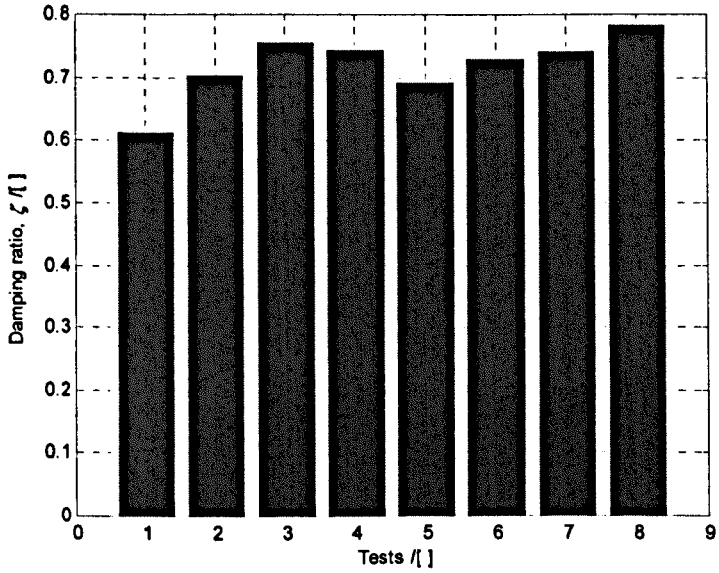

Figure 8.2.7: The values of damping ratio, ζ for each of the system identification tests. System identification results reveal a reasonably constant damping ratio in all tests.

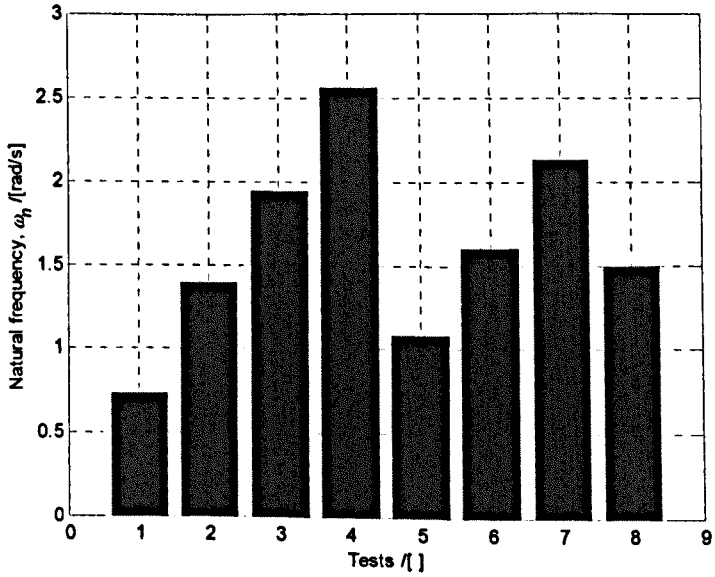

Figure 8.2.8: The values of natural frequency, ω_n for each of the system identification tests. System identification results reveal significant changes in ω_n between each test.

The increase in the lower limit of the flow from close to U_{mf} to 76.9 mm/s increased the response rate of the bed to the incurred changes in flow. The lower limit of flow determined the initial gas laden in the bed before it was subjected to the supply of more gas. The more the bed was laden with gas (and consequently bubbles) the easier and hence the faster it responded to the increase in gas supply. As an example, the bed was faster to respond to increase in gas supply to 103 mm/s above U_{mf} when it was initially at 76.9 mm/s above U_{mf} than the bed did when it responded to an increases in gas supply to 25.6 mm/s above U_{mf} from being initially at a quiescent state. The similar explanation applies to the cases with intermediate variation in gas supply (Test 5 to 7). The bed was also faster to respond when the increase in gas supply was larger (comparing ω_n of Test 1 of 0.686 rad/s to that of Test 5 at 0.948 rad/s). As expected, Test 8 registered the highest ω_n at 1.4 rad/s compared to Test 1 and Test 5.

8.2.4.3 *The justification of second order transfer function estimation of bed transient dynamics relating to behaviour of bubbles affecting the bed*

The system identification tests gave an insight into how the bubbles created in the bed affected the bed transient dynamics. As a consequence of introducing more gas into the bed during the tests, more bubbles were created. Depending on the amount of gas supplied, bubbles that were produced, interacted and then coalesced into larger ones rising faster up the bed. This resulted in the bed reaching its steady state faster reflected in the increase in ω_n obtained. This was more pronounced with the change in gas supply being a step rather than a more gradual one.

Chapter 7 has demonstrated that a bubbling bed could be well described by the theoretical model shown earlier in (7.3)

$$\frac{K_{b,ZOH}}{s}\left(1-e^{-sT}\right) \tag{8.2}$$

both in the frequency domain with a Bode diagram and in the time domain as shown in *Figure 8.2.9* for a step response. A step increase in gas supply at time, t = 1 s generated bubbles continuously such that the BVF increases up to a steady-state after a rise period of 2.2 s, corresponding to the bubble residence time, T. The steady-state value was equal to

$K_{b,ZOH}$*T. Bubbles were assumed to have similar sizes and with (8.2), do not expand with height in the bed. Therefore, the start and end of increase in magnitude were sudden. Indeed, this was a simple representation of bed step response since (8.2) applies to idealised bubbling.

A second order transfer function was used to approximate the step response of the bed in the system identification process and has shown success in estimating the bed transient dynamics. In fact, the dynamical parameters constituting the transfer function have close association with the physical bubbling process described by (8.2). In order to have a better approximation, a zero (a numerator root, $s = -\alpha_{if}$) was added to the second order transfer function such that it took the form

$$\frac{\lambda\omega_n^2(s+\alpha_{if})}{\alpha_{if}(s^2+2\zeta\omega_n s+\omega_n^2)} \tag{8.3}$$

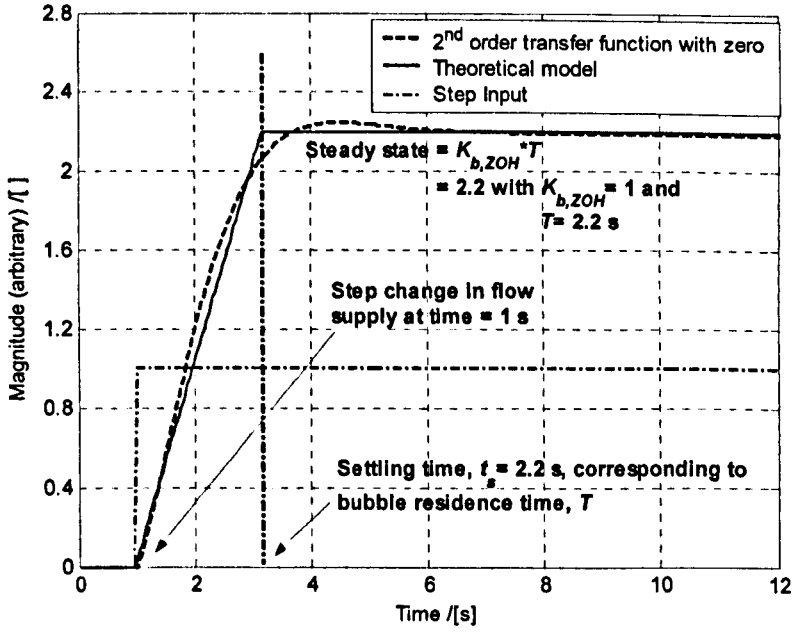

Figure 8.2.9: The step response of the bed described by the theoretical model in (8.2) and estimated using transfer function in (8.3) assuming bubbles were produced to have similar sizes.

This is basically a high frequency differential term within the plant and was used reduce the a roll-off rate to – 20 dB/decade in its Bode plot from the original – 40 dB/decade with a pure second order transfer function, so that the roll-off rate is consistent with that of (8.2). Presumably, (8.3) needs to have a fast zero having a quick but negligible effect on the bed slower dynamics apart from the initial pure second order transfer function

estimation. *Figure 8.2.9* shows the comparison of the step response of the bed described by the theoretical model (8.2) and the estimated transfer function (8.3).

The fitting of (8.3) with the estimation of the best dynamical parameter values via least-square method onto several bed step response conditions with different T values have derived several interesting relationships. It was shown that the damping ratio, ζ in (8.3) was approximately between 0.7 and 0.8. This was a consequence of fitting the transfer function onto the theoretical model and should not be mistaken as a characteristic value of an under-damped system like a mass-spring-damper system. The natural frequency, ω_n was found to relate to the bubble residence time, T by

$$\omega_n \approx \frac{\pi}{T} \tag{8.4}$$

indicating the response of the bed to a step increase was similar to a quarter cycle sinusoidal oscillation with an inversely proportional relationship to the bubble residence time, or more generally, proportional to the amount of gas supply.

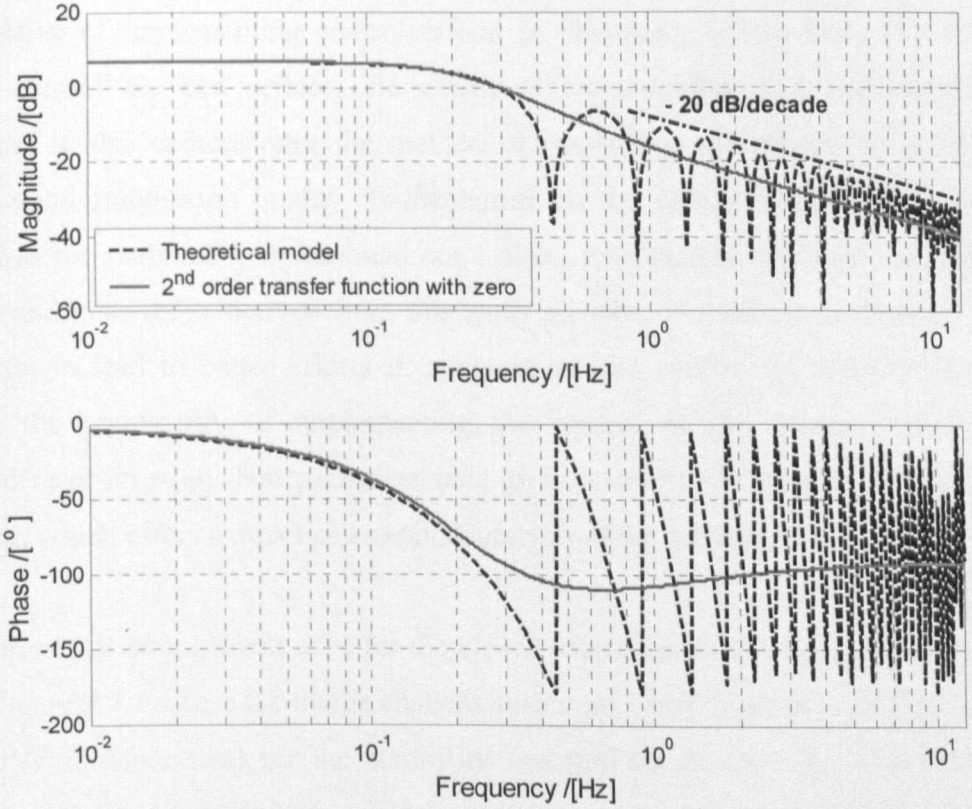

Figure 8.2.10: The Bode diagram for the theoretical model in (8.2) and the approximated second order with a zero transfer function describing the step response of a bed from U_{mf} to a state with bubbles spending 2.2 s in the bed.

Figure 8.2.10 shows the corresponding Bode diagram (both gain and phase) for the theoretical model and the estimated transfer function. Both plots appear to agree well with the transfer function breaking off to a start of – 40 dB/decade roll-off rate that gradually shifted to a – 20 dB/decade decay similar to that of the theoretical model. Both phase curves also settled close to a -90° asymptote characteristic of a first order transfer function at high frequency. Ideally, the second order with zero transfer function approximation to the step response of the bed should be compared more realistically to the theoretical model built to describe a normal bubbling bed, of which the Bode diagram was shown in *Figure 7.7.5*. The simple analysis presented here purely serves to both justify the theoretical model and to demonstrate the use of the transfer function to model the bed step response keeping issues bare and simple to understand and work with. Therefore, the pure second order transfer function form was used in the controller design instead of (8.3).

8.3 The design and implementation of linear control strategies

The objective of implementing control efforts in this study is two-fold. The ability to properly control the bed reflects the extent of the bubbling bed behaviour that is understood. It also demonstrates the method of controlling the process to achieve and maintain good fluidisation quality. Implemented on the planar bed, the control of the process was for analytical purposes and not a direct extension to practical use. However, the ideas and knowledge derived from this study on what is required to properly control such a system lead to better efforts in applying similar control to industrial beds. For example, the practicality of implementing the control of the process via the BVF measurement or an equivalent parameter onto an industrial bed could be assessed on the planar bed, which offers a direct and explicit analysis of the bubbling phase.

The experimental arrangement used for the closed-loop control of the fluidised bed can be seen in *Figure 2.2.1* where the image analysis system in ControlLab provides the feedback signal (BVF measurement) for the controller. ControlLab changes the valve position to control the gas flow into the bed, which in turn translates into a corresponding change in the instantaneous BVF value. Real-time closed-loop control could be implemented by continuously comparing the desired and the obtained BVF values and making appropriate flow variations.

A low-pass filter was applied to the raw BVF signal fed-back in real-time from the image analysis system to clean out low magnitude high frequency fluctuations intrinsic in the process that could hamper the control effort. To prevent the actuator from suffering any stiction problems, the dithering technique was also used by superimposing a low amplitude high frequency (20 Hz) excitation onto the valve control signal such that the valve was always vibrating slightly.

8.3.1 Characteristic equation and the root-locus analysis method for controller design and gains selection

If the transfer function of a system is represented as $G(s)$ then

$$\frac{output(s)}{input(s)} = G(s) = \frac{num(s)}{den(s)} \tag{8.5}$$

where $output(s)$ and $input(s)$ are the input and output parameter measured from the system, $num(s)$ is the numerator and $den(s)$ is the denominator of the transfer function $G(s)$. Rearranging (8.5) gives

$$output(s)den(s) = input(s)num(s) \tag{8.6}$$

A null input signal into the system delivers a response consisting of only the transient component since the steady-state response would be zero, therefore by equating $input(s) = 0$, gives

$$output(s)den(s) = 0 \tag{8.7}$$

Apart from the trivial solution of $output(s) = 0$, the transient response for a system could be determined by the equation

$$den(s) = 0 \tag{8.8}$$

known as the characteristic equation of the system where its solution indicates the form of transient response of the system to any given input signal. The characteristic equation could be used to determine both the open-loop as well as the closed-loop transient response (characterised by the poles or roots) of the system.

However, the roots of the transfer function equation for a system with degree of higher than 3 are complicated and laborious to determine. The closed-loop transfer function of the fluidised system (estimated to be essentially a pure second order system) combined with the Proportional + Integral + Derivative controlled scheme, is effectively higher than second order. Therefore, the root-locus analysis method was used to design the controller

where the series of root values of the characteristic equation are plotted for all the values of a system parameter or controller gain. The basic characteristic of the transient response of a closed-loop system is related to the location of the closed-loop poles. Root-locus analysis is carried out by presenting the results of closed-loop pole variation on the *s*-plane diagram as a root-locus plot that vividly shows how the closed-loop poles migrate with certain controller gain variation. Changes in the controller gains cause loci of variation in the locations of the closed-loop poles, or roots, and therefore the system closed- loop transient response.

The following describes the procedure with which the controllers were designed. To properly construct the root-locus plot, the characteristic equation must be obtained taking the form

$$1 + G_c(s)G_p(s)H_c(s) = 0 \tag{8.9}$$

$G_c(s)$ is the controller and $G_p(s)$ is the plant transfer function with poles, p_i and zeros, z_i such that

$$G(s) = \frac{(s+z_1)(s+z_2)...(s+z_m)}{(s+p_1)(s+p_2)...(s+p_n)} \tag{8.10}$$

The closed-loop transient response of the system depends on the selection of the value of a gain parameter, usually the proportional gain, k_p, which could be obtained by rearranging the characteristic equation into

$$1 + \frac{k_p(s+z_1)...(s+z_m)}{(s+p_1)...(s+p_n)} = 0 \tag{8.11}$$

where z is the zero and p is the pole. Depending on the location of the root-locus plot, the value of gain parameter k_p varies giving a range of system closed-loop transient response. Choosing the desired transient response will determine the gain parameter value required for the controller.

Attempts were made to control the bubbling process using the Proportional + Integral + Derivative (PID) schemes, which is standard linear strategy. PID controller provides a control action that proportionally takes into account the direct and integral of the errors between the desired and measured output as well as the rate at which the measured output changes.

8.3.2 Proportional +Integral + Derivative (PID) controller design and implementation

PID controller is popular for controlling industrial processes such as many in chemical, petroleum, power and manufacturing industries where the systems are usually slow, complex and characterised by relatively incomplete or uncertain mathematical description. The PID controller, with parameters that could be adjusted experimentally, is therefore particularly attractive for such processes and therefore in the control of the bubbling fluidisation process as well.

Applying the root-locus method in the design of the PID controller, the required closed-loop characteristic equation takes the form

$$1+\frac{k_p T_d\left(s^2+s/T_d+1/(T_i T_d)\right)}{s(s^2+2\zeta\omega_n s+\omega_n{}^2)}=0 \tag{8.12}$$

where T_I is the integral gain and T_d is the derivative gain.

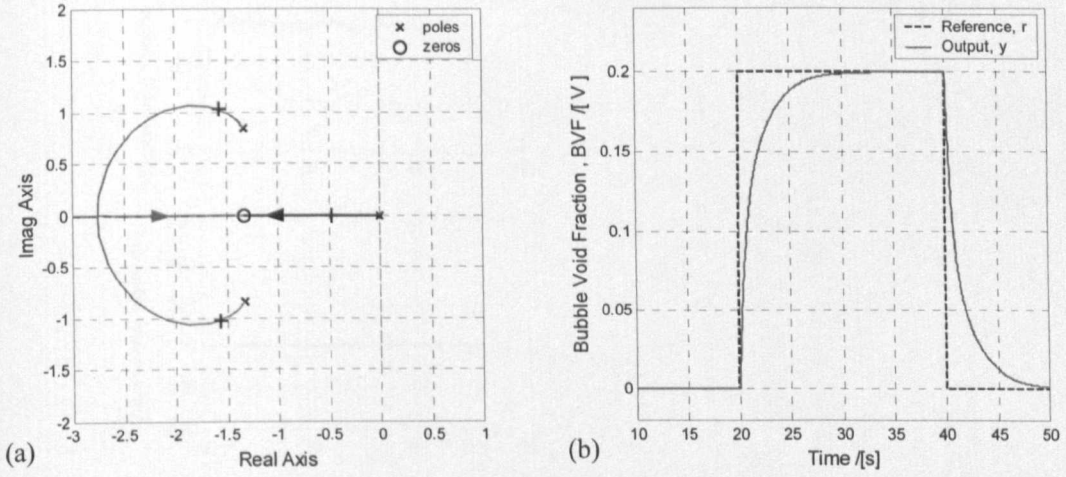

Figure 8.3.1: (a) the root-locus plot and the position in the locus for the chosen gain k_p. (b) the corresponding simulated time response of the system with the designed gains: $k_p = 10.02$, $T_i = 1.50$, and $T_d = 0.38$. The demand signal steps between 0 and 0.2 BVF. The '+' markings indicate the position of the roots in the loci where the gain k_p was chosen.

The controller was first designed to cope with control over approximately the whole bubbling regime where the control demand was a step change in BVF at 0.01 Hz between 0 to 0.2 BVF. The choice of $T_i = 1.50$, and $T_d = 0.38$ created a root-locus plot as shown in *Figure 8.3.1(a)* and were chosen so that the placement of the controller zeros with those values would cancel out the effect of real roots of the plant poles. Pole or zero cancellation

in design of controllers is an effective technique used to cancel out the dynamical effect imposed by a plant pole or zero from affecting the overall behaviour of the closed-loop system. Selecting the value of k_p = 10.02 indicated by the location of '+' markings in the root-locus plot gave a corresponding time response shown in *Figure 8.3.1(b)*. The settling time, t_s is approximately 10 s.

The designed gains for the PID controller were tested on the experimental rig for the same control demand and the results can be seen in *Figure 8.3.2* where *(a)* shows the reference and the output signals over time with the corresponding control effort and valve position shown in *(b)* and *(c)*. The BVF was measured in volts, V. It is typical in control implementation where all parameters or signals are measured in voltages. A positive 'valve control signal' acted to open and a negative value to close the valve while 0 V kept the valve at rest. The 'PID controller demand' dictated the required valve position.

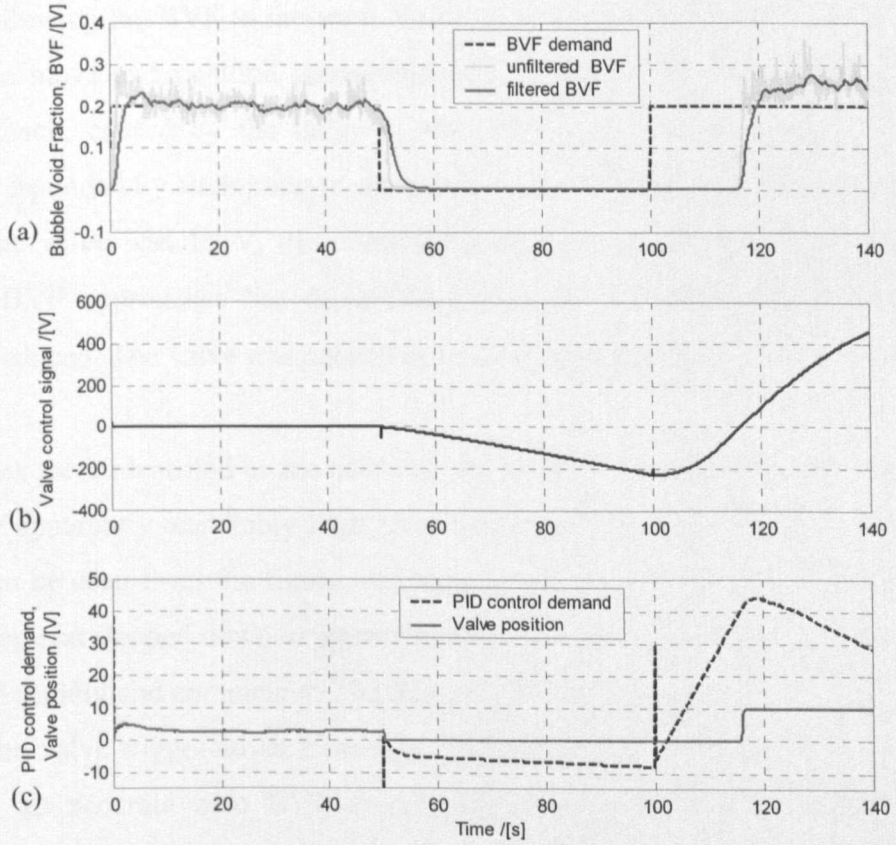

Figure 8.3.2: (a) the reference and the output signal from the experimental bed resulting from close-loop control for a demand of 0 to 0.2 BVF at 0.01 Hz step excitation using the designed gains (k_p = 10.02, T_i = 1.50, and T_d = 0.38). (b) the corresponding control effort exerted onto the valve and (c) the PID controller demand on valve position and the resulting measurement of valve position.

The first cycle of demand excitation witnessed a desirable response of the bed with the measured BVF following the demand closely apart from the expected transient response characteristic and intrinsic fluctuations (*Figure 8.3.2(b)*). At t = 50 s, the demand stepped down from 0.2 to 0 BVF where in response, the valve was directed by the controller to rapidly shut. At this point, a problem surfaced where the valve control signal (*Figure 8.3.2(b)*) continued to increase in negative voltage due to the PID control demand that required the valve to move to a below zero voltage position (*Figure 8.3.2(c)*). This was not possible for the valve as the lower limit, upon complete shut-off of the valve, was 0 V.

The next increase in demand to 0.2 BVF at t = 100 s saw no increase in the measured BVF from 0. This was because the valve was still shut with the valve control signal remained negative. As the controller recovered from the previous control performance setback, the zero-crossing of the PID control demand at approximately t = 103 s, brought the valve control signal gradually back to zero and upon its zero-crossing ($t \approx 117$ s), the valve reopened allowing the BVF to increase. However at this point, the PID control demanded the valve to move to a position corresponding to around 35 V. This is an again another control setback, caused by the delay in the BVF in increasing as demanded and the controller responded by attempting to open the valve even further. While the upper voltage limit for the valve was 10 V, the controller's attempt was hampered. However, as the measured BVF approaches the demanded value, the controller demand peaked, then gradually reduced. The valve was opened to its limit allowing BVF to peak ($\approx$ 0.25 BVF).

Two sources were identified as the cause of the problem, the first being that the designed gains were apparently unsuitably high to be experimentally implemented to the bubbling bed. As can be seen from the figure, the control initially started off well but failed when the BVF demand stepped down to approximately U_{mf}. Due to the high gains, the valve was forced shut rapidly and completely. The high magnitude (peaking at –200 V) of the control signal to the valve suggested an extreme control effort detrimental to the actuator. Apart from that, an accurate zero BVF to correspond to an incipiently fluidised bed was sometimes experimentally unachievable. Occasionally, the image analysis system might record a value very close to zero even when the bed was already defluidised due to problem such as electrical noise picked up in this measurement of BVF. Failure for the bed

to reach this value was worsen by the large gains that amplified the errors and feeding it to the controller that further deteriorated the situation.

The controller integral gain windup was also partly the cause of this complication. The controller algorithm used was not designed prior to the tests to restrict any gain saturation, which leads to many controller faults including complication such as this. A gain saturation limiter was later used to ensure this did not reoccur. At this point, the control of the process could be considered ineffective and might already have drifted into instability. In this case, it is the failure of the controller to perform due to the choice of controller gain values obtained via theoretical controller design without some prior knowledge of system characteristics. An alternative set of design criteria was pursued, moderating the values of the controller gains from those initially chosen. The trial and error choice of moderated gains $T_i = 0.60$, and $T_d = 0.26$ resulted in the root-locus plot shown in *Figure 8.3.3(a)*. $k_p = 2.65$ gave the designed closed-loop response as shown in *Figure 8.3.3(b)* with t_s approximately 10s.

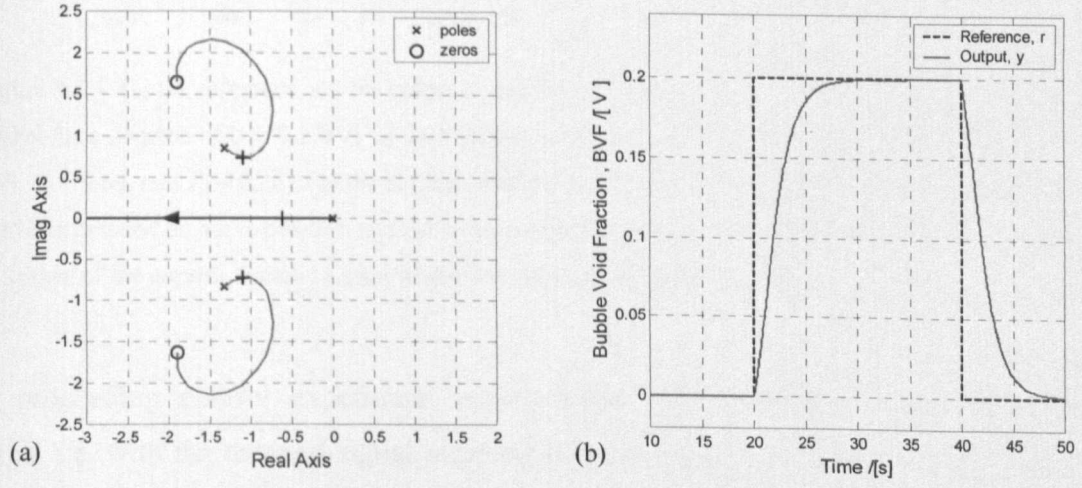

Figure 8.3.3: (a) the root-locus plot and the position in the locus for the chosen gain k_p. (b) the corresponding simulated time response of the system with the designed gains: $k_p = 2.65$, $T_i = 0.60$, and $T_d = 0.26$. The demand signal steps between 0 and 0.2 BVF. The '+' markings indicate the position of the roots in the loci where the gain k_p was chosen.

Figure 8.3.4 shows the corresponding experimental implementation of the PID gains. The control was desirable with approximately 10s settling time. The control signal to the actuator was also moderated compared to the previous effort. The moderation of the gains prevented an extreme response to the error generated between the demand and the fed-back

output signal hence avoiding the saturation of the controller gains and the actuator and subsequently destabilising the controller.

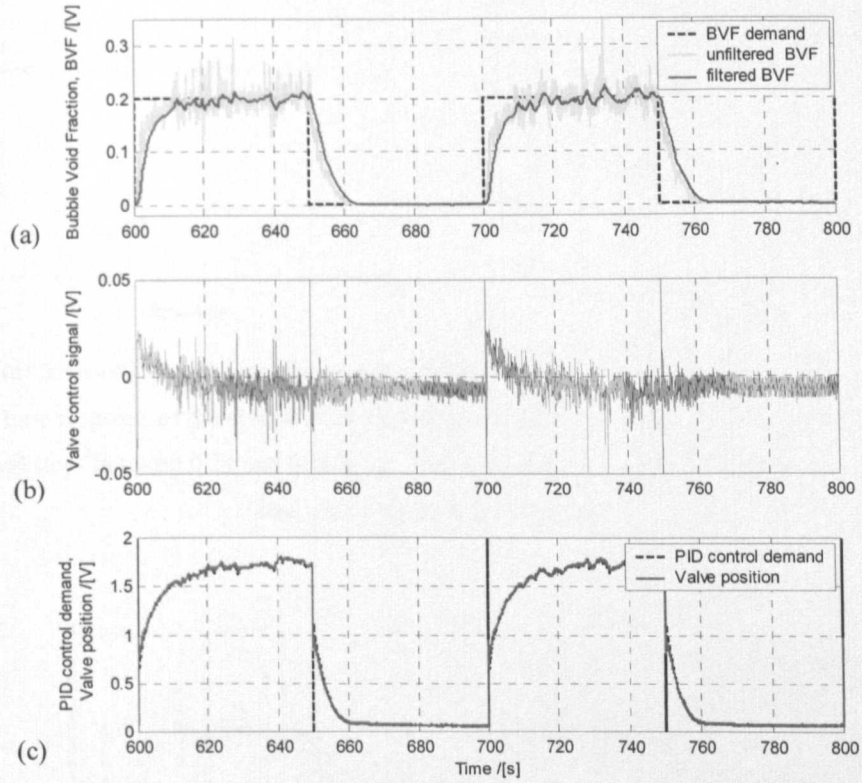

Figure 8.3.4: (a) the reference and the output signal from the experimental bed resulting from close-loop control for a demand of 0 to 0.2 BVF at 0.01 Hz step excitation using experimentally designed gains (k_p = 2.65, T_i = 0.60, and T_d = 0.26). (b) the corresponding control effort exerted onto the valve and (c) the PID controller demand on valve position and the resulting measurement of valve position. Apart from the sharp spikes of the control demand signal where there are step changes, both signals completely overlap.

The proceeding control experiment explored the controllability amidst the bubbling regime, i.e. with the demand signal stepping between 0.11 and 0.16 BVF. The root-locus method was applied producing the plot shown in *Figure 8.3.5(a)*. The chosen gain k_p resulted in the time response presented alongside in *Figure 8.3.5(b)* where: k_p = 5.13, T_i = 0.56, and T_d = 0.24. The designed controller gains gave t_s of approximately 5s. Stepping between 0.11 and 0.16 BVF at 0.01 Hz, the experimental implementation with the designed gains resulted in the closed-loop BVF output as shown in *Figure 8.3.6(a)* with the corresponding control effort and valve position measurements shown in *Figure 8.3.6(b)*. The control was acceptable with the settling time differing from that designed at approximately 10 s instead of 5 s. Due to the large fluctuations, it was difficult to properly determine t_s from the experimental results.

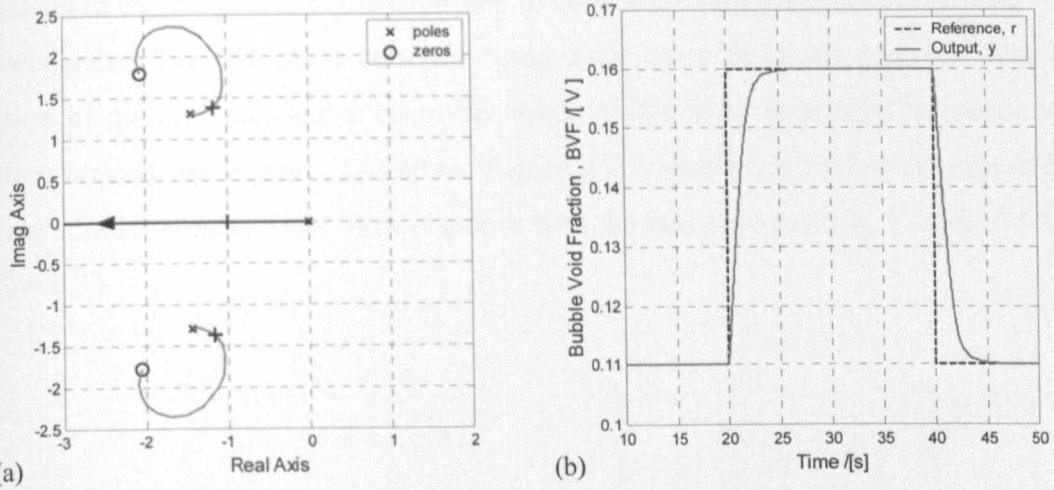

Figure 8.3.5: (a) the root-locus plot and the position in the locus for the chosen gain k_p. (b) the corresponding simulated time response of the system with the designed gains: $k_p = 5.13$, $T_i = 0.56$, and $T_d = 0.24$. The demand signal steps between 0.11 and 0.16 BVF. The '+' markings indicate the position of the roots in the loci where the gain k_p was chosen.

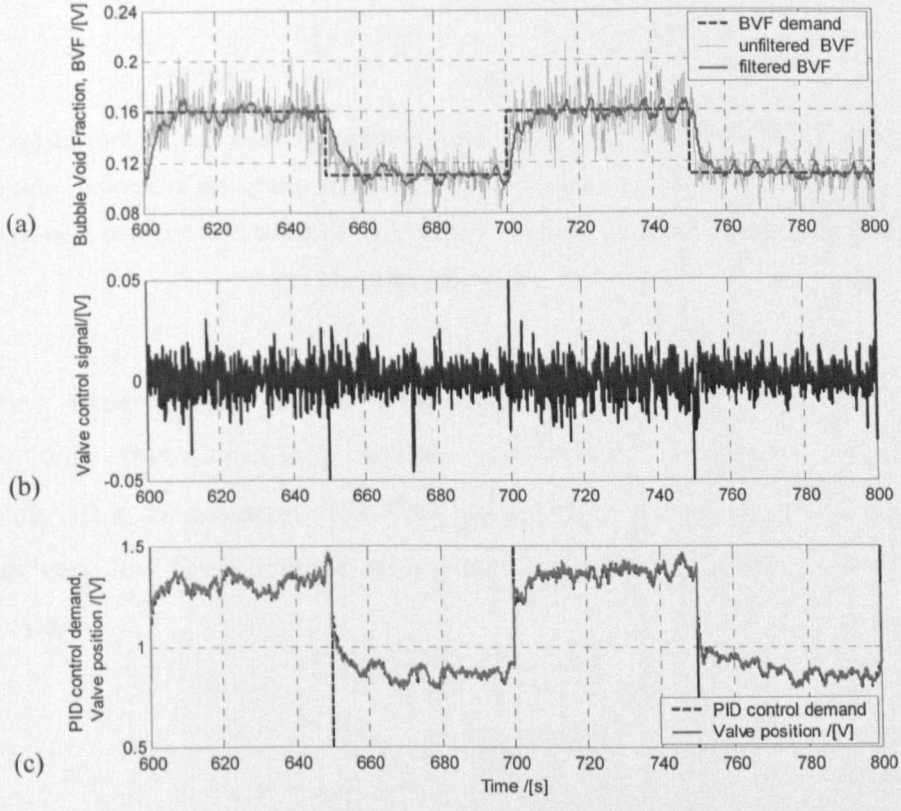

Figure 8.3.6: (a) the reference and the output signal from the experimental bed resulting from close-loop control for a demand of 0.11 to 0.16 BVF at 0.01 Hz step excitation using designed gains ($k_p = 5.13$, $T_i = 0.56$, and $T_d = 0.24$). (b) the corresponding control effort exerted onto the valve and (c) the PID controller demand on valve position and the resulting measurement of valve position. Apart from the sharp spikes of the control demand signal where there are step changes, both signals completely overlap.

It is crucial to test the ability of the controller to cope with a BVF demand very close to the quiescent state. The transition between being incipiently fluidised and bubbling is a condition of discontinuity and a controller might suffer from instability problems when operating around this regime. Therefore, *Figure 8.3.7* shows the root-locus plot and the resulting simulated closed-loop time response with the designed gains $k_p = 3.26$, $T_i = 0.75$, and $T_d = 0.33$.

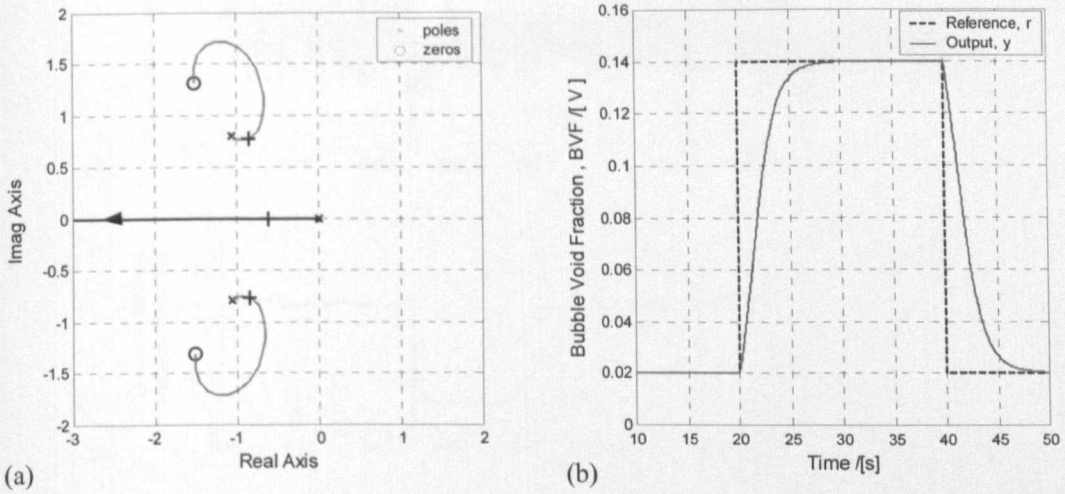

Figure 8.3.7: (a) the root-locus plot and the position in the locus for the chosen gain k_p. (b) the corresponding simulated time response of the system with the designed gains: $k_p = 3.26$, $T_i = 0.75$, and $T_d = 0.33$. The demand signal steps between 0.02 and 0.14 BVF. The '+' markings indicate the position of the roots in the loci where the gain k_p was chosen.

The resulting experimental control implementation as shown in *Figure 8.3.8* was satisfactory with the closed-loop control settling to a desirable steady state in approximately 10 s, as designed. The PID controller scheme was sufficiently robust in coping with very low BVF demand with good manoeuvre of flow control close to the quiescent state.

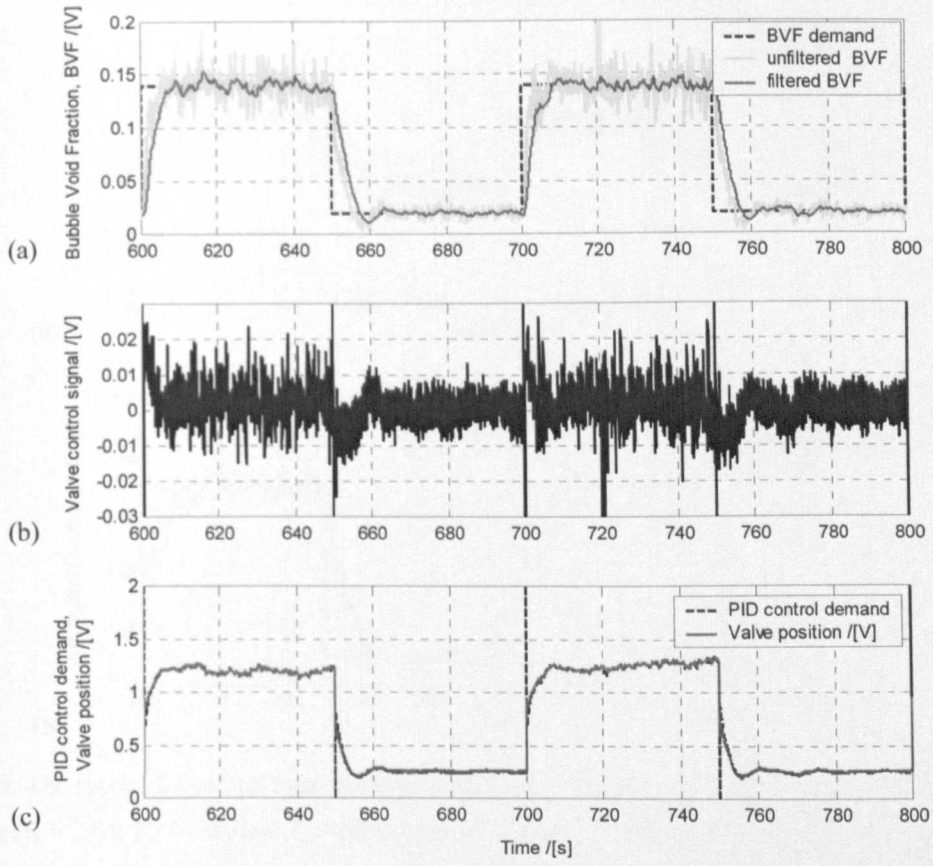

Figure 8.3.8: (a) the reference and the output signal from the experimental bed resulting from close-loop control for a demand of 0.02 to 0.14 BVF at 0.01 Hz step excitation using designed gains ($k_p = 3.26$, $T_i = 0.75$, and $T_d = 0.33$). (b) the corresponding control effort exerted onto the valve and (c) the PID controller demand on valve position and the resulting measurement of valve position. Apart from the sharp spikes of the control demand signal where there are step changes, both signals completely overlap.

Although the system identification of the bubbling bed indicated a non-linear system with different transfer function parameters required for different operating conditions, the robustness of the PID scheme and the linear approximation of the bubbling bed dynamics allowed a fixed gain policy to be implemented for the control of the process over various operating conditions. The non-linearity in the bed dynamics will nevertheless affect the closed-loop control performance features such as the settling time and steady state value to a certain degree. This was demonstrated and the results are shown in *Figure 8.3.9*.

When a much faster settling time was desired from the closed-loop response of the bed, designed by the choice of PID gains of $k_p = 5$, $T_i = 0.9$ and $T_d = 0.4$, the results as shown in *Figure 8.3.10* exhibit several unexpected oscillations in the response to a drop in BVF demand.

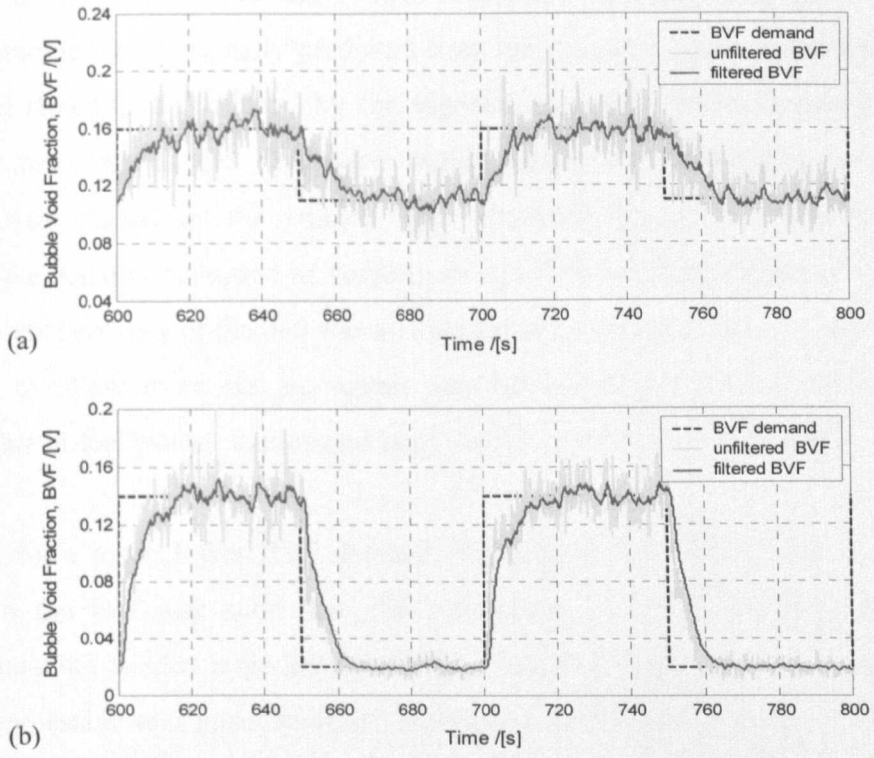

Figure 8.3.9: The successful control implemented using fixed gain policy for the PID controller scheme with gain values ($k_p = 2.65$, $T_i = 0.60$, and $T_d = 0.26$) used for the control of BVF between 0-0.2. (a) BVF control result for step demand between 0.11 and 0.16 BVF, and (b) BVF control result for step demand between 0.02 and 0.14 BVF.

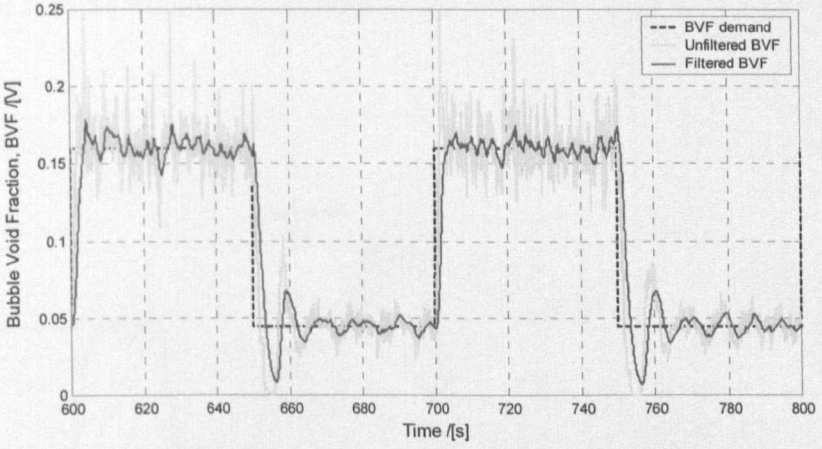

Figure 8.3.10: The reference and the output signal from the experimental bed resulting from close-loop control for a demand of 0.045 to 0.16 BVF at 0.01 Hz step excitation using designed gains ($k_p = 5$, $T_i = 0.9$ and $T_d = 0.4$) with a faster time response.

The designed high gain k_p value was intended to enable rapid system response to the step change in demand. However in a system like this, this sort of control effort manifested into

oscillations in the output when the control responded to a step drop in the demand, a different outcome from originally predicted from the designed gains. The valve was made to open and shut rapidly induced by the vigorous control exertion to cause large flow changes in response to the demanded rapid settling to steady-state condition. The oscillation was caused by the sudden large reduction in gas supply that temporary defluidised the bed and collapsed its suspension and therefore suppression of bubble voids. The subsequent recovery of the bed was accompanied by the controller reopening the valve excessively to allow more gas in, which was the reason for further oscillation in the response. This ordeal causes sudden and large oscillatory changes in the BVF.

In addition, for a much lower BVF demand, the degree of bubbling was minute and the condition in the bed was such that slight variation in the flow determines between quiescent state and sudden large increase in the degree of bubbling. Therefore, the control effort was excessive and unsuccessfully spent on attempting to achieve a stable steady-state condition. The control action would also eventually lead to actuator wear. The results suggest that it is undesirable to expect a rapid response in the control of the bubbling process. As a relatively slow response system, it is impossible for it to fulfil such a demand hence resulting in the problem as demonstrated. *Figure 8.3.11* shows the PID controller's performance in controlling the process over various BVF demands, summarising on the general control success achievable through its implementation.

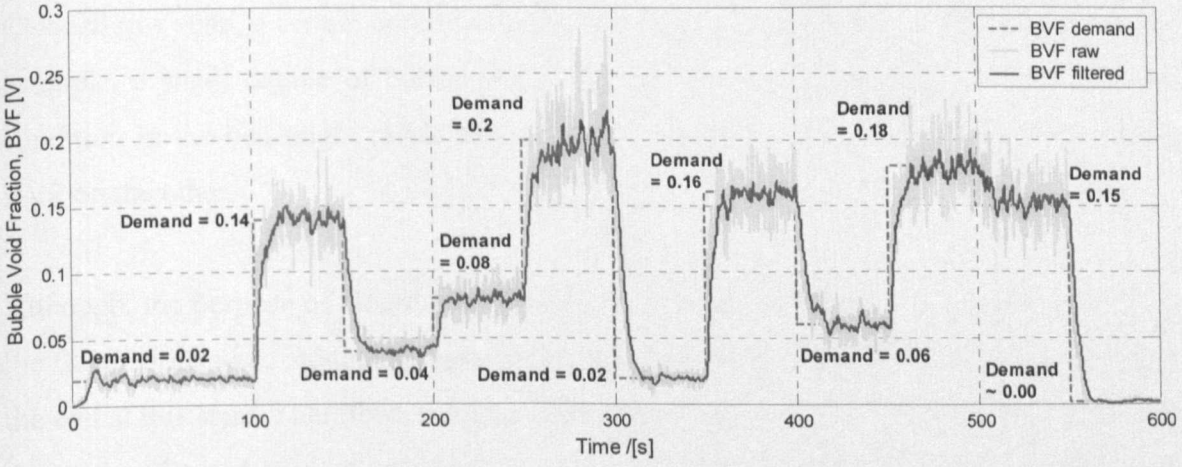

Figure 8.3.11: The time series of the closed-loop control of the process with PID controller conducted over a range of BVF demand.

8.3.3 Discussion

The immediate observation from the study is that the designed gains needed some retuning experimentally for a more desirable closed-loop response in the control of the process, typical for the PID controller scheme. The presence of intrinsic feedback signal (BVF) fluctuation caused by the activities of the bubbles required a moderate derivative gain, T_d. This prevents the controller from rigorously attempting to correct controller errors based on the magnitude of the derivative of the BVF fluctuation (rate of change of fluctuation), which leads to undesirable and ineffective control effort exerted on the actuator and would therefore concurrently prevent actuator wear.

The generally slower propagating effect of gas reduction on the decrease of bubble voids over the whole bed (geometry, i.e. height dependent) requires a more lenient response policy on the rate of settling to the steady state condition during a drop in the BVF demand. This could be offered by moderate proportional and integral gains, k_p and T_i allowing a more gradual shutting off of gas supply and hence giving time for the effect to propagate through compared to an initial more rapid action.

Bubble expansion and bubble void disappearance and reappearance in the emulsion phase are phenomena where the column of bubbling bed can be considered as an open-loop system such that the outcome of a control action not necessarily be as expected from what was predicted during controller design especially in the regime close to its incipient state. Close to this state, a certain control effort might be predicted to deliver an outcome of, for example, a small degree of bubbling with low BVF value. However, the instantaneous condition in the bed might result in a close to zero BVF on one hand or a much higher BVF on the other.

Although, the purpose of closed-loop control is meant to deal with situation such as these, the fluctuations were induced by non-linearity in dynamics associated with the condition of the bed at this state. Therefore, it is important not to expect a swift response to a change in demand and rapid settling to steady state as it will be detrimental to the stability and controllability of the fixed gain control of the bubbling process. The input of gas is not directly linked to how many bubbles are being produced. The degree of bubbling, hence proportion of voids, is governed by the availability of excess gas which balances the

amount of gas supplied and that required by the emulsion phase and is affected by both the global and local condition in the emulsion phase.

The control of the bubbling process becomes difficult especially when a very small BVF value was demanded where the flow of gas just exceeded that required for incipient fluidisation. At this regime, the existence of bubbles is unstable such that some of the nucleated bubbles are too small to be accurately detected and some experience disappearance and reappearance of their void area in the emulsion phase. This causes many fluctuations in the measurement for an accurate BVF and therefore the control becomes complicated. However, the use of a low-pass filter has improved the control in this regime. This problem is also caused by the method of measuring BVF on the planar bed using the image analysis system.

As demonstrated, the implementation of control of the bubbling process using the PID control scheme exhibited acceptable controllability. However, due to the employed fixed-gain policy, the shift in the bubbling condition of the bed, depending on the level of BVF demand, may render the chosen gain values unsuitable in delivering exactly the desired closed-loop response. This was noticeable in the transient response of the BVF where the desired settling time was occasionally compromised depending on the instantaneous BVF demand change (see *Figure 8.3.11*).

The presence of non-linear features especially when close to incipient condition ideally requires changes made to the controller gains to continuously deliver desirable control over the process. Although the moderation of the controller gains allowed the gain values to be continuously used to control the process for various BVF demands, it compromises on the swift response and settling time that were initially desired for some closed-loop responses. It is then worth considering implementing a different controller scheme where the gains could be adjusted according to the condition and the demand in the closed-loop control. This could be found in an adaptive controller scheme and for purposes of case study, the Minimal Control Synthesis scheme (Stoten & Benchoubane, 1990a, 1990b, 1995; Stoten, 1990, 1995; Benchoubane & Stoten, 1990) was implemented and is described in the next section.

Generally, the overall control implementation was successful and it goes to show that a good understanding of the system allows a relatively simple implementation of control. The slight time delay sometimes found intrinsic in the bed dynamics in certain conditions did not pose any formidable problems, in fact, treated as non-existent in the PID implementation.

8.4 Implementation of adaptive controller strategies (a case study of MCS implementation)

8.4.1 Introduction

The Minimal Control Synthesis, MCS, conceived at Bristol University (Stoten, 1990, 1995), is an extension of the Model Reference Adaptive Controller, MRAC (Landau, 1974) that moderates some of the criteria required by MRAC, resulting in a simpler implementation of control scheme requiring no *a priori* knowledge of the plant. Its performance is comparable, if not better than, that of linear controller strategies. The MCS adaptive controller scheme is, for the first time, implemented for the fluidisation system in efforts to handle problems associated with process discontinuity (close to quiescent state), and process non-linearity (hysteresis effect as well as the complication associated with regime transition) that may arise during the period of operation. The aim of this study is therefore to assess and benchmark the performance of adaptive controller tactics on fluidised systems as well as a reflection of it on other processes of such nature.

Figure 8.4.1 shows the typical block diagram of MCS implementation. The function of MCS much resembles a model reference control block with the output of a basic closed-loop control of a plant being compared with the output of a reference model so that appropriate changes could be made to the controller gains based on MCS policies. MCS requires a suitable choice of a set of parameters to be made concerning its adaptability rate, (parameters α and β) and the rate of gain decay that determines how fast the gain values decay over time. This is a 'forgetting-factor' policy applied to help moderate the rate of increase of the gains so that they do not saturate over time and destabilise the control effort.

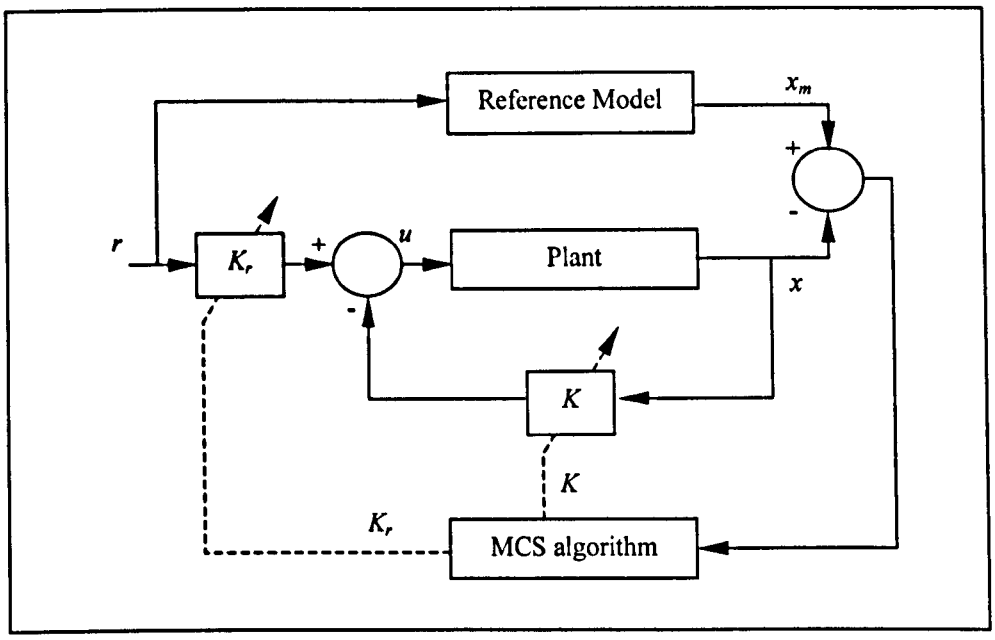

Figure 8.4.1: The typical MCS block diagram.

Typically, the basic implementation of MCS adjusts the gains matrix K and K_r accordingly based on the error calculated between the reference model and the actual plant output until a desired plant output is delivered. MCSIA (Stoten, 1993) is an extended implementation of MCS incorporated with an explicit integral action intended to compensate for relatively low-bandwidth plant bias and any non-zero steady state and transient phase errors calculated between the reference signal and the controlled plant output.

MCSIA was therefore implemented to the experimental bubbling fluidised bed with the appropriate set of controller parameters. Two different reference models were used; the first being a second order model consistent with the approximation of the bed dynamics found in the system identification work. The second reference model, a zero-order-hold model, was meant to incorporate the theoretical model (7.3), found simply to describe the effect of bubble introduction on the bed BVF, into the control of the bed to assess how well will MCS control the bed having been given a model more descriptive of the process itself.

8.4.2 MCSIA with second order reference model

With a second order reference model, MCSIA performed reasonably well in response to a closed-loop BVF demand as shown in *Figure 8.4.2*. The second order reference model demanded a critically damped response with a settling time, t_s of 10s for the given step demand in BVF. Varying between 0.02 and 0.14 BVF, the control of the process using the filtered BVF measurement as the feedback signal resulted in an excellent trailing of the reference model by the output. The steady state value was also desirable coping well at both levels of BVF demand. The adaptability rate parameters, α and β of 10 and 1 respectively were used.

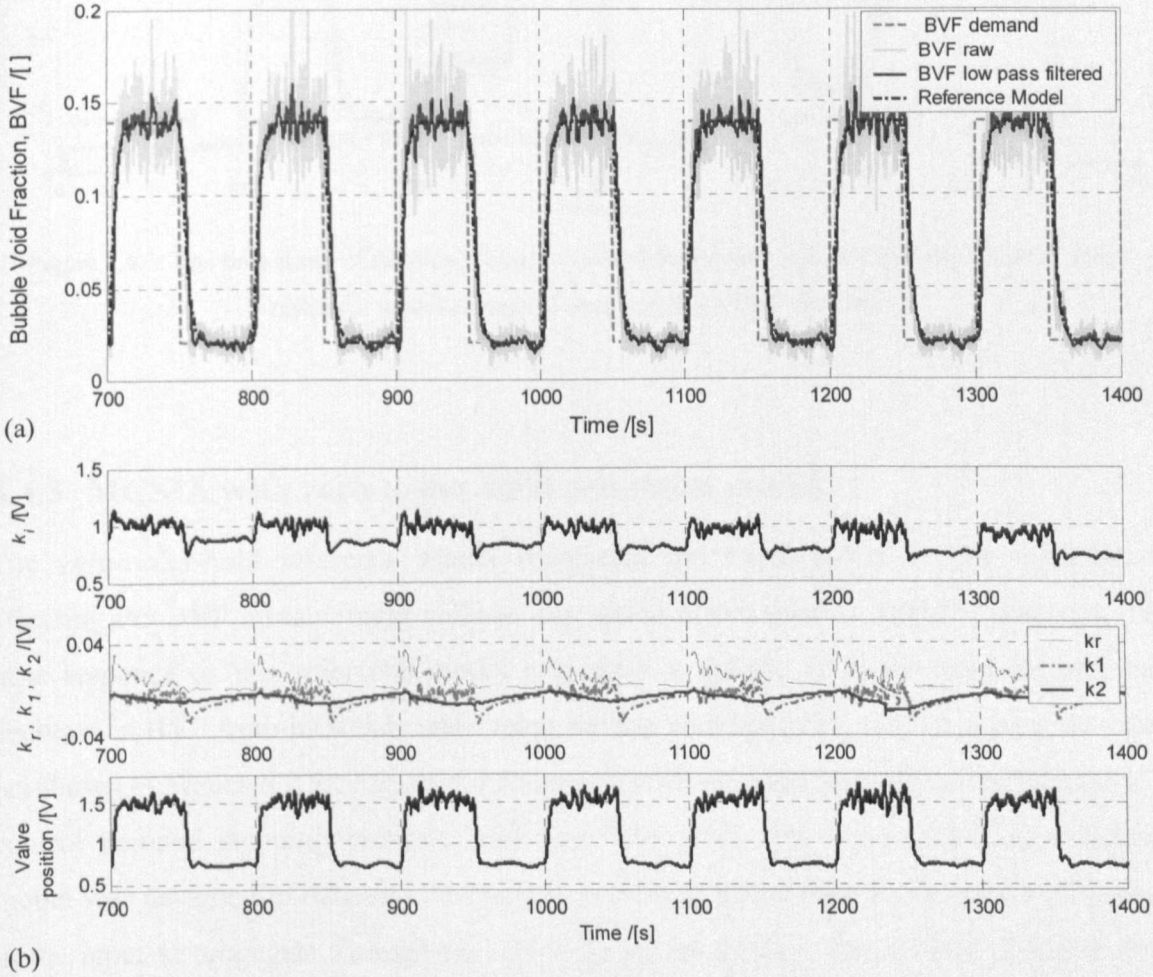

Figure 8.4.2: (a) the results of closed-loop control of the bed for BVF demand between 0.02 and 0.14 BVF at 0.01 Hz step excitation using MCSIA with a 2nd order reference model. (b) the corresponding adaptive gains, k_i, k_r, k_1 and k_2 and the valve position.

The controller gains varied according to the change in demand, periodically shifting between two bounds with a slight drift of the gain values with time, especially observable

for k_i on every low BVF demand intervals. *Figure 8.4.3* subsequently shows the ability of MCSIA in performing continuous control on the process with a range of BVF demand variation. MCSIA demonstrated a good control with continuous delivery of desired closed-loop response. The second order reference model was critically damped with a settling time, t_s of 10 s.

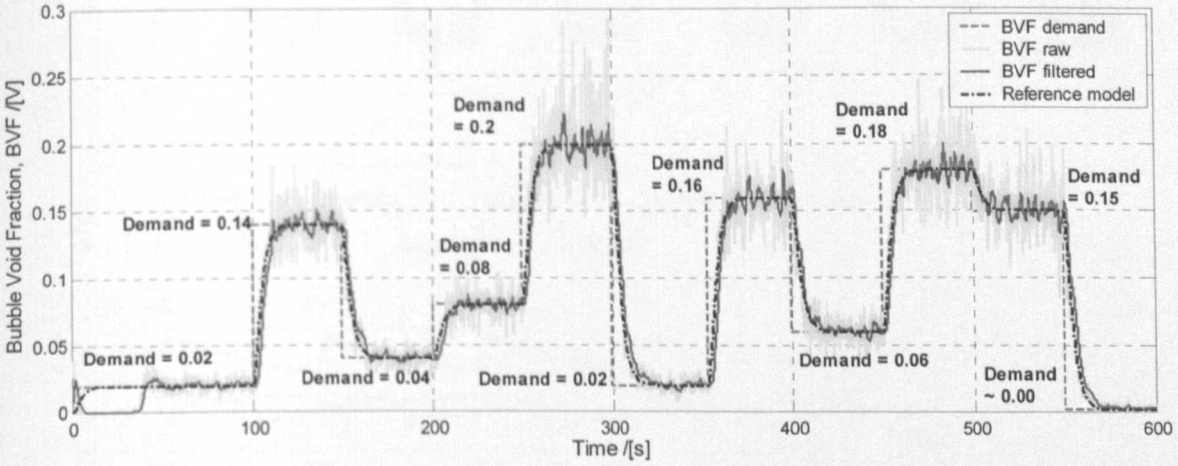

Figure 8.4.3: The time series of the closed-loop control of the process with MCSIA using the 2nd order reference model conducted over a range of BVF demand.

8.4.3 MCSIA with zero-order-hold reference model

The zero-order-hold reference model represents the basic effect of gas introduction affecting the BVF measurement without any added effect such as bubble expansion. The time response of this reference model resembles a unique gradient ramp increase and decrease in BVF from its steady state value for any corresponding step change in the input (as shown in *Figure 8.2.9*). *Figure 8.4.4* shows the closed-loop response of the process to a control demand stepping between 0.02 and 0.14 BVF. The zero-order-hold reference model was designed to deliver a settling time of 5 s to allow time for the effect of change in the input to propagate through the whole height of the bed. The control of the process using the filtered BVF signal as the feedback was desirable although this caused the measured BVF settled in more than the intended 5 s. The adaptability rate parameters, α and β of 10 and 1 respectively were again used.

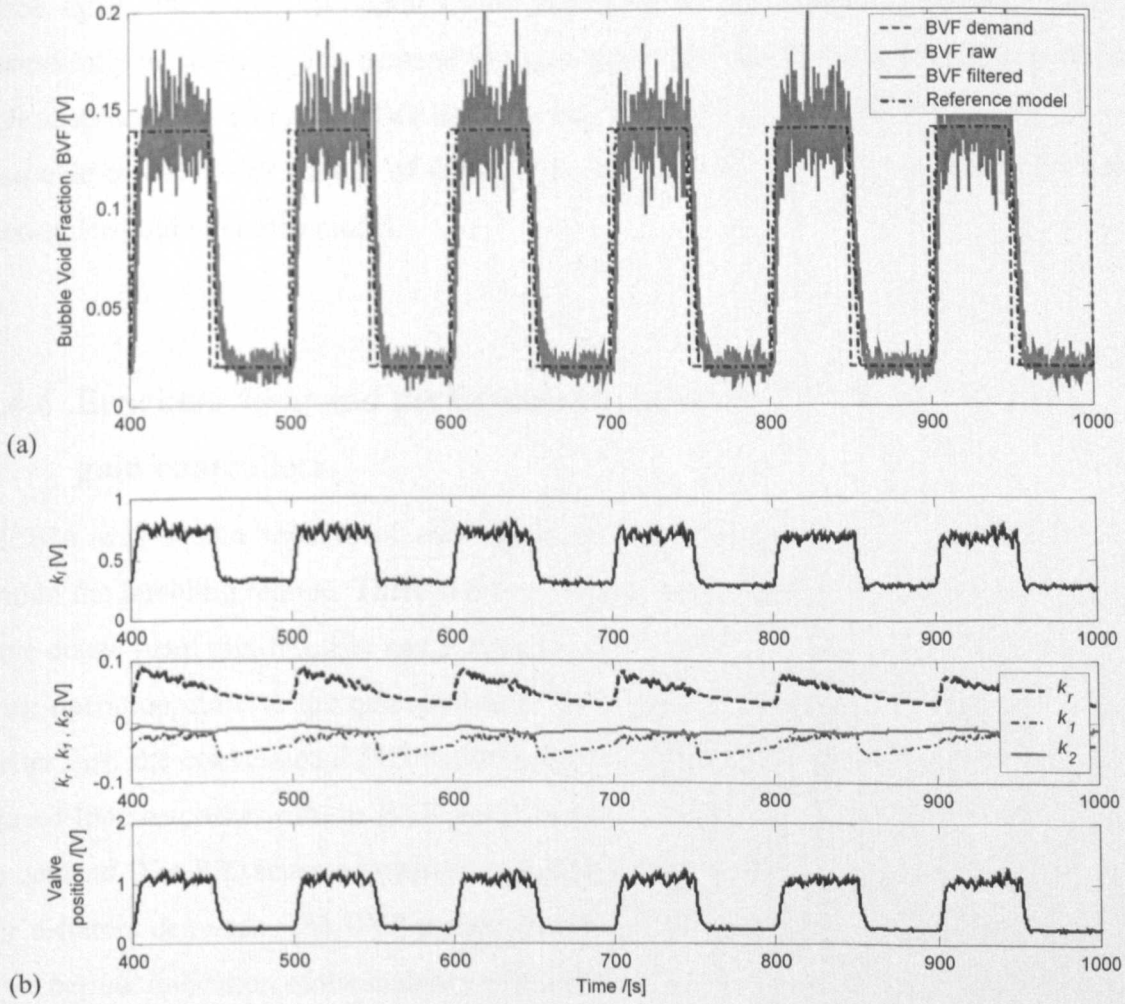

Figure 8.4.4: (a) the results of closed-loop control of the bed for BVF demand between 0.02 and 0.14 BVF at 0.01 Hz step excitation using MCSIA with a zero-order-hold reference model. (b) the corresponding adaptive gains, k_i, k_r, k_1 *and* k_2 and the valve position.

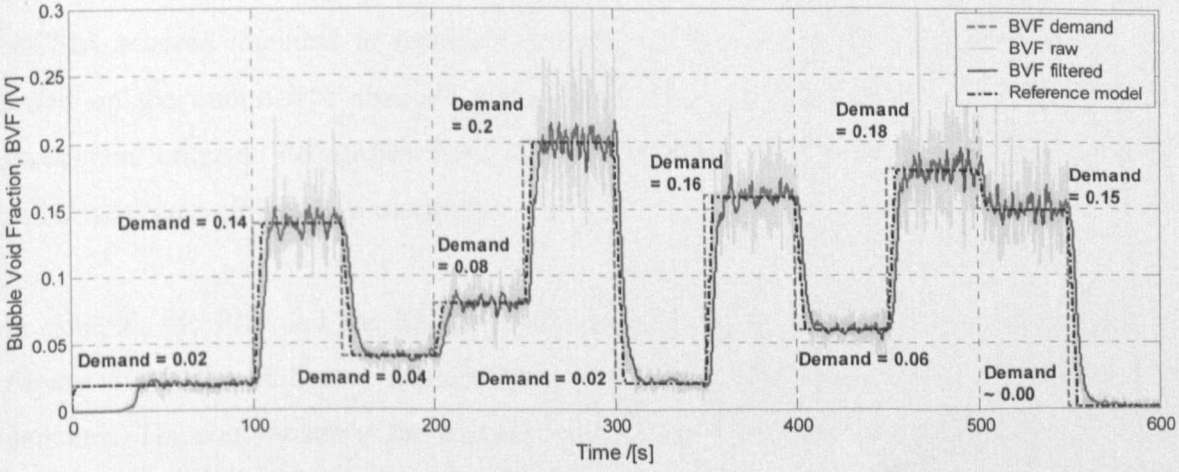

Figure 8.4.5: The time series of the closed-loop control of the process with MCSIA using the zero-order-hold reference model conducted over a range of BVF demand.

Once again, the controller gains varied according to the change in demand, shifting periodically between the two demand values with a slight drift of the gain values with time still observable on every low BVF demand intervals. *Figure 8.4.5* shows that MCSIA was also able to cope with control of the process over various BVF demands with the same zero-order-hold reference model.

8.4.4 Benchmarking and performance assessment of MCS over fixed-gain controllers

MCSIA was shown capable of controlling the process over a range of BVF demands within the bubbling regime. There were no control issues surfacing from intrinsic process time delay, plant non-linearity and hysteresis effect as well as the complication associated with operation close to the quiescent state of the bed. MCSIA was shown to be slightly better than the conventional PID controller scheme by constantly delivering the designed closed-loop response with the BVF measurement settling within 10s for every rise and fall in demand. The PID scheme however may demonstrate a variation in closed-loop response for different demands. The BVF measurement occasionally settled with varying degree of time period, indication of the inability of fixed gain policy in coping fully with the effect of non-linearity in the plant when a certain set of gains designed for a specific condition were used to control the bed over a different condition.

Therefore, an assessment of performance was carried out on the MCSIA controller with the PID controller to investigate the improvements brought about by the implementation of MCSIA scheme intended to resolve these issues. The comparison of performance was based on the cumulative absolute error of the BVF measured in voltage values. This assessment criterion determines how well the controller performed during both transient and steady state closed-loop demands.

In general, the PID and the MCSIA controllers have demonstrated (presented again in *Figure 8.4.6*) the ability to appropriately control the bubbling process of various BVF demands. The comparison of the cumulative absolute error between the controller schemes presented in *Figure 8.4.7* strongly indicated that the PID controller, despite being a fixed-gain control policy, delivered the least error with time between the desired and the

measured process output. The errors were incurred when the measured BVF deviated from the demanded BVF, which will inevitably increase with time. Higher cumulated absolute error indicates a poor controller performance in producing an output that closely match the demand.

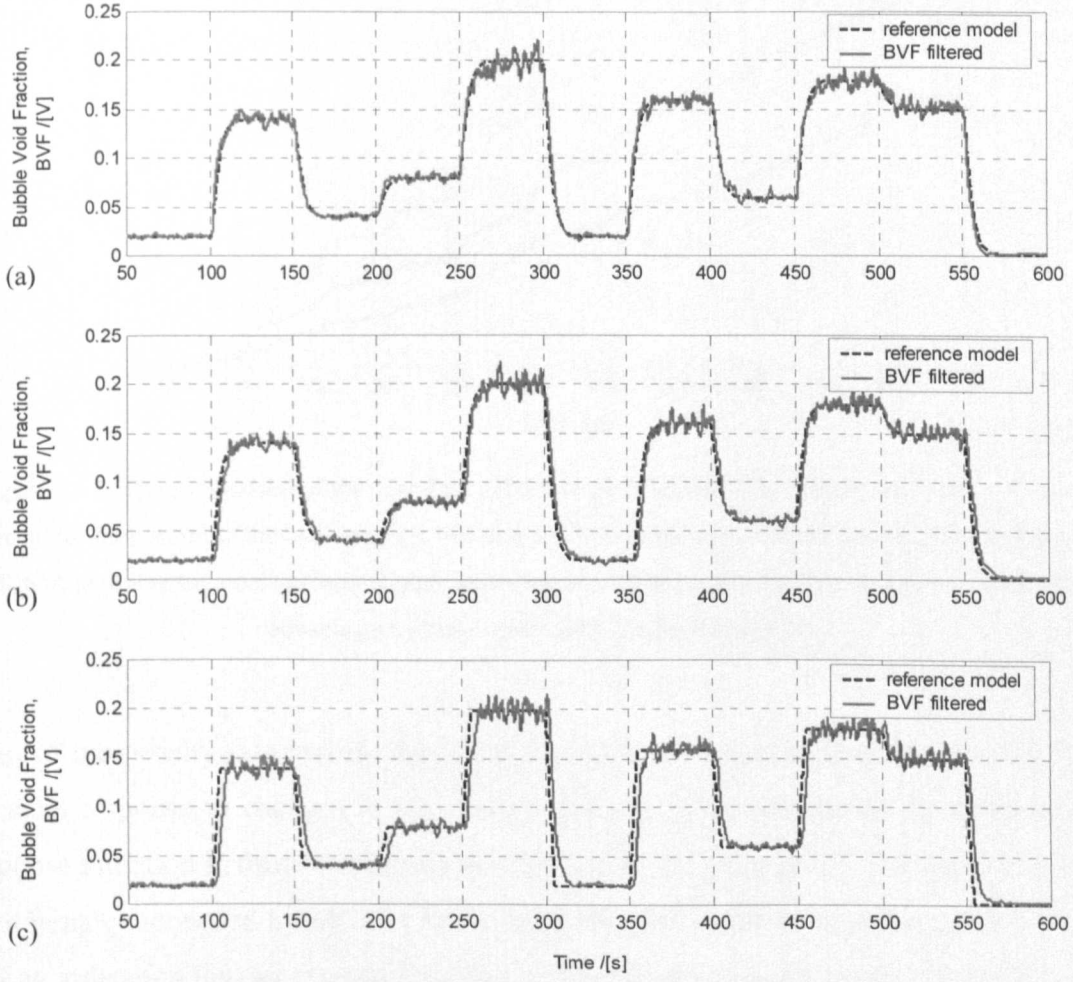

Figure 8.4.6: The respective subplots compare the time series of the filtered measured BVF and the corresponding BVF demand for the control of the process using (a) PID controller and (b) MCSIA controller with second order reference model and (c) MCSIA controller with zero order hold model.

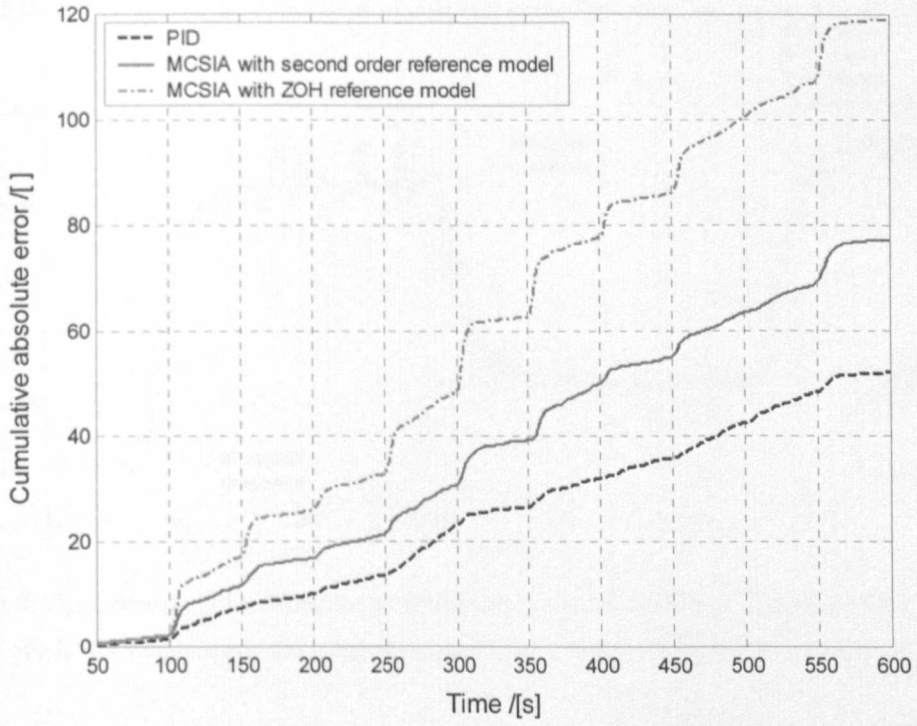

Figure 8.4.7: The comparison of the cumulative absolute error between the filtered measured BVF and the demand for the control of the bed using the PID and MCSIA controllers. In comparison to fixed-gain policy, MCSIA appeared to under-perform slightly indicating that adaptive strategy not necessarily always more advantageous than conventional fixed-gain strategy.

Most of the penalty incurred by the MCSIA scheme was conceded during its closed-loop transient response to changes in the process demand. This was due to its rather sluggish response initiation in those conditions as can be seen in *Figure 8.4.8.* The exceedingly high error penalty conceded by MCSIA while using the zero-order-hold as the reference model was an indication that an extended version of the that model is required for a more realistic replication of the actual bubbling process dynamics that could then be more practically achievable by MCSIA. The model as it is currently reported operated to only describe the dynamics of introducing a single bubble into an idealised bed with no bubble expansion, details of which could be readily found in *Chapter 7.*

The primary shortcoming of the adaptability capability of MCS scheme was the rate at which the controller gains adapted to changes in process demand and process dynamics. The high adaptability rate chosen in some of the control tests affected the controller stability found to be perhaps case specific and therefore, a compromise was taken on the adaptability criteria by moderating on values of α and β.

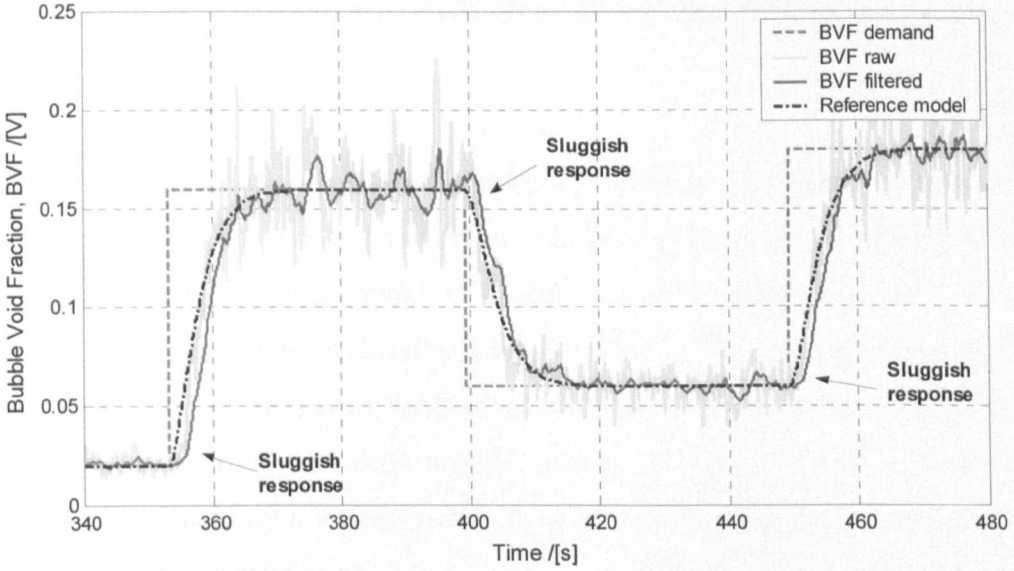

Figure 8.4.8: The close-up of the closed-loop transient response time series of the process under the control of MCSIA emphasising the sluggish response initiation to a sudden change in demand.

The predicament was also partly due to the relatively primitive algorithm that currently makes up the steady state gain decay policy function. Currently, this policy does not allow flexibility in the rate at which the gains decay with respect to the proximity of the closed-loop output to the steady state demand. It may be possible to develop a more versatile gain decay policy in future. The gross drift in the gain values indicated the on-going effort by MCS in adapting to a large variation in demanded controlled condition in the process and was also caused by the present gain decay function. Another part of the control problem faced in a system such as this is induced by the control effort itself. The control action exerted by the controller to rectify errors between the output and demand induces large disturbances to the natural dynamics (open-loop) of the system itself that in turn alters the desired outcome (closed-loop) of the already tuned controller settings.

In general, the control implemented on the fluidisation process has met great success with the adaptive scheme and prospect lay ahead for much more improvements. At this stage of study, the comparison of MCSIA with PID shows that PID remained better for the control of this system. However, MCSIA should be applied to ensure that the closed-loop system can cope with any large changes in process dynamics where PID controller will definitely fail.

8.5 Advanced control of bubbling fluidised beds

8.5.1 Background

The principle objective of controlling the bubbling process in a fluidised system found in many processes is to achieve a good degree of fluidisation quality. Once achieved, the process control must be maintained to ensure that the desired quality is preserved throughout the process duration. Ideally, a good quality of fluidisation requires the vessel to be populated by high density of bubbles of relatively small sizes such that an excellent gas-solid contact is promoted while a good mixing is induced by the presence of the bubbles. This is ensued by a longer residence time of bubbles in the bed and indefinitely leads to a good process efficiency.

The spatial distribution of bubble population within the bed column plays a crucial role in determining the state of the fluidisation quality. As pointed out in *Chapter 3*, the natural tendency in the bed is such that the spatial distribution of bubbles is good at low gas supply close to its quiescent state with bubbles reasonably well distributed in the bed. This profile deteriorates at higher flow of gas where larger population of bubbles coalesce severely and congregate around the centre of the bed. The distribution of bubbles tapers with height, depriving regions near the walls of bubbles. However, it is possible to modify the gradual deterioration of the profile at higher flow conditions if the natural spatial configuration of predecessor and successive bubbles could be rearranged. Many workers (Toei & Matsuno (1967); Clift & Grace (1970); Miwa et al. (1972); Werther & Molerus (1973b)) have shown that as bubbles in fluidised beds interact, the leading bubbles influence the lateral positioning of trailing bubbles and subsequently all successively produced bubbles. This phenomenon could be minimised if a controlled introduction of bubbles is implemented so that bubbles are arranged such that they are less likely to coalesce readily.

The strategy of controlling the bubbling process in relation to promoting good fluidisation quality is two-fold. Firstly, control must be maintained over the amount of bubbling that is occurring in the bubbling column. The supply of gas into the bed should be kept to the amount that preserves an optimal level of bubble population in the bed so that the control over the introduction of the bubbles could be effective in manoeuvring a profile of well-distributed bubbles across the bubbling column.

The study was hence carried out to investigate the prospect and to determine the ability of controlled bubble introduction in creating a better performance bubbling fluidised bed. However, meant to be brief and objective, the study was conducted using the simulated bubbling fluidised bed developed for the research. It was a planar bed and uses imaging techniques to measure properties in the bed by detecting voids in the emulsion phase associated with bubbles. Thoughts were also given to gauge the practicality of implementing this in conventional vessels.

8.5.2 Implementation of controlled bubble introduction techniques

The migration of bubbles towards the bed centre could be prevented or minimised if the leading bubbles were made to maintain a course of travel up the bed without significantly migrating inwards from the walls so that successive bubbles, due to the pre-positioning of the leading bubbles, are encouraged to reside close to the walls along their rise routes. This becomes necessary at high flow rate and is possible with a spatially controlled insertion of bubbles by a distributor that proactively discourages the natural congregation of bubbles at the bed centre. In addition, as bubbles are spatially well distributed they are prohibited from readily coalescing. Previously, Korte et al. (2001) have demonstrated the ability of controlled bubble introduction at the distributor in promoting the existence of a good bubble size distribution in the bed and discouraging the coalescence of bubbles.

A multi-mode distributor was assumed for the simulated bed such that the introduction of bubbles could be performed for any form of distributor, e.g. resembling a porous plate, orifices, or even a perforated plate. The simulations were carried out to assess the improvement brought about by the controlled introduction of bubbles compared to when the bed was left to freely bubble with a normal porous plate distributor. Several assessment measures were used and are listed below:

- bubble spatial distribution
- bubble residence time
- exiting bubble size and population distribution
- bubble population and size distribution within the bed

In the first test, the bubbles were introduced in a normal-bimodal (NBM) fashion where, in sequence, bubbles were first randomly (normally distributed) introduced around the centre of the distributor for a short duration followed by an instance where streams of bubbles were introduced at the extreme edges of the distributor. The introduction configuration switching between the two modes should provide a good average bubble spatial distribution in the bed, dispersing bubble throughout the bed therefore helping to prevent excessive coalescence, preserving the desired bubble sizes and prolonging general bubble residence time.

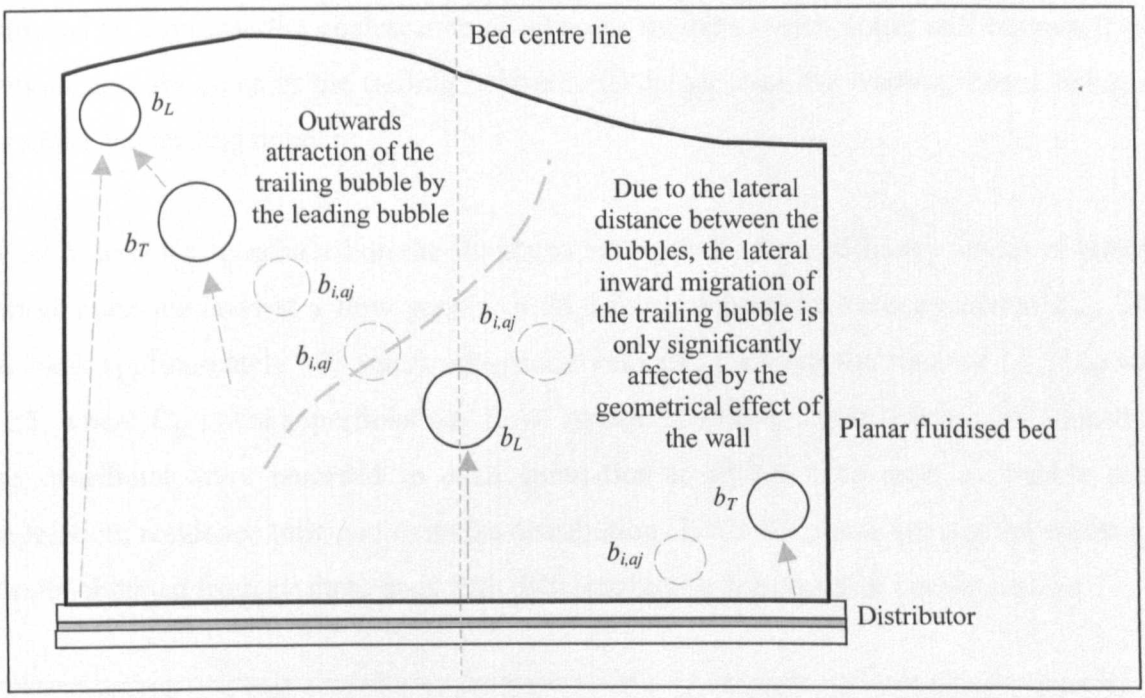

Figure 8.5.1: The proposed arrangement of bubbles in the bed with an inverted pyramid configuration of bubble introduction.

The subsequent test saw bubbles being introduced in a somewhat bimodal-inverted pyramid (IPBM) fashion. It involved a looped sequence of bubble introduction beginning from both ends of the distributor that gradually translated inwards towards the bed centre. This generates a row of bubbles rising up the bed taking some form of an inverted pyramid or 'V' profile. This formation of bubble placements minimised the gross migration of bubbles to the centre of the bed by placing immediate leading bubbles, b_L, or any trailing bubbles, b_T, closer to the walls than the latter. The trailing bubbles would be attracted away from the bed centre by the leading bubbles. Then, at the start of each sequence bubbles formed near the wall would be least affected by its immediate leading counterparts (near

the bed centre) as they were placed horizontally far away. *Figure 8.5.1* illustrates the description.

The profile of bubble introduction was simulated by assuming an orifice type distributor was used. Streams of bubbles near the walls at the distributor were also generated intermittently to encourage a more dispersed bubble distribution around the bed. In all the three simulations, bubbles were introduced with a size of approximately 20 mm in equivalent diameter allowing for minute random deviation (minimum $d_{b,e} \approx 17$ mm). The size of bubbles generated as well as the transverse speed of bubble introduction must be adjusted to minimise the coalescence of adjacent bubbles which could still happen if the bubbles are too close or the trailing bubble is far larger than the leading, hence rising to overtake the leading bubbles.

A set of tests was conducted on the simulated bed with the three different modes of bubble introduction methods at a flow supply of 25.6 mm/s superficial velocity above U_{mf}. The U_{mf} was approximately 103 mm/s superficial velocity, meaning the ratio of U_{fg}/U_{mf} was 1.25, where U_{fg} is the superficial gas flow. Approximately 15, 000 bubbles introduced at the distributor were recorded in each simulation to obtain data such as bubble size, population, residence time and exit size distribution. *Table 8.5.1* summarises the statistical results obtained from all three beds with different bubble introduction configurations.

	Normal freely bubbling	Normal-Bimodal (NBM)	Inverted pyramid-Bimodal (IPBM)
Exiting bubble frequency /[Hz]	3.02	3.59	4.11
Mean bubble population in bed /[ ]	39	38	49
Mean exiting bubble size /[mm^2]	87.0	80.5	78.4
Maximum exiting bubble size /[mm^2]	198.6	163.7	160.2
Mean bubble residence time /[s]	2.00	2.03	2.11

Table 8.5.1: A summary of the statistical results obtained from all three beds with different bubble introduction configurations.

Figure 8.5.2 shows the time- averaged bubble spatial distribution for the bed for the three different bubble introduction modes. It could be seen that there are general improvements in the spatial distribution of bubbles when bubble introduction was controlled using the two proposed modes. The respective contour plots indicated a more pronounced activity of bubbling on both horizontal extremes along the whole height of the bed caused by streams of bubbles created to help disperse bubbles throughout the bed and preventing them from migrating to the centre.

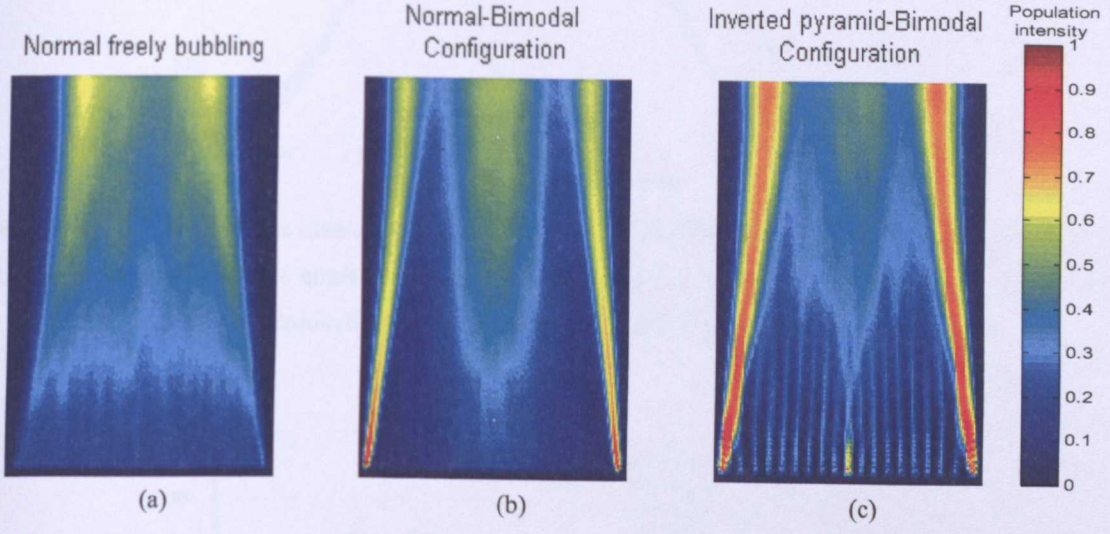

Figure 8.5.2: The contour plots of the bubble spatial distribution average over the simulation duration for the simulated bubbling bed bubbling at 25.6 mm/s superficial gas flow above U_{mf} (a) without and with controlled bubble insertion at the distributor using (b) NBM and (c) IPBM techniques. Population intensity shows the normalised tendency of bubble passing an area in the bed.

Figure 8.5.3 shows the corresponding bubble residence time distribution for the bed with and without controlled bubble insertion respectively. Although there is no significant gross shift in bubble residence time distribution (and its peak), there is a general shift in skewness of the distribution registering a much better overall bubble residence time. A large proportion of the bubbles that were registered spent a longer time in the bed as a result of controlled introduction of bubbles. As bubbles were more dispersed, they were discouraged from readily coalescing and therefore rose through and left the bed smaller in size.

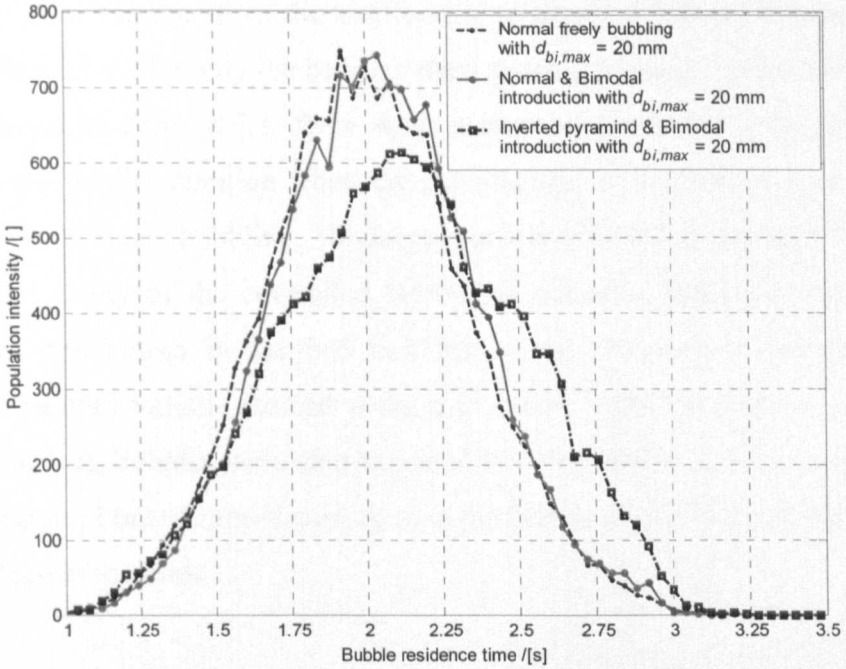

Figure 8.5.3: The residence time distribution of bubbles (of 15, 000 recorded bubbles) for the simulated bubbling bed bubbling at 25.6 mm/s superficial gas flow above U_{mf} with the three different modes of bubble introduction: Normal freely, NBM and IPBM methods.

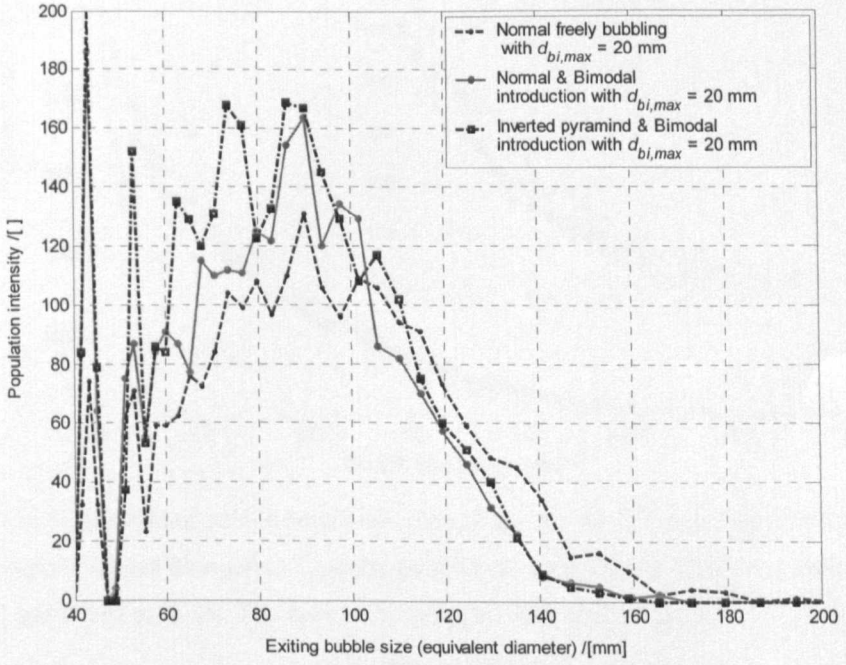

Figure 8.5.4: The distribution of exiting bubble size (equivalent diameter) for the simulated bubbling bed bubbling at 25.6 mm/s superficial gas flow above U_{mf} with the three different modes of bubble introduction: Normal freely, NBM and IPBM methods.

This is reflected by the record of the distribution of sizes of bubbles leaving the bed as shown in *Figure 8.5.4*. Not only the bubbles were generally smaller when leaving the bed, as already shown in *Table 8.5.1,* there were higher number of bubbles leaving at the freeboard for the similar duration when the introduction of bubbles was controlled than when it was normal freely bubbling. The larger number of bubbles exiting at the freeboard was due to the ability of the controlled bubble introduction method to sustain a good bubble spatial distribution in the bed that minimised coalescence and preserved the population of bubbles initially formed at the distributor. With a reduction in coalescence occurring in the bed, bubbles were also expected to be generally smaller as could be seen by the distribution of bubble population sizes in the bed in *Figure 8.5.5* shown for all three bubble introduction methods.

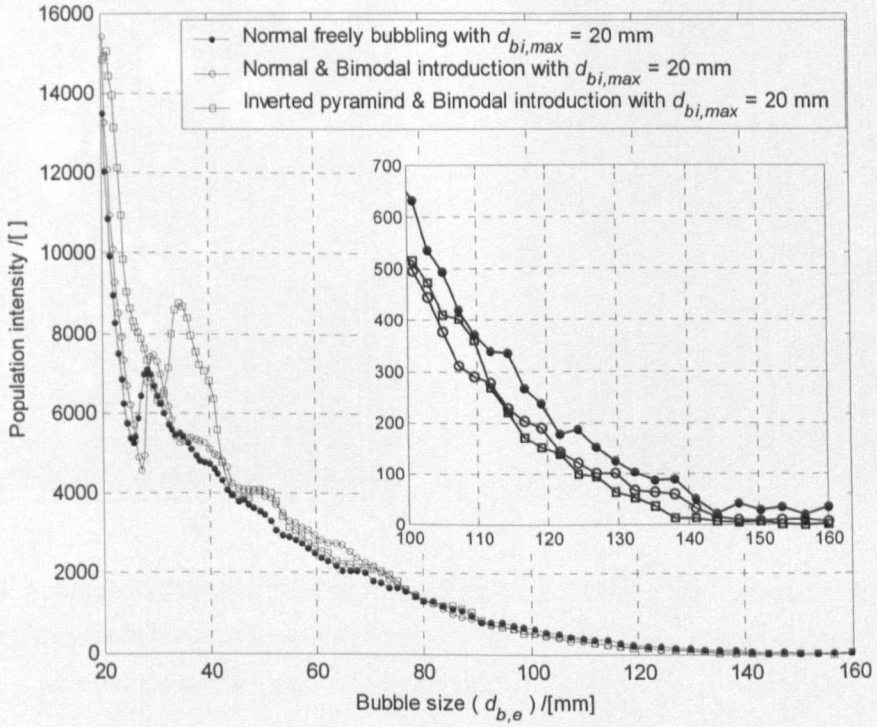

Figure 8.5.5: The distribution of bubble population sizes in the bed for the simulated bubbling bed bubbling at 25.6 mm/s superficial gas flow above U_{mf} with the three different modes of bubble introduction: Normal freely, NBM and IPBM methods. The inset is the enlarged view of the distribution from bubble size, $d_{b,e}$ ≈100 mm to 160 mm.

The bubbles formed in the three simulations mentioned were kept to similar size range for simplicity of analysis. The use of slightly smaller initial bubble size range compared to those previously used ($d_{b,e}$ ≈ 17 mm to 20 mm) brought about other factors to consider in this study. The production of smaller bubbles at the distributor at the similar gas supply as

previously will result in a larger number of bubbles. Although, this is favourable it might not be desirable when the control of the spatial distribution of bubbles is concerned. The higher density of bubbles populating a specific region encouraged bubbles to readily coalesce and further randomise their lateral arrangements leading to even further undesirable reactive coalescence elsewhere in the bed. This could render the control of bubble introduction ineffective. *Figure 8.5.6(a)* and *Figure 8.5.6(b)* show snapshots of the simulated bed with the use of the IPBM method at 25.6 mm/s superficial flow above U_{mf} with initial bubbles size of approximately 15 mm and 20 mm in equivalent diameter respectively. It could also be seen in snapshot *(a)* that the bubble arrangement is more unstable and unpredictable than in snapshot *(b)*.

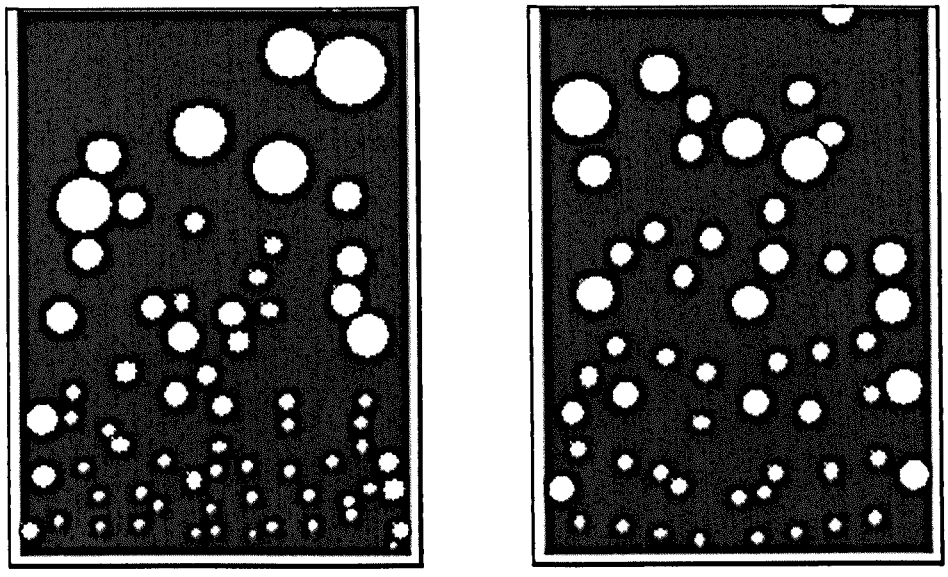

(a) (b)

Figure 8.5.6: A snapshot of the simulated bubbling bed fluidised at 25.6 mm/s superficial flow above U_{mf} with the inverted pyramid-bimodal method with (a) 15 mm and (b) 20 mm initial bubble diameter. It can be seen that the bubble spatial distribution was more stable and ordered in (b).

There is no doubt that improvement in the spatial distribution of bubbles was evident compared to when similar sized bubbles ($d_{b,e} \approx 15$ mm as maximum initial size) were produced in a normal freely uncontrolled bubbling bed. However, other parameters were found to be similarly achievable compared to when 20 mm diameter initial bubble size were used without compromising the effectiveness of controlled bubble introduction on the spatial distribution of bubbles. Therefore, it is a recommendation that sensitive parameters to consider in the design of a controlled bubble introduction technique are the initial bubble

size and distance of separation between adjacent bubble nucleation site that do not compromise the controller effort with time. It is also crucial to realise the importance of amount of bubbling flow rate supplied is influencing the effectiveness of the suggested strategies.

8.5.3 The importance of controlling the degree of bubbling

There is presumably an optimal proportion of bubble phase that is possible to exist within the bed in which good spatial distribution and other desirable bubbling properties can exist and the aim of controlling the degree of bubbling in the bed is to achieve this optimal level (*Section 3.2*). The control of the bubbling process via the feedback signal of the BVF measurement implemented in *Section 8.3* and *Section 8.4* serve to address this requirement in support of the control of bubble introduction in achieve good fluidisation quality. The BVF provided a measure of the degree of bubbling within the bed where closed-loop control of the gas supply could be applied.

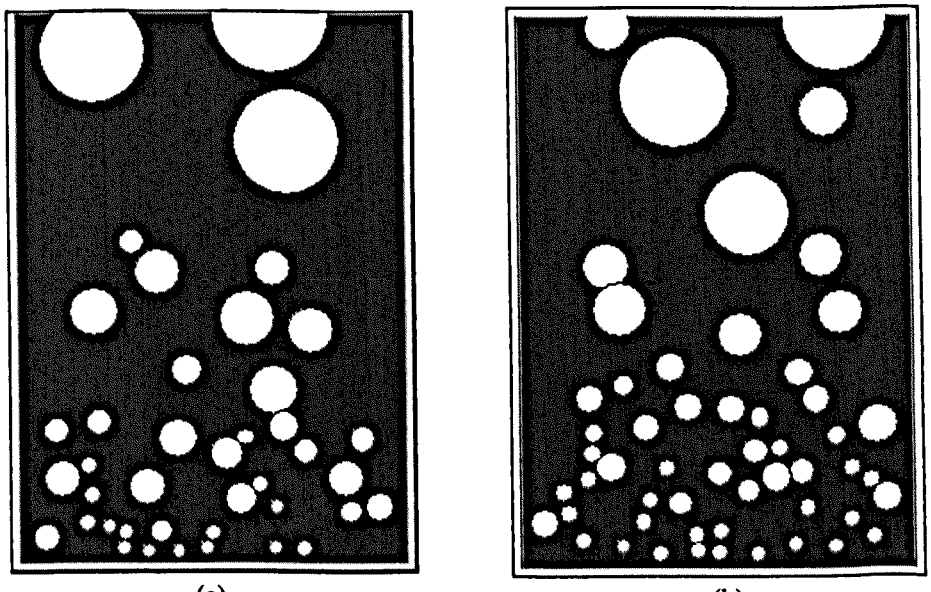

(a) (b)

Figure 8.5.7: The snapshot of the simulated bubbling bed controlled at BVF of 0.15 for (a) freely bubbling bed and (b) IPBM method of bubble introduction. It can be seen that the snapshots of both the beds appear to look similar away from the distributor. This shows that the controlled bubble introduction method was not effective in improving the bubble spatial distribution due to too high a population of bubbles.

Figure 8.5.7(a) shows the normal freely bubbling bed controlled to have BVF of approximately 0.15. Then, with the inverted pyramid-bimodal (IPBM) method, bubbles were introduced at a maintained BVF of 0.15 as shown in *Figure 8.5.7(b)*. It is evident that the controlled bubble introduction was not effective in efforts to improve the distribution of bubbles to achieve that for a good quality bed. The desired arrangement of bubbles produced was quickly upset by severe coalescence of densely placed bubbles. The corresponding contour plots of their respective bubble spatial distributions are shown in *Figure 8.5.8*.

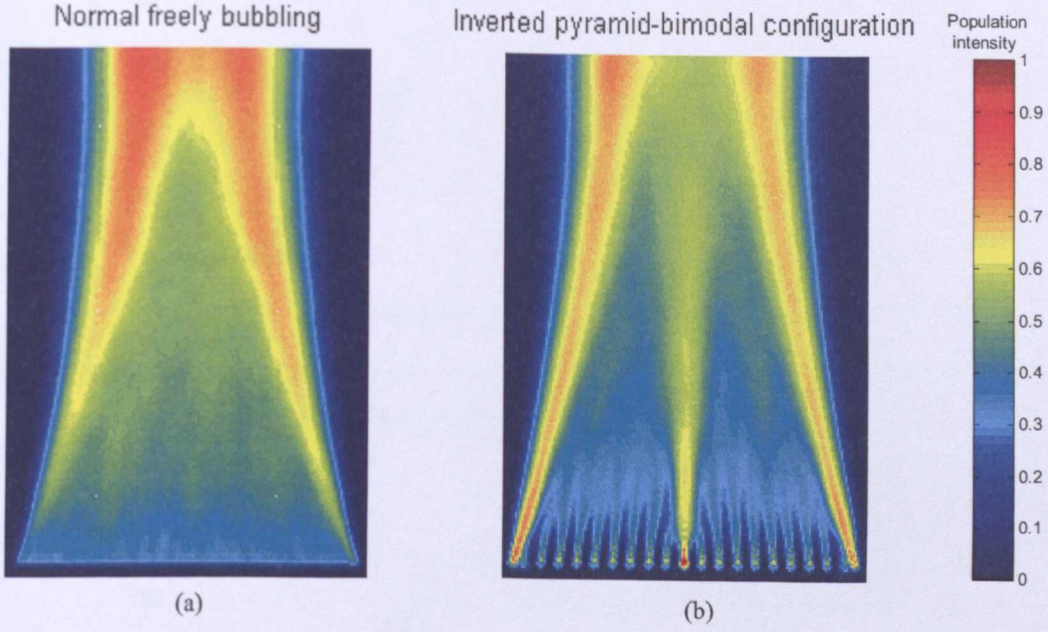

Figure 8.5.8: The bubble spatial distribution contour plot of the simulated bubbling bed controlled at BVF of 0.15 for (a) freely bubbling bed and (b) IPBM method of bubble introduction. Population intensity shows the normalised tendency of bubble passing an area in the bed.

Other statistical results do indicate that controlled bubble introduction in this flow condition brought about some improvements such as that shown in *Figure 8.5.9* for the distribution of bubble residence time in the bed and *Figure 8.5.10* for the distribution of exiting bubble size. With a controlled introduction, there were more, smaller bubbles leaving the bed after spending longer time in the bed. Relatively less coalescence were occurring and therefore allowing a higher population of bubbles within the bed. The average bubble population was approximately 50 compared to an approximately 40 when there was without any control. However, the improvements were inadequate for ensuring good fluidisation quality condition in the bed. Bubbles were still generally large, fast and

concentrated in the bed centre than if the gas supply was lower to further reduce the degree of bubbling.

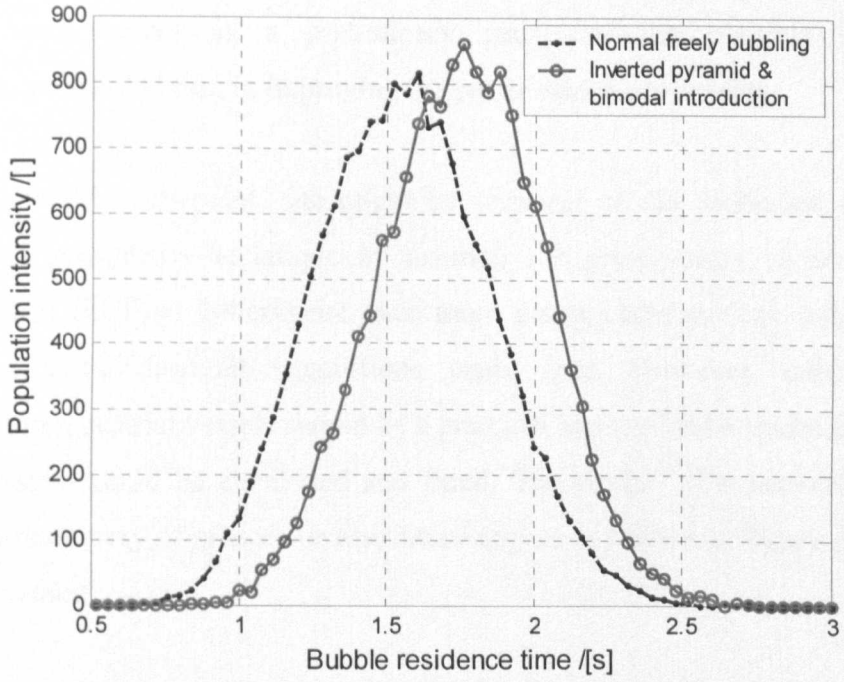

Figure 8.5.9: The distribution of exiting bubble size in the simulated bubbling bed controlled at BVF = 0.15 for a normal freely bubbling and IPBM mode of bubbling.

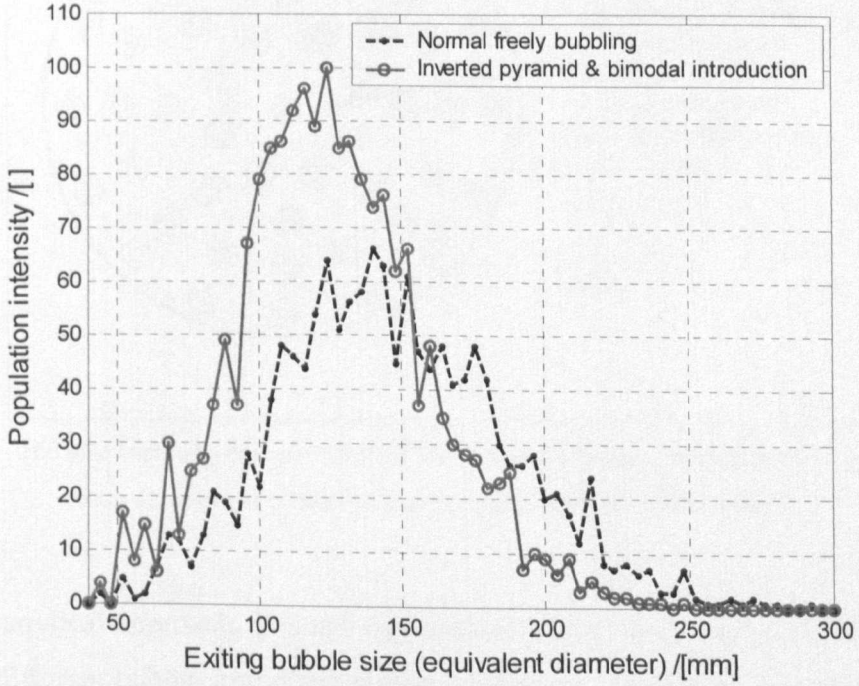

Figure 8.5.10: The distribution of bubble residence time in the simulated bubbling bed controlled at BVF = 0.15 for a normal freely bubbling and IPBM mode of bubbling.

8.5.4 Discussion

The obtained results indicated that improvement has been obvious when a controlled introduction of bubbles was implemented. However, due to the nature of the study, the simulated work serves as a preliminary gauge of the possible successes this implementation would bring in improving the performance of the beds.

From a practicality viewpoint, one might be sceptical of the controlled introduction of bubbles as a prospective technique in ensuring the preservation of desirable process attributes. Real fluidised systems are even more complicated and are subjected to other factors that could discredit suggestions made here. However, controlling bubble introduction in industrial vessels should be a practical and applicable technique from which a control system could be developed and fitted. The control of a network of manifolds servicing certain array of orifices or distributor region as shown in *Figure 8.5.11* could be a possible method.

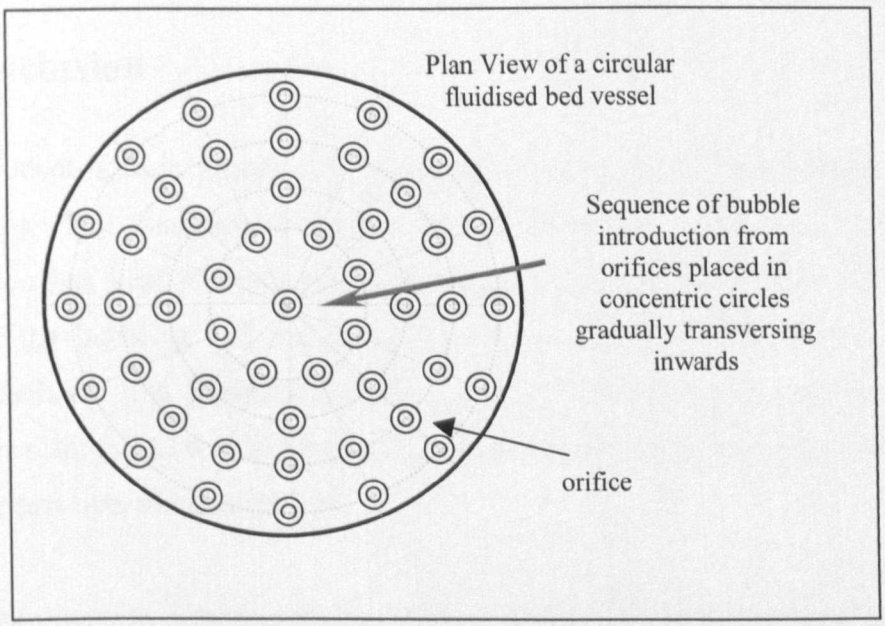

Figure 8.5.11: The plan view of a circular fluidised bed with the suggested management of gas introduction from networks of orifices to create bubbles with the IPBM method.

Purely an analytical approach, it is not essential to publish the numerals of the parameters used in the different bubble introduction methods such as the spacing of distributor orifices or the time interval between consecutive bubble introduction on adjacent orifices. Furthermore, the study was carried out in a simulated environment and made simple for

analytical studies by the used of a planar bed. It is essentially a qualitative study and one set of parameter values may not necessarily uniquely apply to any other bed configuration (e.g. different geometry or bed material) let alone to real life vessels, which are subject to other more complicated factors that could altogether prevent this idea from materialising successfully. The study provides an insight into the possibility on an option available to improve the bed quality.

Referring to the work by Rafailidis et al. (1991) the use of standpipes or orifice distributor could be more advantageous compared to porous plate distributors, leading to stable bubbling patterns but consequently the resulting gross solid circulation pattern within the bed may lead to localised wear of internals. On the other hand, the use of porous plate distributor or larger number of orifices that creates small bubbles offers a more diffused but unstable arrangement of bubbles such that it would create a gross bubble migration to the bed centre through coalescence and wall-effect.

8.6 Conclusion

The system identification process was conducted on the planar fluidised bed system by approximating the complicated and complex bubbling process as linear. This approximation has kept analysis and study simple and has shown that the dynamical response of the bubbling bed was non-linear but reasonably controllable using linear controller methods. The bubbling process was shown to be well approximated with a second order plant model with different plant parameters required to estimate the model for different process operating conditions.

The PID controller was then shown to be a robust controller coping reasonably well with a wide range of operating conditions. Fixed-gain controller implementation has shown that complication in control might arise during a large sudden change in demand, especially when the bed is operating close to its quiescent state. A suggestion, if any problem or controller instability should arise, is a slower response and settling demand imposed on the close-loop control to allow the change in flow to propagate throughout the bed to ensure a more stable transition of the process condition.

A non-linear system ultimately requires a more suitable controller found in adaptive control tactics. Therefore, the adaptive control strategy was subsequently implemented on the system via the Minimal Control Synthesis algorithm, carried out as a case study with the MCS + Integral Action (MCSIA) scheme. MSCIA performed well in controlling the bubbling process considering how noisy systems such as this pose a variety of control problems. MCSIA could appropriately control the process for various BVF demands given by two reference models: a second order plant model and a zero-order-hold plant model.

A more advanced and practical form of control has also been considered where the controlled introduction of bubbles was carried out alongside the control of the degree of bubbling in the bed to achieve good spatial distribution of bubble as well as other bubbling properties that ensure good fluidisation quality. This analysis was carried out only in the simulated environment as a first and objective approach to assessing the potential of this strategy. Results have shown good prospect for considering this form of control in future research.

Chapter 9

Conclusion

The dissertation set out to investigate a series of aspects of the bubbling fluidisation process that needed either readdressing or further study. This has been the dissertation's core motivation, carried out using techniques common in the field of dynamics and automatic control. Much has already been said about the process in the literature but there is still a lack of understanding of the fundamental physical factors that govern the overall mechanics of the process itself. The fluidisation process is generally a difficult and complex system. It consists of two different phases interacting inside an operating column. The process offers a complicated blend of individual physical processes operating both independently and collectively to affect the overall behaviour of the bed. The bubbling regime of the process characterised by the existence of voids in the homogeneous phase associated with as bubbles has been an intriguing subject of research.

The dissertation seeks to pursue a simple route towards understanding something perceived as complex and has done so by analysing the bubbling process in its two-dimensional form. The use of a planar bed led to the measurement and characterisation of the bubbling process through image analysis techniques with real-time acquisition and analysis of images of the bubbling bed. It was a simple technique to directly and explicitly study the bubbling process in its simplest form.

The use of a planar bed has enabled an in-depth study of the spatial distribution of bubbles, a crucial aspect that relates to the fluidisation quality of the bed. A set of definitions was drawn out specifying criteria that dictated what is a good degree of fluidisation quality and the consequences of quality deteriorating factors that emerge naturally at different stages of the bubbling regime. The dominant mechanisms that govern the natural distribution of bubble spatially in the bed were shown to be geometrical effects and bubble interaction.

The convenient application of Bode scaled frequency plots allowed more effective identification of salient features in the plots characteristic of the state at which the measurement was made. Frequency domain analysis was also used to distinguish changes in the dynamics of the bubbling process over different heights in the bed as well as suggesting the existence of a critical height below which the dynamics of beds of different heights are similar. The changes in the bubbling dynamics have a close relation to bubble spatial distribution profile development in the bed below that critical height.

The development of a simulated bubbling bed was a crucial necessity in providing a convenient analysis platform. It also facilitated a significant portion of the study not possible in the real world such as by removing certain dynamical features from the simulation, which were unimportant or complicated so that more relevant issues can be better studied. The implementation of the Clift & Grace (1970, 1971a, 1971b) bubble interaction model in the simulation has been successfully validated experimentally. This has also led to the ability to study the bubbling bed in its idealised form. The idealised form of bubbling bed was conceived in line with the attempt to conceptualise an idealistic condition that provides a good fluidisation quality. In its idealised form, bubbles in the bed were created without having any interaction whatsoever with the bed walls as well as other bubbles, hence eliminating bubble coalescence. This is a condition that is only achievable in a realistic bed close to quiescent state. It was shown that a bubbling bed is linear in its idealised form but slips into non-linearity when bubbles are allowed to interact and ultimately coalesce.

The concept of an idealised bubbling process was further supported with the derivation of a theoretical model described by a transfer function that assumes the bed as a temporary store for gas. The introduction of a packet of gas observable as a bubble void results in an increase in bubble void fraction in the bed for the period of time the bubble resides in the bed. The simplicity of the treatment was justified by its ability to appropriately model the dynamics of the bed with the issuing of single bubbles when comparing similar conditions experimentally and with the simulated bed. The model was extended to cases of bed with multiple bubbles accounting for bubble interaction and coalescence, again shown to be well constructed from the basic model of single bubbles by comparison with the simulated bed for the similar conditions. The successes of the theoretical model demonstrates the

progress made in better understanding the fundamental dynamics of bubbling beds capturing the dominating features affecting its overall behaviour.

System identification of the process was carried out to characterise the bed response to transient changes in the gas supply. The bed was found to be non-linear as its dynamical behaviour changes depending on its bubbling condition. Linear control was implemented to control the proportion of bubbling and was shown to be reasonably successful, particularly with a PID controller scheme.

Adaptive control was subsequently attempted with the Minimal Control Synthesis (MCS) scheme to determine the improvements in performance and the necessity of using such controllers. MCS with integral action (MCSIA) was found to be appropriate and control over various demands was carried out. Performance assessment showed that despite being a versatile and flexible controller strategy adaptable to large changes in system dynamics, MSCIA was unable to perform better than the PID linear controller scheme. The main shortcoming of the adaptability capability of MCS scheme was the rate at which the controller gains adapted to changes in process dynamics. The high adaptability rate chosen in some of the tests caused controller instability, which was perhaps case specific.

The second downfall was due to the relatively primitive algorithm that currently makes up the steady state gain decay policy function. At present, this policy does not allow flexibility in the rate of gain decay with respect to the proximity of the closed-loop output to the steady state demand. It was suggested a more versatile gain decay policy is needed and efforts are currently being made to improve on this feature and is therefore part of a future work lined up for the extension of the research.

Part of the control problem faced in a system such as this is caused by the control effort itself. The control action exerted by the controller to rectify errors between the output and demand induces large disturbances in the natural dynamics of the system itself that in turn alters the desired outcome of the already tuned controller settings. This is of interest for future consideration. In general, the control implemented on the fluidisation process has met success for both conventional and adaptive schemes and the prospect lies ahead for much more improvements.

A note on further work

The immediate aspect for extension of the research is the need to extend it to the more practical three-dimensional realm. The bridging between the two domains requires an integration of correlating knowledge and techniques. The image analysis system should be replaced by a more practical measurement system for an opaque vessel, where pressure fluctuation measurements would offer a suitable solution. Efforts in developing this instrumentation system and characterising the pressure measurements to correlate them to the image analysis measurements should be a substantial piece of work.

An in-depth study of the pressure readings should lead to a greater understanding of what the features in the measurements physically relate to in the process and of what dynamical behaviour in the bed that causes the changes in pressure fluctuations. Through this, a better fundamental understand of the behaviour of three-dimensional bubbling beds can be achieved.

The extension of other body of work in this dissertation based on two-dimensional space can then be systematically transferred to the three-dimensional domain based on the pressure system. Both the simulation of bubbling bed and the theoretical model could be readily extended to cater for an addition degree of space where, for a start, the Clift & Grace model has already been derived for three-dimensional bubble interaction cases. This also presents an outstanding issue for future consideration.

In this dissertation, the fluidisation process was demonstrated to be well controllable in the two-dimensional bed using image analysis measurement of the bed conditions. The practicality of this is somewhat limited to analytical purposes due to the type of bed and measurement parameter used. Therefore, this goes to imply that controlling the fluidisation process with pressure fluctuation as the feedback measurement can subsequently lead to more practical and industrial-relevant effort in devising appropriate control strategies. Further improvement on process control with both the linear and MCS adaptive schemes is also the next obvious step. Understanding the process further and designing the controllers so that they are more suited for this task will be beneficial.

In Chapter 4, the idea of a critical height in the bed that allows the complete development of bubble spatial distribution modification was proposed. Experimental observation was used to estimate that probable critical height but no good qualitative reasoning has been established. Effort should therefore be continued to better address this issue as it could be a potentially useful tool to help determine bed fluidisation quality associated with bubble spatial distribution. The mechanism that governs the spatial distribution of bubbles in three-dimensional bed should also be further investigated and compared with what was proposed for two-dimensional beds.

The transfer function or gain Bode plot of the bubbling bed was shown to be a useful tool to identify the bed dynamical features. Similar analysis carried out with the BVF and A_{gb} time series to produce the plot could also be used with other measured parameter such as with pressure fluctuations time series coupled with a suitable input parameter.

The primary 'dip' found as a distinct feature in the transfer function Bode plot was proposed as a means of identifying fluidisation quality changes in the bubbling bed. A bed with a primary 'dip' placed at a higher frequency indicates it has a lower fluidisation quality. It could be demonstrated that by increasing the gas supplied into the bed to generate more vigorous bubbling the corresponding transfer function Bode plot, in comparison with that of a bed with a lower rate of bubbling, has a primary 'dip' that is narrower and is placed at a higher frequency. It will be interesting to extend what that is already demonstrated via simulation to the experimental bed.

A new experimental planar bed will benefit the research further where the distributor is designed such that the introduction of bubbles can be controlled. This leads to further studies on the spatial distribution of bubbles expanding on ideas of an active distributor that proactively determines the placements of bubbles that promotes the desired distribution profile in the bed. This would allow an experimental extension to investigating the initially simulated attempt at the alternative process control technique of proactively managing the bubble spatial distribution in the bed could also be carried out. Subsequently, a proactive distributor could also be considered for the three-dimensional bed when this technique of controlling the bed quality is more understood and is able to be confidently reproduced.

It is hoped that the efforts put into conceiving this dissertation will benefit the field of fluidisation engineering, not so much in solving the mystery of gas-solid interaction, a topic which has been dwelled upon by many, but towards probing better understanding of the fundamentals of the subject and provide means of supporting research from other approaches. This dissertation shows that for specific problems the simple, including heuristic, approaches work well in delivering results. Some of the objectives of the dissertation have been possible to achieve as they lead to a specific rather than broad understanding of issues concerning the bubbling fluidisation process. The dynamics and automatic control approaches employed throughout the work have delivered some remarkable outcomes offering an alternative perspective to the subject different from that of the typical approaches met in the literature.

References

Amplicon Liveline Limited. PC 30AT. Centenary Industrial State. Hollingdean Road. Brighton UK BN2 4AW: Amplicon Liveline Limited. PC 30AT Instruction manual Part 858 931 54 Issue E

Bi, H. T., Grace, J. R. & Zhu, J., 1995. Propogation of pressure waves and forced oscillations in gas-solid fluidized beds and their influence on diagnostics of local hydrodynamics, *Powder Technology*, Vol. 82, pp. 239-253

Beard, G. S., 1998. Adaptive control of energy efficient hydraulic systems, PhD. Dissertation, University of Bristol, 266 p.

Benchoubane, H. & Stoten, D. P., 1990. Convergence Rates of an Adaptive Control Algorithm with Application to the Speed Control of a DC Machine, *Proc 16th Conf IEEE Ind Elec Soc, Monterey (CA)*, pp. 390-395

Brown, R. C. & Brue, E., 2001. Resolving dynamical features of fluidized beds from pressure fluctuations, *Powder Technology*, Vol. 119, pp. 68-80

Brue, E. & Brown, R. C., 2001. Use of pressure fluctuations to validate hydrodynamic similitude in fluidized media: bubbling beds, *Powder Technology*, Vol. 119, pp. 117-127

Burgess, J. M. & Calderbank, P. H., 1975. The measurement of bubble parameters in 2-phase dispersions-I the development of an improved probe technique, *Chemical Engineering Science*, Vol. 30, pp. 743-750

Canada, G. S., McLaughlin, M. & Staub, F. W., 1978. Flow regimes and void fraction distribution in gas fluidization of large particles in beds without tube banks, *AIChE Symp. Series*, Vol. 74, No. 176, pp. 14-26

Cantù, M., 1999. Mastering Delphi 5, Sybex Inc., CA, United States of America, 1085 p.

Choi, J. H., Son, J. E. & Kim, S. D., 1998. Generalized Model for bubble size and frequency in gas-fluidized beds, *Ind. Eng. Chem. Res.*, Vol. 37, pp. 2559-2564 (x)

Chong, Y. O., O'Dea, D. P., White, E. T., Lee, P. L. & Leung, L. S., 1987. Control of the quality of fluidization in a tall bed using the variance of pressure fluctuations, *Powder Technology*, Vol. 53, pp. 237-246

Clift, R., 1970, Ph.D. dissertation, McGill University

Clift, R. & Grace, J. R., 1970, Bubble interaction in fluidized beds, *Chemical engineering progress symposium series*, Vol. 66, No. 105, pp. 14-27

Clift, R. & Grace, J. R., 1971a, The Coalescence of Bubble Chains in Fluidised Beds, *Transaction of the Institute of Chemical Engineers*, Vol. 50, pp. 364-371

Clift, R. & Grace, J. R., 1971b, Coalescence of Bubbles in Fluidized Beds, *AIChE Symposium Series*, Vol. 67, No. 116, pp. 23-33

Clift, R. & Grace, J. R., 1972. The mechanism of bubble break-up in fluidised beds, *shorter communications*, *Chem. Eng. Sci.*, Vol. 27, pp. 2309-2310

Clift, R., Grace, J. R. & Weber, M.E., 1974. Stability of bubbles in fluidized beds, *Ind. Eng. Chem. Fundam*, Vol. 13, No. 1, pp. 45-51

Collins, R., 1965a. An extension of Davidson's theory of bubbles in fluidized beds, *Chem. Eng. Sci.* Vol. 20, No. 8, pp. 747-755

Collins, R., 1965b. The rise velocity of Davidson's fluidization bubble, *Chem. Eng. Sci.*, Vol. 20, No. 8, pp. 788-789

Darton, R. C., LaNauze, R. D., Davidson, J.F. & Harrison, D., 1977, Bubble growth due to coalescence in fluidised beds, *Trans. Instn Chem. Engrs.* Vol. 55, pp. 274-280

Data Translation , Inc. DT 3155. 100 Locke Drive, Marlboro, MA 01752-1192: Data Translation, Inc. DT 3155 Frame Grabber SDK for MACH Series, UM-13442-F

Data Translation , Inc. DT 3155. 100 Locke Drive, Marlboro, MA 01752-1192: Data Translation, Inc. DT 3155 MACH Series Device Driver for Microsoft Windows, UM-13858-H

Davies, R. M. & Taylor, G. I., 1950. The mechanics of large bubbles rising through extended liquids and through liquids in tubes, *Proc. Roy. Soc.*, A200, p.375-390

Davidson, J. F., Paul, R. C., Smith, J.S. & Duxbury, H. A., 1959. *Trans. Inst. Chem. Engrs.*, Vol. 37, p. 323.

Davidson, J. F. & Leung, L. S., 1961. *Trans. Inst. Chem. Engrs.*, Vol. 39, p. 409

Davidson, J.F., Harrison, D. & Guedes de Carvalho, J.R.F., 1977, On the Liquidlike Behaviour of Fluidized Beds, *Ann. Rev. Fluid Mech.*, Vol. 9, pp. 55-86

Dumitrescu, D. T., 1943. Strömung an einer Luftblase im senkrechten Rphr. Z. angew., *Math. Mech.*, Vol. 5, p. 169

Duraiswami, R., Chahine, G. L. & Sarkar, K. 1997. Boundary element techniques for efficient 2-D and 3-D electrical impedance tomography, *Chemical Engineering Science*, Vol. 52, No. 13, pp. 2185-2196

Dyakowski, T., Edwards, R. B., Xie, C.G. & Williams, R. A., 1997. Application of capacitance tomography to gas-solid flows, *Chemical Engineering Science*, Vol. 52, No. 13, pp. 2099-2110

Dye, M. & Stoten, D.P., 1994. WinCtrl Windows based real time control, University of Bristol. Internal report

Fan, L. T., Ho, T. C., Hiraoka, S., 1981. Pressure fluctuations in a fluidized bed, *AIChE Journal*, Vol. 27, No. 3, pp. 388-396

Fan, L. T., Ho, T. C., Walawender, W. P., 1983. Measurements of the rise velocites of bubbles, slug and pressure waves in a gas-solid fluidized bed using pressure fluctuation signals, *AIChE Journal*, Vol. 29, No. 1, pp. 33-39

Fan, Z., Chen, G. T., Chen, B. C. & Yuan, H., 1990. Analysis of pressure fluctuations in a 2D fluidized bed, *Powder Technology*, Vol. 62, pp. 139-145

Farrokhalaee, T., 1979, Ph.D. dissertation, Cambridge University

Franklin, G. F., Powell, J. D. & Workman, M. L., 1990. Digital control of dynamic systems, 2nd ed. Reading, Mass. , Wokingham, Addison-Wesley.

Franklin, G. F., Powell, J. D & Emami-Naeini, A., 1994. Feedback control of dynamical systems, 3rd Edition, Addison-Wesley Publishing Company, Inc.

Geldart, D., 1970. The size and frequency of bubbles in two- and three-dimensional gas-fluidised beds, *Poweder Technology*, Vol. 4, No. 1, pp. 41-55

Geldart, D. & Kelsey, J. R., 1972. The use of capacitance probes in gas-fluidized beds, *Powder Technology*, Vol. 6, pp. 45-60

Geldart, D. 1973. Types of Gas Fluidization, *Powder Technol*ogy, Vol. 7, pp. 285-292

Gibilaro, L. G., 2001. Fluidization dynamics, Chapter 10: Fluidization quality, Butterworth-Heinemann, Oxford, Great Britain, 232 p.

Gilbertson, M. A., Cheesman, D. J. & Yates, J. G., 1998. Observation and measurements of isolated bubbles in a pressurised gas-fluidised bed, *Fluidisation IX, Durango, Engineering Foundation*, pp. 61-68

Glicksman, L., 1984. Scaling relationship for fluidized beds, *Chemical Engineering Science*, Vol. 39, No. 9, pp. 1373-1379

Grace, J. R. & Harrison, D., 1969. The distribution of bubble within a gas-fluidized bed, *Institute of Chemical Engineering Symposium Series*, Vol. 30, pp. 105-125

Grace, J. R., 1971, *AIChE Symp. Ser.*, Vol. 67, No. 116, pp. 159-167

Grace, J. R. & Venta, J., 1973. *Can. J. Chem Eng.*, Vol. 51, pp. 110-111

Halow, J. S. & Nicoletti, P., 1992. Observations of fluidized bed coalescence using capacitance imaging, *Powder Technology*, Vol. 69, pp. 255-277

Harold, D., 1995. Delphi power toolkit for Windows :cutting-edge tools & techniques for programmers, Research Triangle Park, NC, 750 p.

Harrison, D. & Davidson, J. F., 1961. On the nature of aggregative and particulate fluidisation, *Trans. Instn. Chem. Engrs.*, Vol. 39, pp. 202-211

Harrison, D. & Leung, L. S., 1962. Symposium on Interaction between Fluids and Particles, *Instn. Chem. Eng.*, London, p. 127

Hay, J. M., Nelson, B. H., Briens, C. L. & Bergougnou, M. A., 1995. The calculation of the characteristics of a chaotic attractor in a gas-solid fluidized bed, *Chemical Engineering Science*, Vol. 50, No. 3, pp. 373-380

Horio, M. & Nonaka, A., 1987. A generalized bubble diameter correlation for gas-solid fluidized beds, *AIChE Journal*, Vol. 33, No. 11, pp. 1865-1872

Jackson, R., 1963. *Trans. Inst. Che. Engrs.*, Vol. 41, pp. 13- 21

Ji, H. S., Ohara, H., Kuramoto, K., Tsutsumi, A., Yoshida, K. & Hirama, T., 2000. Nonlinear dynamics of gas-solid circulating fluidized-bed system, *Chemical Engineering Science*, Vol. 55, pp. 403-410

Johnsson, F., Svensson, A., Andersson, S. & Leckner, B., 1995. Fluidization regimes in boilers, *Fluidization VIII* (preprints), Tours, pp. 129-136.

Johnsson, F., Zijerveld, R.C., Schouten, J.C., van den Bleek, C.M. & Leckner, B., 2000. Characterization of fluidization regimes by time-series analysis of pressure fluctuations, *Int. J. Multiphase Flow*, Vol. 26, pp. 663-715

Johnsson, F., Larsson, G. & Leckner, B., 2002. Pressure and flow fluctuations in a fluidized bed – interaction with the air-feed system, *Chemical Engineering Science*, Vol. 57, No. 8, pp. 1379-1392

Judd, M. R., 1965. Ph.D. dissertation, University of Cape Town

Justat, A., 1949, *Przemyst Chem.*, Vol. 28, No. 16

Kaart, S., Schouten, J. C. & Bleek, C. M., 1998. Chaos control applied to the hydrodynamics of gas-solid fluidized bed reactors to improve chemical performance, *Fluidisation IX, Durango, Engineering Foundation*, pp. 621-628

Kaart, S., Schouten, J. C. & Bleek, C. M., 1999. Improving conversion and selectivity of catalytic reactions in bubbling gas-fluidized bed reactors by control of the nonlinear bubble dynamics, *Catalysis Today*, Vol. 48, pp. 185-194

Kage, H., Agari, M., Ogura, H. & Matsuno, Y., 2000. Frequency analysis of pressure fluctuation in fluidized bed plenum and its confidence limit for detection of various modes of fluidization, *Advanced Powder Technology*, Vol. 11, No. 4, pp. 459-475

Kay, S. M. & Marple, S. L., 1981. Spectrum Analysis - A Modern Perspective. *Proceedings of the IEEE*, Vol.69 (11), pp. 1380-1419 Power Spectral Density

Kobayashi, H., Arai, F. & Chiba, T., 1965. *Kagaku Kogaku (Chem. Eng. Japan)*, Vol. 29, p. 858

Korte, R. J., Schouten, J. C. & Bleek, C. M., 2001. Controlling bubble coalescence in a fluidized bed model using bubble injection, *AIChE Journal*, Vol. 47, No. 4, pp. 851-861

Kunii, D., Yoshida, K. & Hiraki, I., 1967. The behaviour of freely bubbling fluidized beds, *Proceedings to the International Symposium on Fluidization*. pp. 243-256

Kunii, D. & Levenspiel, O., 1969. Fluidization Engineering, John Wiley & Sons, Inc.New York, United States of America, 534 p.

Landau, I. D., 1974. A survey of model reference adaptive techniques: Theory and application, *Automatica*, Vol. 10, No. 3, pp. 353-379

Leckner, B., Palchonok, G. I. & Johnsson, F., 2001. Pressure fluctuations in gas fluidised beds, *IEA Technical Meeting*, Lisbon, Portugal

Leva, M., 1962. The use of gas-fluidized systems for blending particulate solids, *Symp Interaction between Fluids and Particles*, p. 143

Lim, K. S. & Agarwal, P. K., 1990a. Conversion of pierced lengths measured at probe to bubble size measures: an assessment of the geometrical probability approach and bubble shape models, *Powder Technology*, Vol. 63, pp. 205-219

Lim, K. S. & Agarwal, P. K., 1990b. Measurement and modelling of bubble parameters in a 2D gas-fluidized bed using image analysis, *Powder Technology*, Vol. 60, pp. 159-171

Lim, K. S. & Agarwal, P. K., 1992. Bubble velocity in fluidised beds: the effects of non-vertical bubble rise on its measurement using submersible probes and its relationship with bubble size, *Powder Technology*, Vol. 69, pp. 239-248

Lim, K. S., Gururajan, V. S. & Agarwal, P. K., 1993. Mixing of homogeneous solids in bubbling fluidized beds: theoretical modelling and experimental investigation using digital image analysis, *Chemical Engineering Science*, Vol. 48, No. 12, pp. 2251-2265

Lirag, R. C. & Littman, H.,1971. Statistical study of the pressure fluctuations in a fluidized bed, *AIChE Symp. Ser.* Vol. 166, No. 67, pp. 11-22

Lischner, R., 2000. Delphi in a nutshell: A desktop quick reference, O'Reilly & Associates, Inc., CA, United States of America, 561 p.

Lee, P. L., Chong, Y. O. & Leung, L. S., 1986. Experimental investigation of the quality control of fluidized beds, *Powder Technology, short communication*, Vol. 46, pp. 77-80

Lockett, M. J. & Harrison, D., 1967. The distribution of voidage fraction near bubbles rising in gas-fluidized beds, *Proceedings of the International Symposium on Fluidization* (edited by Drinkenberg), The Netherlands University Press, Amsterdam, pp. 257-267

Makkawi, Y. T. & Wright, P. C., 2002a. Fluidization regimes in a conventional fluidized bed characterised by means of electrical capacitance tomography, *Chemical Engineering Science*, Vol. 57, No. 13, pp. 2411-2437

Makkawi, Y. T. & Wright, P. C., 2002b. Optimization of experimental span and data acquisition rate for reliable electrical capacitance tomography measurement in fluidization studies – a case study, *Measurement Science and Technology*, Vol. 13, pp. 1831-1841

Mano, M. M, 1991. Digital Design, Second Edition. Prentice-Hall, Inc., 516 p.

Manohar, M., & Ramapriyan, H. K., 1989. Connected Component labelling of Binary Images on a Mesh Connected Massively Parallel Processor, *Computer Vision, Graphics and Image Processing*, Vol. 45, pp. 133-149

Mischke, L., Antoni, J., & Sobolewski, C., 1938, Poland Patent 27,665, class 12 g, 4 (o)

Miwa, K., Mori, S., Kato, T. & Muchi, I., 1972. Behaviour of bubbles in a gaseous fluidized bed, *International Chemical Engineering*, Vol. 12, No. 1, pp. 187-194

Morse, R. D. & Ballou, C. O., 1951. The uniformity of fluidization, its measurement and use, *Chem. Engng. Prog.*, Vol. 47, pp. 199-211

Mostoufi, N. & Chaouki, J, 2001. Local sold mixing in gas-solid fluidized beds, *Powder Technology*, Vol. 114, pp. 23-31

Mudde R. F., Schulte H. B. M. & Akker H. E. A., 1994. Analysis of a bubbling 2-D gas-bubbling bed using image processing, *Powder Technology*, Vol. 81, pp. 149-159

Murray, J. D., 1965. *J. Fluid Mech.*, Vol. 22, pp. 57-80

Murray, J. D., 1966. *Chem. Eng. Progr. Symp. Series*, Vol. 62, No. 62, pp. 71

Musmarra, D., Poletto, M., Vaccaro, S. & Clift, R., 1995. Dynamic waves in fluidized beds, *Powder Technology*, Vol. 82, pp. 255-268

Mussio, P., & Padula, M., 1985. An Approach to the Definition, Description and Extraction of Structures in Binary Digital Images, *Computer Vision, Graphics and Image Processing*, Vol. 31, pp. 19-49

Newby, R. A. & Keairns, D. L., 1986. Test of the scaling relationships for fluid-bed dynamics. In: Ostergaard, K. & Sorensen, A. (Eds.), *Fluidization V*, Engineering Foundation, New York, pp. 31-38.

Nicastro, M. T. & Glicksman, L. R., 1984. Experimental verification of scaling relationship for fluidized bed, *Chemical Engineering Science*, Vol. 39, No. 9, pp. 1381-1391

Nicklin, D. J., 1962. Two-phase bubble flow, *Chemical Engineering Science*, Vol. 17, pp. 693-702

Ogata, K., 1997. Modern Control Engineering, Third Edition. Prentice-Hall International, Inc., 997 p.

Okhi, K., Akehata, T. & Shirai, T.,1976. A new method for evaluating the size of moving particles with a fibre optic probe, *Powder Technology*, Vol. 11, pp. 51-57

Osier, D., Grobman, S. & Batson, S., 1997. Teach yourself Delphi 3 in 14 days, Sams Publishing, Indiana, United States of America, 599 p.

Park, W. H., Kang, W. K., Capes, C. E. & Osberg, G. L., 1969. The Properties of Bubbles in Fluidized Beds of Conducting Particles as Measured by an Electroresistivity Probe, *Chemical Engineering Science*, Vol. 24, pp. 851-865

Potter, O. E., 1971. Chapter 7: Mixing, Fluidization, (Eds Davidson, J.F. & Harrison, D.), p. 293

Pyle, D. L. & Harrison, D., 1967. The rising velocities of bubbles in two-dimensional fluidised beds, *Chemical Engineering Science*, Vol. 22, No. 4, pp. 531-535

Rafailidis, S. V. & Clift, R., 1991. Study on the influence of bubble formation at the distributor on fluidized bed behaviour, *AIChE Symposium Series*, Vol. 87, No. 281, pp. 47-57

Ramayya, A. V., Venkateshan, S. P. & Kolar, A. K., 1998. Bubble detection with horizontal gradient measurements ingas-fluidised beds, *Powder Technology*, Vol. 97, pp. 77-84

Reuter, H., 1963. *Chem.-Ing.-Tech.*, Vol. 35, No. 98, p. 219

Reuter, H., 1966, *Chem. Eng. Progr. Symp. Ser.*, Vol. 62, No. 62

Rippin, D. W. T., 1959. The rise of gas bubbles in liquids, PhD dissertation, University of Cambridge

Ronse, C., & Devijver, P. A., 1984. Connected Components in Binary Images: The Detection Problem, Research Studies, Letchworth, Herts, England

Rosenfeld, A., & Pfaltz, J. L., 1966. Sequential Operations in Digital Picture processing, *Journal of the Association for Computing Machinery*, Vol. 13, pp. 471-494

Rowe, P. N. & Partridge, B. A., 1962. Particle movement caused by bubbles in a fluidized bed, *Symp Interaction between Fluids and Particles, Inst. Chem. Engrs.*, p. 135

Rowe, P. N., Partridge, B. A. & Lyall, E., 1964, Cloud formation around bubbles in gas fluidized beds, *Chemical Engineering Science*, Vol. 19, pp. 973-985

Rowe, P. N., Partridge, B. A., Cheney, A. G., Henwood, G. A. & Lyall, E., 1965. The mechanism of solids mixing in fluidized beds, *Trans Inst Cehm Engrs*, Vol. 43, p. 271

Rowe, P. N. & Partridge, B.A., 1965. *Trans. Inst. Chem. Engrs.*, Vol. 43, T 157

Rowe, P. N., 1971. Chapter 4: Experimental properties of bubbles, Fluidization, (Eds Davidson, J. F. & Harrison, D.), p. 121

Rowe, P. N. & Goldsmith, J. A., 1975. The coalescence and splitting of bubbles in gas fluidised beds, *2nd Iranian Congr. Chem. Eng.*, Teheran

Rowe, P. N. & Matsuno, R., 1971. Single bubbles injected into a GFB & observed by Xray, *Chemical Engineering Science*, Vol. 27, pp. 923-935

Rowe, P. N., 1976. Prediction of bubble size in a gas-fluidised bed, *Chemical Engineering Science*, Vol. 31, pp. 285-288

Rowe, P. N. & Yacono, C. X. R., 1976. The bubbling behaviour of fine powders when fluidised, *Chemical Engineering Science*, Vol. 31, pp. 1179-1192

Rowe, P. N. & Masson, H., 1980. Fluidised bed bubbles observed simultaneously by probe and by X-rays, *Chem Eng Science*, Vol. 35, pp. 1443-1447

Rowe, P. N. & Masson, H., 1981. Interaction of bubbles with probes in gas fluidised beds, *Trans. Instn Chem. Engrs.*, Vol. 59, pp. 177-185

Roy, R., Davidson, J. F. & Tuponogov, V. G., 1990. The velocitty of sound in fluidised beds, *Chemical Engineering Science*, Vol. 45, No. 11, pp. 3233-3245

Satija, S. & Fan, L. S., 1985. Characteristics of slugging regime and transition to turbulent regime for fluidized beds of large coarse particles. *AIChE J.*, Vol. 31, pp. 1554-1562

Schaaf, J., Schouten, J. C. & Bleek, C. M., 1998. Origin propogation and attenuation of pressure waves in gas-solid fluidized beds, *Powder Technology*, Vol. 95, pp. 220-233

Schaaf, J., Schouten, J. C., Johnsson, F. & Bleek, C. M., 2002. Non-intrusive determination of bubble and slug length scales in fluidized beds by decomposition of the power spectral density of pressure time series, *Int. J. Multiphase Flow*, Vol. 28, pp. 865-880

Schouten, J. C., Stappen, M. L. M. & Bleek, C. M., 1992. Deterministic chaos analysis of gas-solid fluidization, *Fluidisation VII*, pp. 103-111

Schouten, J. C., Stappen, M. L. M. & Bleek, C. M., 1996. Scale-up chaotic fluidized bed hydrodynamics, *Chemical Engineering Science*, Vol. 51, No. 10, pp. 1991-2000

Schouten, J. C. & Bleek, C. M., 1998. Monitoring the quality of fluidization using the short-term predictability of pressure fluctuations, *AIChE Journal*, Vol. 44, No. 1, pp. 48-60

Schügerl, K., 1967. Comment, *Proceedings of the International Symposium on Fludization*, p. 662, Eindhoven

Schwarzenbach, J. & Gill, K. F., 1992. System modelling and control, 3rd ed., John Wiley & Sons Inc, London, 340 p.

Shichi, R., Mori, S. & Muchi, I., 1968. Kagaku Kogaku, *(Chem. Eng. Japan)*, Vol. 32, pp. 343-348

Stappen, M. L. M., Schouten, J. C. & Bleek, C. M., 1995. Application of the deterministic chaos theory in understanding the fluid-dynamic behaviour of gas-solids fluidization, *AIChE Symposium Series*, Vol. 89, No. 296, pp. 91-102

Stewart, P. S. B., 1968. Isolated Bubbles in Fluidised Beds – Theory and Experiment, *Trans. Inst. Chem. Engrs.*, Vol. 46, pp. T60-T66

Stoten, D. P. & Benchoubane, H., 1990a. Robustness of a minimal controller synthesis algorithm, *Int. J. Control*, Vol. 51, No. 4, pp. 851-861

Stoten, D. P., 1990. Model Reference Adaptive Control of Manipulators, Research Studies Press Ltd., Taunton, England, 238 p.

Stoten, D. P. & Benchoubane, H., 1990b. Empirical Studies of an MRAC Algorithm with Minimal Controller Synthesis, *Int. J. Control*, Vol. 51, No. 4, pp. 823-849

Stoten, D. P. & Benchoubane, H., 1995. The extended minimal controller synthesis algorithm, *Int. J. Control*, Vol. 56, No. 5, pp. 1139-1165

Stoten D. P., 1993. An overview of the minimal control synthesis algorithm, *I Mech E Conference on Aerospace Hydraulics and Systems*, London, paper C474-033.

Stoten D. P., 1995. The Adaptive Minimal Control Synthesis Algorithm with Integral Action, *Proc. 21st IEEE Conf. Ind. Elec., Control and Inst., Orlando (FLA)*, pp. 1646-1651

Svensson, A., Johnsson, F. & Leckner, B., 1996. Fluidization regimes in non-slugging fluidized beds: the influence of pressure drop across the air distributor, *Powder Technology*, Vol. 86, pp. 299-312

Toei, R., Matsuno, R. & collaborators, 1964. Preprint for the 3rd Annual Symposium, *Soc. Chem. Engrs.*, Japan, Nagoya

Toei, R., Matsuno, R., Kojima, H., Nagai, Y., Nakagama, K. & Yu, S., 1965, *Memoirs Fac. Eng. Kyoto. Univ.*, Vol. 27

Toei, R., Matsuno, R., Ishii, H. & Kojima, H., 1965. *Kagaku Kogaku (Chem. Eng. Japan)*, Vol. 29, p. 851

Toei, R. & Matsuno, R., 1967. *Proc. Intern. Symp. On Fluidization*, Netherlands Univ. Press, Amsterdam

Toei, R., Matsuno, R. & Tejima, T., 1967. *Kagaku Kogaku, (Chem. Eng. Japan)*, Vol. 31, pp. 1238-1239

Waterfall, R. C., He, R. H. & Beck, C. M., 1997. Visualizing combustion using electrical impedance tomography, *Chemical Engineering Science*, Vol. 52, No. 13, pp. 2129-2138

Werther, J. & Molerus, O., 1973a. The local sructure of gas fluidized beds-I. A statistically based measuring system, *Int. J. Multiphase Flow*, Vol. 1, pp. 103-122

Werther, J. & Molerus, O., 1973b. The local sructure of gas fluidized beds-II. The spatial distribution f bubbles, *Int. J. Multiphase Flow*, Vol. 1, pp. 123-138

Whitehead, A. B. & Young, A. D.,1967. Fluidization in large scale equipment, *Proc. Int. Symp. on Fluidization, The Netherlands University Press, Amsterdam*, pp. 294-302

Xu, L. J., Han, Y. T., Xu, L. A. & Yang, J. S., 1997. Application of ultrasonic tomography to monitoring gas/liquid flow, *Chemical Engineering Science*, Vol. 52, No. 13, pp. 2171-2183

Yasui, G. & Johanson, L. N., 1958. Characteristics of Gas Pockets in Fluidized Beds, *AIChE Journal*, Vol. 4, No. 4, pp. 445-452

Yates, J. G., Cheesman D. J. & Sergeev, Y. A., 1994. Experimental observations of voidage distribution around bubbles in a fluidized bed, *Chem. Eng. Sci.*, Vol. 49, No. 12, pp. 1885-1895

Zabrodsky, S. S., 1966. Hydrodynamics and heat transfer in fluidized beds, Cambridge, Mass. London, MIT Press, 379 p.

Zenz, F. A. & Othmer, D. F., 1960. Fluidization and fluid-particle systems, Reinhold Chemical Engineering Series, Reinhold Publising Corporation, New York, 513 p.

Zijerveld, R. C., Johnsson, F., Marzocchella, A., Schouten, J. C. & Bleek, C. M., 1998. Fluidization regimes and transitions from fixed bed to dilute transport flow, *Powder Technology*, Vol. 95, pp. 185-204